

CRANFIELD UNIVERSITY

I. D. HARRIS

HIGH-SPEED GMAW AND LASER GMAW HYBRID WELDING OF
STEEL SHEET

SCHOOL OF APPLIED SCIENCES

PhD THESIS

CRANFIELD UNIVERSITY

SCHOOL OF APPLIED SCIENCES

PhD THESIS

Academic Year 2008-2009

I. D. Harris

High-Speed GMAW and Laser GMAW Hybrid Welding of Steel Sheet

Supervisor D. Yapp

March 2009

Cranfield University 2009. All rights reserved. No part of this publication may be reproduced without the written permission of the copyright owner.

TABLE OF CONTENTS

ABSTRACT

ACKNOWLEDGEMENTS

LIST OF FIGURES

LIST OF TABLES

NOMENCLATURE

ABBREVIATIONS

1.0 INTRODUCTION

1.1 Background

1.1.1 Dispelling the Myths about GMAW-P

1.1.2 The Common Myths

1.1.3 The Good News

1.2 Summary

2.0 LITERATURE REVIEW

2.1 Process Studies and Welding Productivity

2.2 Gas Metal Arc Welding

2.2.1 Gas Metal Arc Welding (GMAW) Including Pulsed GMAW (GMAW-P)

2.2.2 GMA-Brazing and Variable Polarity Gas Metal Arc Welding - GMAW-VP

2.2.3 STT GMAW

2.2.4 CSC and CMT GMAW

2.2.5 Tandem and Twin-Wire GMAW

2.3 Plasma Arc Welding

2.4 Hybrid Laser Arc Welding

2.5 Hybrid Laser Welding – LBW/GTAW and LBW/PAW

2.6 Hybrid Laser Welding - LBW/GMAW

2.6.1 Laser/GMAW and LBW for Galvanized Steel

2.7 Arc Power versus Laser Power

2.7.1 GMAW Melting Rate

2.7.2 GMAW Melting Efficiency

2.7.3 Laser Power and Efficiency

2.8 Diode Lasers

2.9 Fibre Lasers

2.10 Weld Bead Humping

2.11 Weld Pool Dynamics and Humping Mechanisms

2.12 Modeling

2.13 Calorimetry

2.14 Weld Sizing

2.15 Gap Weldability

2.15.1 Tack Welds

- 2.15.2 Self-Fixturing
- 2.16 A Brief Summary of Papers and Conference Presentations by the Author during the Course of This Research
- 2.17 Summary of the Literature Review and Work Scope in the Thesis Research

3.0 RESEARCH AIMS AND OBJECTIVES

4.0 EQUIPMENT AND MATERIALS

- 4.1 Welding Process and Equipment for Weld Sizing
- 4.2 Trumpf Programmable Focusing Optics PFO
- 4.3 CO₂ Laser System
 - 4.3.1 High-Voltage Power Source
 - 4.3.2 Resonator
 - 4.3.3 Shutter
 - 4.3.4 Main Relay Cabinet
 - 4.3.5 Laser Cooling System
- 4.4 Trumpf HAAS 4006D Neodinium Yttrium Aluminum Garnet (Nd:YAG) Laser
- 4.5 Workpiece Manipulation
 - 4.5.1 Single-Axis Welding Carriage
 - 4.5.2 CNC Worktable
 - 4.5.3 Robotic Manipulation
 - 4.5.4 Fixturing
- 4.6 Data Acquisition
 - 4.6.1 Data Acquisition for Arc Welding
- 4.7 High-Speed Video (HSV)
- 4.8 Measurement and Analysis Tools
 - 4.8.1 PRIMES Laser Beam Monitor

5.0 EXPERIMENTAL TECHNIQUES

- 5.1 Weld Acceptance Criteria
- 5.2 Weld Sizing Applications for Sheet Less than 3 mm
 - 5.2.1 Welding Parameter Selection Technique
 - 5.2.2 Weld Acceptance Criteria
 - 5.2.3 Design of Experiments
- 5.3 Experimental and Theoretical Work – High-Speed GMAW-P Lap-Fillet Welding Trials
- 5.4 Experimental and Theoretical Work – Hybrid Welding, Laser Beam Splitting, and Toe Wetting
 - 5.4.1 Scanning Laser Nd:YAG and Dual Spot
 - 5.4.2 CO₂ Dual Beam
 - 5.4.3 CO₂ Offset Beam
- 5.5 Calorimetry
- 5.6 Experimental Procedure for High-Speed Video
- 5.7 Accuracy and Inaccuracy of Methods, Verification, and Repeatability

6.0 RESULTS

- 6.1 Welding Parameters for Weld Sizing
 - 6.1.1 2.4-mm Material Thickness
 - 6.1.2 2.0-mm Material Thickness
 - 6.1.3 1.6-mm Material Thickness
- 6.2 High-Speed GMAW-P for Lap-Fillet Joints
- 6.3 High-Speed GMAW-P for T-Joints
- 6.4 High-Speed Video (HSV)
- 6.5 Results for Hybrid LBW/GMAW-P
 - 6.5.1 Welding Trials – GMAW with 1-kW Laser Power and PFO
 - 6.5.2 Hybrid GMAW-P/LBW using the Trumpf HAAS 4006 Nd:YAG Laser
 - 6.5.3 Hybrid GMAW-P/LBW with Rofin Sinar CO₂ Laser, Model RS-850
- 6.6 Results for Calorimetry
- 6.7 Humping Experiments

7.0 DISCUSSION

- 7.1 Weld Sizing
 - 7.1.1 Deposit Area
 - 7.1.2 Travel Angle
 - 7.1.3 Work Angle
 - 7.1.4 Travel Speed
 - 7.1.5 Arc Length
 - 7.1.6. Contact Tip to Work Distance
- 7.2. Energy Input and Arc Efficiency
- 7.3 Calorimetry
- 7.4 Conduction versus Convection
- 7.5 Wire composition and wetting
- 7.6 Effect of Shielding Gas
- 7.7 Spatter in GMAW-P
- 7.8 GMAW-VP and LBW/GMAW-VP
- 7.9 Hybrid Welding
 - 7.9.1 Comparison of Welding Speed for GMAW-P and LBW/GMAW-P Hybrid
 - 7.9.2 GMAW-P and LBW/GMAW-P Bead Humping – Lap Joints
 - 7.9.3 GMAW-P and LBW/GMAW-P Bead Humping – T-Butt Joints
 - 7.9.4. Laser Spot Size, Spacing and Power Density
 - 7.9.5. Hybrid GMAW-P/LBW with Trumpf HAAS 4006 Nd:YAG Laser
 - 7.9.6 Hybrid CO₂ Laser/GMAW-P Using the Rofin Sinar RS850
 - 7.9.7 Laser Power versus Arc Power
 - 7.9.8. Laser Power Distribution
- 7.10 Weld Bead Humping
 - 7.10.1 Periodicity of Weld Humping in GMAW-P
 - 7.10.2. Weld Pool Dynamics and Humping Mechanisms
- 7.11 High-Speed Video (HSV) Images
- 7.12 Impact of Results and Process Economics

8.0 CONCLUSIONS

9.0 RECOMMENDATIONS FOR FUTURE WORK

10.0 REFERENCES

ABSTRACT

Arc welding is the most widely used set of joining technologies in industry today. The automotive tier supplier network and light manufacturing are significant users of arc welding, particularly gas metal arc welding (GMAW) and pulsed GMAW (GMAW-P). For sheet metal welding the majority of welds are single pass fillet welds on T-butt, lap, or edge joints. A fundamental problem and limitation to the use of higher travel speeds in GMAW is the phenomenon of weld bead humping, a weld profile defect with a wavelike profile to the weld bead that has peaks and troughs in the longitudinal direction.

The initial hypothesis was that the humping defect can be suppressed and continuous beads deposited at much higher speeds by using a laser beam welding (LBW) in the conduction mode at the weld toes to improve bead wetting thus minimizing bead convexity which, at toe angles below 90 degrees, tends to promote the formation of the humping defect. This was investigated by a research program intended to develop an understanding of the cause of the humping defect, and included extensive use of high-speed video (HSV) to determine the root cause, from which the mechanisms were determined. The main elements of the research were as follows;

- GMAW-P parameters for welding with 0T and 1T gaps (T is sheet thickness)
- High-speed GMAW-P with 0T gap
- Hybrid LBW/GMAW-P using CO₂ and Nd:YAG lasers
- High SpeedVideo (HSV) of GMAW-P and bead humping

The hypothesis that weld pool humping can be suppressed to a travel speed (TS) well beyond that achievable with GMAW-P by directing a laser at the weld toes was demonstrated in the results achieved and their comparison to data generated for single wire GMAW-P. For the welding techniques investigated, the following maximum TS can be stated:

1. Conventional GMAW-P – typical maximum TS of 1 m/min
2. High-speed GMAW-P – typical maximum TS of 2 m/min
3. Hybrid conduction mode laser with GMAW-P – typical maximum TS of 3.3 m/min

The main conclusions are as follows:

1. Laser assisted GMAW-P allows increases in TS before humping. The hypothesis that weld bead humping can be suppressed by using laser melting at the GMAW-P weld toes was shown by experiment to be valid.
2. HSV of GMAW-P showed a repetitive arc instability that caused the weld pool to move first forward and then backward at the moment of the instability. It also showed arc shorting leading to the end of one hump and the beginning of the next.

3. A 30-degree lead travel angle for the GMAW welding torch achieved a maximum welding speed in GMAW-P and LBW/GMAW-P welding and was beneficial in suppressing humping.
4. A work angle of 60 degrees, wire on the top edge of the top sheet, and aiming the laser at the bottom toe of the GMAW-P weld is the best configuration.
5. Aiming the wire at the top edge of the top sheet delayed the onset of bead humping to higher TS than aiming at the root.
6. Long weld pools (12:1) and no humping were achieved with a single 4 kW laser spot. Only one beam spot is required – aimed at the lower weld toe - to result in wetting.

The major benefit of this work is the increased understanding of high-speed welding and the potential to significantly increase welding productivity.

ACKNOWLEDGEMENTS

My particular thanks to my Supervisor at Cranfield University Mr. David Yapp, for interesting discussion, input, direction, and encouragement during this course of research study.

Thanks are due to the noted technical staff and colleagues at Edison Welding Institute (EWI) who have contributed in many ways. I particularly wish to thank Mr. Michael Fallara, Mr. Brian Baughman, Mr. Matt Boring, and Ms. Joyce Hinkle of EWI for their help. I would also like to thank Professor David Farson, and Mr. HaeWoon Choi, Mr. Min Cho, and Mr. Yong Lim of The Ohio State University for their part in interesting discussion and conduction of some of the experimental work under EWI Project No. 47412GTO.

I would like to thank EWI for allowing me the opportunity to pursue this course of study, for their financial support in terms of tuition reimbursement, and for providing the extensive laboratory facilities required during a portion of the experimental program.

I would also like to thank the many member companies of EWI and the Ohio Department of Development for their mutual funding of the EWI Cooperative Research Program (CRP) which enabled the research to be conducted.

Most importantly, I wish to thank my wonderful wife Jean, and my beautiful children Avery, Paige, and Brandon for their love and support in this, as in many other endeavors. Were it not for their forbearance and understanding of my time away from the family to complete the process, it could not have been accomplished.

LIST OF TABLES

Table 2.1.	Lasers and Optics Used for Welding
Table 6.1.	Measurement of Fillet Weld Leg Lengths, Area, and Toe Angle Against Lower Sheet
Table 6.2.	Nd:YAG Trials with PFO
Table 6.3.	4-kW Nd:YAG/GMAW Hybrid Trials With Split Optics – Lap Joints
Table 6.4.	Parameters for CO ₂ Laser/GMAW-P Hybrid BOP, Lap and T-Butt Joints
Table 6.5.	Weld Leg Length, Weld Area and Weld Toe Angles
Table 6.6.	Results for GMAW-P Calorimetry and Plot of Results
Table 6.7.	Weld Type and Welding Parameters for HSV Trials
Table 6.8.	Results for Hybrid LBW/GMAW-P Calorimetry and Plot of Results
Table 7.1.	Calculated Weld Deposit Areas for all Three Material Thicknesses Using Preferred WFS and TS
Table 7.2.	Weld Deposit Area Measurements Made with ImagePro™ Software of All Three Material Thicknesses Welded Using Preferred WFS and TS
Table 7.3.	Causes and Remedies of Undercut
Table 7.4.	Methods of Reducing Various Welding Process Defects in GMAW Including the Humping Defect
Table 7.5.	Oxidation Potential of Various Metals and Oxides and their Stability (AWS, 2004)

LIST OF FIGURES

- Figure 2.1 Gas Metal Arc Welding Process
- Figure 2.2 Features of GMA-Brazing
- Figure 2.3 Nominal Comparison of Penetration and Wire Melting Rate for GMAW-DCEP and GMAW-DCEN
- Figure 2.4 Miller Jetline CSC Gun Showing Dual-Wire Drive Motors
- Figure 2.5 Fronius CMT Gun with Integrated Dual-Wire Feed Motors
- Figure 2.6 Twin-Wire and Tandem GMAW
- Figure 2.7 Tandem GMAW Torch with Dual Contact Tips
- Figure 2.8 Typical Arrangement of a Tandem GMAW Welding Torch Head
- Figure 2.9 Schematic of LBW/GMAW Operation
- Figure 2.10 Plasma Welding Torch With Cold Wire Feed
- Figure 2.11 Fronius Hybrid LBW/GMAW Welding Head for Robotic Applications
- Figure 2.12 Schematic of LBW/GMAW Operation and Features of Hybrid Welding
- Figure 2.13 Twin-Spot (Dual-Beam) Optics for Nd:YAG Lasers (Goebels et al., 2003)
- Figure 2.14 Representation of the Forces on an Electrode Drop in GMAW (Norrish and Richardson, 1988)
- Figure 2.15 Changes in the Forces on an Electrode Drop as the Welding Current Increases (Pintard, 1966)
- Figure 2.16 Laser Spot Diameter versus Laser Power Required for Stabilization
- Figure 2.17 Laser Melting Efficiency in Mild Steel (Ream, 2004)
- Figure 2.18 Classic Continuous Bead Humping in GMAW BOP (top)
- Figure 2.19 Weld Appearance for Classic Discontinuous Bead Humping in GMAW
- Figure 2.20 Weld Pool Fluid Flow as Observed and Proposed by Bradstreet for High-Speed GMAW

- Figure 2.21 Contact Line Behaviour – (Schiaffino and Sonin, 1997 [2])
- Figure 2.22 Rearward Weld Metal Fluid Flow Including the Effect of Arc Pressure and Wire Droplet Addition (Kim and Na, 1995)
- Figure 2.23 Flow 3-D Simulation of GMAW-P Droplet Crossing the Arc to the Weld Pool (Cho and Farson, 2007)
- Figure 2.24 BOP Bead Humping Simulation at 2.5 m/min TS and 25 m/min WFS (Cho and Farson, 2007)
- Figure 2.25 Hybrid Welding Process Concept for GMA Spot Welding
- Figure 2.26 Arc Melting Efficiency (DuPont and Marder, 1995).
- Figure 2.27 The Principle of Self-Fixturing of the Weld Components
- Figure 2.28 Tab-and-slot Assembly Procedure (Caterpillar)
- Figure 4.1 Standard Fixture for Lap-Fillet Joints
- Figure 4.2. Welding Power Supply and Wire Feeder (left), Data Acquisition System (Right) used for Gap Weldability Testing
- Figure 4.3. Assembled Variable Joint Gap Weldability Fixture
- Figure 4.4 Side View of Joint Setup to Determine Critical Support Location
- Figure 4.5 Gap Geometry for DOE Trials
- Figure 4.6 Equipment Setup for High-Speed GMAW-P Welding Trials to Establish Humping Limits
- Figure 4.7 Principle for Rapid Beam Manipulation in the PFO Scanner
- Figure 4.8 The Trumpf Programmable Focusing Optics Device
- Figure 4.9 CNC Nd:YAG/GMAW-P Setup for PFO Evaluation, Including HSV, DAQ, and LASEdit Laser Programmer/Controller
- Figure 4.10 Rofin Sinar 850 CO₂ Laser Was Used for Single- and Dual-Beam LBW/GMAW-P Hybrid Welding
- Figure 4.11 Waveguide for Beam Delivery to the GMF Robot
- Figure 4.12 Single-Spot Laser Mirror System for Robotic CO₂ Laser Welding
- Figure 4.13 Rear Face of Split (wire EDM) Copper Mirror for Dual-Spot Experiments with a CO₂ Laser

- Figure 4.14 GMF Robotics Karel L-100 Robot Controller
- Figure 4.15 Laser Spot Alignment Using Low Power Visible Red He-Ne Laser
- Figure 4.16 Console for Laser Parameter Selection
- Figure 4.17 Trumpf Haas HL 4006 4-kW Continuous-Wave Nd:YAG
- Figure 4.18 Motoman SK16 Robot with Fibre-Delivered Nd:YAG Laser and ESAB GMAW-P Equipment Setup on a Lap Joint
- Figure 4.19 GMAW-P Waveform from Arc Impact DAQ at 10-kHz Sampling Frequency
- Figure 4.20 Kodak Ektapro HS HSV Camera Setup for Viewing the Weld Pool Perpendicular to the Welding Direction
- Figure 4.21 Cover Lens and IR Band-Pass Filter Attached to the Camera Lens
- Figure 4.22 Digital Download Interface for Triggering and Capturing HSV Data
- Figure 4.23 Typical Screen Image and Frame Data Using the Kodak Ektapro HS System
- Figure 4.24 Phantom HSV Camera With Filter Mount Between the Camera and Lens Assembly
- Figure 4.25 Primes™ Beam Power Analysis System Setup to Measure Distributed Power in Dual-Beam Nd:YAG Laser
- Figure 4.26 WISC Laser Profilometer
- Figure 4.27 Equipment Used for Calorimetry Experiments
- Figure 5.1 Gap Geometry for DOE Trials
- Figure 5.2. Sample of Completeness of Fusion Rating used by Richardson
- Figure 5.3. Illustration of a “Skip”, or Incomplete Fusion, Encountered During Welding Denoting the End of the Acceptable Weld
- Figure 5.4 Typical Bead Humping Defect in a Lap-Fillet Weld
- Figure 5.5 100-W Dual-Beam Nd:YAG Laser Burn Pattern on Thermographic Paper to Illustrate TEM 01 Laser Mode
- Figure 5.6 Fibre-Delivered Nd:YAG Laser and ESAB GMAW-P Equipment Setup on a Lap Joint for Single- and Dual-Spot Welding Trials

- Figure 5.7 100-W Dual Beam Nd:YAG Laser Burn Pattern on Thermographic Paper to Illustrate TEM 01 Laser Mode
- Figure 5.8 Fibre-Delivered Nd:YAG Laser and ESAB GMAW-P Equipment Setup on a Lap Joint for Single- and Dual-Spot Welding Trials
- Figure 5.9 CO₂ Laser Burn Pattern on Perspex for Dual Beam in TEM 01 Mode
- Figure 5.10 Control Block Diagram of the Calorimetry Experiments
- Figure 5.11 Calibration Image for HSV Using a Millimeter Scale
- Figure 6.1. WFS versus Voltage Relationship for Maintaining a Constant 3.2-mm Arc Length Using GMAW-P with a 19-mm CTWD and a 1.2-mm-Diameter ER70S-3 Electrode
- Figure 6.2 SWAT Results Showing the Visually Acceptable Weld Area Curve for 2.4-mm Mild Steel with a 0T Joint Gap
- Figure 6.3. SWAT Results Showing the Destructively Tested Acceptable Weld Area Curve for 2.4-mm Mild Steel with a 0T Joint Gap
- Figure 6.4. Macrosection Map for 2.4-mm Lap Joints with a 0T Joint Gap
- Figure 6.5. SWAT Results Showing the Acceptable Weld Area Curve for 2.4-mm Mild Steel with a 1T Joint Gap.
- Figure 6.6. Macrosection Map for 2.4-mm Lap Joints with a 1T Joint Gap
- Figure 6.7. SWAT Results Showing Acceptable Weld Area Curve for 2.0-mm Mild Steel Lap joints with a 0T Joint Gap
- Figure 6.8. Macrosection Map for 2.0-mm Sheet Lap Joints with 0T gap
- Figure 6.9. SWAT Results Showing Acceptable Weld Area Curve for 2.0-mm Mild Steel Lap Joints with a 1T Joint Gap
- Figure 6.10. Macrosection Map for 2.0-mm Lap Joints with a 1T Joint Gap
- Figure 6.11. SWAT Results Showing Acceptable Weld Area Curve for 1.6-mm Mild Steel Lap joints with a 0T Joint Gap
- Figure 6.12. Macrosection Map for 1.6-mm Lap Joints with a 0T Joint Gap made using a 1.2-mm-Diameter ER70S-3 Electrode Wire
- Figure 6.13. SWAT Results Showing Acceptable Weld Area Curve for 1.6-mm Mild Steel Lap Joints With a 1T Joint Gap
- Figure 6.14. Macrosection Map for 1.6-mm Lap Joint with a 1T Joint Gap Made Using a 1.2-mm-Diameter ER70-S3 Electrode Wire

- Figure 6.15. Developed Weld Area for the 2.4-mm Mild Steel Sheet Applied to a 0T Joint Gap (left) and 1T Joint Gap (Right)
- Figure 6.16. Developed Weld Area for the 2.0-mm Mild Steel Sheet Applied to a 0T Joint Gap (left) and 1T Joint Gap (Right)
- Figure 6.17. Developed Weld Area for the 1.6-mm Mild Steel Sheet Applied to a 0T Joint Gap (Left) and 1T Joint Gap (Right)
- Figure 6.18. Macrosections of Fillet Welds on T-Butt Joints for the Three Material Thicknesses Studied.
- Figure 6.19. Continuous Humping Defect Generated at a 1T Gap on a Joint at a 'High' Travel Speed of 1.0 m/min.
- Figure 6.20. 2.4-mm Sheet, WFS 12.7 m/min, TS 1.0 m/min, 1T Gap
- Figure 6.21. Further Examples of Humped Bead Profiles for 2.4- and 2.0-mm Sheet
- Figure 6.22. Bead Humping Limit for High-Speed GMAW-P versus 'Conventional' GMAW-P
- Figure 6.23. Bead Humping Limit for High-Speed GMAW-P versus 'Conventional' GMAW-P
- Figure 6.24. Bead Humping Limit for High-Speed GMAW-P versus 'Conventional' GMAW-P for Lap-Fillet Joints in 1.6-mm Sheet
- Figure 6.25. Weld Appearance Map for 2.4-mm Sheet Lap-Fillet Joints with 0T Gap
- Figure 6.26. Bead Humping Limit and Acceptable Weld Area for High-Speed GMAW-P versus 'Conventional' GMAW-P for 2.4-mm Sheet
- Figure 6.27. Weld Appearance Map for 2.0-mm Sheet Lap-Fillet Joints with 0T Gap
- Figure 6.28. Bead Humping Limit and Acceptable Weld Area for High-Speed GMAW-P versus 'Conventional' GMAW-P
- Figure 6.29. Weld Appearance Map for 1.6-mm Sheet Lap-Fillet Joints with 0T Gap
- Figure 6.30. Bead Humping Limit and Acceptable Weld Area for High-Speed GMAW-P versus 'Conventional' GMAW-P
- Figure 6.31. Macrosections Through Bead Humps at the Limits of Travel Speed for Each Material Thickness

- Figure 6.32. Weld Appearance Map for Fillet Welds on T-Butt Joints Using 2.4-mm Sheet
- Figure 6.33. Weld Appearance Map for Fillet Welds on T-Butt Joints Using 2.0-mm Sheet
- Figure 6.34. Weld Appearance Map for Fillet Welds on T-Butt Joints Using 1.6-mm Sheet
- Figure 6.35. HSV Images (GMAWP186- GMAWP214) for GMAW-P
- Figure 6.36. Initial PFO Trials With 1-kW Nd:YAG Laser
- Figure 6.37. Spot and Scanned Nd:YAG Laser Profiles in BOP Form
- Figure 6.38. HSV of GMAW-P Metal Transfer and 1-kW PFO Laser Spot
- Figure 6.39. Nd:YAG Spot and Corresponding LBW/GMAW-P BOP Weld
- Figure 6.40. 2-mm Scanned Nd:YAG and Corresponding LBW/GMAW-P BOP
- Figure 6.41. 4-mm Scanned Nd:YAG and Corresponding LBW/GMAW-P BOP Weld
- Figure 6.42. Classic Bead Humping Suppressed with 1-kW Nd:YAG Laser Energy (WFS/TS of 5 - BOP weld) at 2.0-m/min Travel Speed
- Figure 6.43. Profile for 4-kW Nd:YAG Laser with a Single Beam at Focus with 200-mm Optics
- Figure 6.44. Beam Profile for 4-kW Nd:YAG Laser with Dual-Beam Using 200-mm Focusing Optics (Profile of One Beam is Shown)
- Figure 6.45. 100-W Dual-Beam Nd:YAG Laser Burn Pattern on Thermographic Paper to Illustrate TEM 01 Laser Mode
- Figure 6.46. Single-Beam Laser Offset to GMAW Weld Toe to Increase Toe Wetting Using an Nd:YAG Laser
- Figure 6.47. GMAW-P Fillet Weld on a Lap Joint
- Figure 6.48. Hybrid Nd:YAG/GMAW Fillet Weld on a Lap Joint
- Figure 6.49. 42-mm-Long Weld Pool with 3-mm Bead Width (14:1) Using Single-Spot 4-kW Nd:YAG/GMAW-P Hybrid Welding on a Lap Joint
- Figure 6.50. Bead Appearance for Dual-Spot Nd:YAG Hybrid Weld made at 3.3 m/min on a Lap-Fillet Joint on 2.4-mm Sheet

- Figure 6.51. Macrosection for Dual-Spot Nd:YAG Hybrid Weld Made at 3.3 m/min on 2.4-mm Sheet
- Figure 6.52. Macrosection for Dual-Spot Nd:YAG Hybrid Weld Made at 4.0 m/min on 2.4-mm Sheet
- Figure 6.53. Profile of 6-kW CO₂ Laser Beam at Focus with 254-mm Optics
- Figure 6.54. CO₂ Laser Burn Pattern on Perspex for Dual Beam in TEM 01 Mode Using 3.2, 6.4 and 9.5-mm Dual Spot Spacing
- Figure 6.55. Weld Appearance Map for Hybrid CO₂ LBW/GMAW-P BOP Welds on 2.4-mm Sheet
- Figure 6.56. BOP Weld Made Using Single-Spot Laser at 3.3-kW and 2.5-m/min Travel Speed on 2.4-mm Sheet
- Figure 6.57. BOP Weld Made Using Single Spot Laser at 3.3-kW and 3.0-m/min Travel Speed on 2.4-mm Sheet
- Figure 6.58. Weld Appearance Map for Hybrid CO₂ LBW/GMAW-P Lap-Fillet Welds on 2.4- and 2.0-mm Steel Sheet
- Figure 6.59. Bead Appearance for a Lap-Fillet Joint made using Single-Spot CO₂ LBW/GMAW-P Hybrid Welding With 3.25-kW Laser Power at 4-m/min Travel Speed on 2-mm Sheet
- Figure 6.60. Macrosection for Single-Spot CO₂ LBW/GMAW-P Hybrid Weld Made at 4 m/min on 2-mm Sheet
- Figure 6.61. Weld Appearance Map for Fillet Welds on 2.4-mm Steel Sheet Using CO₂ LBW/GMAW-P Hybrid Welding
- Figure 6.62. Bead Appearance for a T-Butt Joint Made Using Single-Spot CO₂ LBW/GMAW-P Hybrid Welding at 3 m/min on 2-mm Sheet
- Figure 6.63. Macrosection (on Left – Tack on Right) for a Single-Spot CO₂ LBW/GMAW-P Hybrid Weld Made With 3.5-kW Laser Power at 3.0 m/min on 2-mm Sheet
- Figure 6.64. Macrosection for a Dual-Spot CO₂ LBW/GMAW-P Hybrid Weld Made at 1.75 m/min on 2-mm Sheet
- Figure 6.65. Plan View of GMAW-P Weld Pool Cavity for Specimen 72805a WFS 15.2 m/min, TS 2.5 m/min, 225 A, 37 V, 19-mm CTWD
- Figure 6.66. Side View of GMAW-P BOP Humping for Specimen 72805a WFS 15.2 m/min, TS 2.5 m/min, 225 A, 37 V, 19-mm CTWD

- Figure 6.67. Plan View of GMAW-P BOP Humping for Specimen 72805a WFS 15.2 m/min, TS 2.5 m/min, 225 A, 37 V, 19-mm CTWD
- Figure 6.68. HSV Sequence of Bead Humping and Solidification
- Figure 6.69. Plan View of GMAW-P BOP Humping for Specimen 72805 WFS 15.2 m/min, TS 2.5 m/min, 225 A, 28 V, 19-mm CTWD
- Figure 6.70. Side View of GMAW-P BOP Humping for Specimen 72805 WFS 15.2 m/min, TS 2.5 m/min, 225 A, 37 V, 19-mm CTWD
- Figure 6.71. HSV Sequence for GMAW-P Bead Humping
- Figure 6.72. Plan View of GMAW-P BOP Humping and Weld Pool Cavity for Specimen 72805c WFS 15.2 m/min, TS 2.5 m/min, 225 A, 31 V, 19-mm CTWD
- Figure 6.73. Side View of GMAW-P BOP Humping and Weld Pool Cavity for Specimen 72805c WFS 15.2 m/min, TS 2.5 m/min, 225 A, 31 V, 19-mm CTWD
- Figure 6.74. HSV Sequence for GMAW-P Weld 72805c
- Figure 6.75. Plan View of GMAW-P BOP Humping and Weld Pool Cavity for Specimen 72905a WFS 15.2 m/min, TS 2.5 m/min, 225 A, 33 V, 16-mm CTWD
- Figure 6.76. Side View of GMAW-P BOP Humping for Specimen 72905a WFS 15.2 m/min, TS 2.5 m/min, 225 A, 33 V, 16-mm CTWD
- Figure 6.77. Plan View of GMAW-P BOP Humping and Weld Pool Cavity for Specimen 72905-3 WFS 15.2 m/min, TS 2.5 m/min, 225 A, 35 V, 16-mm CTWD
- Figure 6.78. Side View of GMAW-P BOP Humping and Weld Pool Cavity for Specimen 72905-3 WFS 15.2 m/min, TS 2.5 m/min, 225 A, 35 V, 16-mm CTWD
- Figure 6.79. Plan View of GMAW-P BOP Humping (Upper Bead) and Weld Pool Cavity for Specimen 80205a WFS 15.2 m/min, TS 2.5 m/min, 225 A, 34 V, 19-mm CTWD
- Figure 6.80. Side View GMAW-P BOP Humping and Weld Pool Cavity for Specimen 80205a WFS 15.2 m/min, TS 2.5 m/min, 225 A, 34 V, 19-mm CTWD
- Figure 6.81. Plan View of GMAW-P BOP Humping and Weld Pool Cavity for Specimen 80205b WFS 15.2 m/min, TS 2.5 m/min, 225 A, 34 V, 19-mm CTWD WFS 15.2 m/min, TS 2.5 m/min, 225 A, 34 V, 19-mm CTWD

- Figure 6.82. Side View of GMAW-P BOP Humping and Weld pool Cavity for Specimen 80205b WFS 15.2 m/min, TS 2.5 m/min, 225 A, 34 V, 19-mm CTWD
- Figure 6.83. Side View GMAW-P BOP Humping for Specimen 80205b WFS 15.2 m/min, TS 2.5 m/min, 225 A, 34 V, 19-mm CTWD
- Figure 6.84. Plan View of GMAW-P Fillet Weld Humping in a Lap Joint for Specimen 80305a WFS 15.2 m/min, TS 3.0.5 m/min, 225 A, 34 V, 16-mm CTWD
- Figure 6.85. Side View of GMAW-P Fillet Weld Humping in a Lap Joint for Specimen 80305a WFS 15.2 m/min, TS 3.0 m/min, 225 A, 34 V, 16-mm CTWD
- Figure 6.86. Plan View of LBW/GMAW-P Fillet Weld Humping in a Lap Joint for Specimen 80305b with Wire Offset too Much onto the Top Sheet WFS 15.2 m/min, TS 3.0 m/min, 225 A, 34 V, 16-mm CTWD
- Figure 6.87. Side View of LBW/GMAW-P Fillet Weld Humping in a Lap Joint for Specimen 80305b with Wire Offset too Much onto the Top Sheet WFS 15.2 m/min, TS 3.0 m/min, 225 A, 34 V, 16-mm CTWD
- Figure 6.88. HSV Stills of a Lap Fillet Weld Viewed ‘Head-On’
- Figure 6.89. Plan View of GMAW-P BOP Humping for Specimen 82405-5 WFS 15.2 m/min, TS 3.0 m/min, 225 A, 34 V, 16-mm CTWD
- Figure 6.90. Side View of GMAW-P BOP Humping for Specimen 82405-5 WFS 15.2 m/min, TS 3.0 m/min, 225 A, 34 V, 16-mm CTWD
- Figure 6.91. HSV Showing Short Circuiting of the Wire to the Weld Pool in BOP Specimen 082405-4 at the Point when a New Hump is Created
- Figure 6.92. HSV Still Sequence Showing Expulsion and Weld Pool Motion
- Figure 6.93. HSV Still Sequence Showing Expulsion and Weld Pool Motion
- Figure 6.94. HSV Still Sequence Showing Expulsion and Weld Pool Motion
- Figure 6.95. Plan View of GMAW-P BOP Humping for Specimen 82405-8 WFS 15.2 m/min, TS 3.0 m/min, 225 A, 34 V, 16-mm CTWD
- Figure 6.96. Side View of GMAW-P BOP Humping for Specimen 82405-8 WFS 15.2 m/min, TS 3.0 m/min, 225 A, 34 V, 16-mm CTWD
- Figure 6.97. HSV Images Showing Weld Pool Motion through Movement of the ‘White’ Silicate Slag Islands

- Figure 6.98. Three Images in Sequence (082405-8 HSV File) Showing Weld Pool Motion First Forward then Backward
- Figure 6.99. Two Images Five Frames Apart (082405-8 HSV File) Showing Repetition of Weld Pool Forward Motion Every Ten Frames
- Figure 6.100. Plan View of GMAW-P Fillet Weld Humping in a Lap Joint, Specimen 83005-1
- Figure 6.101 HSV Showing Short Circuiting of the Wire to the Weld Pool and Arc Re-ignition in Lap Fillet Specimen 083005-b
- Figure 6.102. Plan View of GMAW-P Fillet Weld Humping in a Lap Joint, Specimen 83005-2
- Figure 7.1. Electrode Locating Error
- Figure 7.2 Plan View of GMAW-P Fillet Weld Discontinuous Humping in a Lap Joint, Specimen 83005-2 Resulting from Wire Mislocation onto the Top Sheet
- Figure 7.3. CTWD Changes
- Figure 7.4. 40-mm-Long Weld Pool with 3-mm Bead Width (14:1) using Single-Spot 4-kW Nd:YAG/GMAW Hybrid on a Lap Joint
- Figure 7.5. Wetting of the Weld Toe Using a Single Laser Spot (Seen at Left of Righthand Weld Bead)
- Figure 7.6 Onset of Bead Humping for Lap Joints Made Using GMAW-P
- Figure 7.7 WFS/TS Versus TS Showing That Smaller Welds Can be Made at Higher TS
- Figure 7.8 Trends for Weld Size Ratio (WFS/TS) versus TS for Lap Joints Made with Conventional GMAW-P, High-Speed GMAW-P, and LBW/GMAW-P
- Figure 7.9 Trends for Weld Size Ratio versus TS for Conventional GMAW-P, High-Speed GMAW-P, and LBW/GMAW-P Hybrid Welding in T-Butt Joints
- Figure 7.10 Plan View - Arrangement of Laser beam Spots (Round) Relative to the Arc Weld Pool (Ellipse) to Achieve Maximum Weld Toe Wetting and Spreading
- Figure 7.11 Cross-Sectional view - Arrangement of Laser beam Spots (Small Ellipses) Relative to the Arc Weld Pool (Larger Ellipse) at Left, to Achieve Maximum Weld Toe Wetting and Spreading, at Right

- Figure 7.12 Plan View - Size and Arrangement of Laser beam Spots (Round) Relative to the Arc Weld Pool (Ellipse) Resulting in Minimum Weld Toe Wetting and Spreading
- Figure 7.13 Cross-Sectional View - Size and Arrangement of Laser beam Spots (Small Elliptical Spot) Relative to the Arc Weld Pool (Ellipse) at Left, Resulting in Minimum Weld Toe Wetting and Spreading at Right
- Figure 7.14 Plan View - Arrangement of Laser Beam Spots (Round) Relative to the Arc Weld Pool (Ellipse) Resulting in Insufficient Melting by the Laser and Thus No GMAW-P Toe Wetting and Spreading
- Figure 7.15 Cross-Sectional View - Arrangement of Laser beam Spots (Small Ellipses) Relative to the Arc Weld Pool (Ellipse) at Left, Resulting in Insufficient Melting by the Laser and Thus No GMAW-P Toe Wetting and Spreading, at Right
- Figure 7.16 36-mm-Long Weld Pool with 3-mm Bead Width (12:1) Using Single-Spot 4-kW Nd:YAG/GMAW-P Hybrid on a Lap Joint
- Figure 7.17 Side View of GMAW-P BOP Humping for 2.4-mm Sheet Specimen 72805
- Figure 7.18 Side View of GMAW-P BOP Humping in 1.6-mm Sheet Metal for Specimen 80205b
- Figure 7.19 Repetitive Forward and Backward Motion of the GMAW-P Weld Pool Within 2 frames (Images 309, 31, and 310) at 250 fps
- Figure 7.20 HSV Still Sequence Showing Weld Wire Expulsion and Weld Pool Motion
- Figure 7.21 HSV Still Showing Weld Wire Expulsion and Weld Pool Motion
- Figure 7.22 HSV Still Showing Weld Wire Expulsion and Weld Pool Motion
- Figure 7.23 HSV Showing Short Circuiting of the Wire to the Weld Pool in BOP Specimen 082405-4
- Figure 7.24 HSV Showing Short Circuiting of the Wire to the Weld Pool and ArcRe-Ignition in Lap Fillet Specimen 083005-1
- Figure 7.25 Classic Bead Humping (Top Bead) for GMAW-P Suppressed with 1-kW Nd:YAG Laser Energy (Middle and Bottom) (WFS/TS of 5 - BOP Weld) at 2.0-m/min TS
- Figure 7.26 Distribution of Welding Consumable Use by Industry (Pekkari, 2004)
- Figure 7.27 Energy Usage and Efficiency for an Array of Commonly Used Welding Processes (Pekkari, 2004)
- Figure 7.28 Laser Operating Cost Summary (Ream, 2004)

Figure 9.1 Extrapolation of TS and WFS for Higher Productivity Using Hybrid
LBW/TGMAW-P

NOMENCLATURE

fps	feet per second
kg/h	kilograms per hour
kJ/mm	kilojoules per millimeter
l/min	litres per minute
m/min	metres per minute
mm/min	millimetres per minute
mm ³ /kJ	millimeters cubed/kilojoules
ppm	parts per million
Mtonnes	Millions of tonnes
W/m ²	Watts per square metre
W/mm ²	Watts per square millimetre

ABBREVIATIONS

A	Amperes (welding current)
AC	Alternating current
AHSS	Advanced high-strength steels
AIP	Average instantaneous power
ANOVA	Analysis of variance
AWS	American Welding Society
BIW	Body in white
BOP	Bead on plate
CMT	Cold metal transfer
CRP	Cooperative Research Program
CAD	Computer-aided design
CAM	Computer-aided manufacturing
CMOS	Complementary metal oxide semiconductor
CNC	Computer numerical control
CSC	Controlled short circuit
CTWD	Contact tip to work distance
CV	Constant voltage
DAQ	Data acquisition
DCEN	Direct current electrode negative
DOE	Design of experiments
DC	Direct current
DCEP	Direct current electrode positive
EDM	Electro discharge machining
EP/EN	Electrode positive/electrode negative
EWI	Edison Welding Institute
FEM	Finite-element modeling
FGD	Flue gas desulphurization
GMAW	Gas metal arc welding
GMAW-VP	Variable-polarity GMAW
GMAW-P	Pulsed-current GMAW
GMAW-SC	Short-circuit GMAW
GMAW-MP	Mechanically pulsed GMAW
GTAW	Gas tungsten arc welding
HSV	High-speed video

HLAW	Hybrid laser arc welding
IR	Infrared
KB-DOE	Knowledge-based design of experiments
LAAW	Laser-assisted arc welding
LANL	Lawrence Livermore National Lab
LED	Light emitting diode
LBW	Laser beam welding
Nd:YAG	Neodymium-doped yttrium aluminum garnet
NG	Narrow groove
ODOD	Ohio Department of Development
OSU	The Ohio State University
PC	Personal computer
PAW	Plasma arc welding
PFO	Programmable focusing optics
PMCS	Power measurement calorimetric system
PSNS	Puget Sound Naval Shipyard
ROI	Return on investment
RSW	Resistance spot welding
RSM	Response surface methodology
RMS	Root mean square
RE-GMAW	Rotating electrode GMAW
RLT-GMAW	Rotating lead tandem GMAW
SC	Short circuit
SEC	Seebeck envelope calorimeter
STT	Surface tension transfer
SWAT	Sloping weld area testing
SUV	Sport utility vehicle
TS	Travel speed
TGMAW	Tandem GMAW
TIME	Transferred Ionized Molten Energy
TTA	Through the arc
VOF	Volume of fluid
V	Volts (arc voltage)
W	Watts
WFS	Wire feed speed

1.0 INTRODUCTION

Arc welding represents the most widely applied set of joining process, and within this suite of processes gas metal arc welding (GMAW) is the most widely used, accounting for 74% of the Western European consumables market, 59% of the market in the USA, and 55% in Japan, in 2002 (Pekkari, 2005). The reason for this is that the process combines the elements of low capital and running cost, simplicity and flexibility in application and can be used to weld a wide range of metals and alloys. The GMAW process can be used by hand (semi-automatic, rather than manual since the wire feed is mechanized), with simple linear or hard automation, or most flexible of all, in conjunction with modern six-axis robots within flexible automation work cells. The latter is of most interest, especially in today's increasingly globally competitive marketplace since it provides the lowest labor cost and highest productivity.

While the use of Al alloys and other metals is increasing, by far the most widely used metal is steel, in a wide array of strengths and thicknesses. In 2003 about 26.4 Mtonnes of Al were produced compared to 855.0 Mtonnes of steel (Pekkari, 2004). To counter the higher use of Al in the automotive industry, the steel industry has introduced advanced high-strength steels (AHSS) in the body and other parts of the structure. In the automotive, shipbuilding, and other industries the use of steel is very high and the trend is increasingly to thinner and higher strength grades. This is reflected in the welding market, wherein the automotive, automotive supplier and general (light) industry account for 60% of the market. Sheet steels and thin plate represent the majority of material consumed and this trend results in the fact that most welds, even in a heavy construction area like shipbuilding are made with a single weld pass. Thus, high productivity welding of joints that can be completed in a single pass is the most prevalent and any process that can increase the productivity of joint completion is of great interest.

While there are several joint types, they can be reduced to only a few basic types, about 80% being fillet welds in either T-butt joints, or lap joints. The other major type is groove welds in butt joints, and makes up the majority of the other 20%. Therefore, it is clear that higher productivity of fillet welding will have the highest impact on overall productivity for single-pass welds.

A fundamental problem and limitation to the use of higher travel speeds in GMAW is the phenomenon of weld bead humping, a weld profile defect with a wavelike profile to the weld bead that has peaks and troughs in the longitudinal direction. In current practice the best way to avoid this is simply to limit the travel speed to one below the threshold for humping. These problems are exacerbated by thinner sheet often associated with the increased use of AHSS.

1.1 Background

The main drivers for increased welding productivity are economic and are associated with the need to reduce weight in the vehicle for increased performance and/or fuel economy. A substantial part of the weight reduction is achieved by increased use of thinner gauge AHSS.

- Weight Reduction - Higher performance, improved economy, and increasing optional equipment create continued pressure on structural and body components. Thinner, higher strength steels, Al, Mg, and plastics are all being introduced and/or substituted to achieve weight targets. Even the larger sport utility vehicle (SUV) and truck categories face this challenge.
- Welding Solutions for AHSS - The biggest change in automotive materials since the broad application of galvanized steel is the introduction of AHSS, which contain sufficient carbon to produce less ductile weld regions (among other challenging issues). In order to achieve acceptable fatigue and impact strengths with these new steels, advances in resistance spot welding (RSW), GMAW, and laser beam welding (LBW) will be required.

High-speed welding of thin sheet, new products, cost pressures, and quality concerns are all driving demand for higher welding speeds on thinner metal components. Higher speed welding processes, such as laser, laser-hybrid, pulsed GMAW (GMAW-P), and plasma arc welding (PAW) are receiving greater attention. Automotive and light manufacturing challenges almost always involve repetitive, automated, welding processes that demand precision motion and accurate control.

In addition to productivity, cost goes hand in hand, and should be considered in terms of capital cost, running cost, and return on investment (ROI). Many capital investments choices are made on the basis of ROI, and the acceptable period for ROI varies from several months to a year in many cases.

The factors relating to the subject matter at hand can be summarized as follows:

- Almost all welds are single pass
- Acceptable quality and productivity are the key items
- Weld sizing is not well defined, especially for welding of sheet metal. Weld sizing refers to the preferred weld cross-sectional area and/or fillet leg length.
- Most data is based on single torch GMAW in either short-circuit (SC) mode or using GMAW with direct current (DC) or GMAW-P
- Use of computer-aided design (CAD) and computer-aided manufacturing (CAM) and computer numerical control (CNC) bending to increase part accuracy and reduce fit-up problems
- Use of CNC laser cutting and CNC punch presses to produce accurate parts and make part changes to improve fit-up
- Welding is expected to cope with the tolerances – and with tolerance stack-up that may lead to significant gaps
- In contrast to the point above, a target of zero gap can be aimed for with accurate forming and fixturing and increased use of CAD/CAM – this will help maximize welding productivity, and minimize production costs
- Sheet metal fabrication is very important in the automotive and light manufacturing industries
- High-strength steels and down-gauging to thinner, lighter weight material – issue of Al versus steel performance and cost
- Cost and performance issues for fabrication of thinner gauge, lighter weight vehicles, and structures of many kinds, even in the shipbuilding arena

In a scenario of continuous improvement and cost reduction, welding productivity increases through robotics and automation have and will continue to be achieved. The development of newer welding techniques and processes is often aimed at higher productivity through the use of higher welding speeds and thus deposition rates. A big impediment to welding productivity is the tendency to over-weld small fillet welds in thin plate and sheet products. Over-welding results in higher welding costs, including additional welding power, electrode wire, higher distortion (and distortion correction costs), and lost productivity.

Prior operations in the fabrication sequence, such as cutting and forming, typically lead to gaps in weld joints. Flexible and fairly gap tolerant welding processes such as GMAW have traditionally been expected to cope with these gaps in the welding operation. However, gaps can severely limit productivity by limiting the TS that can be used. Poor fixturing used during welding can also be a cause of poor part fit-up. The wire fed arc welding processes are most tolerant to gaps as filler material can be deposited to bridge the joint gap.

The use of variable-polarity GMAW (GMAW-VP) has been limited because the power sources are current limited to only 200-300 A. This, in turn, limits the welding speed and has made the equipment of less commercial interest compared to the much greater flexibility and power capabilities of 500-A inverter power sources for GMAW and GMAW-P. Higher power inverter GMAW-P power sources with electronic control of 'arc re-ignition' allows short arc lengths and low arc voltages to be used to control bead width.

Emerging technical capabilities of mechanically pulsed GMAW (GMAW-MP) equipment such as the Controlled Short Circuit (CSC) from Jetline/Miller and Cold Metal Transfer (CMT) from Fronius provide exceptional control of the welding arc for GMAW in SC mode by employing advancing and retracting wire drive. While this is of significant interest for light manufacturing and aerospace, the equipment is also current limited by the nature of the use of the SC current regime, and the equipment is thus not suited to high welding speeds in the 2-4-m/min range of interest here.

Two processes that are relatively new are tandem GMAW (TGMAW) and laser/hybrid GMAW. Both offer the flexibility to apply to plate products and thicker sheet products, with limits generally accepted to be around 1.6-mm thickness at the lower end.

The economics of the welding operation are usually fairly complex, but comparing processes on a use and cost of energy per meter of weld is a reasonable way to present this, especially when energy costs are increasingly high. Such a comparison (Pekkari, 2004) for full-penetration welding of 4-mm-thick carbon steel butt joints, shows the kJ/m for Nd:YAG, lamp-pumped lasers to be almost as high as for GMAW, 1650 kJ/m compared with 1800 kJ/m, respectively. This is quite surprising initially, but the efficiency of such a laser is only 1-2 %, compared to an efficiency of 10-15% for a CO₂ laser. Economically, it is fairly clear that CO₂/GMAW hybrid welding is more energy efficient than Nd:YAG/GMAW hybrid welding, and the capital equipment cost of the CO₂ laser is considerably cheaper than that of the Nd:YAG laser. An

advantage of Nd:YAG lasers is that they are fibre deliverable and thus more suitable for robotic deployment compared with CO₂ lasers. TGMAW, with similar productivity for some applications is an attractive proposition since the capital cost is significantly lower compared to laser systems.

In aerospace the buy to fly cost is of increasingly critical importance and the next level of performance is sought in the arena of hypersonic vehicles. For various performance and strength to weight requirements, the increasing use of lightweight Ti and Ni alloy structures is being actively researched by the author. Material thickness ranges of 0.5 to 1.75 mm are typical in these cases and high-speed GMAW-P, LBW and LBW/GMAW-P are the main contenders for process selection and research.

The concepts and results of the research presented in this thesis can also be used for Ti and Ni alloys, as well as steel, stainless steel, and Al alloys. An example from the author's experience based on process selection for Ni-based alloys comes from a project funded by a major welding equipment manufacturer to highlight the productivity benefits of their new electronically controlled SC GMAW power source (Harris, 1998). The application area of interest was the flue gas desulphurization (FGD) market for power generation market sector. FGD involves scrubbing sulphur compounds from the flue gas before it is discharged and a leading technique is to 'wallpaper' the steel flue stack with a lining of a Ni-based alloy, typically C-276. The context of the research was to compare STT to GMAW-P for low-cost automation of out of position GMAW as a competitor to manual GTAW and semi-automatic GMAW. The research conducted by the author showed mechanized GMAW-P, at 2-4 m/min, to be almost three times more productive than mechanized STT for fillet welding the thin C-276 sheet, and almost nine times more productive than manual GTAW or semi-automatic GMAW. The sponsor was happy since they also made the GMAW-P equipment. This is another practical example of the benefits of GMAW-P as a high-speed welding process, even on sheet material.

Gaps in joints have long been considered a fact of life in the fabrication industry, and welding has a long history as the process that can take care of the poor fit-up, facilitated by the high skill level of a good manual welder. However, productivity suffers considerably with this approach by deposition of excess weld metal, increased heat input and distortion, over and above the high labor cost for a skilled or semi-skilled manual welder, and the limited ability of a human operator to weld at high speeds. The original wave of robotic welding was aimed at replacing the welder and lowering the fabrication cost, but in many cases the gap variation was too large for the application of robotics to work satisfactorily.

The author has seen robotic welding operations where a manual welder has programmed a robot to weave over a large gap producing a large weld size with high heat input and distortion. This was in an automotive Tier 2/Tier 3 supplier producing welded cross-car dashboard beams. The brackets were produced in-house where the stamping tolerances were in direct control of the same company. Rather than alter the stamping to produce a well fitting part, the large gap created by poor fit-up was being bridged by welding, causing the whole assembly to fail to meet final inspection tolerances because of significant bending distortion around this high heat input weld. This is a rather extreme example, but one drawn from first-hand experience in working directly with the supplier to help them identify the source of the problem.

Modern arc welding robots are equipped with through the arc (TTA) seam tracking to cope with gap variation and seam following. However, to maximize productivity the whole fabrication process has to be considered from first-operations such as cutting and bending, through stamping and other forming operations such that good fit-up is achieved. If this is ignored, the welding process, even though it may be robotic, has to slow down to cope with gap-bridging and avoid burn-through on thinner materials.

Part of the issue is that the productivity, of a welding process is relatively poorly understood and thus a hidden cost in many ways. The usual argument is that it is 'too expensive' to improve fit-up, when springback from a forming operation, or poor fit from a stamping operation leaves the welding operation to cope with large gaps. In this case the context of large is a gap of more than $0.5 T$ where T is the material thickness.

1.1.1 Dispelling the Myths about GMAW-P

There have been over 250 articles and papers published on the subject of GMAW-P, and numerous theses for higher degrees. Despite this, the myths persist, perhaps because of the sometimes highly technical nature in which the wide array of possibilities offered by GMAW-P parameter settings have been studied, including metal droplet transfer, synergic logic controls, and algorithms for pulse parameter development. These subjects are usually presented by the technical community to the technical community. While there have been numerous good general articles on the subject over the years, much of the published work may not have been read by the welding community and welders at large, either because it is presented in specialized journals, or not widely published as is the case with many thesis dissertations or consortia projects. For example, the author ran a 2½ year study of synergic pulsed GMAW in the late 1980s, but this was a confidential consortia project. While the results would in themselves address many of the myths described below, they were not available for widespread publication.

GMAW-P was initially developed in the mid 1960s, to exploit the benefits of high arc stability and low spatter offered by the spray mode of metal transfer at wire feed speeds (WFS) and welding currents below the spray transition point for steel wires; for example, below 230A for a 1.2-mm-diameter wire in Ar-CO₂ shielding gases. The generation of power supplies available at that time relied on the manual setting and balancing of pulse parameters, namely the pulse current, pulse time or duration, background current, and background time. While this setup could produce good results, it had two major disadvantages. Firstly, the welder had to understand the interactive nature of the individual pulse parameters to obtain stable transfer for a particular wire speed, and secondly, had to reset the pulse parameters for each WFS selected to maintain stable wire burn-off characteristics.

These major drawbacks led directly to the development of synergic pulsed GMAW, although commercial power sources were not produced in significant quantities until the early 1980s, largely because the more sophisticated power electronic devices required were not initially available, and were too costly for widespread application until the 1980s. The invention and continued development of the inverter power source has been crucial to the development and widespread application of GMAW-P.

In GMAW-P the individual pulse parameters are automatically selected from a set of preprogrammed parameters through solid-state electronic logic controls. The use of such controls effectively allows a welder to dial up a current or WFS, and the power source automatically selects the appropriate pulse current and time parameters and the pulse frequency required to burn off the wire at whatever WFS is demanded, maintaining a stable spray transfer, with concomitant benefits for control of metal transfer at negligible spatter levels.

1.1.2 The Common Myths

There are a wide variety of myths which have been created over the past 15 to 20 years concerning the application of GMAW-P. Some of the more common ones are listed below and explained:

- **Myth 1** – GMAW-P prevents spatter, and is a spatter-free process
- **Myth 2** – GMAW-P is a lower heat input process than conventional constant voltage (CV) GMAW
- **Myth 3** – GMAW-P was invented to weld sheet metal and is more tolerant to burnthrough
- **Myth 4** – A true square wave pulse is better than other pulse shapes
- **Myth 5** – GMAW-P is appropriate for all problems with GMAW, in as much as it is better at any WFS than conventional CV GMAW.
- **Myth 6** – GMAW-P is a slower process than conventional GMAW in terms of welding speed

Many of these myths have become established in industry, often encouraged by the overselling of the equipment as a panacea for all problems. The myths persist and are still promulgated.

1.1.3 Dispelling the Myths

The individual myths are in no particular order, but will be dealt with in the order they are presented above.

Myth 1 – GMAW-P Prevents Spatter, and is a Spatter-Free Process

Unfortunately, the physical nature of the GMAW process, and particularly the way it starts by short circuiting the wire to the workpiece, means that for all practical purposes there will always be some spatter at the start of the weld as the arc is established. This has long been an area of active study, and still awaits a low-cost, robust solution suitable for industrial application. Once in steady-state operation the electronic pulsed control of metal droplet transfer produces a welding condition, which if the torch is manipulated correctly can produce a weld bead which is effectively free from adherent spatter in the vicinity of the joint. In practical terms, GMAW-P offers low spatter operation, which improves weld cosmetic appearance and reduces problems of part fit-up, through spatter deposited on fixturing, in increasingly mechanized and automated welding operations.

However, despite the pulsed current, the arc voltage also needs to be suitable for spray transfer. If the arc voltage is tuned too low, say below 20V, short circuiting may

occur, or the arc action on a larger weld pool may cause metal to be ejected from the pool in the form of spatter. It should be noted that with the wide variety of electronic controls now available, it is also possible to use synergic control for SC transfer, and variants are available such as Lincoln Electric's STT which electronically senses SC droplet detachment to minimize spatter in a SC operating mode.

Myth 2 – GMAW-P is a Lower Heat Input Process than Conventional CV GMAW

The myth states that using discrete current pulses better controls and lowers the heat input to the weld. While may be true for pulsed gas tungsten arc welding (GTAW) where low pulse frequencies, typically 2 to 10 Hz, used in, it is largely a myth with P-GMAW where pulse frequencies are typically 100 to 500 Hz. Pulsing certainly gives much more control over metal transfer, especially compared to conventional short circuiting or globular transfer in CV GMAW of ferritic steels and stainless steels. However, as far as the weld pool is concerned, and the heat flow into the adjacent metal, the heat input of P-GMAW is effectively no different to that of conventional GMAW for the same current and voltage.

Myth 3 – GMAW-P was Invented to Weld Sheet Metal and is More Tolerant to Burnthrough

The GMAW-P process was invented to achieve the best control of metal transfer across the entire range of useable WFS for each particular diameter. This is because spray provides the most arc stability and thus the best opportunity to transfer metal across the arc and deposit it where it is desired. Thus, the development of GMAW-P was aimed as a broad range of material thicknesses, not just sheet metal. Applications range from welding of automotive vehicle frames through welding of circumferential pipe joints. In fact, with the open arc and consequently higher arc voltage, GMAW-P is somewhat less suited to sheet metal applications than controlled short circuit welding, although it can be used with careful control of arc voltage in semiautomatic mode. Mechanized welding of sheet metal, where the travel speed (TS) can be considerably higher is very attractive. A project at EWI (Harris, 1998) demonstrated that GMAW-P could be used to weld lap-fillet joints at 2.8 m/min on Ni alloy C-276 in the 3F vertical down position and 2F H-V fillet welds were made at 2.0 m/min. Welds were free from spatter and had a pleasing slightly convex weld profile desirable for the application. The Ni alloy weld pool is thought to be more viscous than that for other alloy systems, and thus is considered less prone to humping defects.

Myth 4 – A True Square Wave Pulse is Better than Other Pulse Shapes

A true square waveform is only really produced with expensive transistor power sources. Almost all commercial GMAW-P power sources contain some inductance in the circuit resulting in some minimal delay in current rise at the start of the pulse. Many power supplies are now inverter designs which can have an inherent current ripple on the peak and background current waveform associated with the switching frequency of the inverter.

As part of a large group-sponsored project on GMAW-P a study of five power source control designs and waveform shapes for GMAW-P with various pulse shapes determined that there was negligible difference between the performance of each in terms of the effect on weld penetration for the same welding parameters and thus welding power. The important criterion is that enough energy is supplied in the pulse to detach a droplet. Typically the droplet is approximately the size of the wire diameter. For this case, for similar welding power, the results of a variety of waveform shapes are essentially the same in terms of weld bead characteristics such as bead width and penetration depth.

Myth 5 – GMAW-P is Appropriate for all Problems with GMAW, Since it is Better at Any WFS than Conventional CV GMAW

No welding process is a panacea for all welding problems. Each process has niche areas where it can be used more effectively than other processes. The GMAW process is the most widely industrially applied process of any welding process, arc or resistance. In many instances conventional GMAW does an adequate job. However, with ever increasing focus on weld quality and industrial competitiveness, the GMAW-P process should be examined to see whether it can enhance weld quality through spatter reduction, weld profile control, and overall consistency of operation. Results achieved using spray transfer with conventional GMAW will be hard to beat. The GMAW-P technique provides the ability to use the advantages of spray transfer at WFS where SC or globular transfer would otherwise be the options with lower WFS using conventional GMAW.

One of the more important attributes of GMAW-P is that it allows spray transfer to be used out of position. This opens up a number of possibilities, including welding of pipe joints in the 5G and 6G fixed positions.

Myth 6 – GMAW-P is a Slower Process than Conventional GMAW in Terms of Welding Speed

This myth may have come from a parallel drawn from pulsed GTAW where TS needs to be sequenced with pulse frequency to get the required overlap and weld ripple pattern. With GMAW-P the pulse frequency is in the range of 100 to 500Hz, rather than the typical 2 to 10 Hz used for pulsed GTAW, so there is no need to weld slowly. There is no technical justification for supposing that GMAW-P should be slower than conventional GMAW for the same wire feed speed. As mentioned earlier a recent project at EWI demonstrated that GMAW-P could be used to weld lap-fillet joints at 3.75 m/min on Ni alloy C-276 in the vertical down position. This is a very high welding speed, and suitably indicates the potential for high welding speeds with GMAW-P.

1.1.4 The Good News

While the myths persist, many users have found GMAW-P to be a very effective tool, and the use of this variant of GMAW has found widespread applications from welding of sheet metal through welding pressure vessel steels. The level of sophistication of the power sources available today is daunting to some, but for the end user, should be viewed as offering a wider array of possibilities and flexibility

than ever before. While most applications reflect the general usage of materials, i.e., ferritic steels, stainless steels, and Al alloys in that order, the process is very suitable for welding Ni alloys, Cu alloys, and even Ti alloys. For the majority of applications and users the preprogrammed parameters for steel, stainless steel, and Al alloys for various wire sizes and shielding gases are sufficient for most needs. These are set up as simple toggle switches on most power supplies, leaving the welder to simply set the WFS (or current control depending on the labeling of the main control knob) and trim the arc voltage (usually ± 5 to 10% of a preprogrammed voltage). The possibilities for user pulse programming and parameter storage, where needed, are now wider than ever. The current state of developments in solid-state electronics and inverter power sources, has yielded systems such as Lincoln Electric's Wave Designer software which allow almost infinite control of pulse parameters and power source characteristics. Obviously, these sophisticated controls are not for the uninitiated, but with suitable control by qualified personnel, they are very powerful tools. GMAW-P equipment has offered conventional CV GMAW from the earliest days along with preprogrammed parameters for common combinations of wire type, wire diameter, and shielding gas. The most sophisticated power supplies obviously also offer these more conventional operation modes.

1.2 Summary

For sheet metal applications the following are typical;

- Almost all welds are single pass and the majority are lap welds
- Acceptable quality and high productivity are the key requirements
- Weld sizing is not well defined, especially for welding of sheet metal
- Minimizing joint gaps is key to maintaining high welding productivity
- Most data is based on single torch GMAW in either short-circuit (SC) mode or using GMAW with direct current (DC) or GMAW-P
- Weld humping limits travel speed and thus welding productivity for high-speed welds

The maximum potential travel speed to make welds with single torch GMAW-P needs to be evaluated to establish a baseline from which to compare other processes. The limiting effect of joint gaps on maximum travel speed is part of this baseline.

To make significant strides in welding productivity, joint-fit up is a critical requirement rather than a preferable thing if the potential productivity and welding speed improvements offered by hybrid LBW/GMAW-P are to be realized. As such, this process needs to be studied with joint fit-up set at a minimum.

To overcome the problems with productivity from the perspective of the welding process, the primary need is suppressing the weld humping defect to increase the travel speed at which acceptable welds can be obtained. To achieve this, the humping defect needs to be studied as well as welding processes and techniques that can more readily produce a small fillet weld size. The associated research objective is thus to conduct a fundamental study of the humping phenomenon and its mechanisms to understand how to suppress or eliminate it while welding at high travel speed.

2.0 LITERATURE REVIEW AND INDUSTRY SURVEY

Almost 200 papers and articles relevant to the overall subject matters have been reviewed: high-speed GMAW, GMAW-P, GMAW-VP, laser, laser/GMAW hybrid welding, weld pool dynamics and humping, and weld pool modeling. Many of these are cited in this literature review.

2.1 Process Studies and Welding Productivity

GMAW using SC or pulse spray transfer are the preferred methods used by industry for welding light structures because of their lower heat inputs.

The arc welding equipment industry has been busy producing a wide new array of GMAW variants, including twin-wire GMAW, GMAW-VP, STT GMAW, and GMAW-MP in addition to enhanced CV GMAW, and GMAW-P equipment of increasing reliability, stability, and hence weld quality and consistency. The newer GMAW variants and some of their application areas are discussed below.

In a scenario of continuous improvement and cost reduction, welding productivity increases through robotics and automation have and will continue to be achieved. The development of newer welding techniques and processes is often aimed at higher productivity through the use of higher welding speeds and thus deposition rates. A big impediment to welding productivity is the tendency to over-weld small fillet welds in thin plate and sheet products. Over-welding results in higher welding costs, including additional welding power, electrode wire, higher distortion (and distortion correction costs), and lost productivity. Two processes that are relatively new are TGMAW and laser/hybrid GMAW. Both offer the flexibility to apply to plate products and thicker sheet products, with limits generally accepted to be around 1.6-mm thickness at the lower end.

The productivity of GMAW, GMAW-VP, GMAW-P, TGMAW, and LBW/GMAW hybrid processes are reviewed here as a context and benchmark for the present research. Arc welding processes use electrical energy to melt or fuse metals to produce a joint between two or more parts. All processes are characterized by an electrical arc between an electrode and the workpieces. These processes, their advantages and disadvantages, and their applications for welding sheet products are described in the following sections.

2.2 Gas Metal Arc Welding

The GMAW process (also known as MIG or MAG welding) is characterized by the fact that an arc is formed between the end of a continuous spool of electrode wire and the workpiece, Figure 2.1. The solid wire is continuously fed through a contact tip in the torch, and melts to form the weld bead joining the base metals. The wire feed rate is balanced to the burnoff rate to maintain a stable arc. The wire type is selected to give the weld metal a matching (but often overmatching) strength compared to the base metal. The weld area around the arc is protected by a shielding gas supplied from the torch.

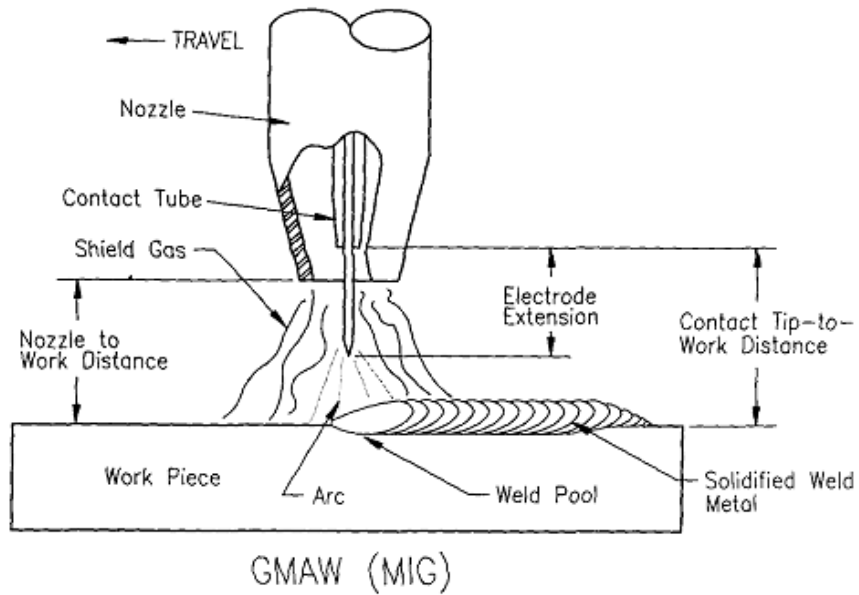


Figure 2.1 GMAW Process

GMAW weldments can be made in all positions, especially using pulsed-current, GMAW-P, thus the process is ideally suited to automation, especially through arc welding robots. Gap tolerance for GMAW is good, with joint gaps up to 1T being tolerable.

The welding parameters that must be controlled to produce acceptable welds include welding current, arc voltage, WFS, torch TS, torch travel and work angles, and shielding gas flow rate. The joint gap should be minimized to achieve the best joint quality and productivity.

The major advantages of the GMAW process are its high productivity and reliability coupled with low cost. The process is suited for automation, and very little cleanup is required after welding. The equipment can be deployed on welding robots with relative ease, and single-side access only is required. In addition, the process is suitable for many different alloys, including carbon and low alloy steels, stainless steels, Al alloys, Ni alloys, Cu alloys, and Mg alloys.

The disadvantages of GMAW are that plant ventilation is required to remove welding fumes, and that protection is needed from strong drafts to avoid loss of shielding gas efficiency which can lead to porosity. Welding of coated steels can cause porosity by volatilization of zinc-rich coatings. This can be mitigated by correct development and implementation of welding procedures.

The GMAW process already has widespread usage in the automotive supplier network, ranging from SUV and light truck frames to exhaust, catalytic converter, seat frames, suspensions, and engine cradles. GMAW is widely used in structural applications for making fillet welds on lap, corner and T-joints, and also in light industrial applications. The process is widely applied using manual, mechanized, and robotic techniques. Consumable electrodes can be solid or metal-cored and used in a variety of metal transfer modes: SC, globular, and spray. Cu-based electrodes are

used for braze welding cast iron and galvanized sheet. Conventional CV power supplies are very affordable.

2.2.1 GMAW Including GMAW-P

As a long-established process, GMAW, and in the last 20-25 years, GMAW-P, have rightly developed a standing atop the most widely used and flexible production welding processes, both in terms of application across a broad range of materials, but especially in terms of flexibility for deployment with a wide array of mechanization and automation. Application experience and production robustness is broadest at relatively modest TS, often stated to be in the 0.5-1.0-m/min range

The GMAW-P process has been widely reviewed before, and the benefits are considered to be well understood in the automotive supplier network, especially among the Tier 1 suppliers. Current pulsing has the benefit that spray transfer can be achieved across the entire range of WFS, maintaining the most stable arc conditions, which relate directly to weld quality, consistency, and very low spatter levels. Attached to a modern six axis welding robot, or other mechanized welding system, this provides a very flexible manufacturing tool. GMAW-P has been heavily used since the late 1980s by automotive suppliers such Tower Automotive which had several hundred machines in production welding operations at that time for welding light truck frames and other parts. Almost all applications until fairly recently were for steel. In the last several years GMAW-P of Al alloys has become of increasing interest and application, especially for components such as suspension parts and engine cradles. For example, the Audi A8 spaceframe is welded predominantly with GMAW-P.

Metal-cored wires offer another dimension for high-quality and high-productivity GMAW whether by GMAW-P or conventional CV GMAW. The metal powder in the wire core offers enhanced deposition rates and welding speeds compared to typical solid wire GMAW. The cored nature of the consumable also offers a cheaper production route for alloyed wires such as the Type 409 wires for welding Type 409 exhaust components, which can be Ti, Nb, or Nb/Ti stabilized for grain size control and enhanced mechanical properties of weldments.

GMAW-P is widely used on applications that compete with SC welding (light gauge) and spray for out-of-position welding. Waveform development tools (software), servo-wire feeders, and real-time parameter monitoring may be provided with these advanced systems. Cost is typically two to four times that of CV equipment.

The GMAW and GMAW-P processes have been very widely studied with attention more often in the realms of optimization for productivity along with production robustness. Various well-known generalized optimization methods such as Taguchi, design of experiment (DOE), and other techniques have been applied to welding.

Successful strategies such as ‘Sloping Weld Area Testing’ (SWAT) (Green, 2001), ‘Arcwise’ (Harwig, 2000), and others have been applied that are more directly tailored by and for arc welding research and development. SWAT was carried out using steel and Si bronze consumables for welding steel sheet and tubes simulating joints anticipated for tubular construction of automotive frames (Green, 2001). This

work determined suitable welding speeds in the range of 0.5 to 1.0 m/min, plotting WFS against welding TS. The ratio WFS/TS gives a measure of weld size. Once a preferred weld size is determined, the ratio can be maintained to increase productivity by increasing both WFS and TS, but maintaining the same ratio.

Little work appears to have been conducted at significantly higher TS, with one exception (Mischler, 1986). In this case fillet welds were made at 3.2 m/min using single-wire GMAW with 100% CO₂ shielding gas. CO₂ shielding is well known to generate high spatter levels from globular metal transfer and to produce high fume levels compared to Ar-based shielding gases, the latter promoting very stable spray or pulsed spray transfer in GMAW and GMAW-P. The results were reported as being considerably lacking in terms of reproducibility and consistency, and also intolerant to small changes in wire offset relative to the joint. They do however point to the productivity potential of the process in a range of TS most would consider improbable for GMAW.

More recent work on high strength galvanized steel sheet (Howse, 2000) reported a 'high' TS of 1.0 m/min for lap joints in 2.0-mm-thick sheet using Ar-5%CO₂ shielding gas. Welding current was only 140 A, and a low arc voltage of 17 to 19 V was employed. This is yet another example of the mindset that single-wire GMAW is limited to linear TS of 1.0 m/min or less. Work is needed to investigate the performance and develop welding procedures for higher speed single-wire GMAW.

Welding wire development (Suzuki and Nakamoto, 2001) examined Si and Mn ratios in the welding wire since they affect surface tension, and fluid flow in the weld pool. Their aim was to increase bead width to increase gap bridging capability (gap weldability). However, a larger bead width is counterintuitive for increasing welding productivity because the weld metal is spread laterally requiring slower welding speeds for the same WFS, while the welding speed needs to be increased for increased productivity. Typical welding conditions for GMAW-P and GMAW-VP of 0.5 to 1.5 m/min were used with Ar-20%CO₂ gas shielding on sheet steels in the 0.6- to 1.2-mm range. Weld bead humping was found either above 1.6-m/min TS or above 34-V arc voltage for a 1.2-mm-diameter wire. Again, work is needed to develop higher productivity single-wire GMAW.

2.2.2 GMA-Brazing and GMAW-VP

While traditional CV GMAW always operated in the DCEP polarity, as does GMAW-P, GMAW-VP (also known as GMAW-AC) operates, as the name suggests, in a variable-EP/EN mode. While GTAW-AC has been available for many years, cost reduction of power electronic devices were required for development of commercially viable GMAW-VP equipment. The ability to minimize distortion associated with the heat input when welding sheet thicknesses made this process potentially attractive for sheet metal body in white (BIW) fabrication.

One of the earlier references to GMAW-VP (Tanimoto et al., 1988), concerns the development and application of a power source in Japan incorporating twin inverter power sources run in DCEP and DCEN mode. This now familiar design concept, enabling adjustment of EN and EP ratios to independently (within reason) change welding power and WFS has been adopted by many Japanese manufacturers

including Panasonic, Hitachi, OTC, and Kobelco, but has not been exploited widely in the U.S. or Europe. Amongst the various issues, the most pertinent one technically and economically is the relatively low current limit, typically 200 to 250 A, provided by such equipment. It has been demonstrated that the available EN and EP adjustment range allows joint gaps of up to 3T to be bridged, in extremis. Work must be done to address first operations (cutting, etc) if the latent productivity advantages of GMAW are to be exploited.

The use of GMAW-VP for welding of thin sheet Al for auto body applications was reported (Ueyama et al., 2005) with the benefits stated as welding with large gaps while avoiding burnthrough defects. The use of GMAW-VP with Si bronze or Al bronze electrode wires (Joseph et al., 2001), (Hackl, 1998), Figures 2.2 and 2.3, has been shown to be very effective for thin steel sheet with large gaps, but this is very much a niche markets for largely non-structural automotive joints such as roof to quarter panel seams where the process is used to fill in seams from prior structural welds made with RSW.

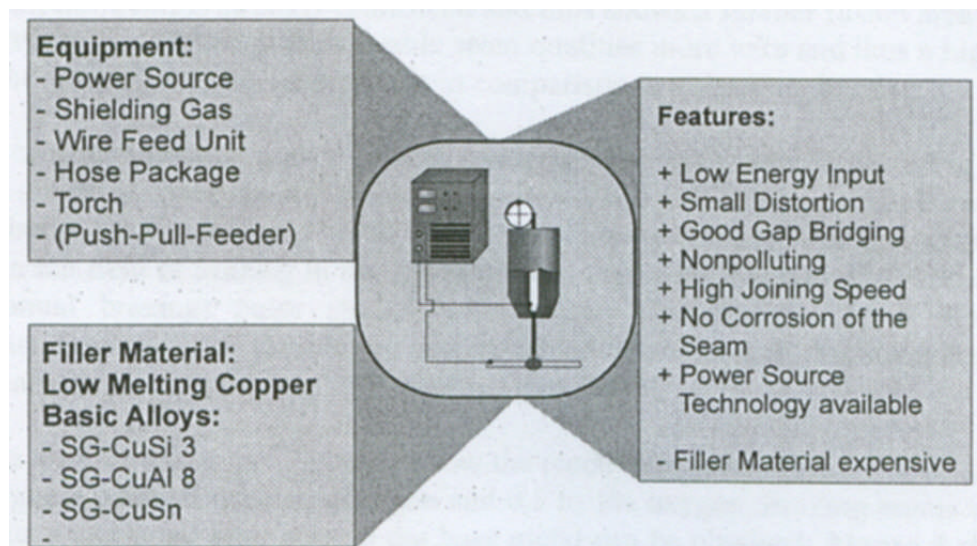


Figure 2.2 Features of GMA-Brazing (Hackl, 1998)

Studies comparing GMAW-VP and GMAW-P (Joseph et al., 2002) for 1.6-mm sheet lap-fillet joints with 1T gap found a productivity improvement of 67% using GMAW-VP at 1.5-m/min TS.

The main advantage of VP-GMAW compared to conventional GMAW, is that the ability to vary the balance of DCEN and DCEP polarity, Figure 2.3, allows a significant improvement in control of weld penetration. This significantly enhances the ability to weld sheet metal components, particularly regarding gap tolerance. VP-GMAW is suitable for welding steel sheet and tube material.

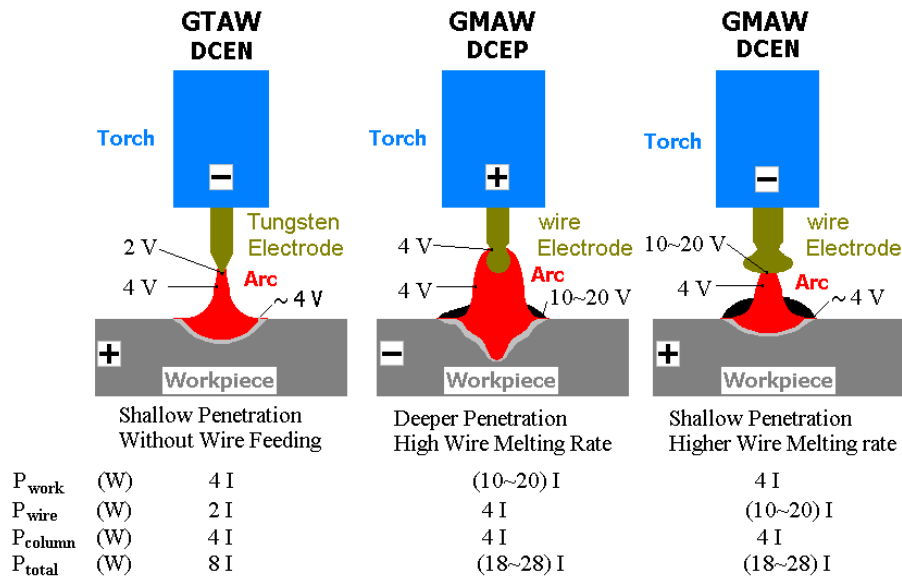


Figure 2.3 Nominal Comparison of Penetration and Wire Melting Rate for GMAW-DCEP and GMAW-DCEN (Joseph, 2002)

Recent research (Harwig, 2003) has continued to discuss the limitations of CV GMAW and GMAW-P for high-speed welding of sheet products, characterizing it as between 0.5 and 1.0 m/min. Based on this characterization, GMAW-VP has been reported to have productivity twice that of GMAW-P (Harwig, 2003). This productivity difference is appropriate when considering relatively large gaps up to 2T, but not when fit up is good (Harris, 2002). When good fit up can be achieved, the productivity of GMAW-P can be considerably higher.

Literature for single-torch GMAW (Fronius, 2005) clearly reflects the commonly held view that single-torch GMAW is limited to 1 m/min for small single-pass fillet welds on lap-fillet joints in the 2F position.. The TGMAW system, while offering a high-speed welding solution, is not considered suitable by the manufacturer for material thinner than 2.0 mm. A welding speed of 2.0 to 3.0 m/min is recommended for hybrid LBW/GMAW for 2.0-mm-thick steel sheet material (Fronius, 2005).

2.2.3 STT GMAW

The STT (a trademark of Lincoln Electric) variant of GMAW is an electronically controlled version of GMAW-SC without the spatter problems typically associated with this transfer mode under traditional CV control. The effective control of metal transfer, with the lower heat input of a lower current operating mode, has potential advantages for welding sheet metal components. An analogy could be made to the increase in metal transfer stability and improvement in weld consistency, quality, and spatter reduction typical of modern GMAW-P equipment which is already widely used by the automotive supplier network at all levels.

2.2.4 CSC and CMT GMAW

In the few years or so a completely new type of GMAW system has become commercially available from two sources: Jetline/Miller CSC, Figure 2.4, and Fronius CMT, Figure 2.5. This equipment type is unique within the family of

GMAW techniques in that it uses both forward and reverse wire movement to control the deposition of electrode wire in a mechanically CSC mode. The wire reverse component allows the welding current to be reduced to only a few amps as the wire is withdrawn and another drop of molten metal is developed. This technique essentially eliminates all weld spatter produced during arc re-ignition, the source of most welding spatter in the conventional forward drive SC metal transfer mode in conventional GMAW. This technique allows very high levels of control for depositing small weld beads and has already been found useful for areas of application development in low dilution cladding and building up of discrete areas of a component for OEM or repair scenarios. The nature of the SC metal transfer, albeit highly controlled, does not lend itself as an appropriate tool for very high welding TS.

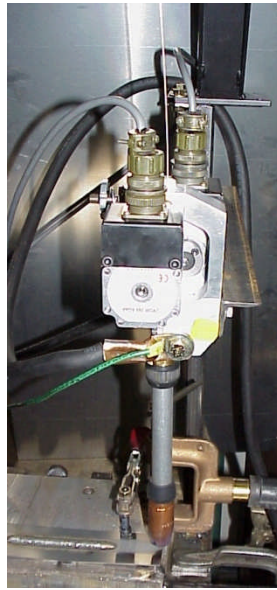


Figure 2.4 Miller Jetline CSC Gun Showing Dual-Wire Drive Motors



Figure 2.5 Fronius CMT Gun With Integrated Wire Feed Motor for Forward and Reverse Wire Drive

2.2.5 Tandem and Twin-Wire GMAW

Tandem and twin-wire GMAW were developed and applied around the same time. The difference between the two is that the former uses two torches with two separate welding power sources, while the latter employs one power source, Figure 2.6. Both have torches with two contact tips and two wire feed systems feeding into the same weld pool. Different power source and welding gun setups are available for twin (common potential) or tandem (independent potential) electrodes. Both will naturally give twice the deposition rate and increased productivity compared to a single wire, but the twin/tandem system can increase productivity and deposition rate by two to four times, depending on the application, based on the thermal efficiency of a single weld pool.

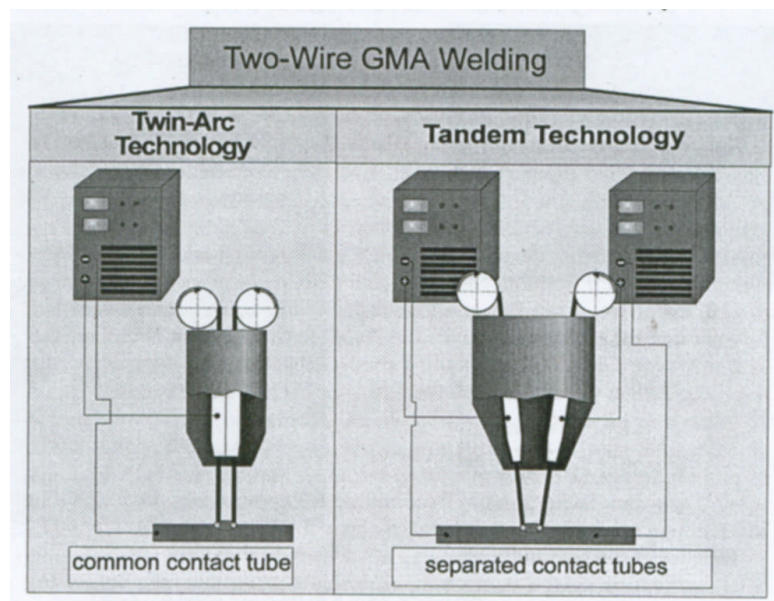


Figure 2.6 Twin Wire and TGMAW (Dilthey, 2000)

TGMAW exploits the benefits of a dual welding gun and two arcs in a single weld pool to achieve productivity gains in excess of three times that of single-wire GMAW. The most suitable systems for robotic operation incorporate two wires in a single torch, Figure 2.7, using two contact tips and sequencing the current pulsing to minimize the potential for arc interference. Several commercial systems are available and applications range from 2.0-mm sheet to thicker materials. Applications include frame manufacturing, such as in light trucks and SUVs, and a wide array of suspension and axle components.

Twin GMAW offers two to three times the deposition rate (or TS) of single electrode GMAW processes. Lower current density and arc coupling minimizes the onset of plasma jet-induced defects. The process is used in robotic applications that have either long joints (greater than 150 mm) or in thick plate applications requiring multi-bead multi-layer deposits in the flat and horizontal positions.

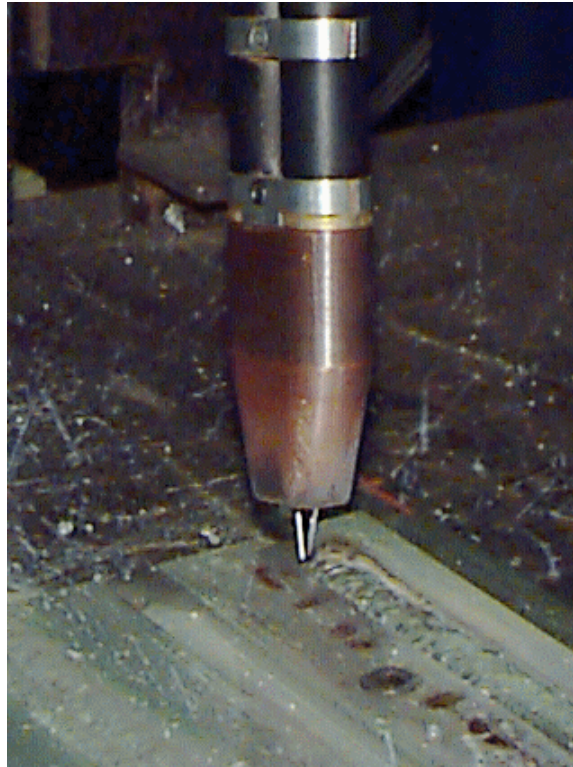


Figure 2.7 TGMAW Torch with Dual Contact Tips (EWI)

This has obvious implications for increased deposition rate and productivity in sheet metal and automotive component fabrication. The main advantage for thinner materials is the high-speed welding speeds which can be achieved up to three to four times faster than single-wire GMAW for suitable applications on thicker material, above 2 mm. The welding power and deposition rates are suitable for production of suspension parts, engine cradles, light truck and SUV frames, etc., but not for thin sheet metal parts below 1.6 mm (Fronius, 2005) or tubular spaceframe components made of thinner tube material.

Typical welding speeds for robotic TGMAW are in the range of 1.2 m/min for a horizontal 6-mm leg length fillet weld, to 3 m/min for a 3-mm lap fillet weld, and 6 m/min for a 2-mm wall thickness cylinder. These speeds are two to three times faster than conventional single-wire GMAW. This makes twin-wire GMAW a very powerful tool for automotive fabrication.

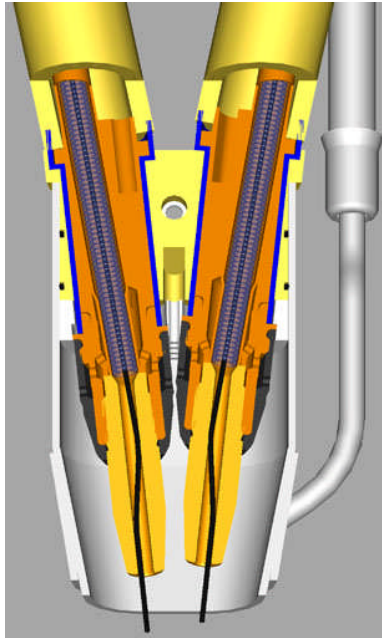


Figure 2.8 Typical Arrangement of a TGMAW Welding Torch Head (Pekkari, 2004)

The development of twin and TGMAW in the 1990s saw considerable application toward the end of the decade for high-speed fillet welding, (Kodama et al., 1997), automotive subassemblies (Rippl, 1998), and automotive and railroad applications (Michie et al., 1999).

Equipment is commercially available from a number of companies, including Fronius, Cloos, Lincoln Electric, and ESAB, Figure 2.8. The TGMAW process is capable of 20-kg/hr deposition rate and operates at current levels up to 1200 A. Over 1000 systems have been installed since the mid 1990s (Moorehead, 2003). Applications continue to be developed as process refinements and parametric development (Ketrion, 2000) are made. These include steels in a wide range of thicknesses, and other alloys such as 1.2-mm-thick Type 409 stainless steel lap fillet welds produced at 5.0 m/min for exhaust tubing (Moran and Kotnik, 2000) and Al alloys down to 1.0-mm thick welded at 2.5 m/min.

In addition to high deposition rate, the process is well suited for high-speed welding. A recent study in Sweden (Hedegard et al., 2004) reported welding speeds of 0.8 to 4.0 m/min for a range of joint and material types. For a lap-fillet joint between two 2.5-mm-thick C-steel sheets a welding speeds of 3.5 m/min was reported.

2.3 Plasma Arc Welding

Melt-mode plasma welding, which can be performed with or without cold wire feed as desired, Figure 2.9 has the advantage over GMAW that the weld fusion characteristics are such that almost the entire weld length can be “counted” as performing a structural role. With GMAW, some of the weld length has to be discounted because of the start and stop characteristics of a GMA weldment, typically 3 mm at either end of the weld. This yields the advantage that shorter welds can be made with PAW, with higher potential productivity. The other advantage is that melt

mode welds can be made which have improved cosmetic appearance for more visible joints.

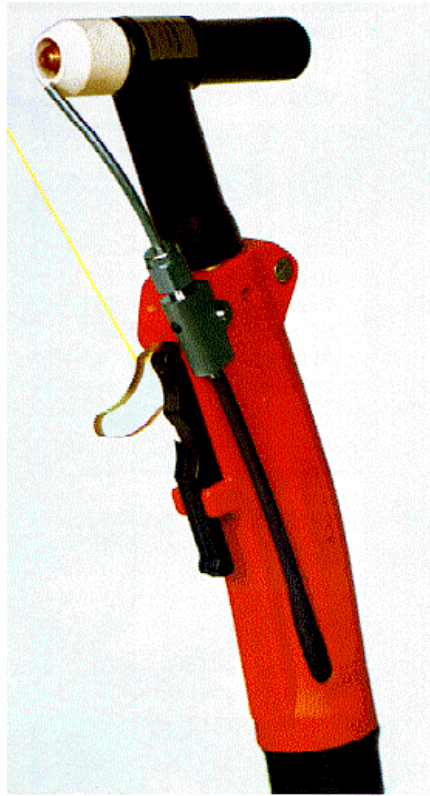


Figure 2.9 Plasma Welding Torch with Cold Wire Feed (Hughes, 2002)

Autogenous welding (i.e., without filler) of 6104 Al alloy sheet for door panels has been successfully carried out without cracking or porosity. Typical welding speeds for a lap-fillet joint are 1 to 2 m/min (Hughes, 2002). Another advantage of PAW of Al is that, with an AC power source and VP switching, parts can be welded with much reduced cleaning time.

2.4 Hybrid Laser Arc Welding

Use of lasers in conjunction with arc welding was first reported in 1978 (Eboo and Steen), and referred to as arc augmented laser welding. Work continued (Steen and Eboo, 1979) examining the effect of welding from one or both sides of thin sheet. It was found that the arc roots preferentially to the laser generated plasma or hot spot (Steen, 1980).

Laser hybrid welding is today almost synonymous with LBW/GMAW, Figure 2.10, and almost all commercial applications employ this method. The practical application of this process, has taken almost 20 years to come to fruition. The first commercial exploitation of this process was claimed in Germany in 2000 at a container manufacturer for welding oil tanks (Petring, 2001).

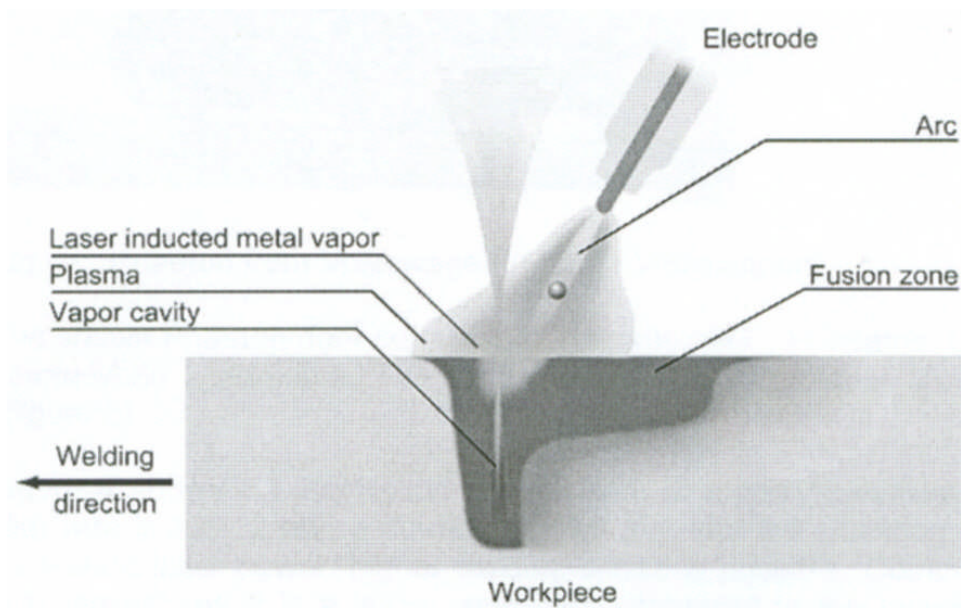


Figure 2.10 Schematic of Hybrid LBW/GMAW Operation (Graf, 2002)

2.5 Hybrid Laser Welding – LBW/GTAW and LBW/PAW

In the 1990s the LBW/PAW work of Steen and Eboo was continued at the University of Coventry, U.K. (Johnson et al., 1995) (Walduck and Biffin, 1994) and further developed for high-speed laser/PAW of 0.25-mm-thick steel for can stock using a butt welding procedure. Very fast partial-penetration autogenous welding speeds up to 67.5 m/min were achieved (Blundell et al., 1995) whereas previous work had found productivity to be limited to 30 m/min. Humping was encountered at high speed but reduced to acceptable levels by adjusting PAW power (used to control the surface profile of the weld bead) with laser power (used for weld penetration).

What became known as hybrid laser/PAW is used predominantly for welding of butt joints in can stock and automotive tailored blank applications (Biffen, 1997) which had used laser welding almost exclusively up to the implementation of hybrid laser/PAW.

Hybrid laser/GTAW has been developed predominantly by ISF at Aachen University (Dilthey and Wieschemann, 2002) for improving laser weld profile in tailor-welded steel blanks for automotive use. Electromagnetic arc control was used to stabilize the GTAW arc in work reported for applications involving 1.2-mm-thick stainless steel sheet (Kim and Suga, 2001).

Study of hybrid laser/GTAW (Hu and Den Ouden, 2003) showed that the combined processes did not increase heat transfer efficiency, but did significantly increase melting efficiency, supported by calculations based on the Rosenthal equation. They attributed this effect to the arc contraction caused by the laser beam. However, it was noted that this effect diminished above 250 A, so is not likely to be high for hybrid laser/GMAW when the welding current for high-speed GMAW will usually be higher. It was found that the arc plasma force and the Lorentz force, the two most

dominant forces for GTAW, are strongly influenced by the GTAW torch inclination. They concluded that the torch inclination has an important influence on the melting rate because of the flow direction of the molten pool. Inclining the torch backwards (torch in front of the laser) favors melting under low current conditions, while inclining the torch forward (in the direction of travel) produces a higher melting rate at high arc current (200 A or above). This effect on bead shape is also true for GMAW so can be used to address the humping defect by maintaining a less convex weld pool by using a lead travel angle in GMAW or laser/GMAW.

Interesting work on hybrid LBW/GTAW has been conducted (Morgan and Williams, 2005) in which conduction mode rather than keyhole mode welding was used for 12.5-mm-thick 2024 Al alloy. In this case welding was, by intention, at slow TS, and conducted with the GTAW torch leading the laser to increase the absorption of the laser power and achieve greater penetration depth. This work, while of limited interest for high-speed welding, serves to illustrate the high level of activity in hybrid laser/arc welding and the innovative methods being investigated in this active field.

2.6 Hybrid Laser Welding - LBW/GMAW

Laser/GMAW hybrid welding has been the most widely studied of the hybrid processes as it offers the most potential for increased productivity and tolerance to fit-up variations typical in most industrial practice. Commercially available systems have been developed by companies including Fronius, Figure 2.11, Fraunhofer (ISF), Cloos, and Daihen.



Figure 2.11 Fronius Hybrid LBW/GMAW Welding Head for Robotic Applications (Fronius, 2005)

One of the limitations of all these welding heads is that the two tools operate in a common plane. While suitable for many applications, this does not allow for innovative solutions which can be developed by using the tools on separately manipulated planes. This is an area that merits further work.

The predominant approach employed to date is to use the laser for penetration and the GMAW wire addition for gap tolerance and joint filling, Figure 2.12. Much of the hybrid LBW/GMAW work has been directed at the shipbuilding and pipelining markets for welding steel plate and pipe products, respectively, by FORCE Technology (Kristensen and Welding, 2003), EWI (Harris, 2008), and Cranfield

University (Yapp, 2008). Probably the best known production application is that at German shipbuilder Meyer Werft, (Herbert, 2004).

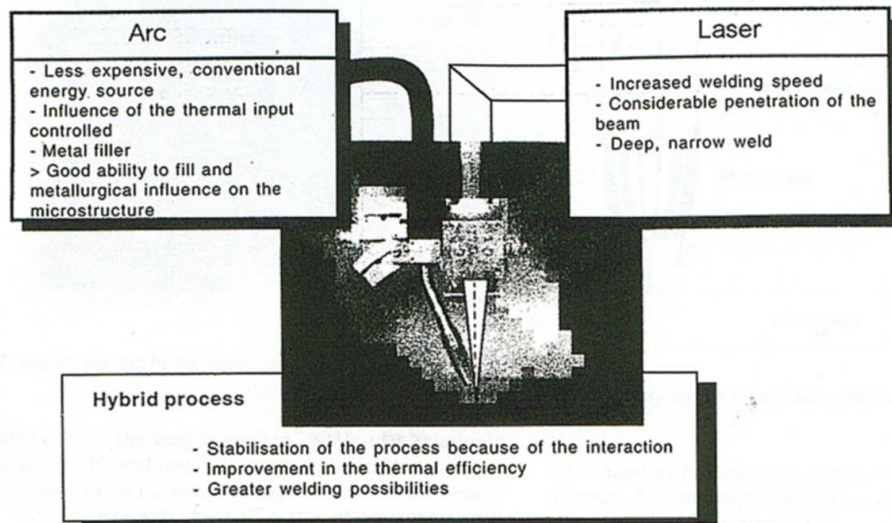


Figure 2.12 Schematic of LBW/GMAW Operation and Features of Hybrid Welding

Significant work has also been conducted in laser/GMA brazing of automotive steel sheet (Dilthey, 2000) and on Al sheet products for BIW applications (Graf, 2002).

Several studies of narrow gap (NG) plate butt weldments made using LBW/GMAW hybrid welding (Abe et al., 1998), [Abe et al., 1998 (2)], (Tusek and Suban, 1999) were reviewed for insight into mechanisms, but this work was applicable mostly to root pass welding of medium-thickness plate. This area was further explored by work with split-beam laser/GMAW of plate (Harris, 2004.) in some preliminary work for narrow-gap welding of steel plate.

(Dilthey et al., 1998) gave a good general overview of the laser/GMAW and laser/GTAW welding processes, operating parameters, and equipment developments including a twin GMAW/laser hybrid head.

A review of CO₂ laser/GMAW hybrid welding and bead-on-plate (BOP) trials on steel plate (Downs and Mulligan, 2002) highlighted the benefits of the process for deep penetration and tolerance to joint gap, but did not address the potential process benefits for sheet products.

Welding of 1-mm steel sheet lap fillet joints at 10 m/min was claimed using 4-kW CO₂ laser power (Petring et al., 2003). These speeds are much higher than reported by any other author and no details were given as to how this was achieved. As such, without any supporting parameters, there is no way to reproduce or verify the claim.

The influence of the laser radiation on the plasma dynamics during laser/GMAW welding has been studied (Aden et al., 1998). Measurements were made that confirmed the arc plasma temperature on the laser irradiated area is increased and thus that the plasma is concentrated by the laser. Temperature measurement in a laser arc

hybrid welding plasma has been conducted (Cho and Na, 2003) and absorption of laser energy by the welding arc has been studied (Hu and Richardson, 2003) and confirmed. Thus, contrary to the concerns of plasma plume interference of the hybrid process by some authors, this work confirms the complementary and synergistic effect of the laser and arc in the hybrid process.

Researchers at MHI in Japan (Ishide et al., 2003) developed a coaxial hybrid welding head capable of Nd:YAG/GTAW and Nd:YAG/GMAW. They investigated the spacing between the arc and the laser in the travel direction and concluded that aiming the arc and laser at the same spot maximized wire heating and minimized penetration compared to aiming the laser 2 mm ahead or 2 mm behind the arc. A welding speed of 1 m/min and a 2-mm penetration depth was achieved using a 3-kW Nd:YAG laser power.

Bratt and Noel, 2004 reported welding of 1.5-mm-thick butt joints for tailor-welded blanks in DP600 AHSS at 4.5 m/min, but struggled to maintain the maximum allowable (20% of material thickness) bead convexity due to poor toe angles on the weld beads. An adjustable twin-spot laser focusing module was used in conjunction with lower GMAW welding current and WFS to reduce the convexity to an acceptable level.

Welding parameter studies for CO₂ laser/GMAW hybrid welding have been carried out on 6-mm carbon steel with a 6-kW laser (Nilsson et al., 2003), (Fellman et al., 2004), and on Type 316L stainless steel with a 10-kW laser (El Rayes et al., 2004) where only BOP studies were carried out. Nilsson reported that the GMAW power was the main effect on weld geometry and quality. Undercut in butt joints was experienced when the arc voltage was high, although a surprisingly high arc voltage range of 30-50 V was used, and no visible undercut was experienced at or below 38 V. Fellman reported undercut on fillet welds in T-butt joints, and this was ascribed to a WFS that was too low, or aiming the wire at the root of the joint rather than more toward the web where the undercut occurred. This indicates that work is needed to control undercut for high-speed hybrid welding.

The use of hybrid LBW/GMAW for improving fatigue life (Farson, 2004) of tee-butt joints in 15-mm-thick plate in the 1F position was reported. With the assistance of welding in the 1F position, weld toe profile was improved and improved fatigue life was demonstrated. The TS used to achieve this was 0.18 m/min. The improved profile of weld toes is well known and well characterized to improve fatigue life through a number of existing methods (Maddox, 1994). As the toe wetting angle increases, producing a smoother transition between the base material and the weld, an increase in fatigue life would be expected. Whether the wetting also occurs at high TS up to 3 or 4 m/min, and the laser power required to achieve this, needs to be investigated.

In reviewing the state of the art for hybrid laser welding Bagger and Olsen (2005) concluded that the ideal thickness to obtain the benefits of the process was greater than 3 mm. Welding of 2-mm-thick steel was also reported at speeds of 3-4 m/min. A welding speed of 3.5 m/min could be maintained for a butt joint with a 0.6-mm gap. This indicates that work on sheet material of 2 mm and less is required to improve the results achieved on these material thicknesses.

A recent paper (Thomy et al., 2006) on high-power fibre lasers highlighted two applications, one of which was butt welding of 4-mm-thick Al extrusions at 8 m/min using 5.5 kW of laser power. Al extrusions 8-mm-thick were also welded at 8 m/min using 10.5-kW laser power. Solid state lasers of 7 kW, 10kW and higher have been available for only the last 2 to 3 years, but clearly demonstrate the rapid pace of welding technology development.

Most recently, laser welding and TIGMAW have been combined to weld automotive components at speeds of 4.2 m/min (Staufer, 2007), the main benefit claimed being increased tolerance to joint gap for butt welds in formed sheet products.

2.6.1 Laser/GMAW and LBW for Galvanized Steel

The use of dual-beam and elliptically shaped Nd:YAG laser beams has significantly improved the performance in the hybrid welding of galvanized and galvanealed sheet steel for automotive BIW applications, Figure 2.13, (Goebels et al., 2003), (Fabbro et al., 2004). Figure 2.13 shows two fibres producing two beams collimated to two spots on the left, and one beam split with a prism and collimated into two spots, on the right (the arrows were not labeled in the referenced paper). This has resulted in significant reduction in porosity and spatter resulting from zinc volatilization in the welding process, particularly in lap-fillet joints. Prior to this only an intentional joint gap setup was considered the solution in terms of weld integrity. This dual-beam approach has not, however, been combined with GMAW.

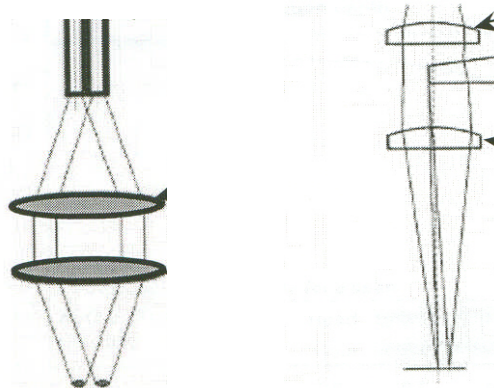


Figure 2.13 Twin-Spot (Dual-Beam) Optics for Nd:YAG Lasers (Goebels et al., 2003)

Use of Nd:YAG/GMAW has been reported (Nakata et al., 2004) for welding galvanized steel. They used a 2-kW laser with a 1.5-mm spot size and a laser to arc distance of 3 mm. An Ar-20% CO₂ shielding gas was used for the GMAW portion. They reported a better performance in terms of reducing pits in the weld metal by using a welding wire with higher Si and Mn which lower the oxygen content and viscosity of the weld metal. Lower viscosity results in higher weld pool fluidity and this is achieved in terms of conventional filler wire availability using AWS A5.18 ER70S-6 wire. Their results correlated well with this expected result.

2.7 Arc Power versus Laser Power

2.7.1 GMAW Melting Rate

The electrical power dissipated in each region of the arc (anode, cathode, and plasma column) is a product of the current flowing in and the voltage across the region. Thus, the simple relationship:

$$Power(Watts) = I \times V \quad (2.1)$$

can be expressed:

$$Power = I \times (Va + Vb + Vc) \quad (2.2)$$

where:

- I = welding current
- Va = Anode voltage
- Vc = Cathode voltage
- Vp = Plasma (arc) voltage.

These regions are referred to as the anode drop, cathode drop, and plasma column.

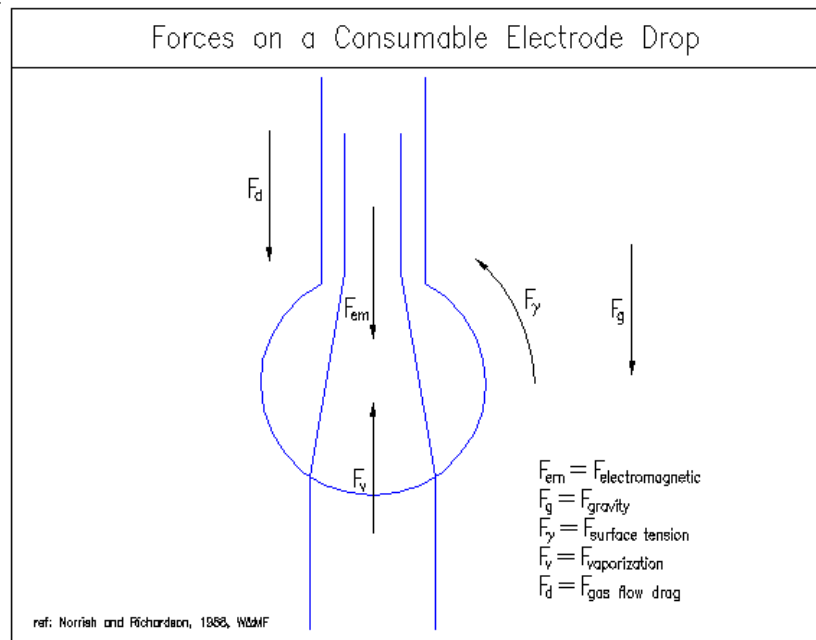


Figure 2.14 Representation of the Forces on an Electrode Drop in GMAW (Norrish and Richardson, 1988)

Norrish and Richardson (1988) concluded that a droplet detaches when:

$$F_g + F_f + F_{em} > F_{st} \quad (2.3)$$

- Of these, F_{em} , F_{st} , and F_g are the most important
- F_{em} is a function of current
- F_{st} depends on material type
- At high current levels, F_{em} dominates, and the drop is pinched off (i.e., spray transfer)

This is illustrated schematically in Figure 2.14 and graphically in Figure 2.15.

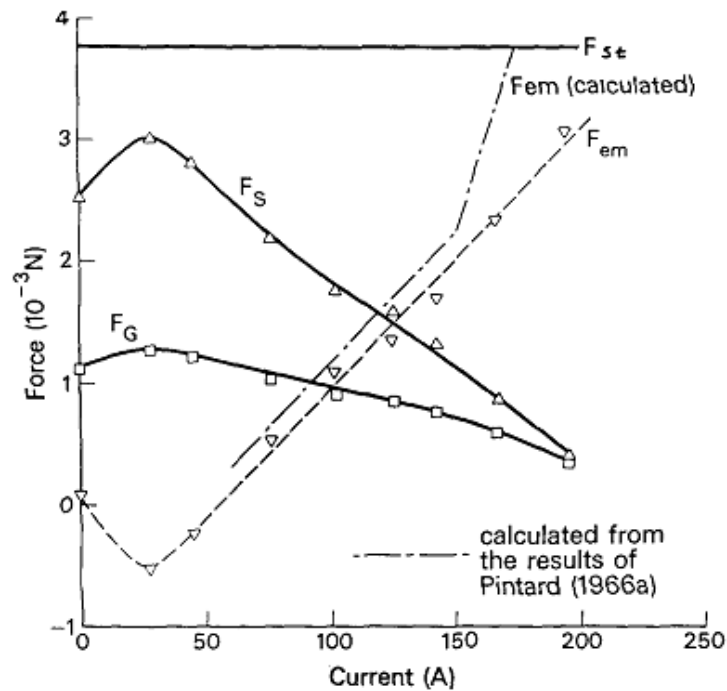


Figure 2.15 Changes in the Forces on an Electrode Drop as the Welding Current Increases (Pintard, 1966)

High current levels are at or above the point where natural spray transfer occurs. Thus, the effect of gravity on the droplet transfer and weld pool is considered less important than the impact of the metal droplets impacting the weld pool. The impact of metal droplets causes the weld pool to oscillate and it is this impact and oscillation which are considered to result in the ‘ripples’ seen on the surface of the weld. The author has seen in HSV of GMAW-P the weld metal clearly oscillate backwards and forwards along the welding direction each time a droplet of electrode material enters the molten weld pool.

For GMAW the anode and cathode voltage drop are relatively fixed. They are a result of the electrical characteristics of the base metal, electrode wire, and the shielding gas. The plasma voltage is a function of the arc length and can be controlled. Most of the arc energy used for melting comes from the voltage drop at the anode or cathode, with substantially more coming from the cathode. When the electrode is the cathode

terminal, considerable influence on the energy is achieved. Energy release at the anode is mostly related to the magnitude of the welding current and the work function of the electrode wire. The plasma column itself contributes relatively little energy in terms of melting the electrode. Therefore, the parameters affecting the plasma column such as arc length and shielding gas have only an indirect effect on the electrode melting rate. In addition to the energy supplied by the welding arc, electrical resistance heating of the electrode by the welding current affects the electrode melting rate. As the heating results from the resistance of the electrode to the current flow it is dependent on Ohm's Law and will be greater with small electrode diameters, long electrode extensions, and high electrical resistance of the electrode. This infers that any work scope to increase melting rate should include CTWD longer than the 19-mm typical for spray transfer GMAW.

The melting rate is the amount of electrode wire melted in unit time. In GMAW it is usually referred to in kg/hr. This effect is significant in GMAW where the use of small-diameter electrode wires, and long electrode extensions result in relatively high resistance, particularly with steel wires, which have high resistivity. The equation for electrode melting rate is typically expressed as shown below (AWS, 2001):

$$MR = aI + bLI^2 \quad (2.4)$$

where

- MR = Electrode melting rate, kg/hr
- L = Electrode extension, mm
- I = Welding current, A
- a = Proportionality constant for anode or cathode heating
- b = Proportionality constant for electrical resistance heating including the electrode resistivity, kg/hr \times A² [squared] mm

2.7.2 GMAW Melting Efficiency

Melting efficiency is the term used to describe the portion of the net energy input, H_{net} , that melts metal. While heat transfer efficiency, f_1 , is a heat source characteristic, melting efficiency is a characteristic of both the heat source and the process of heat transfer in the metal being welded. The melting efficiency for a given set of welding parameters can be determined from the area of the weld, the metal welded, and the net energy input. Measurement of a weld cross section can determine the area of base metal melted, and the area of filler metal added with respect to the original metal surface, such that:

$$A_w = A_m + A_f \quad (2.5)$$

where

- A_w = cross sectional area of the weld metal, mm²
- A_m = cross sectional area of melted base metal, mm²
- A_f = cross sectional area of filler metal added, mm²

For an arc, the melting efficiency, f_2 , (AWS, 2001) is:

$$f_2 = \frac{Q_{Awv}}{(f_1VI)} \quad (2.6)$$

where

A_w = cross sectional area of the weld metal, mm^2
 V = Welding arc voltage, V
 I = Welding arc current, A
 v = Travel velocity of the heat source, mm/s
 f_1 = Heat transfer efficiency
 Q = Melting enthalpy, 10.5 J/mm^3 for steel

Solving the equations for 2-D heat flow in thin plate has been used to predict melting efficiency as follows (AWS, 2001):

$$f_2 = \frac{1}{\left[\left(\frac{8a}{5vw} \right) + 2 \right]} \quad (2.7)$$

where

f_2 = melting efficiency
 a = Base metal thermal diffusivity, mm^2/s
 v = Travel velocity of the heat source, mm/s
 w = Weld width, mm

This equation shows that melting efficiency increases with increasing welding speed. In addition, it predicts that melting efficiency cannot be higher than 0.5 for 2-D heat flow.

2.7.3 Laser Power and Efficiency

Higher arc power compared to laser power has been reported (Denney et al., 2004) to have a very beneficial effect on arc stability through cathode rooting of the welding arc when conducting Nd:YAG laser/GMAW hybrid welding of Ti, Figure 2.16.

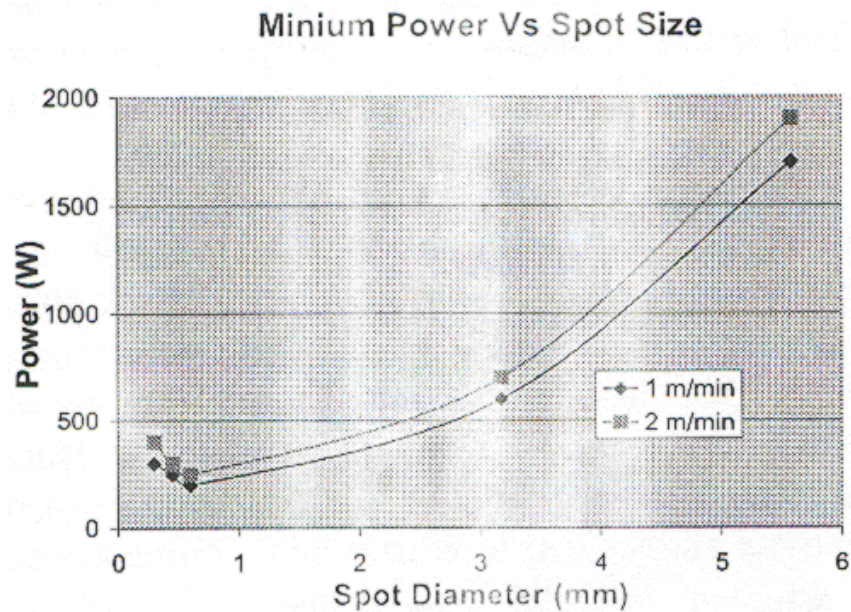


Figure 2.16 Laser Spot Diameter versus Laser Power Required for Stabilization (Denney et al., 2004)

In this case the arc power was about 4 kW while the laser power range was 0.2-2 kW. The laser spot size versus laser power required for arc stabilization is shown in Figure 2.16. The distinct advantage of a lower laser power is lower capital cost for the laser portion of the welding equipment. More efficient and industrially reliable diode and fibre lasers offer future increases in the overall production reliability of the laser/GMAW hybrid welding processes.

Shinn et al (2005) documented the phenomenon of cathode spot stabilization when using low-current GMAW for fabrication of sheet structures in Ti alloys. Using low laser power of 200 to 600 W, the cathode spot of the GMAW process was stabilized by the laser spot providing a consistent arcing point on the surface of the weld pool. At low current with GMAW-only, the cathode spot tends to wander in a left-right manner relative to the welding direction. The arc wandering produces an erratic bead shape, while the laser-stabilized weld has a consistent straight profile. This is an interesting phenomenon, but is much less relevant at high welding current for high-speed welding where the arc force is much higher and the arc has more directionality. The author has direct experience developing pulse parameters and producing all weld metal structure in Ti at high GMAW current (confidential client-sponsored research). In this case the arc force is sufficient to produce consistent bead shape suitable for deposition of multiple passes stacked one upon another when sufficiently shielded with Ar to avoid contamination.

In work performed at EWI (Ream, 2004) three of the four lasers under consideration were available at EWI:

- PRC, 6 kW, CO₂ laser
- IPG, 4 kW, fiber laser (beta unit at 3.8 kW)
- Trumpf, 4 kW, lamp pumped, YAG laser

Data from the fourth laser, a 4-kW disc laser, was generated by Trumpf in Germany.

Partial-penetration, BOP welding was performed on mild steel samples over a speed range of 1 to 10 m/min. Lasers were operated at rated power in all cases. Various focal lengths and focal point positions were evaluated at EWI, and data from the highest penetration conditions were analyzed. The basic set-up conditions for the four lasers are shown in the table below.

Table 2.1 Lasers and Optics Used for Welding

	CO ₂	YAG	Fiber	Disc
Power on work	5190	4000	3640	4000
Focal length (mm)	150	200	200	?
Spot diameter (μm)	na	600	300	200

Metallographic weld cross sections were prepared and imaged for area analysis. Laser welding efficiencies were calculated based on actual power measured at the work:

$$Efficiency = Nugget\ Area \times \frac{TS}{Power\ on\ Work} = \left(\frac{mm^3}{kJ} \right) \quad (2.8)$$

Clearly the volume melted per kJ is not efficiency per-se, but it is a practical measurement of efficiency when compared to the theoretical amount of material which should be melted based on 100 % efficiency. The summary of laser welding efficiencies is presented graphically in Figure 2.17. For Fibre and CO₂ lasers the curves are produced from several data points. However, only two data points were available for the Nd:YAG and the Trumpf disc laser.

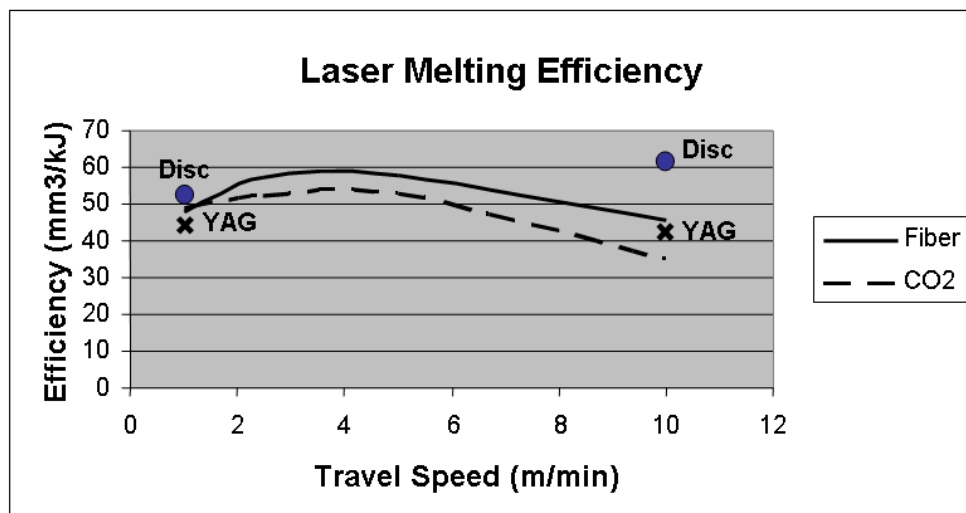


Figure 2.17 Laser Melting Efficiency in Mild Steel (Ream, 2004)

All four lasers produced high efficiency in the mid-speed range, with values to 60 mm³/kJ, which equate to 66% absolute efficiency. This is notably higher than Swift-Hook and Gick's prediction of 48% maximum efficiency, (Swift-Hook and Gick, 1973) In any event it is clear that all four of these lasers can produce nearly optimal melting efficiencies.

Penetration and weld width and hence cross-sectional area are essential considerations for determining process tolerance and robustness. In high-volume applications, such as tailored blank welding, transmission component welding, and BIW lap welding, there will be a minimum weld width or area that is established either by specification or by process reliability requirements. Welding productivity then is the product of area and speed based on the volume of material melted. Therefore, it is possible to predict various combinations of weld width and speed for a given penetration, based on the welding efficiency value.

2.8 Diode Laser

High-power diode lasers have been available on the industrial market for metals processing for only about 7 years in power of 2 kW [Abe et al., 1999 (3)], and have been used for welding of high-strength steel (Ng and Watson, 1999), (Klimpel and Wolnik, 2002).

Since the commercialization of equipment is fairly recent, it is not surprising to see a significant amount of work reported in diode laser applications in recent years, especially at ICALEO 2003 and ICALEO 2004. Using 3-kW laser power, 2-mm steel sheet was butt welded at 1.9 m/min, while 3-mm sheet was butt welded at 0.6 m/min (Salminen et al., 2003). Welding of AISI 1045 steel plate was reported (Schnitzler et al., 2003) using a 1.5-kW laser. Welding was mostly on a gapped butt joint in 5-mm plate and the welding speed was only 0.24 m/min, achieving penetration of up to 2 mm (Sanchez-Castillo et al., 2003).

High-power diode lasers have a wavelength between 800 and 940 nm (Petring et al., 2003), a little shorter than the 1.06 μ m typical of Nd:YAG lasers. This also results in somewhat higher absorption by metallic surfaces (Petring et al., 2003) and assists with conduction welding as used in sheet thicknesses. Typical beam power is up to 3 kW. A 2-kW laser was used to make BOP welds in mild steel and achieved welding speeds of 4 m/min for 1-mm penetration, and 1 m/min for 2.5-mm penetration [Abe et al., 2000 (4)]. Diode lasers with power ranges from 0.5 to 2.5 kW were used to weld thin steel sheets (Bonss et al., 2004). 2.5-kW welds were made at 1 m/min, achieving only about 1.5-mm penetration.

Tomita et al (2004) reported development of a LBW/GMAW hybrid robotic system comprising a 2-kW diode laser and a 200-A GMAW-VP unit to weld sheet metal and automotive components, primarily for Al alloys. A welding speed of 3 m/min was also reported for 1.2-mm Type 304 stainless steel sheet lap fillet joints. No data was presented for carbon steel.

2.9 Fibre Lasers

High-power fibre lasers (greater than 1 kW) suitable for industrial applications in metals processing are a recent entrant to the field of available processes (Rossi, 2000).

Fibre lasers offer potential for significantly cheaper ownership costs compared to the case for even recent entrants to the field of commercial lasers. The floor space footprint of such lasers is considerably smaller than that of an equivalent powered Nd:YAG laser and the laser 'wall plug' efficiency of 20% is considerably higher than the 3% typical of Nd:YAG lasers, resulting in a significant reduction in the requirements for chiller capacity and hence size also. .

Yb fiber-laser technology (1.07- μm wavelength) has been incorporated into the hybrid welding technique, and with the higher electrical efficiency and smaller footprint of these lasers threatens to replace CO₂ (10.6- μm wavelength) and Nd:YAG (1.06- μm wavelength) lasers where flexible automation and higher laser power (above 5 kW) are considered. This emerging laser technology produces equivalent or superior beam quality to current lasers, but has reduced infrastructure requirements for installations (i.e., cooling water, power, floor space), which simplifies implementation into typical production environments.

Work in Europe (Herbert, 2004) reports use of high-power fibre lasers up to 10 kW. The emission wavelength ranges from 1.07 to 2.0 μm so performance equivalence in terms of fibre-optic beam delivery and its use compared to an Nd:YAG laser is comparable for LMW/GMAW hybrid work.

The latest commercially available fibre lasers are at the point where portability and field use of such systems is being seriously considered. One example is for onshore and offshore pipeline construction, and research is presently being conducted in Europe and at EWI for cross-country pipeline applications, enabled particularly by the small size and rugged portability of the high-power fibre lasers, up to 10 kW, available today.

2.10 Weld Bead Humping

With fusion welding including arc welding and laser welding, as the welding TS increases, the progression is as follows:

- Smooth beads
- Uneven beads
- Undercut
- Continuous bead humping (and undercut)
- Discontinuous bead humping

Humping refers to the formation of an irregular weld bead profile characterized by repeating peaks and valleys in the weld metal, and is a defect found in fusion welding processes as the welding speed approaches a limiting value.

The appearance, at successively higher TS, of first continuous and then discontinuous bead humping is illustrated in Figures 2.18 and 2.19, respectively.

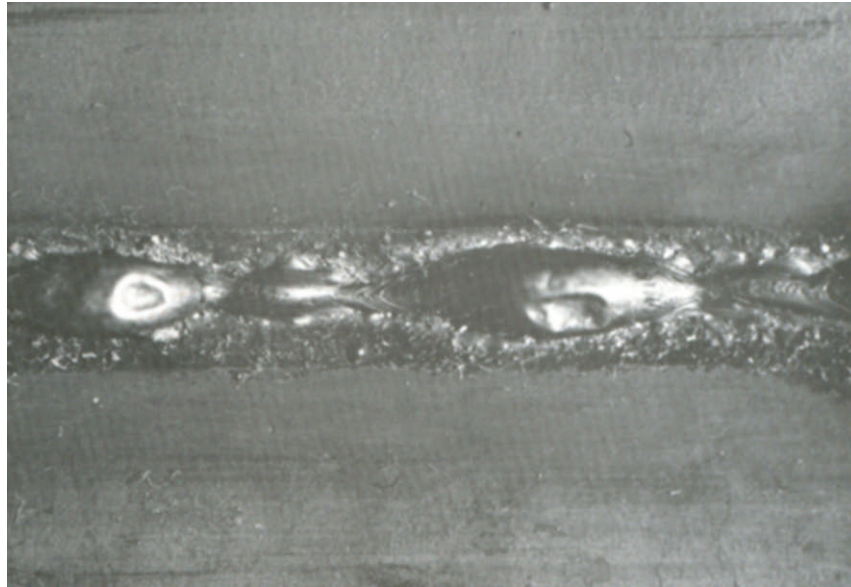


Figure 2.18 Classic Continuous Bead Humping in GMAW-P BOP

In the former case, Figure 2.18, the weld bead, albeit narrower, is continuous between one hump and the next, while in the latter the arc gouged profile can be seen between separated humps of weld metal, Figure 2.19. The welds in Figure 2.18 were made at 2 m/min with 10 m/min WFS, while that in Figure 2.19 was made at 2.5 m/min TS with 10 m/min WFS.

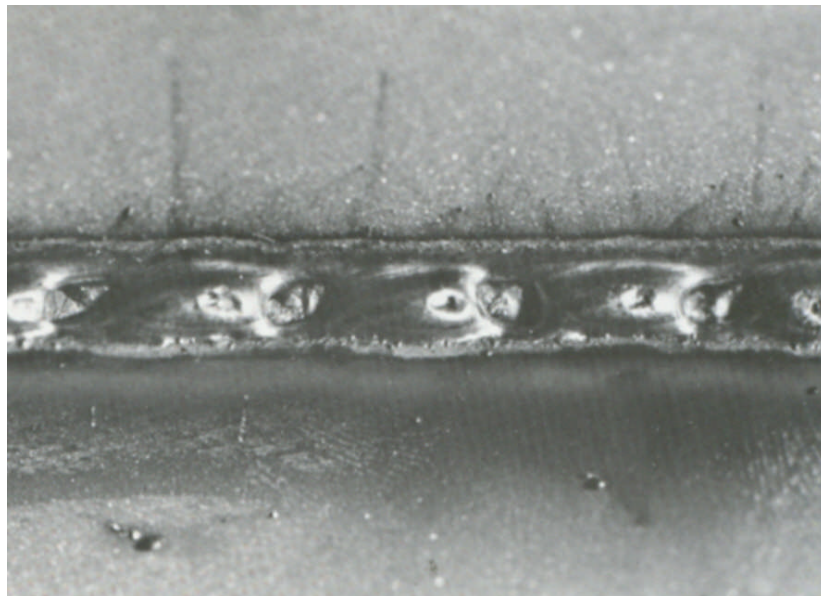


Figure 2.19 Weld Appearance for Classic Discontinuous Bead Humping in a GMAW-P Lap Joint (Paskell, 1989)

The examination of the humping mechanism and its suppression to achieve higher welding speeds for increased productivity is needed to determine the fundamental cause and mechanisms and thus to address a remedy for bead humping. Use of high-

speed video (HSV) is needed for direct observation of metal transfer and weld pool behavior for GMAW and observation of the hybrid LBW/GMAW processes.

No work has been done, and is therefore needed, in the area of laser beam splitting to examine its effect on weld toe wetting of both weld toes simultaneously as a method to overcome weld bead humping for sheet metal applications.

Weld bead humping occurs both in GMAW and LBW, at TS related to maximum weld bead width to length ratios. The observed sequence of events in GMAW is as follows:

1. Circular weld pool
2. Elliptical weld pool
3. Teardrop-shaped weld pool
4. Continuously humping weld pool
5. Discontinuous humping of the weld pool.

The weld pool shape is elongated as TS increases and begins to hump as the weld toe contact angle is reduced below 90 degrees. This has been studied in work on weld bead sizing (Boring and Harris, 2004) and weld bead humping (Harris et al., 2005), from the context of solutions through welding process research and development.

In LBW, humping occurs when TS relative to welding power and weld pool size follows the following sequence (Albright, 1988):

1. Keyhole mode
2. Conduction mode
3. Humping bead in conduction mode

The last mode is analogous to the humping mode in arc welding.

2.11 Weld Pool Dynamics and Humping Mechanisms

The phenomenon of discontinuous bead humping in GMAW was first systematically studied and documented in 1968 (Bradstreet, 1968). Bradstreet used a simple but effective precursor technique similar to weld pool decanting to study weld pool shape and the bead humping phenomenon, whereby the plate was hinged to allow the weld pool to drop out under gravity. His findings from visual observation of weld pool fluid flow are summarized in Figure 2.20, for a weld pool of about 25-mm length. This shows the predominant weld metal fluid flow to be rearward, and also that the unsolidified weld metal, once it reached the rear of the weld pool at the solidification front, travelled back toward the front of the pool.

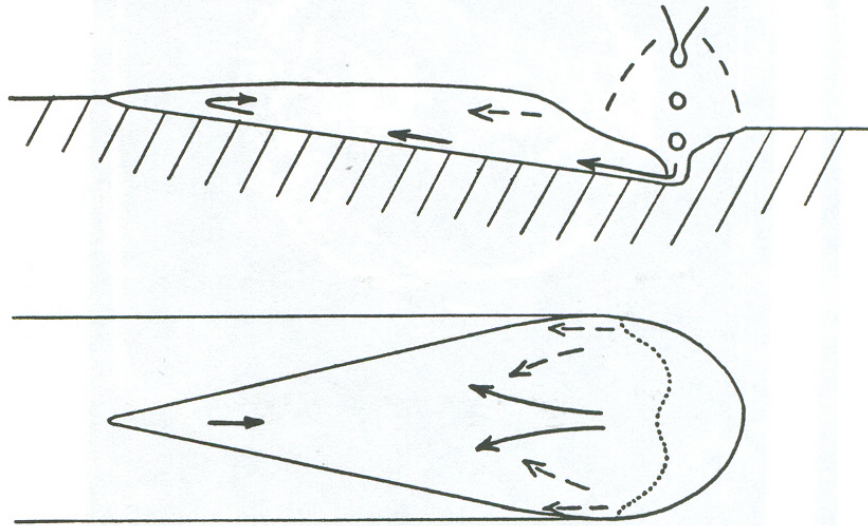


Figure 2.20 Weld Pool Fluid Flow as Observed and Proposed by Bradstreet for High-Speed GMAW (Bradstreet, 1968)

A study of the effect of arc pressure on defect formation in GTA welding (Savage et al., 1979) found higher TS limits before the onset of humping, roughly 1 m/min compared to 0.5 m/min could be achieved by using helium shielding gas rather than Ar shielding. Equipment developed to measure arc force directly found no difference in the arc force measured in the two cases. The arc force varied from 3 g at 100 A up to 15 g at 550 A. They concluded that arc pressure was the dominant mechanism at welding current above 250 A, and surface tension was the cause of defects at welding current below 250 A. This implies that, at least for GTAW, the arc force at higher current can overcome the effect of surface tension as the two compete in terms of weld shape and fluid flow. However, the pool dynamics are considerably more complicated when using GMAW, since the effect of droplet impingement on the weld pool surface is also involved.

The effect of minor amounts of sulphur on weld penetration through reversal of Marangoni fluid flow in stainless steels is well known (Heiple and Roper, 1982). This affect is also caused in steels as well as stainless steels, but is certainly best known and characterized in stainless steels.

Summary work on the phenomena and measurement of weld pool surface tension (Rodwell, 1985) discussed the effect of oxygen content of the weld pool on lowering surface tension and improving weld pool wetting at the bead toes. Weld bead humping and undercutting are normally caused by excessive welding speed that causes the weld metal to solidify before surface depressions created by the arc forces can be completely filled. Surface tension forces control the degree of wetting at the edges of the weld pool, which is improved if oxides are present on the molten weld pool. A low weld pool surface tension promotes good wetting and thus increases the opportunity for the molten metal to refill the groove before solidification occurs. Increasing the oxygen content of the shielding gas from 1 to 5% had an appreciable effect in increasing toe wetting. Since typical shielding gases for GMAW of steel contain CO₂ rather than oxygen, it is worth noting that the oxidizing potential of

oxygen is 2.5 times greater than that of CO₂. Thus a 5% oxygen content has the same oxidizing potential as 12.5% CO₂.

Modeling of phenomena associated with partial wetting (Sekimoto et al., 1987) describes the movement of contact lines at the edges of liquids wet to the surface of a solid. While this has much more in common with wetting of brazing alloys than weld pools, it offers some insight into local instabilities, which have parallels in the weld bead humping mechanism in terms of contact lines at the weld toes, which are not straight, but neck down in the transverse axis between humps.

Significant work on weld profile defects in laser welding (Albright and Chiang, 1988) for sheet steels characterized a number of defect types from cutting and hole formation to undercut, uneven bead, and humping defects. Thin material of 0.13 and 0.25 mm were used along with high welding speeds in the range of 1 to 5 m/min. Laser powers of 450 W to 3.3 kW were used employing a transverse flow CO₂ laser. All welding was conducted in a BOP mode. The results were plotted in discontinuity maps that showed boundary conditions for the various defect types along with regions where smooth (defect free) welds could be produced. As with arc welding processes, smooth beads became uneven, undercut, and then of humped (and undercut) appearance at successively higher TS.

A review (Paskell, 1989) of weld bead humping in GMAW showed that work in the 20 years since that of Bradstreet had not significantly advanced the field in terms of understanding or a solution.

Marangoni convection was proposed as the underlying mechanism for humping (Mills and Keene, 1990) but later work (Gratzke et al., 1992), showed that surface tension, acting in a manner similar to that breaking up a liquid cylinder was an important underlying physical mechanism, and that the length to width ratio of the weld pool was more important, the ratio needing to be less than 10:1 for arc welding to prevent humping.

Heat conduction in finite thickness, i.e., applicable to welding of sheet thicknesses for laser welding was studied (Gratzke et al., 1991) for steel to calculate the fusion boundary position. High-speed laser welding was studied by Albright and Chiang (1988) and characterized a number of welding defects such as humping, undercut, rropy (i.e., uneven) bead shape, cutting and hole formation. For conduction mode welding the molten weld pool increases in length with welding speed and power as is the case in arc welding. They approximated the weld pool to a liquid cylinder as noted in other work involving Gratzke.

Studies on humping effects (Gao and Sonin, 1994) (Schiaffino and Sonin, 1997) showed that the humping instability depends on the conditions at the boundary of the deposit, i.e., the weld toe region, in the case of a weld bead produced by GMAW. They argued, similarly to Gratzke, that the mechanism involved in bead hump formation is the surface tension of the molten metal surface. As TS is increased, the time required for conduction cooling and solidification of the weld deposit is somewhat decreased, but not in proportion to the TS increase. This leads to a molten weld pool with a relatively large length/width ratio, a fluid geometry that is prone to a dynamic shape instability controlled by surface tension. This instability is similar to

the familiar one that causes a thin stream of water falling from a tap to break into droplets. In the case of welding, if the surface tension forces within the weld pool are sufficiently strong, then the bead can develop appreciable humps before cooling freezes the deposit geometry. The humps form as a result of the transverse movement of the molten metal as it tends to neck down laterally driven by surface tension to lower the overall surface energy.

Schiaffino and Sonin in 1997 (2) showed that if the melt and target material (weld pool and base material) are the same then solidification always takes place near a moving contact line, or weld toe. From visual observation, welding forms humps based on a moving contact line as in sketch (b), Figure 2.21, rather than in sketches (a) or (c). This makes sense since naturally a weld solidifies from the fusion boundary into the melt, and the observation takes some account for the shrinkage feature often seen in the surface of the peak of a humped weld bead, based on solidification shrinkage occurring there as it is the last part of the bead to solidify.

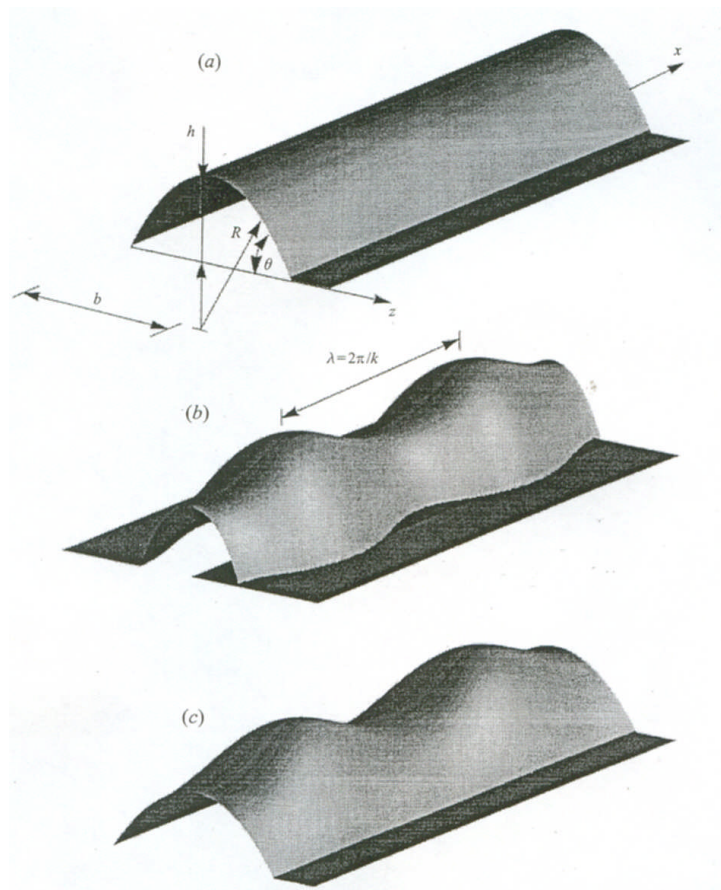


Figure 2.21 Contact Line Behaviour [Schiaffino and Sonin, 1997 (2)]

The Marangoni effects of sulphur in a GTAW pool are well known and have been characterized by many over the years. More recent work (Mills et al., 1998) also characterized the effect of oxygen in terms of slag spots and oxide films. The soluble oxygen is considerably lower than the total oxygen since oxygen readily forms Al_2O_3 in the presence of Al additions in excess of 20 ppm. The soluble sulphur content on the other hand is similar to the total sulphur level unless the steel is Ca or Ce treated.

The combined oxygen has little effect on the surface tension. The situation for GMAW is more complicated since there are more forces at work with the addition of molten droplets from the electrode wire, and as the wire has a sulphur content of its own which may well be different to that of the base material.

The observations of other research (Schiaffino and Sonin,1997 (2)) were interesting in that they noted that Gratzke et al. (1992) rejected the thermocapillary mechanism and proposed that humping was caused by Rayleigh instability, i.e., the breakup of a liquid cylinder by the action of surface and gravity forces. Gratzke concluded that (i), the width/length ratio of the weld pool was the most important factor ,and that (ii) the surface tension does not affect the onset of humping, only the kinetic behaviour. Mills et al. observed that this latter conclusion seems to be inconsistent with the observation that humping is prevalent in high sulphur casts of base metal. Based on the competing findings and opinions of Schiaffino and Sonin, Gratzke, and Mills et al, it seems most likely that surface tension is indeed one of the dominant forces involved in the mechanism of humping. Gratzke's proposed Rayleigh instability theory has some merit, but mostly as it involves the effect of surface tension, rather than gravity.

Work on weld pool dynamics and weld pool fluid flow in the 1980s concentrated mostly on the GTAW process (Kujanpaa, 1983), (Oreper and Szekely, 1984), (Lin and Eagar, 1985), lower welding currents, and significantly lower TS than typical of GMAW. Recent work (Mendez and Eagar, 2003) dealt with higher current GTAW. However, the GTAW process, without the addition of filler metal, is more amenable to analysis than the considerably more dynamic GMAW process. Theoretical work on GMAW (Ushio and Wu, 1997) and contact tip to workpiece effects in GMAW (Kim and Na, 1995) dealt with welding currents up to 250 A, and the latter showed the results of modeling on the weld pool fluid flow, Figure 2.22. This is consistent with the observations of Bradstreet (Bradstreet, 1968). However, no observations were made on the velocity of motion of the weld pool. Work is needed in this area to generate data for the speed of weld metal fluid flow in the weld pool. Such work could be conducted using HSV.

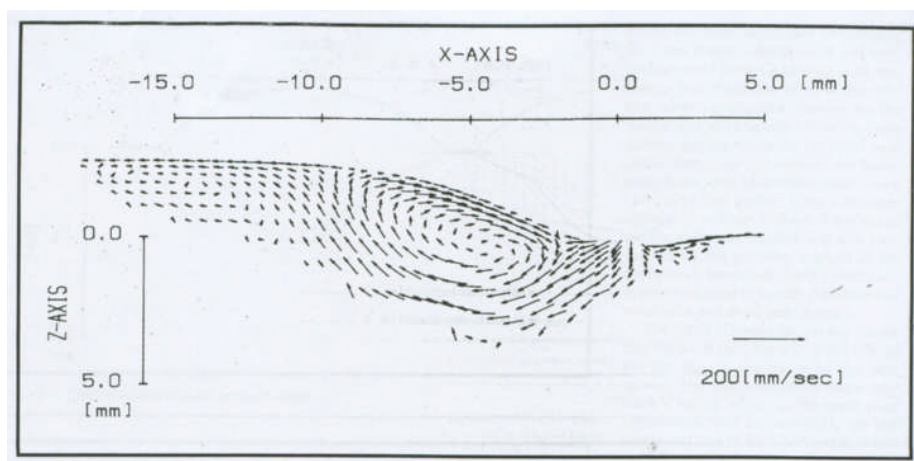


Figure 2.22 Rearward Weld Metal Fluid Flow Including the Effect of Arc Pressure and Wire Droplet Addition (Kim and Na, 1995)

Independent research was conducted and reported (Nguyen et al., 2005) within the timeframe of the author's research. The study is the first one since Bradstreet to address the phenomenon of humping in GMAW in a process-specific and systematic method. The work used LaserStrobe equipment with nitrogen laser backlighting. Video image capture was used to examine the formation of the humps and they concluded that the humping defect was caused essentially by the dominant rearward motion of the weld metal flow. The rearward motion was established by earlier researchers, but does not explain the mechanism by which one hump ends and the next begins. Evaluation and determination of this mechanism is therefore needed. Images presented in the paper show the welding torch was used at a perpendicular angle to the workpiece and weld pool. Suggestions in the conclusions of the paper were made to incline the workpiece 10-degrees downhill to use gravity assistance to overcome the rearward momentum of the weld pool and achieve higher welding speeds. This is considered an impractical suggestion for most applications. However, the use of a leading torch travel angle to alter the process and metal transfer dynamics was absent from their work and needs to be studied to increase the TS for the onset of weld bead humping. A very significant practical factor was that all the welds were made in bead on plate mode, with no evaluation on welded joints. They evaluated Transferred Ionized Molten Energy (TIME) gas and achieved high welding speeds up to 3 m/min before humping. They also used a benchmark of Ar shielding gas which is not a typical gas used for GMAW of steel. The differences in TS for the onset of humping between the Ar-CO₂ shielding gas they used and the TIME gas were not significant for most arc powers, only being higher at 5-kW arc power – 3.6 m/min for the TIME gas versus 2.5 m/min for Ar-CO₂. The ability to minimize humping with a larger weld pool depth has to be balanced with the need to avoid excessive penetration and burnthrough when welding sheet products and is a limiting condition or boundary condition for the upper TS for humping suppression.

Another conclusion of their work was that the metal transfer, known technically as rotational spray transfer, occurred at arc power above 7.5 kW for the 0.9-mm diameter electrode wire, reduced the vertical component of the arc force and caused less arc gouging depth, thus increasing the TS at which humping occurred.

Weld pool decanting was used in a weld pool modeling study (Wahab and Painter, 1997) to determine weld pool shape and the effect of higher welding current and TS on the length and metal flow in the weld pool. Higher currents produce higher arc force and droplet impact on the weld pool. This creates a rearward flow of molten weld metal to the rear of the pool. Thus, as current increases and TS increases, the weld pool lengthens. They determined experimentally through weld pool decanting that the development of a tail on the weld pool is directly linked to welding current and TS.

The possibility of combining LBW with GMA (MIG/MAG) welding was studied, (Choi, Farson, and Cho, 2006) to enable high-speed welding whilst avoiding hump formation in the weld bead. BOP welds were prepared on hot-rolled 1008 mild steel sheet of 1.6- and 2.0-mm thickness. GMA welds were produced using a pulsed power source, ER70S-5 filler wire, contact tip-to-workpiece distance of 22 mm, and Ar or Ar-10%CO₂ shielding gas. In the welds made using the hybrid process, the laser spot (2.0- to 3.5-kW power, 3- to 5-mm diameter) preceded the arc by 3-5 mm. TS, laser power, and laser spot width were varied. Weld bead shape was characterised by

measurements of height and weld toe angles. Weld bead height was compared for welds made by the GMA and hybrid processes. This recently published work used in-line GMAW and laser heat sources to alter the heat input, weld pool shape, and weld pool fluid flow. These researchers found that the humping defect could be reduced at 2 m/min travel speed and concluded that this was associated with increased heating and weld toe wetting, not only capillary instability. The work was a precursor to research conducted as part of the experimental approach in this thesis, where offset laser beam spots were used to impinge the weld toes rather than the centerline of the weld.

2.12 Modeling

Computer modeling (Wahab et al., 1998) has been used to predict weld pool length using 2- and 3-D models for conductive heat flow. Underprediction of weld pool length was attributed to the failure of the models to adequately compensate for convective heat flow.

Modeling of hybrid laser GMAW has been conducted (Zhou et al., 2003); however, the model was based on laser keyhole formation in plate weldments and so is less relevant to laser conduction welding of sheet metal which is of primary interest in this research.

With advances in computational power and weld pool simulation packages such as Flow-3D™ and Fluent™ more recent work (Cao et al., 2004) has dealt with higher welding currents in GMAW that are applicable to the present work and assisted improved modeling of the process. The newly available TRUCHAS software (Telluride project at LANL, 2004) offers high potential for weld modeling, but is only equipped at present for internal, rather than external (arc or laser) heat input simulation for melting, heat treatment, etc. To accurately simulate weld pools in GMAW, and the humping phenomenon, the use of constant volume of fluid (VOF) algorithms, and the ability to model free surfaces, i.e., the surface motion of the weld pool outside the original mesh of the unmelted surface, are critical requirements for the model. Modeling of free surfaces of weld pools (Choo et al., 1990) is important because the shape of these surfaces markedly affects the circulation of molten material in the weld pool. The Fluent™ software can do this reasonably well. Difficulties have been experienced using the Flow-3D™ package in that the use of viscosity is averaged across liquid and solid regions, preventing the appropriate simulation of necking of the weld pool between humps. This can be overcome by the addition to the finite-element modeling (FEM) mesh of a series of elements representing the ‘mushy zone’ adjacent to the fusion boundary in the solid.

The characteristics of commercially available Fluent (Cao et al., 2004) software and the new Truchas (Telluride Project at LANL, 2004) have also been assessed. Flow-3D allows a free surface and constant VOF in modeling the free surface, but the Fluent and Truchas cases do not. Fluent is designed around modeling of castings but does not enable free surface modeling outside the original surface mesh. Presently, the Truchas software does not include algorithms for external heat sources such as welding but deals much better with representing solid and liquid interfaces.

Modeling of humping in relation to humping suppression was carried out using Flow 3-D software. A weld bead humping modeling study was conducted by OSU (Cho and Farson, 2007) using the Flow-3D fluid dynamics software package to model the weld deposit to predict humping formation. A model was created that incorporated the addition of molten metal droplets at an angle normal to the workpiece surface, and was initially based on the findings of others (Cao et al., 2004).

The 3-D numerical simulation of heat, fluid flow, and phase change in pulsed MIG/MAG welding was used to understand the mechanism of hump formation and the way in which the use of a leading laser beam in a hybrid process can suppress the phenomenon (Cho and Farson, 2007). Pulsed MIG/MAG and hybrid-pulsed MIG/MAG BOP welding experiments were simulated; the hybrid process included a defocused laser beam located in front of the weld pool which controls weld shape by increasing the spreading and wetting of the weld pool. The relationship between laser beam intensity, spot size, and bead width was considered. A calculation to determine the critical bead width to prevent capillary instability (which leads to hump formation) was suggested. This work was conducted only for BOP welds and thus does not necessarily represent the conditions for a joint made with faying surfaces.

The modeling work enabled simulated humping to be produced, but was limited by the inability to run the model without an averaging effect in terms of viscosity. This did not allow the transverse necking or pinching effect of the molten weld pool to be simulated. Introduction of mesh elements to create a boundary layer between solid and liquid was undertaken to overcome this. The model simulated heat and arc pressure inputs with traveling Gaussian distributions, accompanied by filler metal droplet addition, Figure 2.23. The latter is not trivial and this is why most modeling prior to this dealt predominantly with autogenous GTAW.

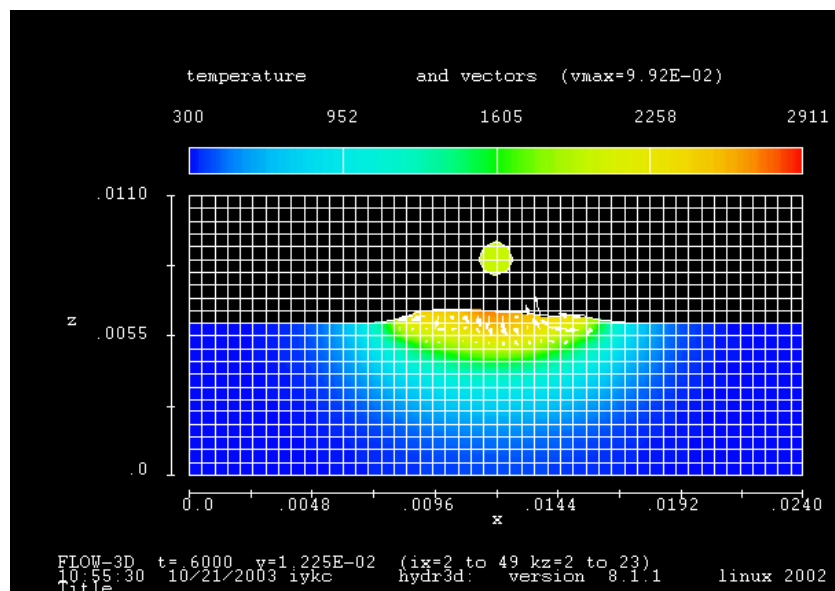


Figure 2.23 Flow-3D Simulation of GMAW-P Droplet Crossing the Arc to the Weld Pool (Cho and Farson, 2007)

Laser heat input was represented by additional Gaussian heat sources with locations displaced from the arc sources. The advantage was that some insights into the hump

formation was gained, and fluid flow in the weld pool, driven by surface tension and wetting was shown to be a significant factor. The simulation results were compared to the experimental results for GMAW. Humping could be simulated, Figure 2.24, but the model could not predict the event that leads to the end of one hump and the formation of the next one. This work remains to be done. Before this can be simulated correctly the experimental work needs to be done that identifies the critical event, the mechanism, that leads to the end of one hump and the formation of the next. Based on the author's firsthand knowledge of the work, the representation of several beads in the paper by Cho (Cho and Farson, 2007), is based on a simple sequential replication of the bead shape shown in Figure 2.24.

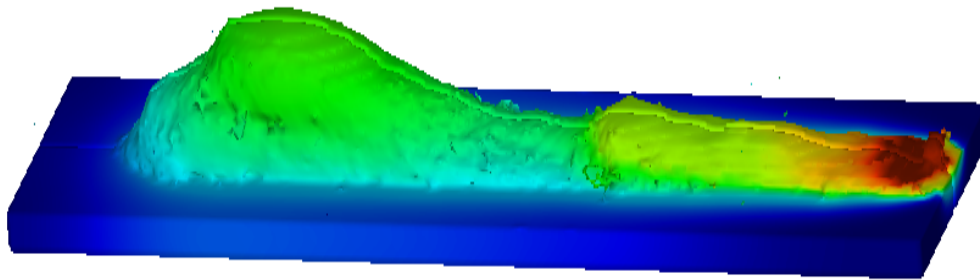


Figure 2.24 BOP Bead Humping Simulation at 2.5-m/min TS and 25-m/min WFS (Cho and Farson, 2007)

Recent associated work (Cho et al., 2006) in the modeling field discussed modeling of a stationary spot weld in GMAW-P. HSV was used to measure the growth and contact angle of the developing GMAW spot weld and this data was used to model the GMA welding process. The addition of a defocused laser spot adjacent to the GMA spot weld was described.

A 3-D numerical simulation of a high peak current pulsed MIG/MAG welding process was developed based on the VOF technique. HSV images from welding experiments on 6.4-mm-thick A-36 steel plate provided data for the simulations (Cho, Lim, and Farson, 2006). Real-time weld pool radius, temperature history and final weld shape were simulated; the results were validated with experimental measurements. The effects of process conditions on the heat and fluid flow in the molten weld pool and on the final weld shape were also investigated. The effects of parameters such as current density, arc pressure, drag force, and Lorentz force on weld shape were discussed. This work was limited to a stationary GMA spot weld in a BOP context, Figure 2.25, and thus does not represent the conditions of a dynamic traveling weld bead, or the condition of welding, for example, a lap joint. The stationary nature of the setup allows the laser spot to heat the base material, form a conduction mode weld pool, and then for this to grow. When it impinges the molten GMAW spot the two weld pools become one, wetting the GMA weld toe as shown at right in Figure 2.25.

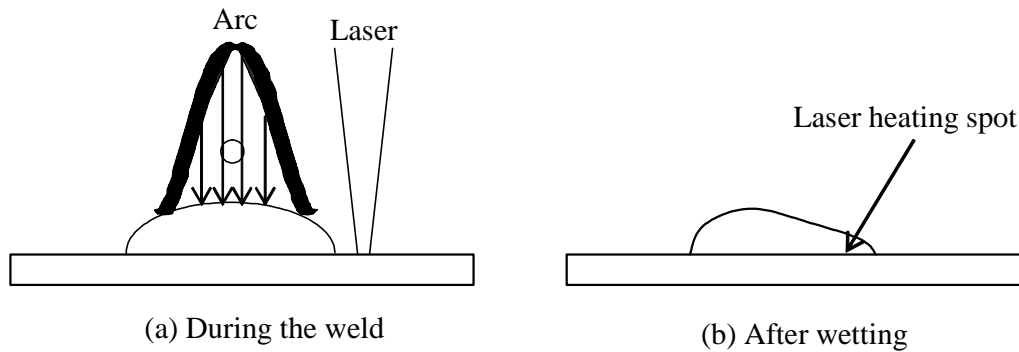


Figure 2.25 Hybrid Welding Process Concept for GMA Spot Welding

Work by Kumar (Kumar, 2006) discussed an attempt at a unified theory for weld bead humping in mechanized GTAW. Humping increases with increased arc current as, with other factors equal the depth of penetration is higher at higher current. This effect has been known for over 30 years and is not new. The most significant conclusions were that use of a leading GTAW torch angle relative to the welding direction suppresses humping while use of a drag angle favors humping; lead and drag angles of 25 degrees were used in the experiments. Thus, the most important conclusion indicated that a leading travel angle assists with the avoidance of humping, or, more particularly, the suppression of the onset of the humping defect to higher TS. However, welding parameters were summarized and TS were generally slow ranging from 0.3 m/min to only 0.7 m/min. The use of a lead travel angle to reduce weld penetration and minimize weld bead convexity has been known for a long time in GMAW (AWS, 1991).

Welding of sheet steel is governed by 2-D heat flow rather than 3-D heat flow. The GMAW process results in the highest heat and penetration along the bead centerline and the wetting angle is controlled by the overall heat input, particularly the welding current and TS, and Marangoni convection, namely the inward, surface tension driven fluid flow within the weld pool. The Lorenz force in arc welding, results in a downward fluid flow within the weld pool, under the arc. The subsequent motion of the weld pool is toward the rear as welding progresses in the opposite direction. The heat input, and particularly the weld speed in relation to the weld pool size, results in the well-known phenomenon of the weld pool shape changing from round to elliptical to teardrop shape as the welding TS is progressively increased. The ability to increase the weld penetration by addition of laser energy is known and used to good effect in welding of plate thicknesses when arranged in axial alignment with the welding arc. There is a need to examine the benefits of non-axial use of laser energy for sheet products.

2.13 Calorimetry

Liquid nitrogen calorimetry is the technique most commonly employed and was established at INEL (Kenney et al., 1998). The technique involves recording weight change due to liquid nitrogen boil-off with time. After welding, the part is immediately dropped into an insulated liquid nitrogen container and the change in

weight as liquid nitrogen boiled off was used to calculate the heat content of the part. Equipment calibration is achieved by dropping the same part at room temperature into the liquid nitrogen, enabling adjustment of the results to compensate for the room temperature heat content of the weldment.

Results obtained by other researchers (Joseph et al., 2003), (Kenney et al., 1998), using liquid nitrogen calorimetry, correlate well with those achieved using the older and more laborious technique involving a water-cooled Seebeck arc welding calorimeter (DuPont and Marder, 1995), Figure 2.26.

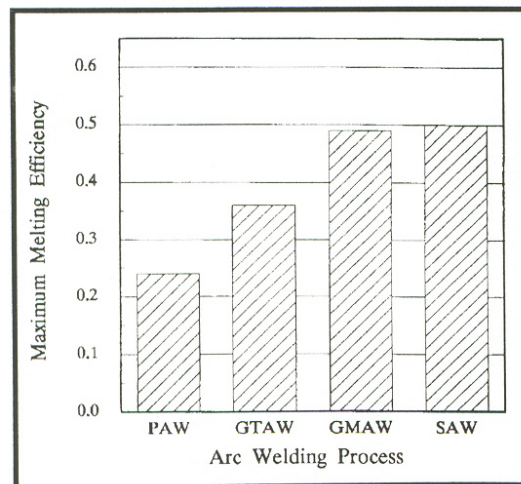


Figure 2.26 Arc Melting Efficiency (DuPont and Marder, 1995)

Work on a new calorimetric technique was conducted (Malin and Sciammarella, 2004) to enable calculation of net power transfer of high-power diode laser beams. Named the Power Measurement Calorimetric System (PMCS) it is capable of taking measurements in 3 min instead of the 6 h needed to collect data in the Seebeck Envelope Calorimeter (SEC). The system was built for PSNS and is capable of measurements for GTAW as well as any commercial laser system. The system is currently in test mode and not available for routine testing.

2.14 Weld Sizing

Sizing of welds for sheet metal is dependent on the joint gap anticipated and has been expressed (Harwig, 2003) in terms of the material thickness and the gap as follows:

Case 1 – Horizontal lap fillet welds with gap

$$A_{HF} = \frac{\pi a(bt)}{4} + G^2 \quad (2.9)$$

where:

A = weld deposit area

t = sheet thickness

a = normal leg, t + G

G = gap
 b = parallel leg factor, 2.0 to 4.0

Therefore, the substitutions can be made resulting in the following equation:

$$A_{HF} = \frac{\pi(t+G)bt}{4} + G^2 \quad (2.10)$$

Case 2 – Vertical-down lap fillet welds with gap

$$A_{VDF} = (ab) - \frac{\pi a(bt)}{4} + G^2 \quad (2.11)$$

Therefore, with joint parameter substitutions the equation becomes:

$$A_{VDF} = (t+G)bt - \frac{\pi(t+G)bt}{4} + G^2 \quad (2.12)$$

Case 3 – Flat fillet with gap

$$A_{FF} = 0.5(t+G)^2 \quad (2.13)$$

Case 4 – Horizontal T-joint fillet welds with gap

$$A_{HTF} = 0.5l(l+G) + G^2 \quad (2.14)$$

where l = leg size of fillet

For lap and T-butt joints having no gap, both Cases 3 and 4 can be simplified to:

$$A = 0.5t^2 \quad (2.15)$$

This is a straightforward way to calculate the smallest theoretical mitre fillet weld cross-sectional area, and can be used to size fillet welds for both lap-fillet and T-butt joints.

For a mitre fillet weld, the theoretical minimum weld size represented using the simplified case above, and ignoring the weld penetration area, is:

- 1.3 mm² for 1.6-mm sheet
- 2 mm² for 2.0-mm sheet
- 2.9 mm² for 2.4-mm sheet

Clearly, it is not possible to produce such a small weld area in practice, but the aim of producing the smallest practical bead size and highest welding speed that can be obtained without humping formation is a reasonable goal. Bead size can reasonably be based on a ¼ ellipse when determining WFS/TS for parametric development of fillet welds for lap and T-butt joints.

Strategies such as SWAT (Green, 2001) involve plotting WFS against welding TS and using the desired outcome in terms of weld quality to determine a window or tolerance for welding procedure robustness. The ratio WFS/TS gives a measure of weld size. Once a preferred weld size is determined, the ratio can be maintained to increase productivity by increasing both WFS and TS, but maintaining the same ratio.

2.15 Gap Weldability

Prior operations in the fabrication sequence such as cutting and forming typically lead to gaps in weld joints. Flexible and fairly gap tolerant welding processes such as GMAW have traditionally been expected to cope with these gaps in the welding operation.

The wire-fed arc welding processes are most tolerant to gaps as filler material can be deposited to bridge the joint gap.

Measuring process capability to cope with joint gaps is not a new idea. The driving force for the development of a standard method of measuring process capability with respect to joint gaps is the ability to quickly select an appropriate weld size based on the gap condition and highlight productivity benefits if gap can be reduced. Standards typically characterize the acceptable gap limits for a specific joint configuration and material thickness. Although the tolerances vary with the specific standard, such as AWS/ANSI D8.8-97 'Specification for Automotive and Light Truck Components Weld Quality – Arc Welding', (ANSI/AWS D8.8, 1997), and the 'Structural Welding Code – Sheet Steel', ANSI/AWS D1.3-98 (ANSI/AWS D1.3, 1998), the acceptance criteria are uniform; i.e., there should not be excessive undercut, burnthrough, or overlap present in the finished weld.

Harwig (Harwig et al., 2000) used the parallel shim technique for the GMAW-VP and GMAW-P welding of 1.6-mm mild steel lap joints. The weld trials started on a constant joint gap equal to the thickness of the material (1T) to be welded. Harwig experimented with two GMAW-VP power supplies and compared the results to GMAW-P for the same materials and joint setup. Visual inspection was used to determine the acceptable weld range. The maximum welding speed achieved with the GMAW-P process on steel was 0.76 m/min. The GMAW-VP process achieved 1.27 m/min on the same joint, representing a 67% increase in productivity with steel compared with GMAW-P. This increase can be attributed to the characteristics of the GMAW-VP process, producing large welds with minimal penetration, which is preferred when welding on sheet metal with gaps.

Richardson (Richardson et al., 2002) also used parallel shims. Richardson produced GMAW welds on 1.6-mm Type 409 stainless steel lap joints using metal-cored wire with a constant joint gap. The gaps ranged from 0 to 1.6 mm using a 1.2-mm-diameter wire.

2.15.1 Tack Welds

Tack welding can be used to maintain a preset gap during welding. The tack also maintains the location of the two base materials, relative to each other, in 3-D space. As with shimming, weld tacking can be applied to many joint types.

Experiments carried out on butt joints in 1.0- × 0.8-m sheets of mild steel using a laser welding process (Makhnenko et al., 1997) resulted in difficulty in maintaining zero gap during the welding process. Research was performed to determine the effect of tack weld spacing. Reducing the tack spacing from 0.2 to 0.1 m, at the same 3.3-kJ/mm heat input and 1.8 m/min TS, the maximum deflection of the butt joint edge changed from 2.2 to 0.6 mm. Using tack welds, the gap opening could thus be significantly reduced. However, in the case of precision welding, the required distance between the tack welds is very small. The small spacing is needed because of the intolerance to joint gaps in autogenous laser welding.

Tack welds have the significant disadvantage of the time taken to make the welds, and for a single-pass weld on sheet metal structures, the presence of a tack is a profile irregularity that can lead to defects associated with welding over a tack at high welding speeds. For high-speed welding, use of appropriate tolerances on cut parts and good fit-up along with appropriate fixturing to eliminate gaps as much as possible, is considerably more preferable to facilitate successful high-speed welding.

2.15.2 Self-Fixturing

A precision-cutting technique has also been used to maintain a gap. This method used a laser to cut base material into shapes that were placed together in an interlocking 'puzzle piece' orientation. The parts were then shape locked thus avoiding thermal expansion of the gap during welding. An illustration of the precision cutting technique is shown below, Figure 2.27.

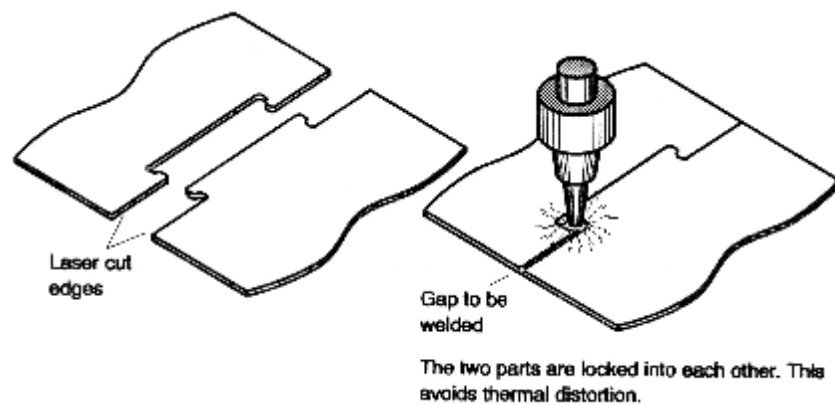


Figure 2.27 Principle of Self-Fixturing of the Weld Components (Kristensen et al., 1994)

The self-fixturing technique was applied (Kristensen et al., 1994) to a butt joint using 1-mm mild steel cut with a laser. The technique is started on a no gap condition to establish a stable keyhole and then traverses a constant joint gap. The major limitation of the technique is that it is only suitable for butt joints. The shape fitting of the pieces restricted movement in the horizontal direction, while the mild steel sheets were limited in the vertical direction by magnets. Some deformation from the heat-affected zone was evident, however, the sheets were joined in a plane without any deformation.

A more practical approach for self-fixturing is a tab-and-slot process patented by Caterpillar, in which a slot is cut in one member and a tab on another. The tab is pushed through the slot in the assembly and the tab is then twisted to lock the materials in intimate contact without joint gap, Figure 2.28. This technique can be used for sheet metal and plate products.

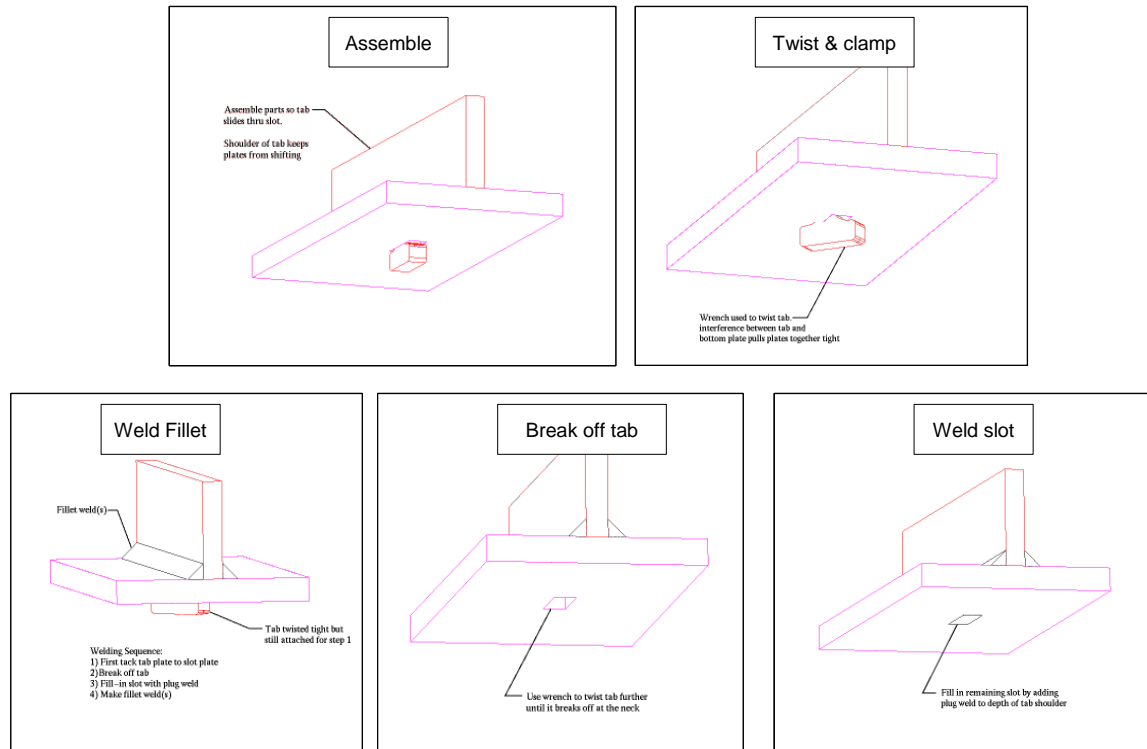


Figure 2.28 Tab-and-Slot Assembly Procedure (Caterpillar)

2.16 Brief Summary of Papers and Conference Presentations by the Author During the Course of this Research

I presented a paper in an automotive AI session at the ASM Fall Conference in Columbus in 2001 (Harris, 2001).

I presented a paper at the Sheet Metal Welding Conference X in Detroit in 2002, (Harris, 2002) based on weld sizing and procedural tolerances for robust production welding with GMAW-P and GMAW-VP.

As a result of work on hydroformed gas tanks, I was invited to an AISI/SASFT meeting defining and discussing alternative joining technologies for 'next generation steel gas tanks, held in Detroit in July 2002.

EWI Members Reports were completed in early 2004 on EWI Project 44634IRP 'Weld Sizing and Gap Weldability for Arc Welding Production Robustness in Sheet Metal' (Boring and Harris, 2004) and in 2005 on EWI Project 47412GTO 'Hybrid Laser-GMAW Welding for Sheet Metal and Fill Passes on Plate' (Harris et al., 2005). OSU was funded to conduct some of the latter work on behalf of EWI, directed and managed by the present author.

A paper on LBW/GMAW hybrid welding with the LBW aimed at the weld toes for increased wetting, based on the results of my research, was presented at the AWS Annual Convention in April 2005 (Harris, 2005). This led to three commercially sponsored projects worth over \$100,000 with the heavy fabrication industry for high-speed hybrid LBW/GMAW of steel products.

2.17 Summary of the Literature Review and Work Scope in the Thesis Research

A summary of known items from the literature review is as follows:

- Weld bead humping limits welding travel speed
- Existence of weld bead humping is documented
- Several theories exist but there is a lack of current practical solutions in the literature
- Modeling of the humping event has been conducted, but this, at best, is based on bead on plate work and does not identify the key event between one hump and the next.

A study of weld bead humping was first documented by Bradstreet (1968) but little work was done in the following 25 years. In studying the formation of the humping defect, the observations of (Schiaffino and Sonin, 1997 (2)) were interesting in that they noted that Gratzke et al. (1992) rejected the thermocapillary mechanism and proposed that humping was caused by Rayleigh instability, i.e., the breakup of a liquid cylinder by the action of surface and gravity forces. Gratzke concluded that (i), the width/length ratio of the weld pool was the most important factor, and that (ii) the surface tension does not affect the onset of humping, only the kinetic behaviour. Mills et al. observed that this latter conclusion seems to be inconsistent with the observation that humping is prevalent in high sulphur casts of base metal. Based on the competing findings and opinions of Schiaffino and Sonin, Gratzke, and Mills et al, it seems most likely that surface tension is indeed one of the dominant forces involved in the mechanism of humping. Gratzke's proposed Rayleigh instability theory has some merit, but mostly as it involves the effect of surface tension, rather than gravity. Surface tension affects wetting angles both in brazing and welding. It seems likely that anything in the welding process that promotes good wetting and higher contact angles between the base metal and the weld will work to reduce the humping defect. Therefore, although the welding fraternity does not understand the phenomenon, the answer would seem to lie in further study of weld geometry, viscosity, and weld toe wetting. This is the basis for the area of study conducted in this dissertation.

There is evidence (Choi et al) that use of lasers along with GMAW-P can increase the wetting angle of a spot weld, and that some increase in toe wetting angle can be achieved in large fillet welds at slow to moderate travel speeds. However, there has been no work to evaluate the effect of lasers directed at the weld toes for small fillet welds in sheet materials. It seems reasonable that, with sufficient power density, this can be achieved.

A summary of the experimental work needed is as follows:

- Weld sizing for sheet metal to minimize over-welding and excessive distortion
- Examination, using high-speed video (HSV), of weld bead humping mechanisms at high travel speeds that explain the event occurring between the end of one bead hump and the beginning of the next
- Practical solutions for high-speed welding of sheet metal without humping are needed.

Even fairly recent research (Harwig, 2003) has continued to discuss the limitations of CV GMAW and GMAW-P for high-speed welding of sheet products, characterizing it as between 0.5 and 1 m/min. Based on this characterization, GMAW-VP has been reported to have productivity twice that of GMAW-P (Harwig, 2003). This limitation needs to be evaluated experimentally, and the results achieved with GMAW-P need to be applied to laser/GMAW-P hybrid welding for high-speed fillet welding of lap and T-butt joints.

The productivity of GMAW, GMAW-VP, GMAW-P, TGMAW, and LBW/GMAW hybrid processes have been reviewed here as a context and benchmark for the present research. There is contradictory evidence on the relative productivity of GMAW, GMAW-VP, GMAW-P as noted above, depending on whether one is welding on joints with significant gaps, or on joints with good fit-up. Certainly GMAW-VP has good gap bridging capabilities, but the typical 200-250 A current limit for these power sources makes them of limited use for high-speed GMAW.

Much work has been conducted over the years in the field of welded design for plate structures in terms of fillet weld size requirements. By comparison, little effort, or published work exists in weld sizing for sheet metal structures. Part of the reason for the latter is that sheet products are generally characterized as having thicknesses of 3 mm or less, and that GMAW of fillet sizes smaller than 3 mm is relatively difficult, even for mechanized welding. The area of interest in terms of material thickness is 2 mm and less, as this thickness range is less well suited for welding by conventional processes at high speeds.

In the past, the tendency of over-welding fillet sizes has been less of an important issue, but with the trend toward thinner and higher strength steels, and the continuing emphasis on productivity and global competitiveness, higher welding speeds and reduced distortion are ever more important to reduce cost while meeting the required welding quality standards.

Based on this literature and industry review, the intent was to test and develop the thesis that modification of fluid flow within the GMAW-P weld pool using laser beams can suppress the onset of bead humping by increasing the wetting angle at the bead toes, thus increasing the maximum speed and productivity for production of fillet welds in GMAW-P. It is anticipated that the laser power required to achieve this will be lower than that typically used in 'conventional' LBW/GMAW as the laser energy will be directed at the weld toes, rather than in alignment with the axis of the welding arc. A study using HSV recording, to examine the humping defect formation in GMAW-P is needed to gain further insight into the mechanisms and use this in conjunction with weld bead toe wetting with lasers to suppress the humping defect to higher welding speeds.

Although there has been significant work on weld pool fluid flow and modeling of bead humping over the years, almost all of it has been conducted with GTAW. In contrast, there has been very little study of humping in GMAW. The work by Bradstreet in 1968 was the first to study this in any detail. However, little significant further study is reported until that recently reported by Nguyen et al. in 2005. Although this work used a LaserStrobe technique to examine metal transfer, it involved little direct viewing of the weld pool dynamics and fluid flow. Hence, a study of the mechanisms for formation of bead humping using HSV is needed to investigate this.

Looking beyond mechanisms, little work has been done to provide practical welding solutions and welding parameters establishing higher welding speeds. Thus, this was also an area requiring more work and in which new knowledge has been added to this field.

Work reported to date has been done with bead on plate only and has not progressed to look at practical welded joints. The work scope presented in this thesis addresses this often overlooked area, addressing differences in weld pool behaviour in this situation.

Work reported to date has been done on plate, and there is no work found in the literature on humping in sheet metal for GMAW. As such, this thesis research involved conducting trials to generate and evaluate weld bead humping in sheet metal joints where the weld pool depth is, by necessity, shallow. Deeper weld pools in sheet products lead to GMAW 'cutting' as the weld penetrates completely through the sheet. The balance between adequate penetration while avoiding cutting is quite fine when welding on sheet metal.

The bead humping defect has been responsible for the limitation of GMAW and GMAW-P to 1-m/min TS for the welding industry at large. There is a need to demonstrate that the process is capable of higher TS using modifications to the welding setup and parameters that have not been adequately developed or demonstrated to date. This work was also planned to develop and also publish suitable welding parameters that can achieve twice the welding speed, 2 m/min, typically attributed to the GMAW process.

A lot of studies of pool dynamics have been carried out, especially in GTAW, but little work has been conducted with GMAW. The situation for arc physics, process modeling, and other aspects is complicated considerably when molten metal is added to the scenario in the form of metal droplets crossing the arc and impacting the liquid weld pool. In the past, modeling in particular has been confined almost completely to GTAW based on the complexity and computational power needed to address GMAW. This has changed in the last few years based on high processing power of modern computers outside of the supercomputers.

3.0 RESEARCH AIMS AND OBJECTIVES

The main issues for high-speed welding lie in the three areas; namely,

- Weld sizing for sheet metal
- Weld bead humping mechanisms
- Lack of current solutions

The key event that leads to the end of one hump and the formation of the next needs to be determined experimentally. Before this can be simulated the experimental work needs to be done that identifies the critical event that leads to the end of one hump and the formation of the next.

The aims and objectives of this work were to generate useful new knowledge and understanding in the field of high-productivity sheet metal welding, and provide a new contribution to knowledge in this field. The two main needs, based on the review of literature, were to study the mechanisms for weld bead humping, and to use this knowledge, combined with hybrid laser welding with both Nd:YAG and CO₂ lasers for very high-speed welding applications on sheet products to significantly increase the welding speed achievable without humping.

This research, conducted to support the thesis for improved productivity through humping characterization and suppression, was designed to show the effect of the following:

1. Joint gap variation from 0T to 1T for conventional GMAW-P.
2. The ability to increase this speed using known welding engineering concepts for 0T gap joints
3. The use of GMAW-P with leading torch angles to control bead shape

and then to apply some new concepts and experimental techniques, namely:

1. Use HSV to examine the formation of bead humping in the liquid weld pool
2. Use offset laser beams (rather than in-line laser and GMAW heat sources) to affect the wetting of single-pass GMAW beads to suppress the humping defect characteristic of high-speed GMAW
3. Use transverse beam splitting of CO₂ and Nd:YAG laser beams to wet both the weld bead toes of high-speed GMA welds

using as a basis a process of emerging commercial interest called hybrid laser arc welding (LBW/GMAW), also known as HLAW.

However, using the laser energy predominantly to change the toe angle of the weld pool has not been previously investigated. This technique was used in the present work by intentionally directing the laser energy to one or both of the weld toes, with the aim to increase the superheat and fluidity of the weld pool and thus increasing the contact angle and wetting between the weld bead and the parent material such that higher welding speeds could be obtained before the onset of weld bead humping.

The concept of using offset laser beams and dual, transversely split, laser beams to wet the toes of moving arc welds is also a new concept. Through the research presented here it was intended to suppress the humping defect, and develop understanding of the mechanisms involved.

A long-standing aim has been to reinforce, through research and resulting data, the idea that GMAW, and GMAW-P is a useful tool for high-speed welding at speeds above 1 m/min.

4.0 EQUIPMENT AND MATERIALS

In developing the thesis associated with weld bead humping and its mechanisms HSV data collection and analysis of pool dynamics was conducted to compare mechanisms for BOP welds and lap-fillet welds. To achieve this a series of experiments were conducted concerning humping in the following cases:

- Conventional GMAW with gaps ranging from 0T to 1T to determine appropriate weld sizes
- Increasing welding speeds achieved without humping by changes in welding parameters using GMAW-P
- Use of single- and dual-offset laser impingement at GMAW-P weld toes to alter weld toe wetting angles and fluid flow in the weld pool to suppress bead humping to higher TS
- HSV data collection and analysis of pool dynamics to compare mechanisms for BOP welds and lap-fillet welds

The welding equipment, data acquisition hardware, and materials are described below.

4.1 Welding Process and Equipment for Weld Sizing

The weld samples were produced and the welding parameters were recorded using the following equipment:

- ESAB Digipulse 450i GMA welding power source, Figure 4.2
- ESAB Digipulse wire feeder, Figure 4.2
- CRC – Evans ADM Data Monitor 3 with Epson printer, Figure 4.2

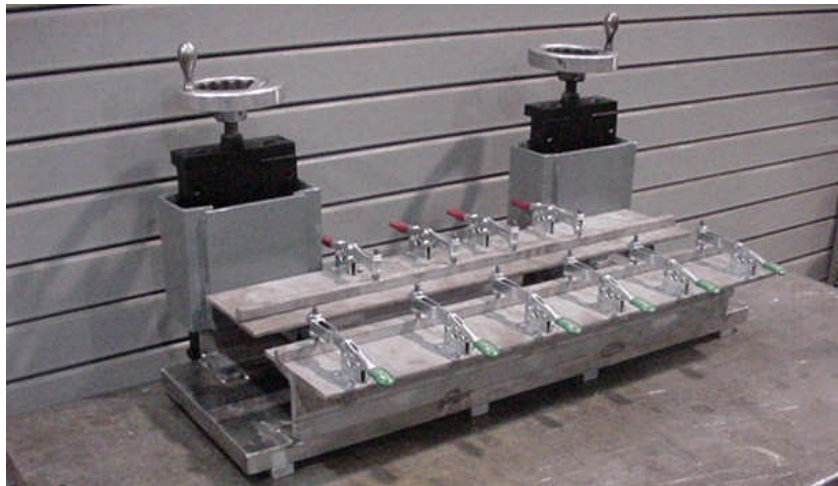


Figure 4.1 Standard Fixture for Lap-Fillet Joints



Figure 4.2 Welding Power Supply and Wire Feeder (left), Data Acquisition System (right) used for Gap Weldability Testing

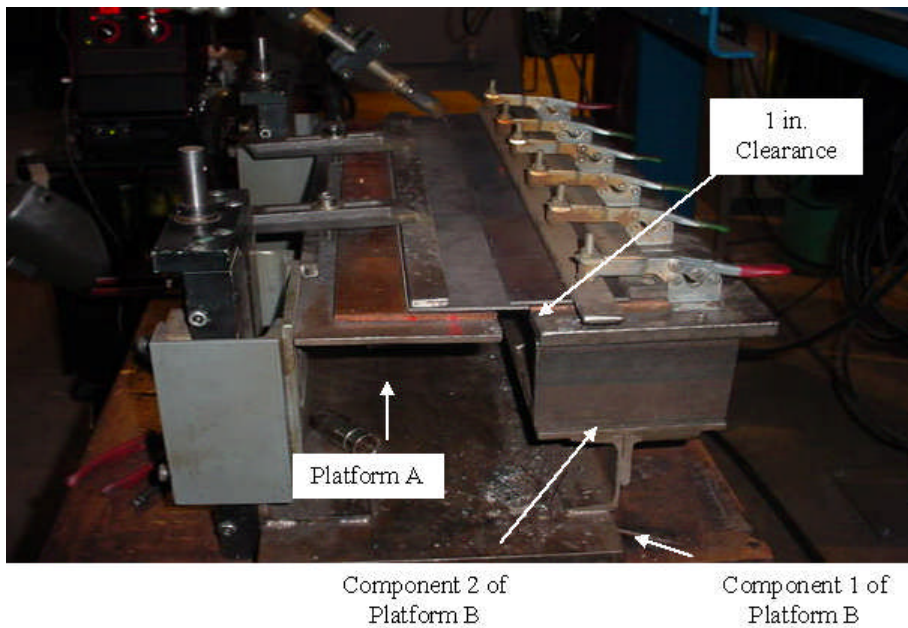


Figure 4.3 Assembled Variable Joint Gap Weldability Fixture

The main components of the new fixture design are two platforms connected to a base plate. The design of the fixture allowed for one platform to move independently of the second, allowing for any type of gap geometry. The first platform, Platform A, is the variable component of the fixture and can be moved vertically. The platform is a 660- × 125- × 6-mm piece of mild steel. Two 300- × 100- × 6-mm Cu plates were screwed into the top of the platform. The joint member was clamped to the platform by two clamps that apply force to a 610-mm-long steel hold-down bar. This applied enough force to restrict the plates from moving during welding.

The vertical slides allowed for either side of Platform A to move 115 mm vertically while the other end of the platform did not move, which gave the fixture the ability to produce variable gaps. Figure 4.4 shows the completely assembled variable joint gap weldability fixture. The weld is made between the top sheet where the wire is aimed, and the lower clamped sheet.

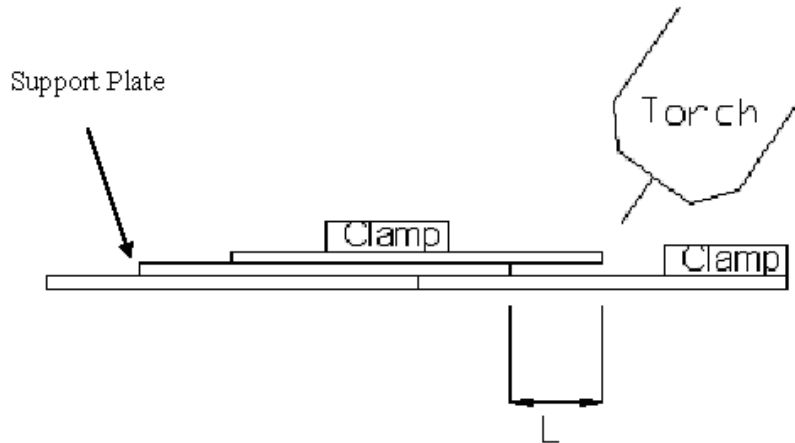


Figure 4.4 Side View of Joint Setup Showing 1T gap Introduced at the Weld Region

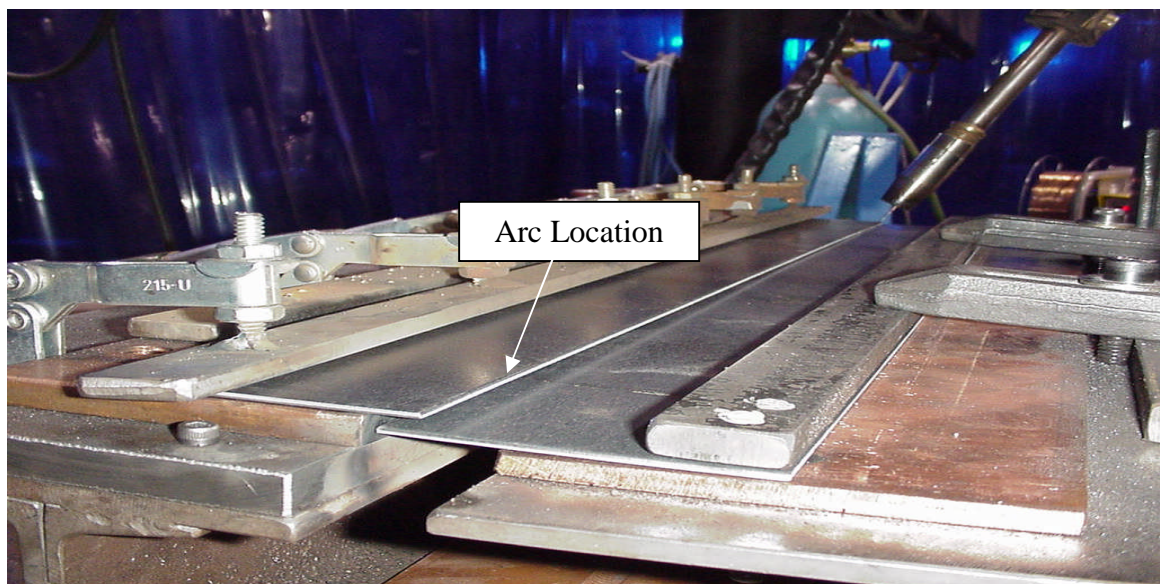


Figure 4.5 Gap Geometry for DOE Trials

A calibrated Hall Effect current shunt was used for measurement of welding current and the arc voltage signal was taken by a lead connected within the welding torch, as close as feasible to the arc. Voltage drop at this proximity is negligible, less than 0.1 V.

GMA WFS measurements were taken using a calibrated WFS sensor mounted just before the drive rolls in the four-roll drive system in the wire feeder.

Shielding gases for welding were supplied from standard K size cylinders from commercial suppliers. Pressure and flow rate were controlled by two stage regulators.

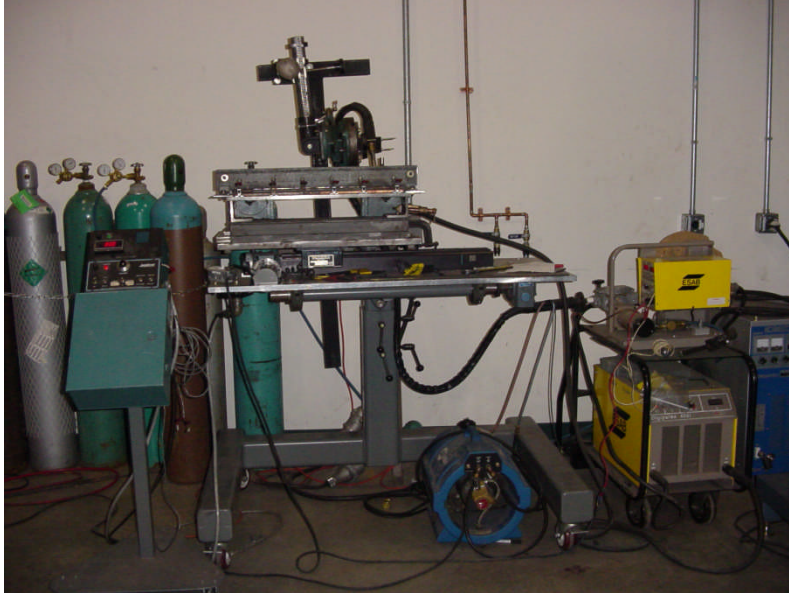


Figure 4.6 Equipment Set-up for High-Speed GMAW-P Welding Trials to Establish Humping Limits

4.2 Trumpf Programmable Focusing Optics PFO

The Trumpf Programmable Focusing Optics (PFO) scanning head galvanometers are limited to 1 kW of laser power. This system uses a high-bandwidth scanning mirror system Figure 4.7, which can be mounted to a robot or CNC system, to provide highly flexible laser beam delivery capability, Figure 4.8. Although dual-beam welding has been employed to enlarge a laser weld pool to avoid porosity from zinc fuming when welding coated steel sheet (Forrest and Lu, 2003) a rastered laser beam, used to affect weld bead shape and wetting, had not been studied before.

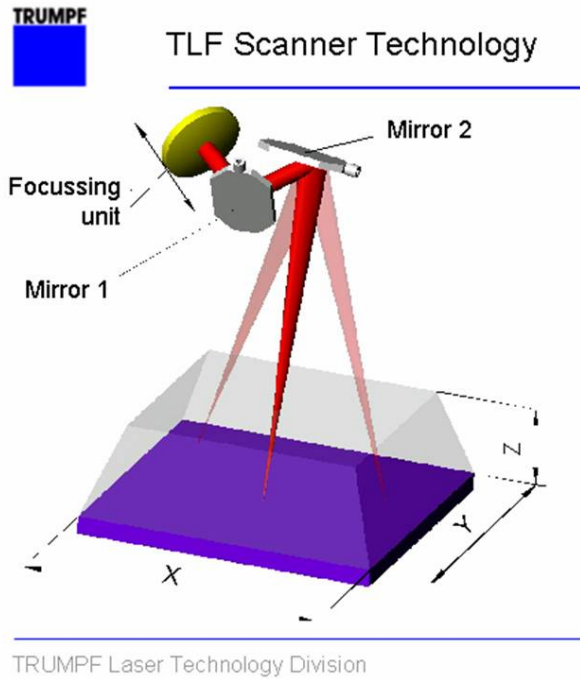


Figure 4.7 Principle for Rapid Beam Manipulation in the PFO Scanner

The rapid beam manipulation in the PFO scanner is controlled by mirrors operated by galvanometers as shown above. The PFO head, Figure 4.8, was attached to the Nd:YAG laser but is limited to 1-kW output power. Above this power the laser damages the mirrors.

The scanning pattern of the laser is controlled through the LASEdit program to produce the desired scan profiles. The PFO head was attached to a CNC workstation, Figure 4.9, and was operated with HSV and DAQ for the GMAW-P portion of the hybrid operation.



Figure 4.8 Trumpf PFO Device



Figure 4.9 CNC Nd:YAG/GMAW-P Setup for PFO Evaluation, Including HSV, DAQ, and LASEdit Laser Programmer/Controller

A Rofin Sinar 850 CO₂ laser was used for single- and dual-beam LBW/GMAW-P hybrid welding, Figure 4.10.

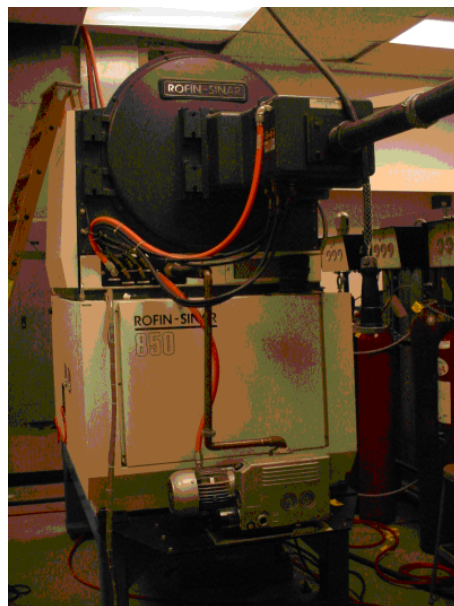


Figure 4.10 Rofin Sinar 850 CO₂ Laser was Used for Single- and Dual-Beam LBW/GMAW-P Hybrid Welding

The beam was delivered through a waveguide with mirrors, Figure 4.11.

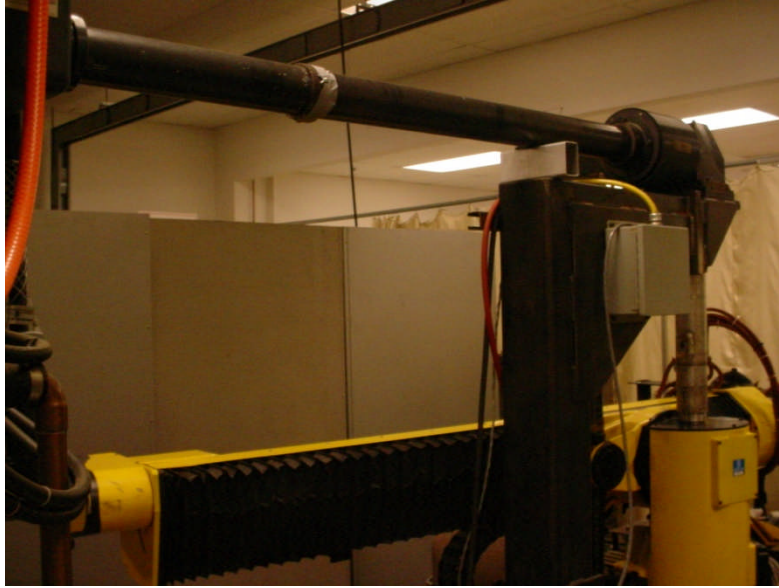


Figure 4.11 Waveguide for Beam Delivery to the GMF Robot

Dual-beam optics based on a polished and EDM split Cu mirror, Figures 4.12 and 4.13, were built to suit the GMF Fanuc L-100 robot.

The distance between the dual laser beams was adjusted by a pair of set-screws, to produce an array of beam separation distances, Figure 4.13. TS was controlled by a Jetline 9020XZ single-axis carriage with digital TS control having a maximum TS capability of 4 m/min.

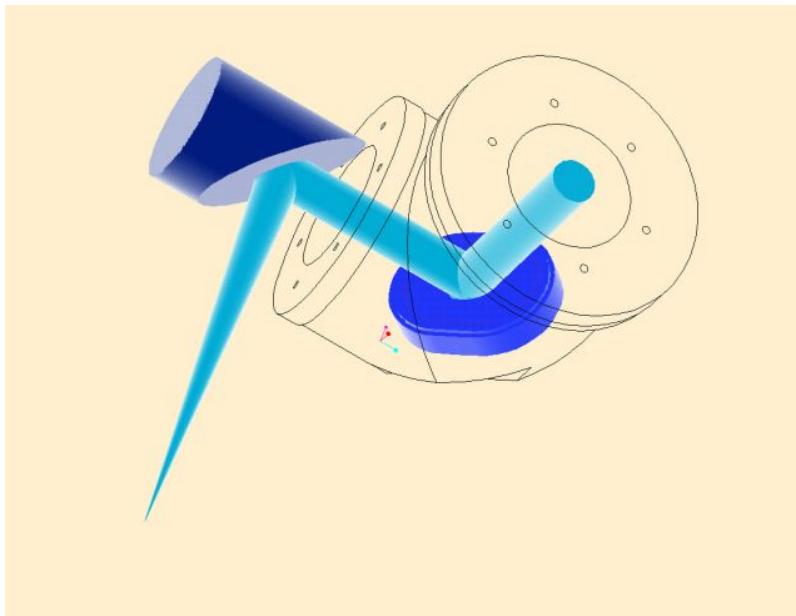


Figure 4.12 Single Spot Laser Mirror System for Robotic CO₂ Laser Welding (Trumpf)

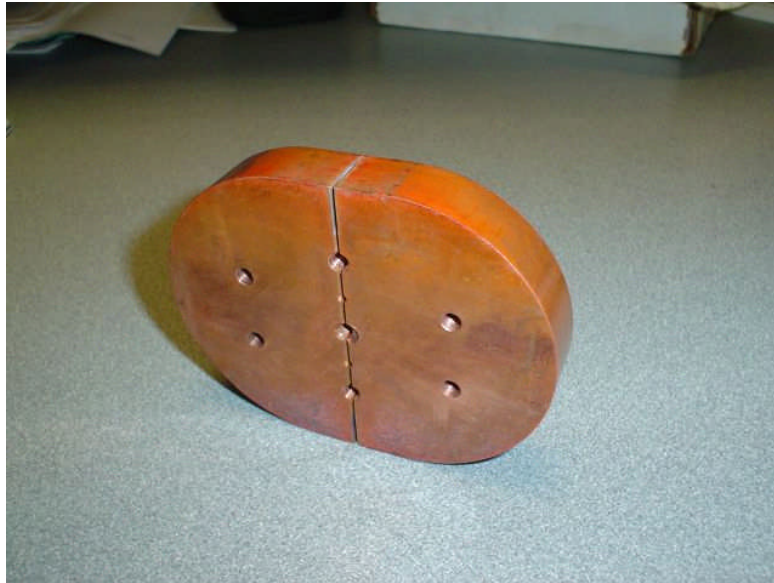


Figure 4.13 Rear Face of Split (wire EDM) Cu Mirror for Dual-Spot Experiments with a CO₂ Laser

The robot was controlled using a Karel Robotics L-100 controller, Figure 4.14.



Figure 4.14 GMF Robotics Karel L-100 Robot Controller

An integrated system was used for controlling and recording welding parameters, initiating the arc welding and laser welding power, and fixture motion.



Figure 4.15 Laser Spot Alignment Using a Low-Power Visible Red He-Ne Laser

Laser beam alignment was conducted using a He-Ne sighting laser centered to the axis of the beam delivery guide, Figure 4.15.

Set screws on the sighting laser enabled adjustment of the red light beam generated by the laser itself.

4.3 CO₂ Laser System

The CO₂ laser system is comprised of the following elements:

4.3.1 High-Voltage Power Source

The power source is used to produce the high-voltage DC that creates the discharge that excites the gases within the resonator. For continuous wave operation only one power source is used.

4.3.2 Resonator

The resonator contains the lasing cavity which is a series of glass tubes and laser optics which contains the laser gases as they are excited by an electrical discharge. Each glass tube contains a cathode and anode and the discharge creates a plasma when the high voltage DC passes between the cathode and anode.

4.3.3 Shutter

The shutter can safely absorb the full power of the laser beam when it is closed, and when open, allows the beam to exit the enclosure and perform the desired welding operation. A He-Ne diode laser emitting a visible red light is used as a pointing tool to indicate where the invisible CO₂ laser beam will impact the part, Figure 4.15.

4.3.4 Main Relay Cabinet

The main relay cabinet controls the electrical systems and interfaces with the main control cabinet. Laser parameter settings were entered by the operator, Figure 4.16.



Figure 4.16 Console for Laser Parameter Selection

4.3.5 Laser Cooling System

The cooling system provides cooling water to maintain the temperature within the laser enclosure to within $\pm 2^{\circ}\text{C}$. Water was provided by a separate re-circulating chiller and contained corrosion and biochemical inhibitors.

4.4 Trumpf HAAS 4006D Nd:YAG Laser

A Trumpf Haas HL 4006 4-kW continuous-wave Nd:YAG laser system, Figure 4.17, was used with both single-beam and adjustable dual-beam optics. This continuous-wave lamp-pumped laser operates with the lasing action stimulated by high-power flashlamps.



Figure 4.17 Trumpf Haas HL 4006 4-kW Continuous-Wave Nd:YAG

This system was interfaced to a 6-axis Motoman SK16 welding robot and was set up with a hybrid laser + GMAW welding head built in-house, Figure 4.18. Work was conducted on lap-fillet joints and T-butt joints in sheet metal thicknesses, for bare steels.

The laser operation and parameter selection was controlled via a PC running HAAS LASEdit software.

4.5 Workpiece Manipulation

The type of workpiece manipulation was in some cases determined by the type of welding equipment employed.

4.5.1 Single-Axis Welding Carriage

A servo-motor driven single-axis welding carriage was used for most of the work. The maximum TS provision was 4 m/min.

4.5.2 CNC Worktable

A CNC worktable was used to manipulate the parts when welding using the PFO for low power (1 kW max) Nd:YAG laser GMAW-P operations, Figure 4.9.

4.5.3 Robotic Manipulation

A Motoman SK16 six-axis welding robot was used to mount the hybrid welding head consisting of the fibre-optic delivery of the Nd:YAG laser beam and focusing optics, along with the GMAW welding torch for hybrid welding operations.

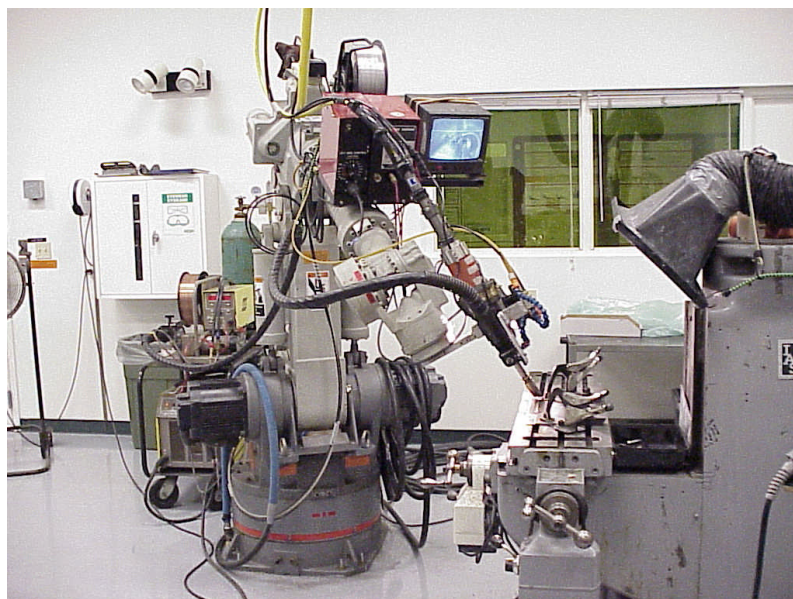


Figure 4.18 Motoman SK16 Robot with Fibre-Delivered Nd:YAG Laser and ESAB GMAW-P Equipment Setup on a Lap Joint

4.5.4 Fixturing

Fixturing for welding was kept as consistent as possible, but running trials on three different installations; it was not possible to use the same fixturing all the time in terms of the platen on which the specimens were mounted. As sheet metal welds are subject to 2-D heat flow and the welding speeds used in most of the work were very high, conductive cooling by the platens on which the specimen sheets were mounted is considered to have had a minimal effect on the results achieved.

4.6 Data Acquisition

Data acquisition equipment was used for both arc welding and laser welding components of the system.

4.6.1 Data Acquisition for Arc Welding

Calibrated Hall Effect shunts were used for monitoring welding current, and calibrated WFS sensors were used to measure WFS accurately.

Data acquisition for the arc welding operation employed an Arc Agent™ system from Impact Engineering with sampling frequency adjustable up to 10 kHz. A typical GMAW-P waveform is shown in Figure 4.19.

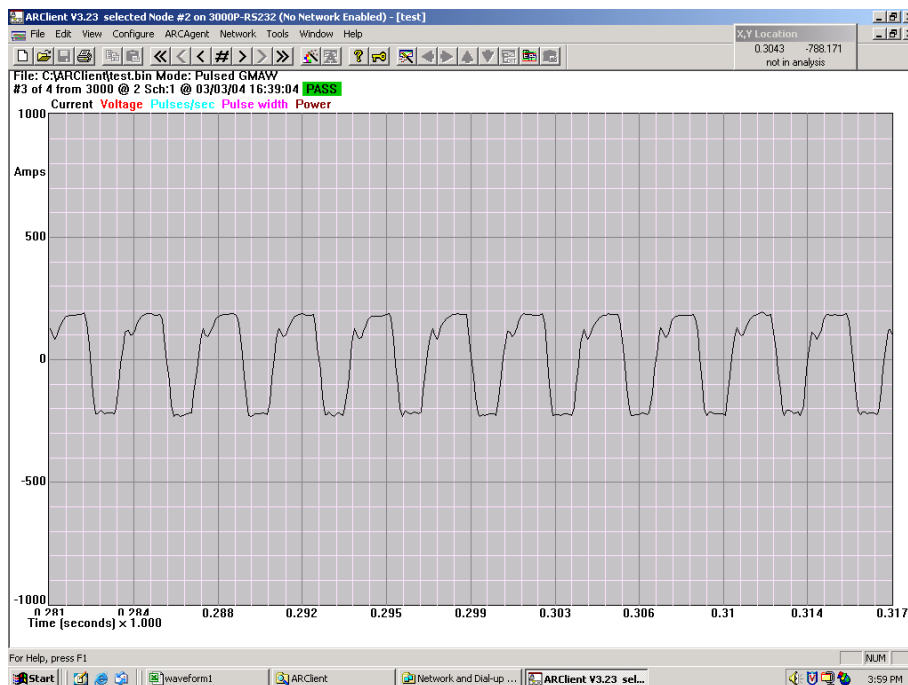


Figure 4.19 GMAW-P Waveform from Arc Impact DAQ at 10-kHz Sampling Frequency

4.7 High-Speed Video (HSV)

HSV imaging, using a Kodak Ektapro HS, Figure 4.20, was sequenced with a Model 4540 motion analyzer and data acquisition. The Ektapro system has a frame rate capability up to 45,000 fps.

A $950\text{-}\mu\text{m} \pm 10\text{-}\mu\text{m}$ infrared (IR) band-pass filter was placed between the lens and the camera, Figure 4.21, to obtain clear images of weld deposition by filtering unwanted UV arc light. This was used to study the arc characteristics and weld pool dynamics in the hybrid laser/GMAW case, particularly when the relative positions of the laser and GMAW-P arc were being evaluated, Figure 4.18. The HSV output was triggered through an interface, Figure 4.22, and captured by a desktop PC.

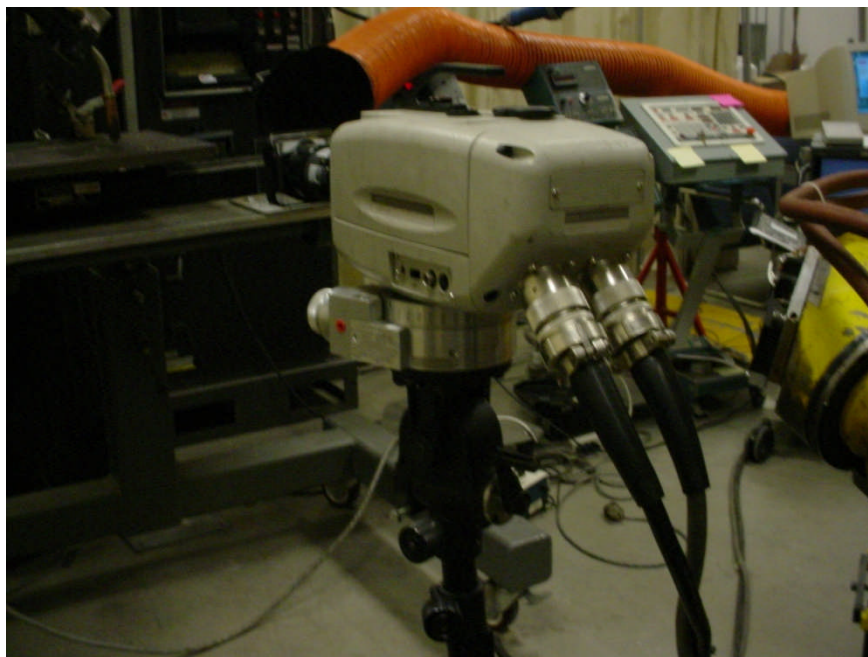


Figure 4.20 Kodak Ektapro HS HSV Camera Setup for Viewing the Weld Pool Perpendicular to the Welding Direction

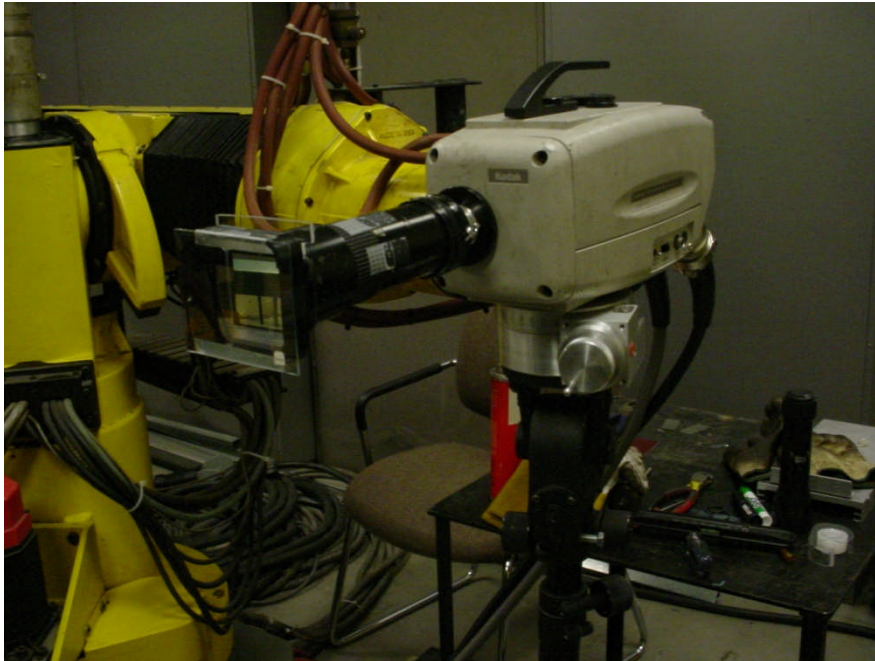


Figure 4.21 Cover Lens and IR Band-Pass Filter Attached to the Camera Lens

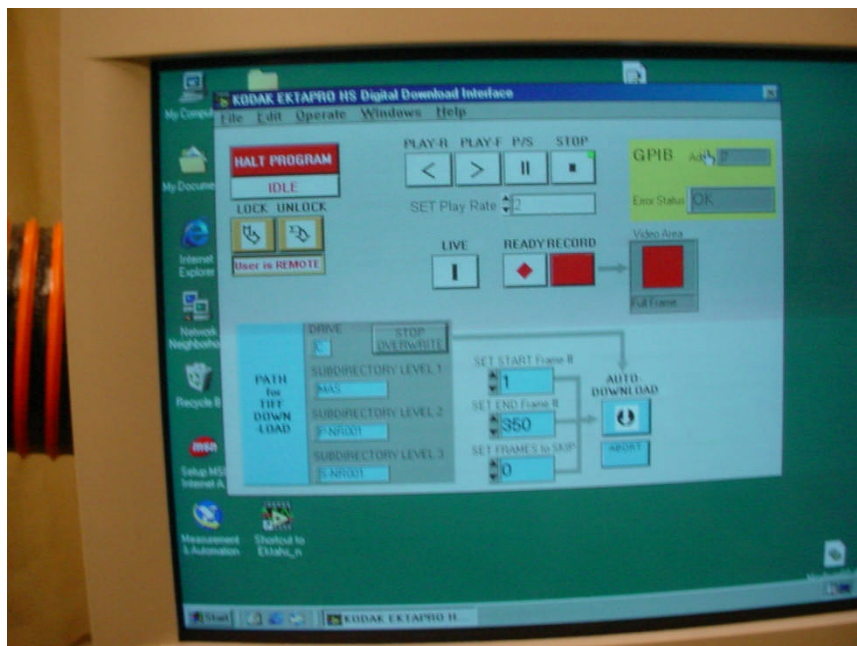


Figure 4.22 Digital Download Interface for Triggering and Capturing HSV Data

The frame-by-frame images were observed on a monitor, so that selected image ranges could be viewed and recorded, Figure 4.23.



Figure 4.23 Typical Screen Image and Frame Data Using the Kodak Ektapro HS System

The residual light ‘noise’ in the LED array within the camera causes reduction in the image resolution. This was neutralized by recording a black image, effectively setting the array elements to the same baseline level. This increased the image resolution, but it was still not as good as that achievable with the Phantom camera described below.

HSV acquisition and analysis was also carried out using a Phantom camera, Figure 4.24, with the capability of a frame rate up to 100,000 fps.

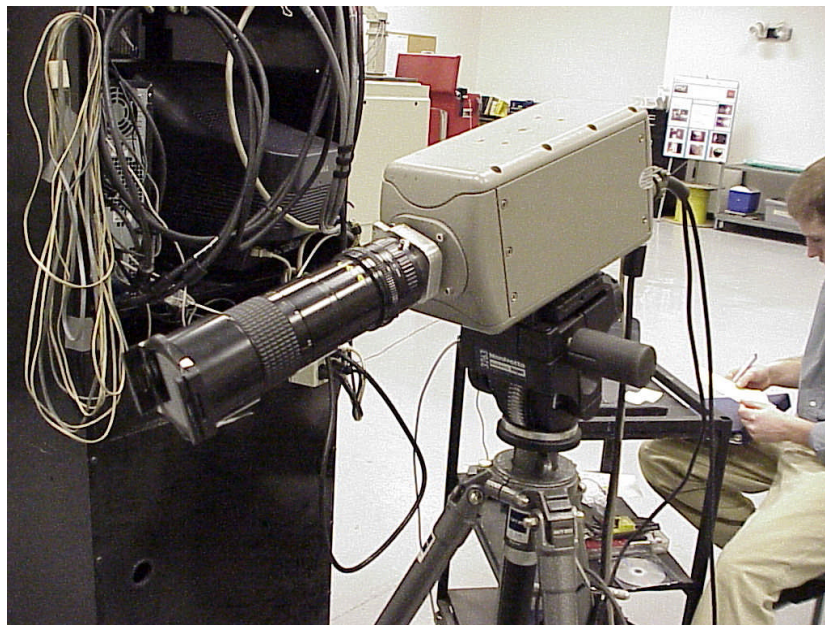


Figure 4.24 Phantom HSV Camera with Filter Mount Between the Camera and Lens Assembly

A similar $950\text{-}\mu\text{m} \pm 10\text{-}\mu\text{m}$ band-pass filter was used to obtain clear images of weld pool motion. The filter was incorporated into an Al mount attached to the camera body that allowed it to be removed and replaced easily for image focusing before welding. Image acquisition was carried out with the Phantom software loaded on a laptop computer. The CMOS camera in the newer Phantom system provided higher image resolution than achievable with the older Ektapro system. The user interface software was also easier to use than the Kodak system.

4.8 Measurement and Analysis Tools

Several tools for measurement and analysis were used during the course of the work. A brief description of each is contained in the following sections.

4.8.1 PRIMES Laser Beam Monitor

The PRIMES Laser Beam Monitor, Figure 4.25, consists of a high-speed rotating disc and a water-cooled beam dump or cup to absorb the beam energy. The thermal sensor in the disc samples the beam intensity and is linked to software that can output a laser intensity map. This tool was used to sample Nd:YAG laser spot size, beam intensity, and beam separation in the case of split beam laser operation.

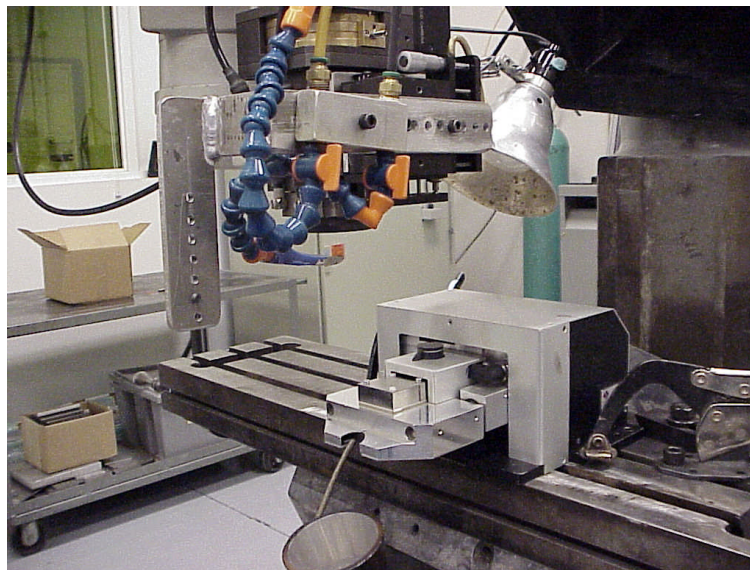


Figure 4.25 Primes™ Beam Power Analysis System Setup to Measure Distributed Power in Dual-Beam Nd:YAG Laser

4.8.2 WISC Laser Profilometer

Typical weld bead profiles were recorded using a WISC handheld laser scanning system, Figure 4.26, which incorporates a He-Ne laser beam used as a rangefinder to record the surface profile of the welds. Data storage was accommodated using a desktop PC.



Figure 4.26 WISC Laser Profilometer

4.8.3 Image Pro Digital Imaging and Measurement

Photographic images of weld bead macrosections and weld profiles was conducted using Image Pro digital imaging software on a desktop PC. Measurement of weld features in terms of leg length toe angles, and weld cross-sectional area was carried out digitally using the Image Pro measurement package.

4.8.4 MINITAB

MINITAB was used for linear regression, response surface data representation from Box-Behnken experimental designs and for DOEs procedures including factors, levels, centerpoints, and run-order randomization. Analysis of variance (ANOVA) for DOE results was also conducted using Minitab.

4.9 Calorimetry

Calorimetry was conducted using the method of differential weight of liquid nitrogen, Figure 4.27, caused by nitrogen boil-off equivalent to the heat removed from a welded plate, adjusted for room temperature. This method was used to measure the efficiency of the GMAW-P and hybrid LBW/GMAW-P processes



Figure 4.27 Equipment Used for Calorimetry Experiments

4.10 Metallography

Metallography was conducted using conventional metallographic preparation techniques. The following procedure was followed for welds of interest:

1. Band-saw cutting of weld cross sections (two per weld, one at one third distance and one at two thirds distance along the weld)
2. Abrasive cut-off to trim the sawn sections to size to fit a standard mount
3. Hot press mounting of specimens in standard 37-mm-diameter Bakelite mounts
4. Grinding on successively finer grit abrasive papers
5. Polishing to 1- μm finish using diamond paste polishing wheels
6. Etching with 2% Nital (2% nitric acid in alcohol)

ImagePro™ software was used to measure weld bead dimensions from photomicrograph images captured digitally. This software allows measurement of bead dimensions, fusion boundary tracing to calculate weld bead cross-sectional areas, and weld toe angles, all of interest in this work.

4.11 Materials

The materials and consumables that were used are listed below:

- AWS A5.18 ER70S-3 and ER70S-6 Cu-coated solid steel welding electrode wires, 1.2-mm diameter on standard 15-kg spools
- 90% Ar/10% CO₂ shielding gas for GMAW-P
- 1.6-, 2.0-, and 2.4-mm-thick AISI 1010 hot-rolled steel sheet sheared into 75- \times 610-mm pieces.

5.0 EXPERIMENTAL PROCEDURE

A series of experiments were conducted concerning humping in the following cases:

1. Conventional GMAW-P with gaps of 0T and 1T to determine appropriate weld sizes
2. Increasing welding speeds achieved without humping by changes in welding parameters using GMAW-P and by improving fit-up to close to 0T
3. Use of single- and dual-offset laser impingement at GMAW-P weld toes to alter weld toe wetting angles and fluid flow to suppress bead humping to higher TS
4. HSV data collection and analysis to compare humping mechanisms

The experimental procedures conducted to develop the thesis are described below and were based on the known occurrence of the humping phenomenon at high welding speeds. HSV data collection and analysis of pool dynamics was conducted to compare mechanisms for BOP welds and lap-fillet welds.

The thesis evolved to examine the optimization of weld size along with welding speed and productivity, within the constraints of an industrially useful bead shape. The use of GMAW alone for welding sheet metal is constrained by the minimum effective bead size that can be maintained without the occurrence of the bead humping phenomenon. Introduction of the additional heat input and the weld toe wetting effect from the laser beam allows a reduction in this effective minimum bead size that also allows considerable increase in welding TS.

The methodology adopted included GMAW-P and hybrid LBW/GMAW-P trials and data input to a modeling project as it pertains to the main subject matter; using laser beams to increase weld toe wetting in GMAW, and thus suppressing bead humping. GMAW-P was combined with CO₂ and Nd:YAG laser beams. HSV monitoring was combined with high-speed data acquisition of LBW/GMAW-P operation. The results were interpreted to advance the work and knowledge in the field of hybrid LBW/GMAW-P, and the suppression of bead humping, and to allow the development of a predictive thermal model of the process.

5.1 Weld Acceptance Criteria

Five acceptance criteria were used as follows:

1. No burnthrough
2. No overlap (cold lap) on the lower weld toe
3. No humping i.e., continuous weld
4. Weld size, measured by WFS/TS above 4.
5. Undercut on the top plate of the lap joint less than 20% of the plate thickness

The work was divided into tasks concentrating on sheet metal joints, as follows:

- CO₂ LBW/GMAW-P Lap-Fillet Welding Trials - Carbon Steel
- Nd:YAG LBW/GMAW-P Lap-Fillet Welding Trials - Carbon Steel
- CO₂ LBW/GMAW-P T-Butt Welding Trials - Carbon Steel

- Calorimetry for LBW/GMAW-P, GMAW-VP and GMAW-P
- Optimization of Welding Procedures; Knowledge-Based DOE (KB-DOE)
- Humping and Humping Suppression in GMAW-P using HSV of GMAW-P for BOP and lap-fillet welds
- HSV of hybrid welding using a CO₂ laser

5.2 Weld Sizing Applications for Sheet Less than 3 mm

Sizing of welds for sheet metal is dependent on the joint gap anticipated. For lap and T-butt joints having no gap studied in this work can be simplified to:

$$A = 0.5t^2 \quad (5.1)$$

This area is for a mitre fillet weld, a right triangle, giving the theoretical minimum weld size, ignoring the weld penetration area as:

- 1.3 mm² for 1.6-mm-thick sheet
- 2 mm² for 2.0-mm-thick sheet
- 2.9 mm² for 2.4-mm-thick sheet.

Clearly, it is not possible to produce such a small weld area in practice, but the aim of the work conducted was to produce the smallest practical bead size and highest welding speed that could be obtained without humping formation.

Bead size was based on a ¼ ellipse when determining WFS/TS for parametric development in hybrid LBW/GMAW-P.

Initial GMAW-P weld trials were done on a standard lap joint fixture without introduction of controlled gaps. A lap joint is the most common joint in sheet metal applications, so a generic mild steel lap joint was used

A variable joint gap was used in this work. The variable gap can be used to represent the inconsistent joint gap as a result of distortion or inaccuracies in fit-up or tooling. Another point is that the gap can be represented as a function of distance traveled along the weld joint, similar to Tanimoto (Tanimoto et al., 1988). This is efficient in terms of runs required for determining the maximum gap that can be welded under a given condition.

For variable gap joints (0T to 1T) the starting location of the weld was on the 0-gap condition to facilitate establishment of a stable arc.

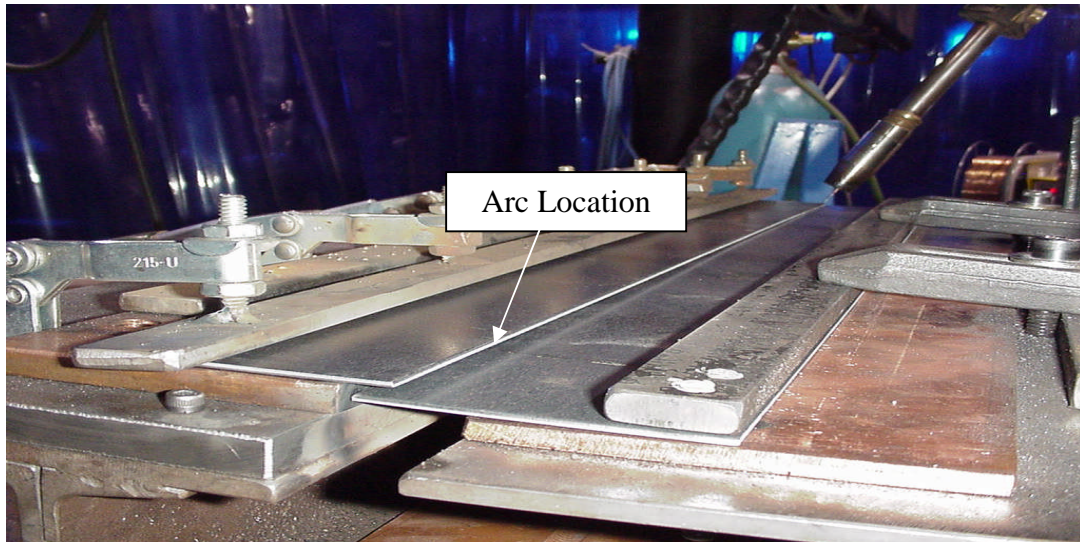


Figure 5.1 Gap Geometry for DOE Trials

5.2.1 Welding Parameter Selection Technique

The welding conditions were selected using a systematic methodology called the SWAT (Green, 2001). The purpose of the SWAT trials was to develop welding conditions that could be used as a baseline during the fixture evaluation and designed experiments. The concept behind SWAT is to produce a region of acceptable weld parameters for a given material and joint type. The acceptable region is outlined on a WFS versus TS graph. The welds were measured against ANSI/AWS D1.3, Structural Welding Code – Sheet Steel (AWS, 1998), for acceptability. The SWAT technique was used to evaluate lap joints with no joint gap (0T) and one material thickness joint gap (1T) using the three base material thicknesses. This resulted in a total of six SWAT WFS versus TS plots.

The SWAT welds were produced with a constant WFS of 3.8 m/min while varying the TS in increments of 250 mm/min starting at 250 mm/min. Once the range of TS that produced acceptable welds for 3.8 m/min were exhausted, the WFS was increased 1.25 m/min to determine the next TS range. These two steps were continued until no acceptable welds could be produced.

The results from the SWAT trials were graphed on WFS versus TS plots. The regions of acceptable welds were then identified on the plot by inspection. A linear model of WFS as a function of TS of the acceptable welds was then determined from a linear regression. This model produces a WFS versus TS relationship that is specific to the weld joint and material type that the test evaluated. The linear equation was plotted as a solid line on each of the six WFS versus TS graphs.

The 0T and 1T joint gap WFS versus TS relationships, for each thickness of material, were mathematically averaged and a new relationship for that thickness was derived. The new relationship was chosen to accommodate both a 0T and 1T gap. The three new equations were plotted as a dashed line on each of the representative WFS versus TS figures. The welding parameters from the final three equations were used in the verification of the gap weldability fixture.

When developing the welding conditions several factors were kept constant. The work angle was maintained at 60 degrees from the horizontal plates and no push or drag angles were used. The second factor, CTWD, was held constant at 16 mm. The final factor of the setup was the arc location. In these experiments the arc was aimed at the top corner of the upper sheet of the lap joint.

5.2.2 Weld Acceptance Criteria

Varying the TS and WFS developed the plots used to determine the welding conditions for all three material thicknesses. Upon completion of the weld visual examination, destructive testing was performed on the weld coupons. To be characterized as an acceptable weld using visual inspection certain criteria needed to be met. Firstly, the amount of undercut on the top plate of the lap joint needed to be less than 20% of the plate thickness. The second factor was no presence of burnthrough after the completion of the weld. The third criterion was the absence of overlap on the lower toe. To a lesser extent, the weld size could be a factor in rating the unacceptability of a set of welding conditions. Failure of any of these conditions resulted in an unacceptable weld.

Destructive tests were also done in accordance with ANSI/AWS D1.3. The test that evaluated the lap joint was the chisel test. A chisel was inserted between the two sheets. Then pliers were used to separate the sheets. ANSI/AWS D1.3 states that any weld that does not show complete fusion is deemed unacceptable.

5.2.3 Design of Experiments

After the proposed variable-gap weldability fixture setup parameters were determined from the fixture evaluation, the designed experiments were carried out. All of the DOE weld trials for the three material thicknesses were performed on the variable gap weldability fixture, Figure 5.1. The type of design that was used for the designed experiments was the Box-Behnken design. Box-Behnken designs are response surface designs that can fit a full quadratic model. Box-Behnken designs use three levels of each factor, this makes them appealing when the factors are quantitative but the set of achievable values is small.

The experiments consisted of systematic variations of the following six factors from the values used during the SWAT trials: travel angle, work angle, deposit area, TS, arc length, and CTWD. The six factors for the DOE were varied around the SWAT trial setup conditions. The values used during the SWAT trials are given below except for the deposit area, which is dependent on the material thickness.

- Travel angle: 90 degrees (no drag or push)
- Work angle: 60 degrees (from the horizontal lap joint)
- TS: 0.5 m/min
- Arc length: 3 mm.
- CTWD: 16 mm.

Each of the factors listed above were varied to represent the three levels of each factor for the DOE. Below is a list of the ranges used.

- Travel angles: 10-degrees drag, 90 degree, and 10-degrees push
- Working angles: 45, 60, and 70 degrees
- Deposit area was changed $\pm 20\%$ of the SWAT weld area for each gauge
- TS: 254, 510, and 760 mm/min
- Arc length was changed by $\pm 15\%$ of the 3-mm arc length
- CTWD: 13 mm, 16 mm, and 19 mm.

For travel angles, a drag travel angle was considered negative and a push angle was considered to be positive. The work angles were all measured from the horizontal plate surface of the bottom piece of the lap joint; a 90-degree work angle is a vertical torch position. The response of the DOE was the maximum weldable gap, which was calculated from Eq. (5.2).

$$\text{Maximum Welded Gap} = 0.83 \times T \times \text{Weld Length} \quad (5.2)$$

In the equation above the variable, T, represents the material thickness. The weld length that is used in the equation is the length of acceptable weld before failure. The equation was developed for a weld joint 610 mm in length that created a 2T joint gap. If either one of these conditions are altered, the constant in the equation changes.

Each DOE consisted of 54 weld trials for each gauge, resulting in a total of 162 weld trials. The top plate was kept horizontal to allow for the arc to always be directed at the upper edge of the top piece, as shown by the arrow in Figure 5.1. The weld coupon was 610 mm in length and welding was started on a no-gap condition and traversed the joint toward a 2T gap. The gap encountered by the welding arc was linearly related to the horizontal distance traveled along the joint, as shown in the equation above.

The criterion that was used to determine the successful weld length was similar to the rating system used by Richardson (Richardson, 2002). One factor that Richardson used was a completeness of fusion rating. This rating was determined by subtracting the total length of areas showing fusion defects from the total length of the weld. An illustration of this rating method is given in Figure 5.2. The completeness of fusion was the only factor that was used to determine the acceptance of the weld in this research. For the DOE welds, the gap corresponding to the first lack of fusion or burnthrough occurrence was the response factor. Figure 5.3 shows an example of a skip that was encountered during one of the DOE trials that resulted in the acceptable weld length and corresponding gap.

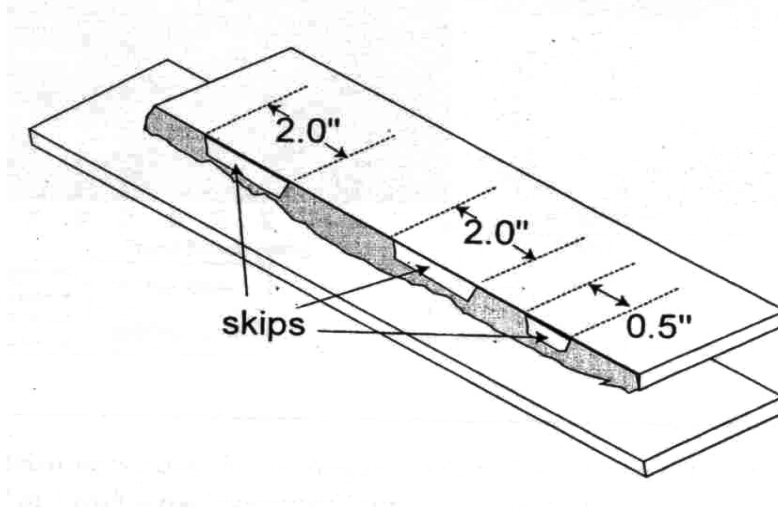


Figure 5.2 Sample of Completeness of Fusion Rating (Richardson, 2002)

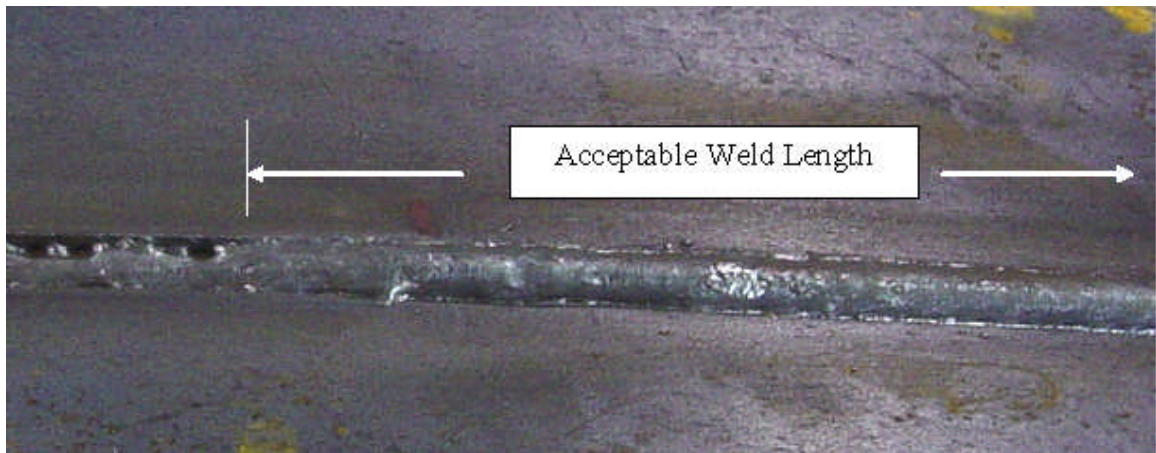


Figure 5.3 Illustration of a Skip, or Incomplete Fusion, Encountered During Welding Denoting the End of the Acceptable Weld

After completing each weld the weld length was measured with an accuracy of 3 mm. The weld length was used in the equation to determine the gap that the weld encountered at the point where a fusion defect was encountered. This gap was determined to be the maximum allowable joint gap for the material thickness and welding variables. Beyond this gap a typical humping morphology was seen, Figure 5.4.



Figure 5.4 Typical Bead Humping Defect in a Lap-Fillet Weld

5.3 Experimental and Theoretical Work – High-Speed GMAW-P Lap-Fillet Welding Trials

The baseline for TS established in the weld sizing work for mechanized GMAW-P on 3-mm CS plate lap-fillet tolerant to 0 to 1T gap was established in the work described above.

A new baseline for suppression of bead humping at high speed using GMAW-P was established for a 0-gap condition on lap-fillet joints for the three material thicknesses studied. This work was conducted to prove that higher welding speed than generally understood can be achieved using GMAW-P when controlling the welding parameters, and developing them around a substantial lead travel angle. The following parameters were used:

- CTWD 16 mm
- Arc length 3 mm
- Torch work angle 60 degrees from horizontal
- Torch travel angle 30-degrees lead angle
- Electrode wire ER70S-6
- Shielding gas 90/10 Ar/CO₂ mixture
- Power Source ESAB Digipulse 450i GMAW-P power supply
- Wire feeder ESAB Digipulse wire feeder
- Torch Binzel water-cooled machine torch

The lead travel angle and its angle of incidence against the front wall of the melted arc gouge is postulated to be a substantially controlling parameter in the flow of molten metal in the weld pool and the ability to suppress the onset of bead humping to higher TS.

5.4 Experimental and Theoretical Work – Hybrid Welding, Laser Beam Splitting and Toe Wetting

Work was conducted to determine the minimum laser power requirement and power density to achieve effective wetting at the weld toe. As such, work with the scanning head was discontinued, and dual laser beam studies have also been concluded in favor of an offset (with respect to the weld centerline) single-beam approach. The use of GMAW-P alone for welding sheet metal is constrained by the minimum effective bead size that can be maintained without the occurrence of the bead humping phenomenon. Introduction of the additional heat input from the laser beam allows a reduction in this effective minimum bead size that also allows considerable increase in welding TS.

Mechanisms in operation and controlling the tendency or otherwise for bead humping to occur are the arc force, bead size, TS, WFS, laser power, laser focus, and power density. The weld bead is prone to a humping discontinuity when the toe angle between the weld and the base material becomes less than 90 degrees.

HSV was used to show the interaction of the laser spot and the GMAW-P weld pool, Figure 5.5. The laser is set up to lead the front edge of the GMAW-P weld pool by 2.0 mm, with a tolerance of ± 0.5 mm. This allows for a stable interaction and focus height for the laser. It is also routinely observed that if the laser is focused at a point on the GMAW-P weld pool surface that significant spatter is generated resulting in a weld bead size that is too small because of volume loss of weld metal.

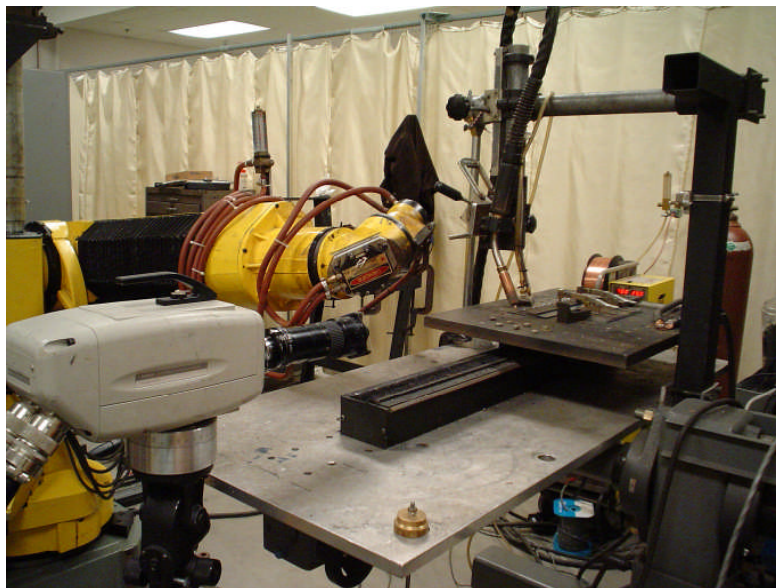


Figure 5.5 Setup for HSV of the CO₂ Laser/GMAW-P Hybrid Welding Process for Evaluation of Optimum Offset between the LBW and GMAW-P Process



Figure 5.6 Adjustable Beam Distance for CO₂ Laser Split Optics showing 3.2-, 6.4- and 9.5-mm Dual Spot Spacing

The experimental work conducted is summarized below for scanning and dual-spot Nd:YAG, and both single- and dual-spot CO₂ lasers, Figure 5.6, used with GMAW-P. A fully integrated system was completed and used for controlling and recording welding parameters, initiating the GMAW and laser welding power, and the fixture motion.

5.4.1 Scanning Laser Nd:YAG and Dual Spot

The Trumpf PFO system is limited to 1-kW laser power, and thus offers limited opportunity to increase welding speed and productivity. As such, a dual-spot technique was used with 4 kW of Nd:YAG LBW power. Beam splitting was accomplished using commercially available split optics, but using each of the two beams on the same weld bead.

Scanning the laser beam using the Trumpf PFO is limited to 1-kW laser power. Trials were conducted to maximize the bead wetting and to increase productivity by increasing the welding speed achievable. Laser/GMAW hybrid welding was also conducted with single and dual beams (split optics), Figure 5.7 using Nd:YAG laser power up to 4 kW, Figure 5.8.

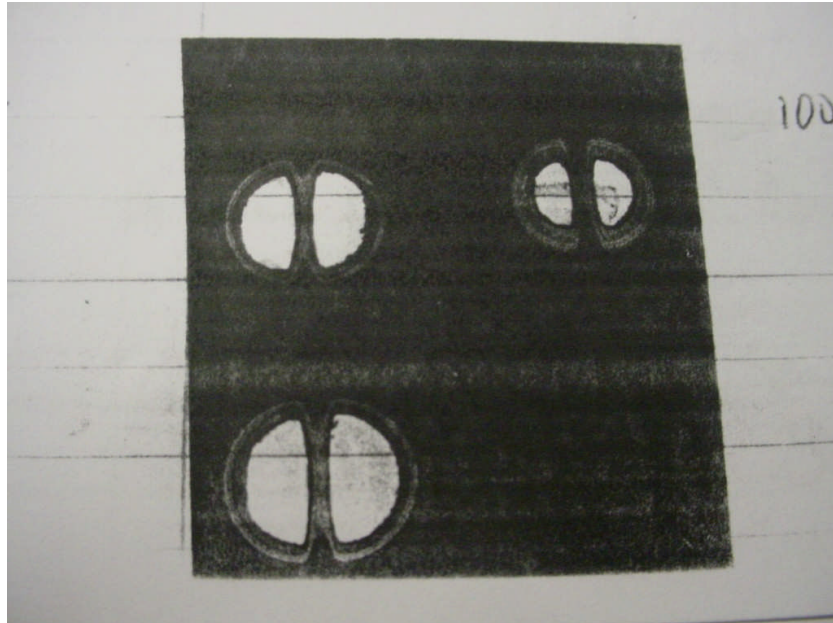


Figure 5.7 100-W Dual Beam Nd:YAG Laser Burn Pattern on Thermographic Paper to Illustrate TEM 01 Laser Mode

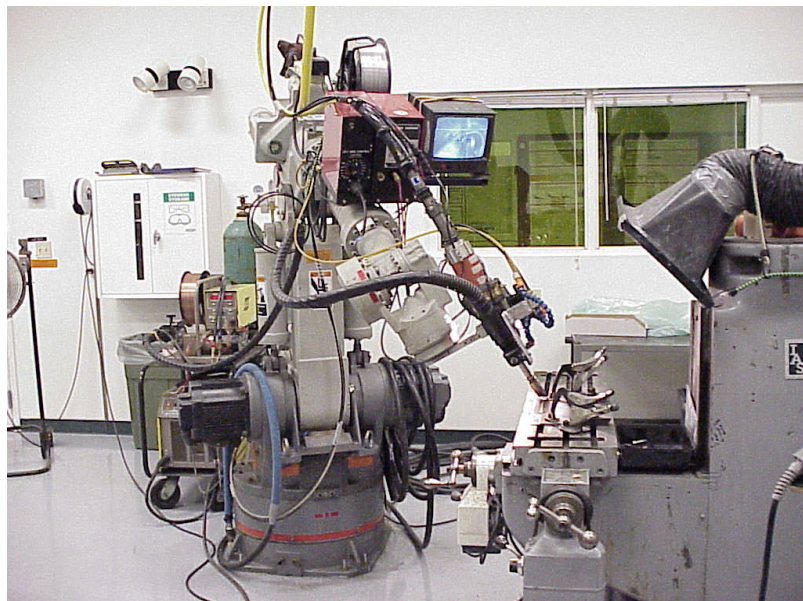


Figure 5.8 Fibre-Delivered Nd:YAG Laser and ESAB GMAW-P Equipment Setup on a Lap Joint for Single- and Dual-Spot Welding Trials

5.4.2 CO₂ Dual Beam

A 4-kW CO₂ laser was used for dual-spot welding, and the productivity evaluated based on the 2 kW available for each laser spot, Figure 5.9, and the available heat input to increase the wetting angle. The coating on the Perspex was applied only to highlight the laser ‘burn pattern’, not for laser absorption.

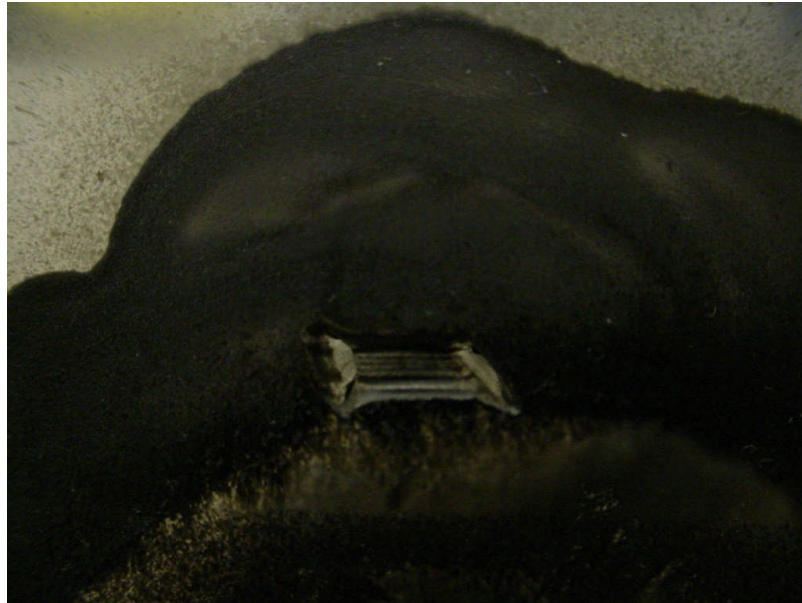


Figure 5.9 CO₂ Laser Burn Pattern on Perspex for Dual Beam in TEM 01 Mode

Work was then conducted with a single-beam approach, the laser beam being offset to the lower sheet in a joint. Work was carried out to establish the minimum laser power requirement to achieve effective wetting at the weld toe. Laser/GMAW-P hybrid welding was conducted with CO₂ laser power up to 4 kW, with CO₂ LBW/GMAW-P trials carried out with an offset (with respect to the weld centerline) single-beam approach.

5.4.3 CO₂ Offset Beam

The beam was offset onto the lower ligament of the joint to increase the wetting of the lower weld toe that was considered the limiting factor in making a continuous high-speed fillet weld. Defocusing the laser spot is a balance of sufficient power density with the beam width. The beam width and beam position relative to the lower GMAW-P weld toe were considered important and were investigated in this work. The same approach was applied to a T-butt weld. The offset and defocused CO₂ laser spot was used in GMAW-P/LBW hybrid welding trials on sheet metal joints

5.5 Calorimetry

Calorimetry was performed for GMAW-P, and LBW/GMAW-P. The technique employed was that established by Smartt et al. at INEL, involving recording weight change due to liquid nitrogen boil-off with time. Calorimetry was conducted for GMAW-P, and CO₂ laser/GMAW-P welding., with the equipment set-up integrated into the data acquisition system, Figure 5.10.

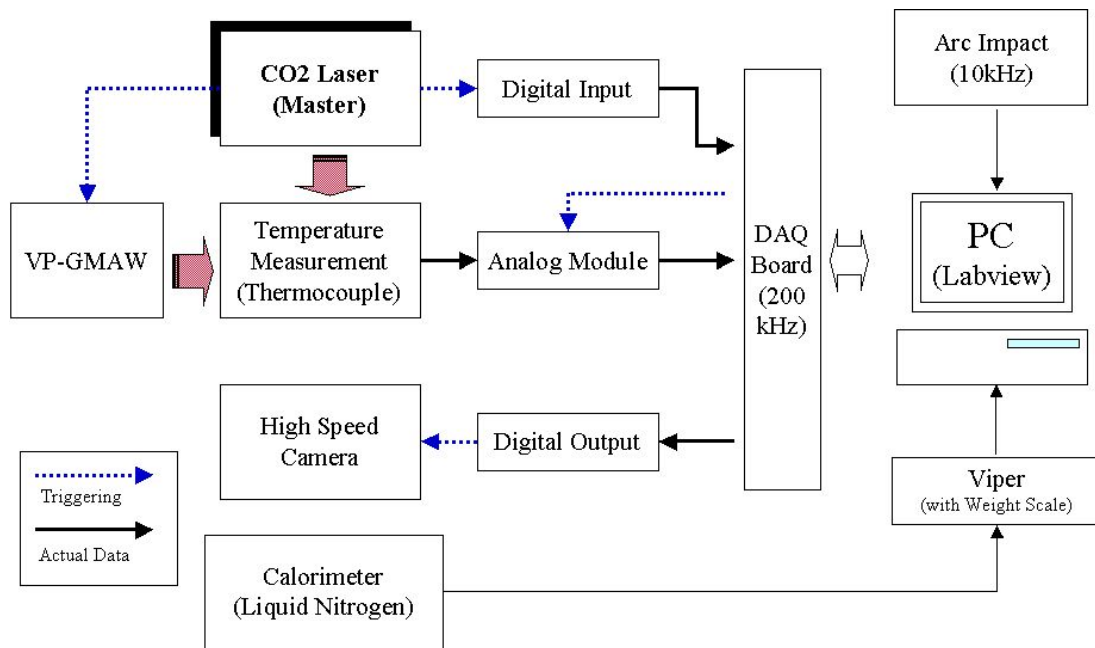


Figure 5.10 Control Block Diagram of the Calorimetry Experiments

5.6 Experimental Procedure for HSV

The following sequence was used to setup and record HSV images on the Kodak HSV system:

1. Depth of focus – extension to lens/aperture.
2. Recorded field of view and calibrated same in mm – used 25- to 40-mm field of view.
3. Aiming point behind the arc to get a good view of the hump formation when using high-speed GMAW-P and LBW/GMAW-P.
4. Calibration of light source – exposure to set light levels across diode array in the Kodak camera.
5. Focus with band-pass filter when arc is running.
6. A fiberoptic lightbox was used to illuminate the area of interest with respect to the GMAW torch for field of view, preliminary focusing and calibration image. Figure 5.11 shows the wire tip, and metal scale indicating a 27-mm field of view.
7. A frame rate of 250 fps provided 2 s of recording time on the Kodak camera. This allowed recording of a 150-mm weld length at a TS of 3 m/min.

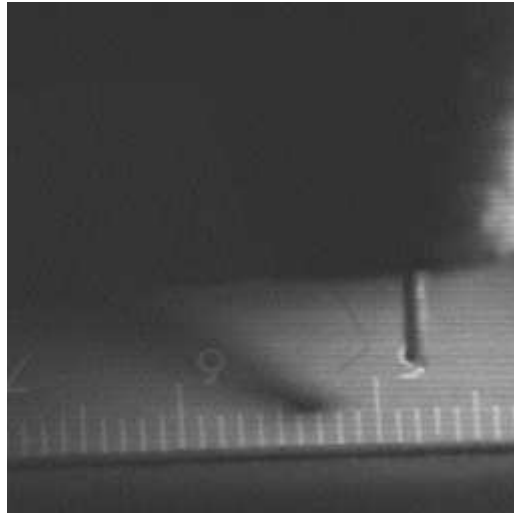


Figure 5.11 Calibration Image for HSV Using a Millimeter Scale

HSV was conducted for both BOP welds and fillet welds in lap joints. The frame rate was selected to record the weld pool dynamics during hump formation, and particularly to record the event which causes the end of one hump and the beginning of the next. This key event between humps has not previously been documented in a way that allows it to be definitively seen. Being able to view and interpret this event is key to the understanding of the humping discontinuity.

5.7 Accuracy and Inaccuracy of Methods, Verification, and Repeatability

During the course of the 6 years of work three DC inverter GMAW-P power sources from ESAB, Miller Electric, and Thermal Arc were used. However, while the power sources themselves were not calibrated, the sensors used to measure welding current, arc voltage, and WFS were calibrated to NIST standards. So also were the weld data acquisition systems, albeit that different equipment was used: the ADM and Arc Agent-type systems.

While each power source uses a different pulse current waveform shape and pulse parameter selection logic control, work by the author in the past has shown this to have a negligible affect on the welding current delivered for the WFS demanded or on the weld bead shape and penetration profile at the same arc voltage and overall heat input.

When setting up sheet material for welding trials, the heat sink was considered such that the technique remained the same. Often the same fixture was used to hold the parts, but when it was not, a similar heat sink, and the same support technique were employed. For example, when performing lap fillet welding trials, a gap of 25 mm was left between the two halves of the fixture in each case. The 2-D heat flow in sheet metal tends to mitigate any small differences, since by its nature it is lateral, away from the weld.

Potential stacking errors in alignment of the GMAW welding torch travel angle, work angle, CTWD, and wire placement in a joint were considered and minimized by careful set-up and measurement of angles with a magnetic angle finder accurate to 1

degree, and formed wire gauges for CTWD consistency. This became even more important when combining GMAW-P with the lasers for hybrid LBW/GMAW-P operation.

Two different lasers were used during the course of the work, an Nd:YAG Laser at EWI and CO₂ laser in the work performed at OSU. The lasers use different light wavelength and have different absorption characteristics. These are sufficiently different that parameters were not simply transferred from one to the other. As such issues of accuracy and repeatability are not really pertinent in these cases, but are when setting up the respective lasers. In each case the laser light intensity and distribution was measured using either the PRIMES tool or by Perspex 'burn patterns' to check for the required spot diameter, for example, when experimenting and deploying different beam diameter and power density effects.

Two significantly different welding robots were used during the work: the GMF six-axis robot and the Motoman K16 to deploy CO₂ and Nd:YAG lasers, respectively. However, the robots were used to make simple linear welds and so are not considered to have had any impact on the results.

When conducting the calorimetry experiments the time to deliver the specimens into the liquid nitrogen bath was carefully controlled to minimize any inaccuracy of the experimental results that may have resulted from different cooling times between one sample and the next before immersion. The bath position relative to the welding operation was maintained constant to minimize errors. A calibrated balance, accurate to several decimal places, was used to minimize overall measurement error because the total weight loss in each specimen is small relative to their weight.

The Phantom camera was equipped with software on a laptop computer for image capture, recording, and analysis. The Phantom employs a modern complementary metal oxide semiconductor (CMOS) camera, and had a built-in IR band-pass filter holder which meant that the IR band-pass filter could be easily inserted and removed when setting up the camera. The Phantom has better resolution and is easier to use; the Kodak system required separate image capture with frequent data exchange errors.

6.0 RESULTS

The results are described in the following sections and are divided as follows:

- Conventional GMAW-P parameters for welding with 0T and 1T gaps
- High-speed GMAW-P with 0T gap
- Hybrid LBW/GMAW-P using CO₂ and Nd:YAG lasers
- HSV of GMAW-P and hybrid LBW/GMAW-P welding

The results aim to establish the operating regimes for each process as they relate to the onset of the humping defect and to the study of this defect for high-speed GMAW-P.

6.1 Welding Parameters for Weld Sizing

The following sections give the results from the SWAT trials that were performed on the 2.4-, 2.0-, and 1.6-mm-thick mild steel sheet. The purpose of these weld runs was to use conventional GMAW-P practice in terms of travel angle to establish nominal welding parameters that could be compared, as a benchmark, to high-speed GMAW-P and welds made using hybrid LBW/GMAW-P.

6.1.1 2.4-mm Material Thickness

The arc voltage and the WFS relationship for maintaining a 3.2-mm arc length is shown in Figure 6.1. This arc length was used during the welding parameter trials for all three material thicknesses.

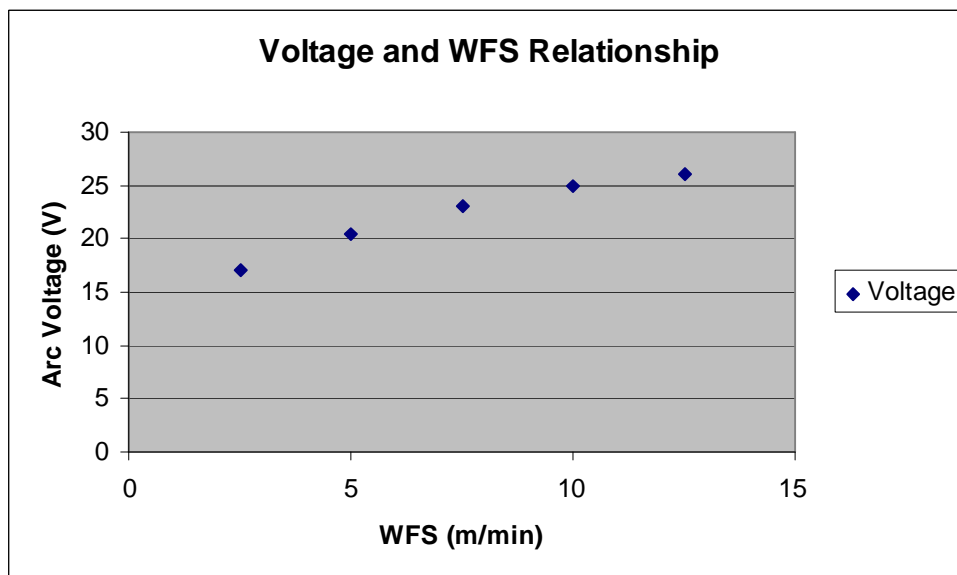


Figure 6.1 WFS versus Voltage Relationship for Maintaining a Constant 3.2-mm Arc Length Using GMAW-P with a 19-mm CTWD and a 1.2-mmER70S-3 Electrode

The welds made at a range of WFS and TS were visually inspected and rated according to the acceptance criteria in AWS D8.8 (AWS, 1998). The acceptable region for welds based on visual inspection, Figure 6.2, was quite narrow.

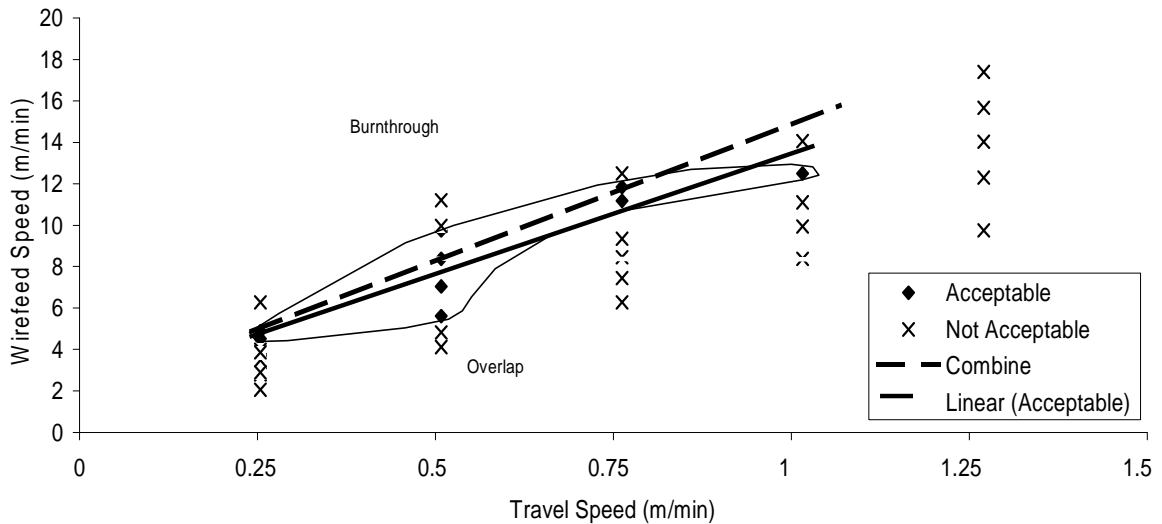


Figure 6.2 SWAT Results Showing the Visually Acceptable Weld Area Curve for 2.4-mm Mild Steel with a 0T Joint Gap

There were two reasons why welds failed visual examination: one was burnthrough and the other was overlap. Burnthrough resulted from excess heat input into the part based on high WFS. Overlap occurs when the heat input (i.e., WFS) is too low and the weld does not fuse properly with the lower joint member. Complete root penetration can be achieved when a weld has an overlap condition, but the overlap is a profile irregularity that is undesirable, especially if the part is subjected to fatigue loading. This is the primary reason that the destructively tested results, Figure 6.3, have a larger acceptability window compared to the visually examined welds. The destructive testing only requires complete fusion with the lower joint member.

The 'linear (acceptable)' result is for the best fit straight line describing the results of all the visually acceptable welds. The dotted line designated 'combine' indicates the combined best fit straight line for the visual and destructively tested welds. These lines are the same in each pair of results, e.g., Figures 6.2 and 6.3.

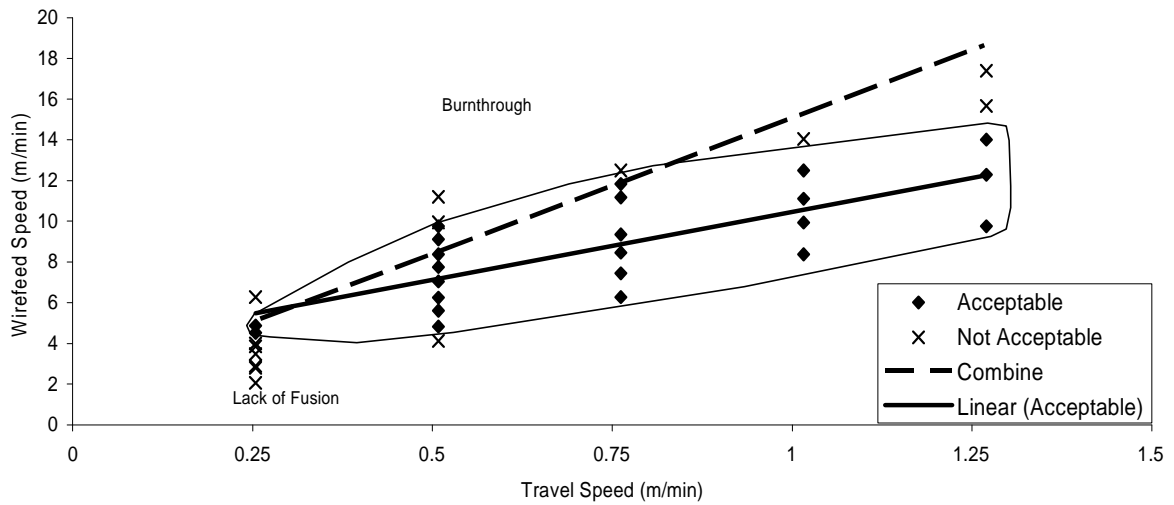


Figure 6.3 SWAT Results Showing the Destructively Tested Acceptable Weld Area Curve for 2.4-mm Mild Steel with a 0T Joint Gap

Visual inspection was the more conservative evaluation and therefore was used for all the subsequent weld evaluations.

Metallographic sectioning was also used to verify the results, Figure 6.4. This is presented as a metallographic map to indicate the typical fusion characteristics and weld surface profiles achieved at each combination of WFS and TS. These welds were made using a nominal 0T gap condition.

The basis for ‘acceptable’ and ‘not acceptable’ for the destructive testing was the presence or absence of fusion defects in the weld cross section judged according to the requirements of ANSI/AWS D1.3 for sheet metal fabrication. The welds can be acceptable based on destructive testing but unacceptable based on visual inspection requirements such as burnthrough, and overlap. Therefore, the more stringent requirements of visual inspection were plotted subsequently.

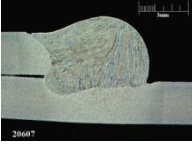
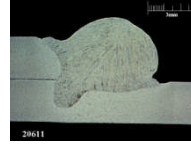


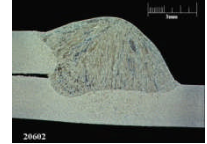
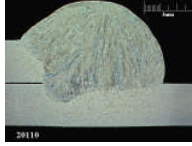
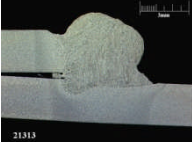
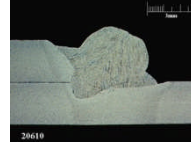

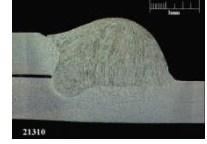
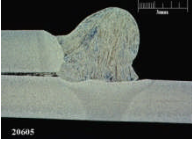
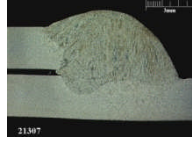





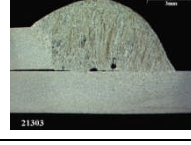

WFS = 14.0 (m/min)					
WFS = 12.7 (m/min)					
WFS = 11.4 (m/min)					
WFS = 10.2 (m/min)					
WFS = 8.9 (m/min)					
WFS = 7.6 (m/min)					
WFS = 6.3 (m/min)					
WFS = 5.1 (m/min)					
WFS = 3.8 (m/min)					
	TS = 0.25 m/min	TS = 0.51 m/min	TS = 0.76 m/min	TS = 1.0 m/min	TS = 1.3 m/min

Figure 6.4 Macrosection Map for 2.4-mm Lap Joints with a 0T Joint Gap

The leg lengths, weld area and toe angle against the lower sheet was measured for several of the welds in 2.4-mm sheet with a 0T gap were measured. Results are shown in Table 6.1 below.

Table 6.1 Measurement of Fillet Weld Leg Lengths, Area, and Toe Angle Against Lower Sheet

Weld No.	Length L1 (mm)	Length L2 (mm)	Area (mm²)	Angle (degrees)
20104	2.9	6.9	31	54
20105	2.9	7.3	37	121
20106	2.9	4.6	16	96
20107	2.9	5.2	24	121
20109	2.9	8.5	35	113
20110	2.9	7.2	39	80
20601	2.8	6	21	100
20602	2.8	8	30	119
21303	2.8	7.5	29	121
21304	2.8	7.4	31	73
21305	2.9	4.3	20	79
21306	2.8	5.6	27	92
21307	3	7.3	28	114
21308	2.8	8.3	34	93
21310	2.8	7.5	26	133
21314	2.8	6.4	28	56

Note: Baseline GMAW-P with normal (90-degree) torch lead angle and ER70S-3 wire

The toe angle is the angle subtended from the surface of the sheet to the toe of the weld, in the case above to the toe of the fillet weld. It is an included angle, such that the larger the angle the smoother the transition between the sheet surface and the weld toe. For the best fatigue performance, the toe angle is preferred to be 120 degrees or higher. For vehicle structures subject to significant fatigue loading, the same is looked for in a fillet weld, either in a T-butt or lap-fillet joint.

Some reentrant angles (less than 90 degrees) were measured. In six cases angles of 115 to 121 were found, with one measured at 133 degrees. The typical lower leg length ranged from 6-8 mm, around two to three times the material thickness. The weld area typically ranged from 25 to 35 mm². These measurements were used as a baseline for improvements made using hybrid welding.

The solid line shown on Figure 6.2 was developed using linear regression from the data points in the acceptable weld region. The results of the welds performed on a 2.4-mm-thick lap joint with a 1T gap are given in Figure 6.5.

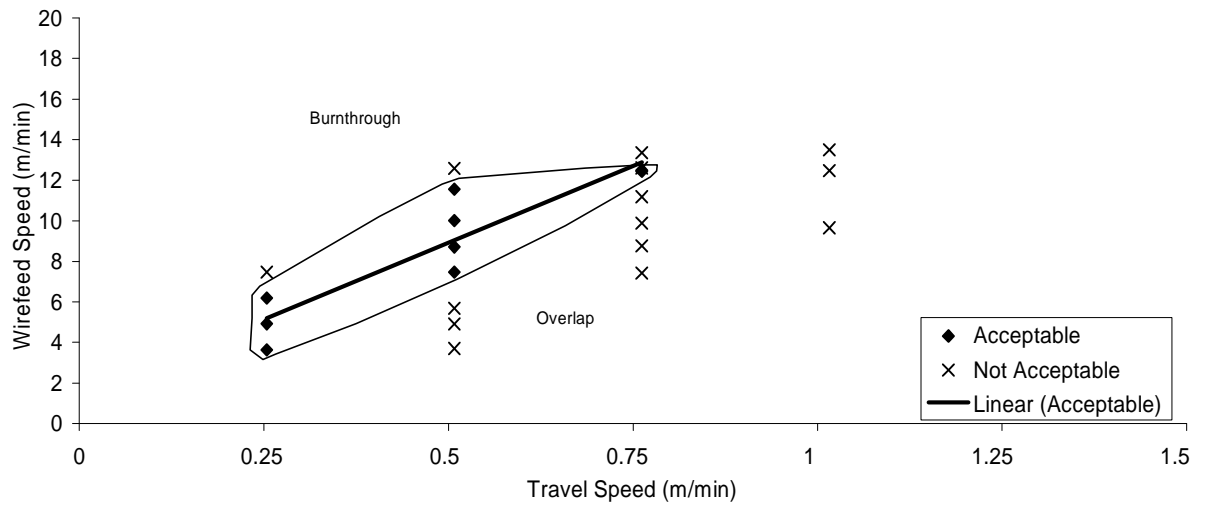


Figure 6.5 SWAT Results Showing the Acceptable Weld Area Curve for 2.4-mm Mild Steel with a 1T Joint Gap Based on Visual Inspection

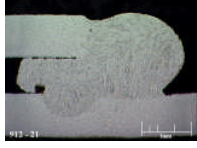
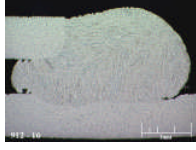
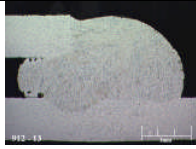


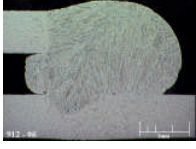

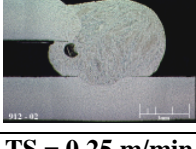
WFS = 12.7 (m/min)					
WFS = 11.4 (m/min)					
WFS = 10.2 (m/min)					
WFS = 8.4 (m/min)					
WFS = 7.6 (m/min)					
WFS = 6.4 (m/min)					
WFS = 5.1 (m/min)					
WFS = 3.8 (m/min)					
	TS = 0.25 m/min	TS = 0.51 m/min	TS = 0.76 m/min	TS = 1.0 m/min	TS = 1.27 m/min

Figure 6.6 Macrosection Map for 2.4-mm Lap Joints with a 1T Joint Gap

The equations for both the 0T and 1T joint gap conditions were averaged and a third equation derived representing the WFS and TS relationship that would produce acceptable results for both a 0T and 1T gap, for 2.4-mm-thick mild steel.

$$\text{WFS m/min} = 13.25(\text{TS}) + 1.66 \quad (6.1)$$

Eq. (6.1) is plotted as a dashed line on Figures 6.2 and 6.3. The dashed line can be seen to overlap the acceptable weld regions of both plots. For both figures, the line overlaps the acceptable region between the 0.255- and 0.760-m/min TS. Since the visual acceptance of the joint was shown to be more conservative in terms of weld acceptance than the NDE results, the dotted line was eliminated from subsequent

graphs. In short, WFS is a function of TS for a good weld, based on visual appearance of welds on 2.4-mm-thick sheet with 0T and 1T gaps. Higher WFS leads to burnthrough and lower WFS leads to overlap.

6.1.2 2.0-mm Material Thickness

A similar series of weld trials was performed on the 2.0-mm thickness. Figures 6.7 and 6.9 depict the acceptable weld regions for the 0T and 1T joint gaps, while the metallographic results are shown in Figures 6.8 and 6.10.

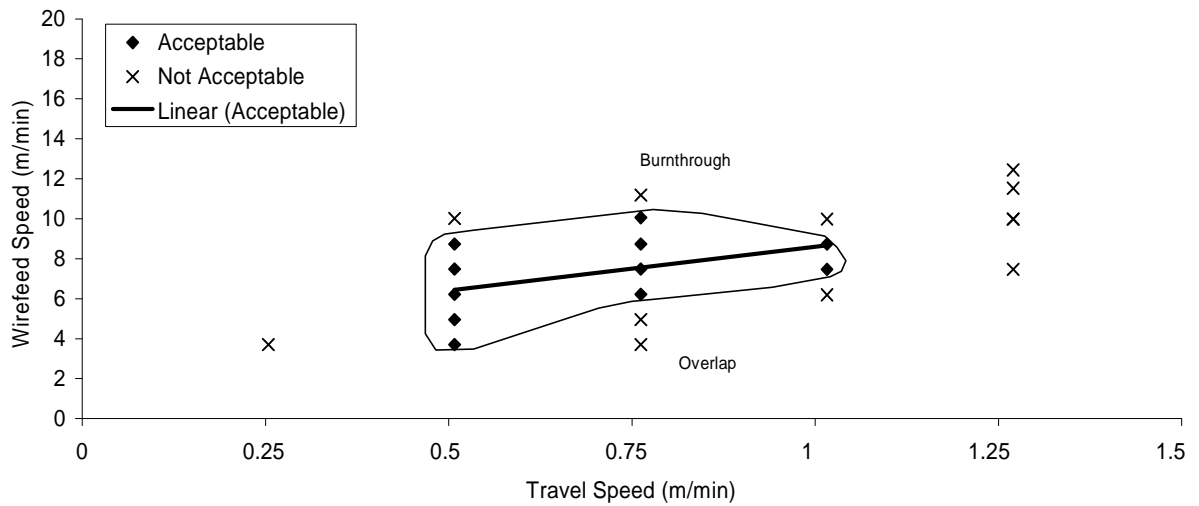


Figure 6.7 SWAT Results Showing Acceptable Weld Area Curve for 2.0-mm Mild Steel Lap Joints with a 0T Joint Gap Based on Visual Inspection

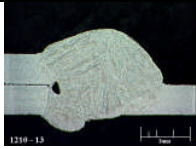
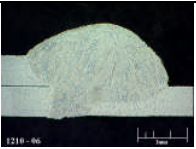
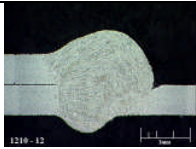
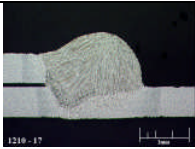
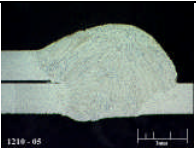
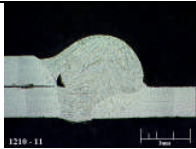
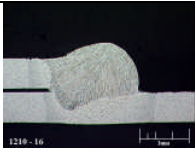
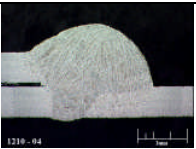
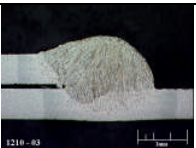
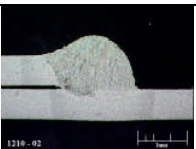
WFS = 10.2 (m/min)					
WFS = 8.9 (m/min)					
WFS = 7.6 (m/min)					
WFS = 6.4 (m/min)					
WFS = 5.1 (m/min)					
WFS = 3.8 (m/min)					
	TS = 0.25 m/min	TS = 0.51m/min	TS = 0.76 m/min	TS = 1.0 m/min	TS = 1.27 m/min

Figure 6.8 Macrosection Map For 2.0-mm Sheet Lap Joints with 0T Gap

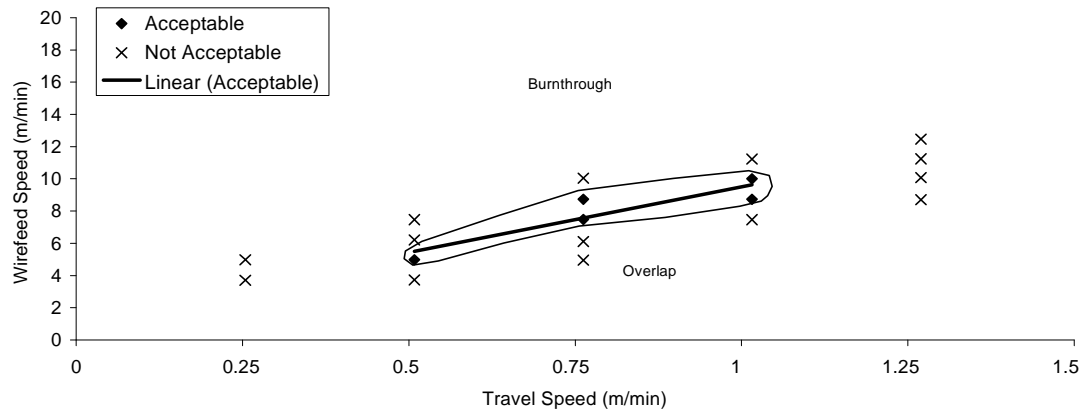


Figure 6.9 SWAT Results Showing Acceptable Weld Area Curve for 2.0-mm Mild Steel Lap Joints with a 1T Joint Gap Based on Visual Inspection

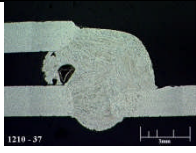
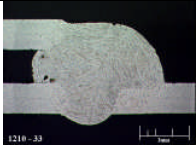
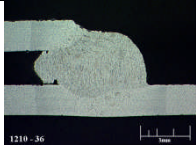
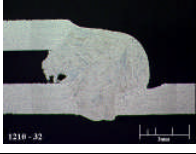
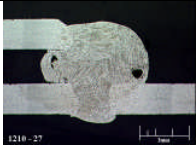
WFS = 10.2 m/min					
WFS = 8.9 m/min					
WFS = 7.6 m/min					
WFS = 6.4 m/min					
WFS = 5.1 m/min					
	TS = 0.25 m/min	TS = 0.51 m/min	TS = 0.76 m/min	TS = 1.0 m/min	TS = 1.27 m/min

Figure 6.10 Macrosection Map for 2.0-mm Lap Joints with a 1T Joint Gap

The dashed line represents the combined WFS versus TS relationship, which produces an acceptable weld, for both a 0T and 1T joint gap.

Eq. (6.2) describes the preferred WFS versus TS relationship for the 2.0-mm mild steel that accommodates a 0T and 1T joint gap while still maintaining an acceptable weld, the dashed line in Figures 6.7 and 6.9.

$$WFS \text{ m/min} = 6.25 (TS) + 2.81 \quad (6.2)$$

6.1.3 1.6-mm Material Thickness

Figures 6.11 and 6.13 depict the acceptable weld regions for 0T and 1T joint gap for the 1.6-mm thickness, while Figures 6.12 and 6.14 show the metallographic results.

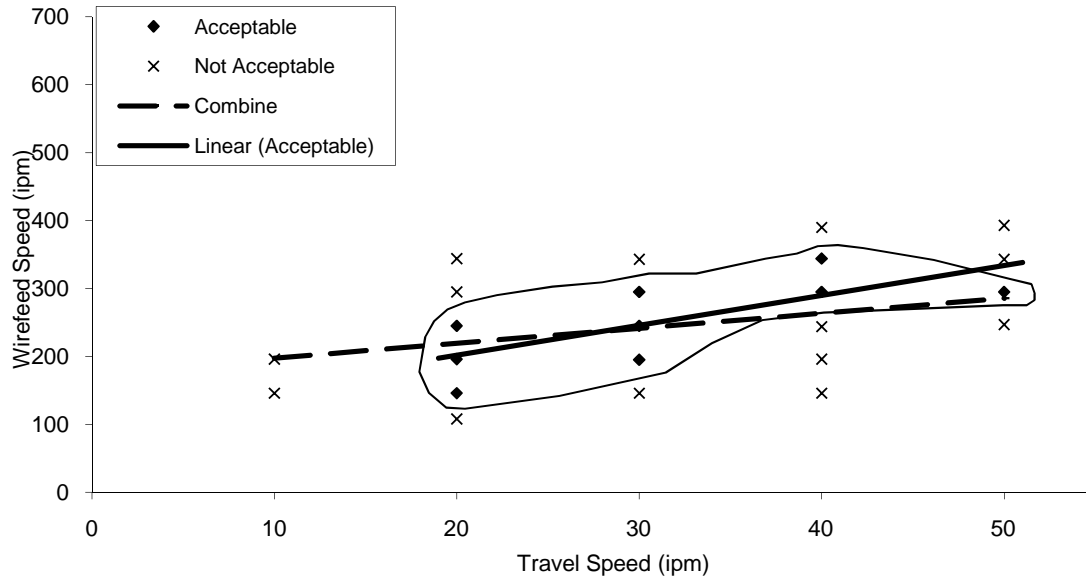


Figure 6.11 SWAT Results Showing Acceptable Weld Area Curve for 1.6-mm Mild Steel Lap joints with a 0T Joint Gap Based on Visual Inspection

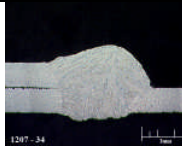
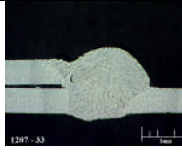
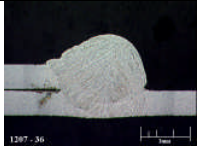
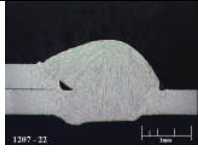
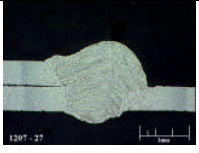
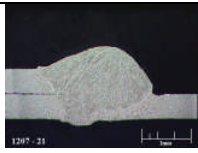
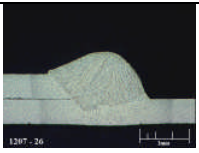
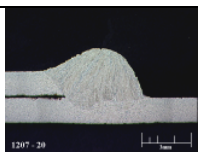
WFS = 8.9 (m/min)					
WFS = 7.6 (m/min)					
WFS = 6.4 (m/min)					
WFS = 5.1 (m/min)					
WFS = 3.8 (m/min)					
	TS = 0.25 m/min	TS = 0.51 m/min	TS = 0.76 m/min	TS = 1.0 m/min	TS = 1.27 m/min

Figure 6.12 Macrosection Map for 1.6-mm Lap Joints with a 0T Joint Gap made using a 1.2-mm-Diameter ER70S-3 Electrode Wire

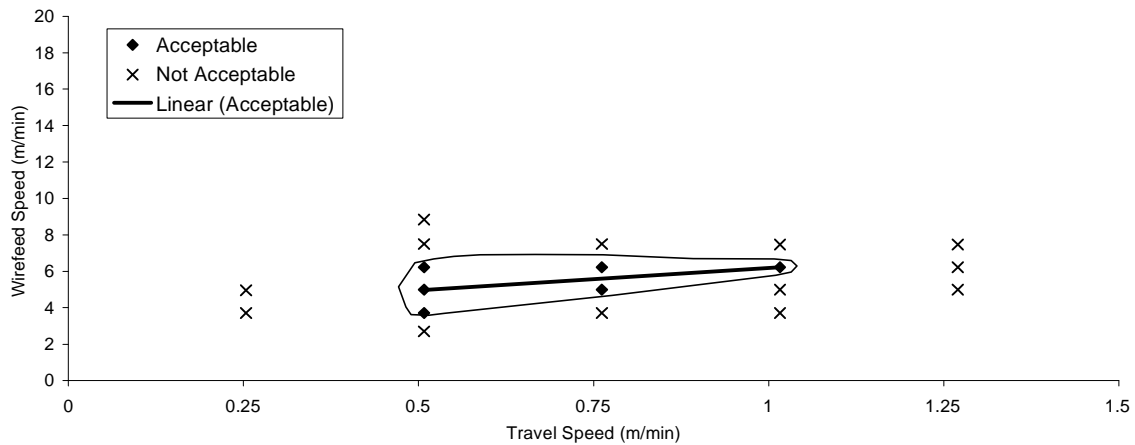


Figure 6.13 SWAT Results Showing Acceptable Weld Area Curve for 1.6-mm Mild Steel Lap Joints with a 1T Joint Gap Based on Visual Inspection

Eq. (6.3) is the derived equation for the welding conditions that accommodate a 0T and 1T joint gap while still maintaining an acceptable weld, the dashed line in Figures 6.11 and 6.13.

$$WFS \text{ m / min} = 2.21 (TS) + 7.16 \quad (6.3)$$

Having developed Eqs. (6.1) through (6.3) for the three material thickness, the highest travel speed producing acceptable results for both 0T and 1T joints was used to calculate the WFS for six more welds made to validate the equations. The six welds at the highest TS are shown in Figures 6.15, 6.16, and 6.17, for the 2.4-, 2.0-, and 1.6-mm-thick sheet lap joints, respectively. All six welds were acceptable, thus validating the equations.

For T-butt joints a range of WFS:TS of 7:1 through 10:1 produced welds of acceptable quality with some minimal undercut (within acceptance limits), Figure 6.18.


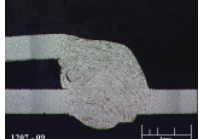
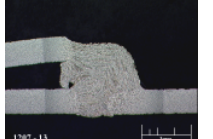
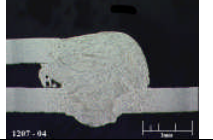
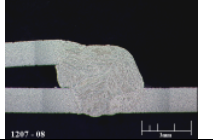
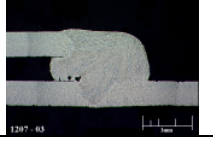
WFS = 6.4 (m/min)					
WFS = 5.1 (m/min)					
WFS = 3.8 (m/min)					
	TS = 0.25 m/min	TS = 0.51 m/min	TS = 0.76 m/min	TS = 1.0 m/min	TS = 1.27 m/min

Figure 6.14 Macrosection Map for 1.6-mm Lap Joint with a 1T Joint Gap made using a 1.2-mm-Diameter ER70-S3 Electrode Wire

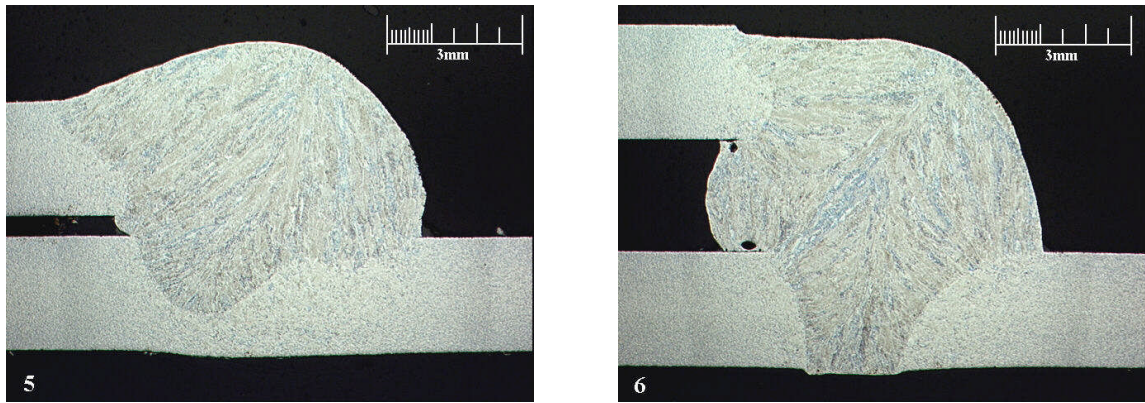


Figure 6.15 Developed Weld Area for the 2.4-mm Mild steel Sheet Applied to a 0T Joint Gap (left) and 1T Joint Gap (right) using 8.8 m/min WFS and 0.76 m/min TS

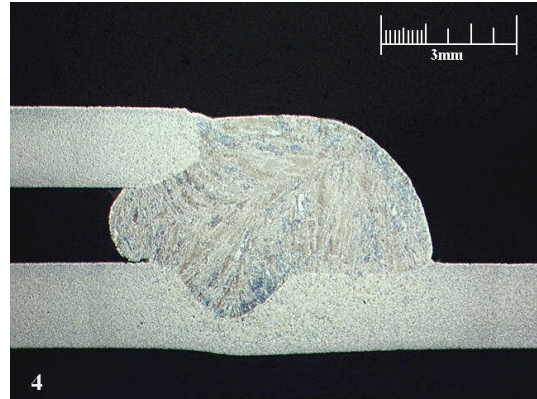
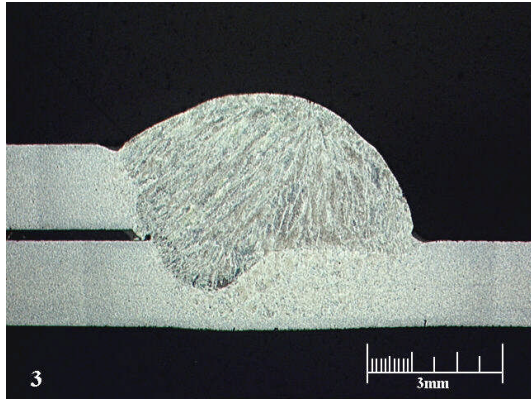


Figure 6.16 Developed Weld Area for the 2.0-mm Mild Steel Sheet Applied to a 0T Joint Gap (left) and 1T Joint Gap (right) using 8.8 m/min WFS and 0.76 m/min TS

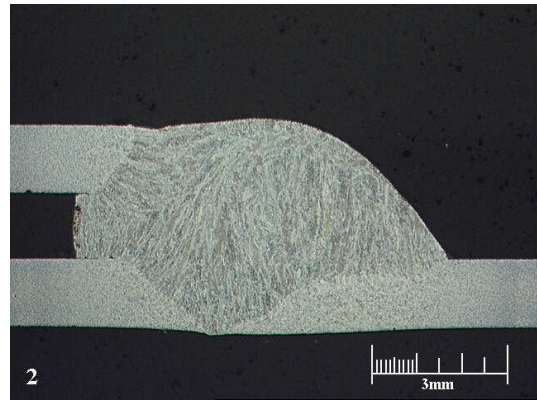
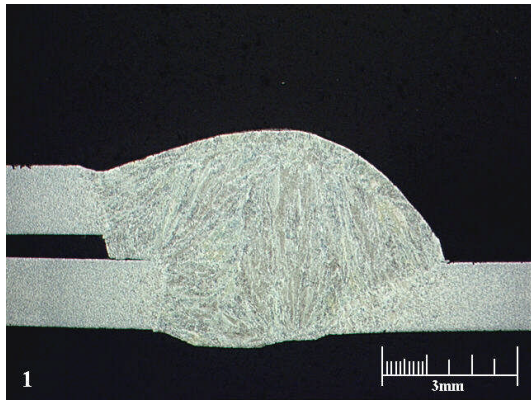
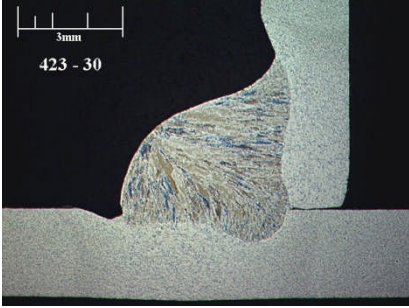
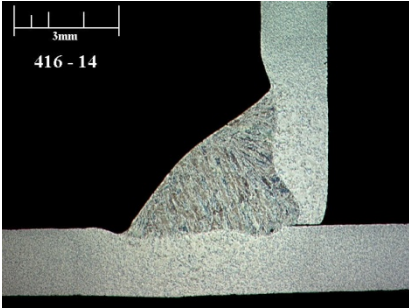


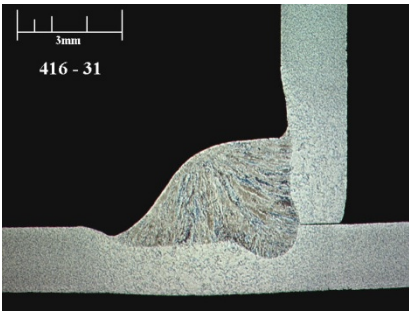
Figure 6.17 Developed Weld Area for the 1.6-mm Mild Steel Sheet Applied to a 0T Joint Gap (left) and 1T Joint Gap (right) using 8.8 m/min WFS and 0.76 m/min TS



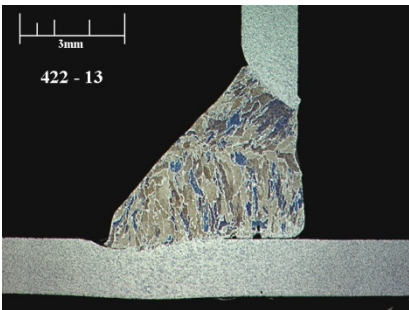
(a) 2.4-mm sheet, WFS 7.6 m/min, TS 0.76 m/min



(b) 2.0-mm sheet, WFS 3.8 m/min, TS 0.51 m/min



(c) 2.0-mm sheet, WFS 7.0 m/min, TS 1.0 m/min



(d) 1.6-mm sheet, WFS 2.5 m/min, TS 0.25 m/min

Figure 6.18 Macrosections of Fillet Welds on T-Butt Joints for the Three Material Thicknesses Studied

A typical humping defect in a fillet produced on a lap-fillet joint with a 1T gap is shown in Figure 6.19.



Figure 6.19. Continuous Humping Defect Generated at a 1T Gap on a Joint at a ‘High’ 1.0-m/min TS

The images in Figure 6.20 shows cross sections of the high and low areas of the humped bead marked in Figure 6.19.

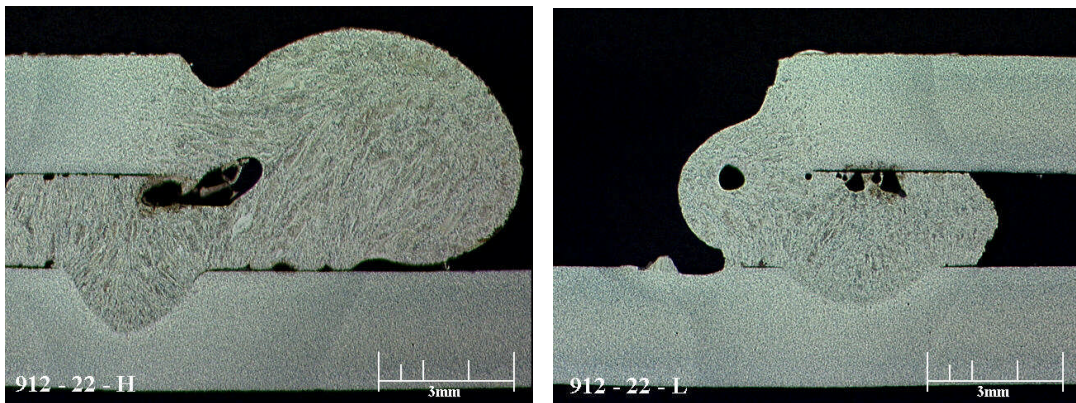
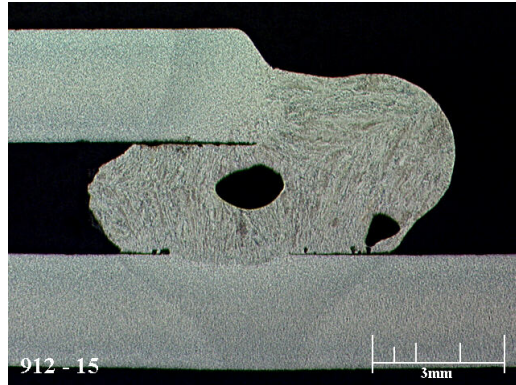
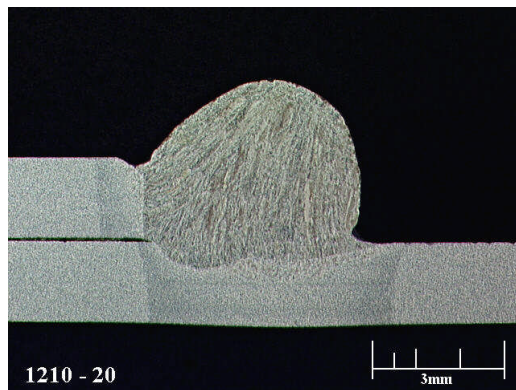


Figure 6.20 2.4-mm Sheet, 12.7 m/min WFS, 1.0 m/min TS, 1T Gap

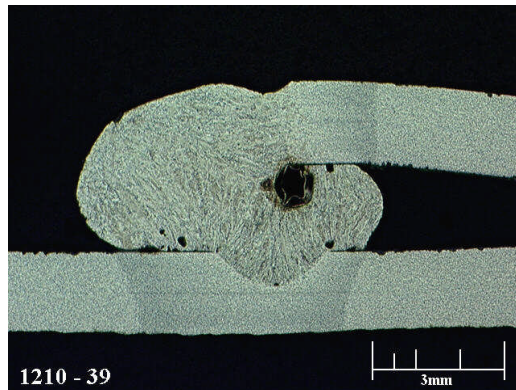
When the gap is 0T the typical appearance of the bead hump cross section is illustrated in Figure 6.21 (b). When there is a 1T gap the typical appearance is similar to those shown in Figures 6.20 and in 6.21 (a) and (c).



(a) 2.4-mm sheet, WFS 10.2 m/min, TS 1.0 m/min, 1T Gap



(b) 2.0-mm sheet, WFS 8.9 m/min, TS 1.27 m/min, 0T Gap



(c) 2.0-mm sheet, WFS 8.9 m/min, TS 1.27 m/min, 1T Gap

Figure 6.21 Further Examples of Humped Bead Profiles for 2.4- and 2.0-mm Sheet

6.2 High-Speed GMAW-P for Lap-Fillet Joints

The high-speed GMAW-P work focused on a higher lead travel angle compared with conventional practice. The latter typically uses a 90-degree travel angle or a lead angle of up to 15 degrees. As a higher lead travel angle tends to produce a shallower weld with less convexity, it is considered a useful approach to increase the maximum travel speed before humping occurs. A 30-degree lead travel angle was selected as the maximum practical angle to avoid potential mechanical interference between the torch nozzle and the weld and to avoid excessive CTWD.

Weld lap joints were made for three material thicknesses (2.4-, 2.0-, and 1.6-mm steel) of carbon steel sheet. The limits of acceptable welds were explored by increasing the TS until the bead humping phenomena appeared. Three WFS were chosen for each material thickness and the TS was increased until the humping was evident. Macrosections were taken of the weld profile (macros sectioned at hump of beads). The electrode wire was aimed at the top edge of the top sheet in the lap joint. The wire (arc) placement was seen to have significant effect on when the humping phenomena appeared. Placing the wire into the middle of the lap joint, aiming at the root of the joint, caused the humping to appear at lower TS.

The results are summarized below:

- **2.4-mm Sheet:**
 - 12.7-m/min WFS: Bead humping at 1.32 m/min 26.4 V
 - 14.0-m/min WFS: Bead humping at 1.9 m/min 27.1 V
 - 15.2-m/min WFS: Bead humping at 2.3 m/min 27.8 V

- **2.0-mm Sheet:**
 - 7.6-m/min WFS: Bead humping at 1.33 m/min 22.9 V
 - 8.9-m/min WFS: Bead humping at 1.71 m/min 23.9 V
 - 10.2-m/min WFS: Bead humping at 2.16 m/min 24.8 V

- **1.6-mm Sheet:**
 - 7.6-m/min WFS: Bead humping at 1.46 m/min 22.9 V
 - 8.9-m/min WFS: Bead humping at 2.03 m/min 23.9 V
 - 10.2-m/min WFS: Bead humping at 2.48 m/min 24.8 V

These results are shown graphically by plotting them (in red) on the same graphs produced using the original work for tolerance to OT and IT gaps where a torch travel angle normal to the workpiece was used.

For the 2.4-mm-thick material, the speed at which humping became a limiting factor was increased to 2.3 m/min at the highest WFS (15.2 m/min), Figure 6.22. Humping occurred

at travel speeds above 1.0 m/min with the conventional travel angle (normal angle to the workpiece), Figure 6.22. Welds above the red line, i.e., below the humping limit would be acceptable in terms of surface profile.

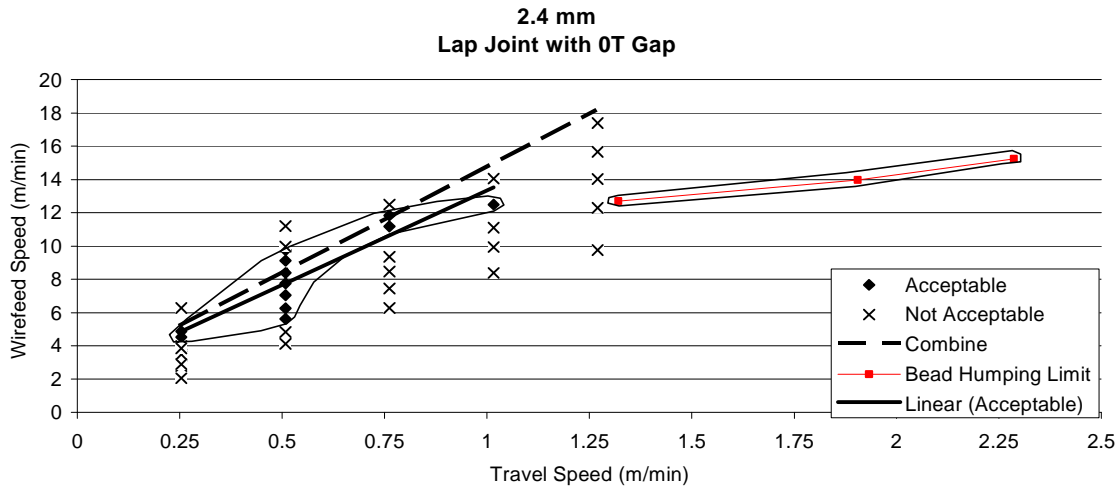


Figure 6.22 Bead Humping Limit for High-Speed GMAW-P versus ‘Conventional’ GMAW-P for 2.4-mm Material

For the 2.0-mm-thick material, the speed at which humping was produced was increased to 2.16 m/min at the highest WFS (10.2 m/min), Figure 6.23.

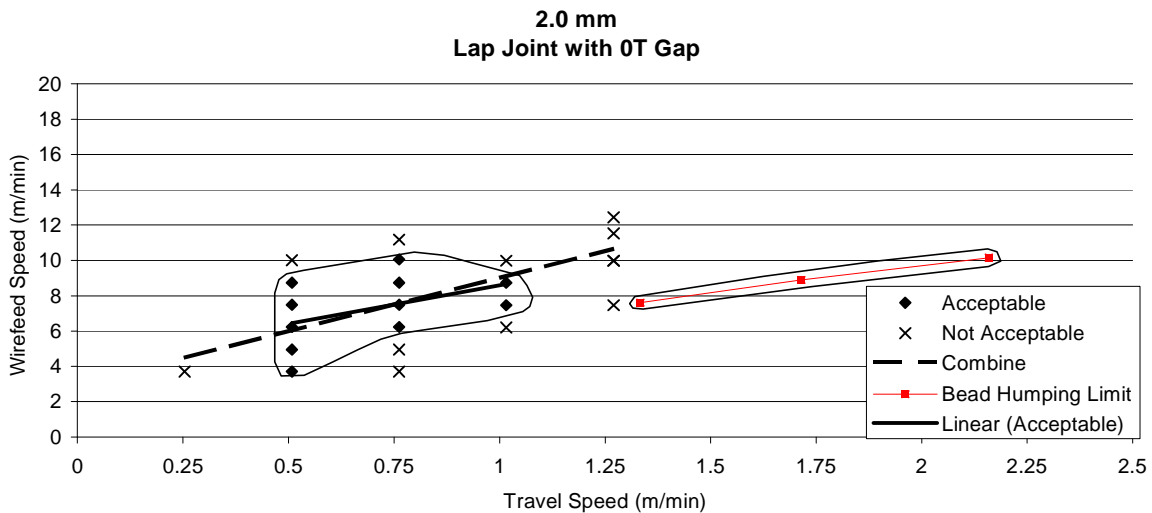


Figure 6.23 Bead Humping Limit for High-Speed GMAW-P versus ‘Conventional’ GMAW-P for 2.0-mm Material

For the 1.6-mm-thick material, the speed at which humping was produced was increased to 2.48 m/min at the highest WFS (10.2 m/min), Figure 6.24.

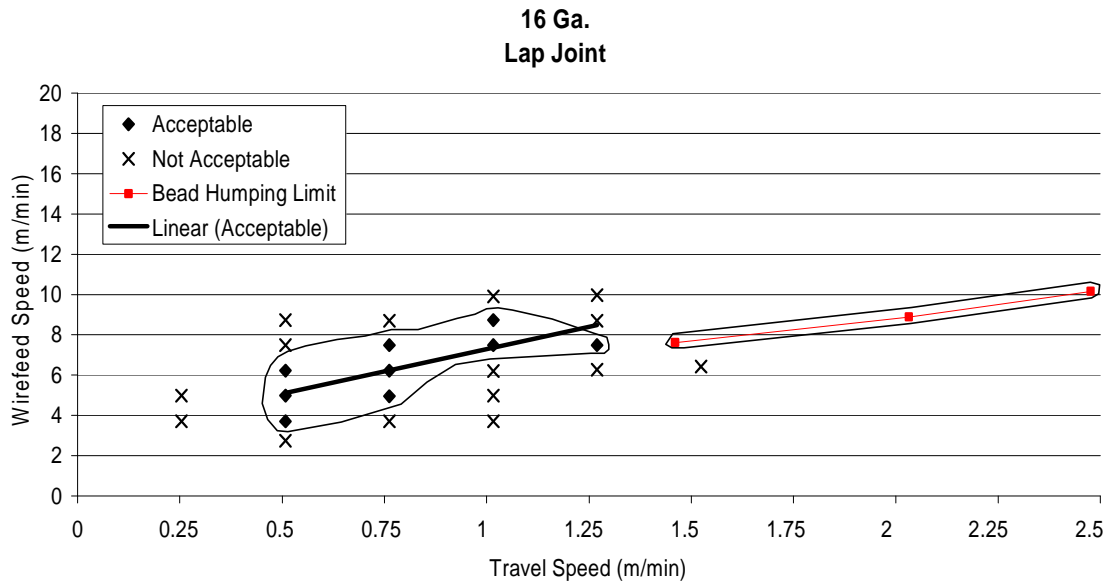


Figure 6.24 Bead Humping Limit for High-Speed GMAW-P versus ‘Conventional’ GMAW-P for Lap-Fillet Joints in 1.6-mm Sheet

A weld appearance map showing the appearance of welds made is shown in Figure 6.25.

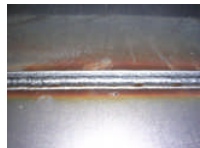

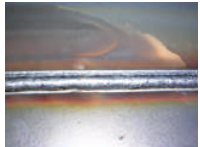



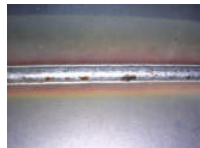
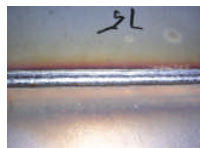
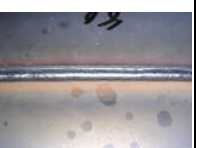
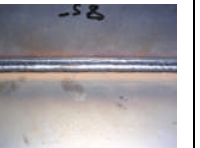


WFS (m/min)	TS (m/min)					
	1.15	1.3				
12.5						
	1.15	1.78	1.85	1.9		
14.0						
	1.15	1.9	2.0	2.1	2.2	2.3
15.25						

Figure 6.25 Weld Appearance Map for 2.4-mm Sheet Lap-Fillet Joints with 0T Gap and 30-Degree Lead Travel Angle

Plotting the other acceptable welds on the respective graphs for the three material thicknesses significantly expanded the regions of acceptable welds produced using the 30-degree lead travel angle. This is illustrated below for the 2.4-mm-thick sheet, Figure 6.26. Two weld regions are shown, one with the zero-degree travel angle on the lower left and one with the 30-degree travel angle at the upper right. Using the higher WFS/TS along with the higher travel angle allowed the area of acceptable welds to be increased significantly to higher welding speeds. The lead travel angle is considered to have positively influenced the convex shape of the weld pool to make it less convex, thus delaying the onset of poor wetting and bead humping to higher travel speeds.

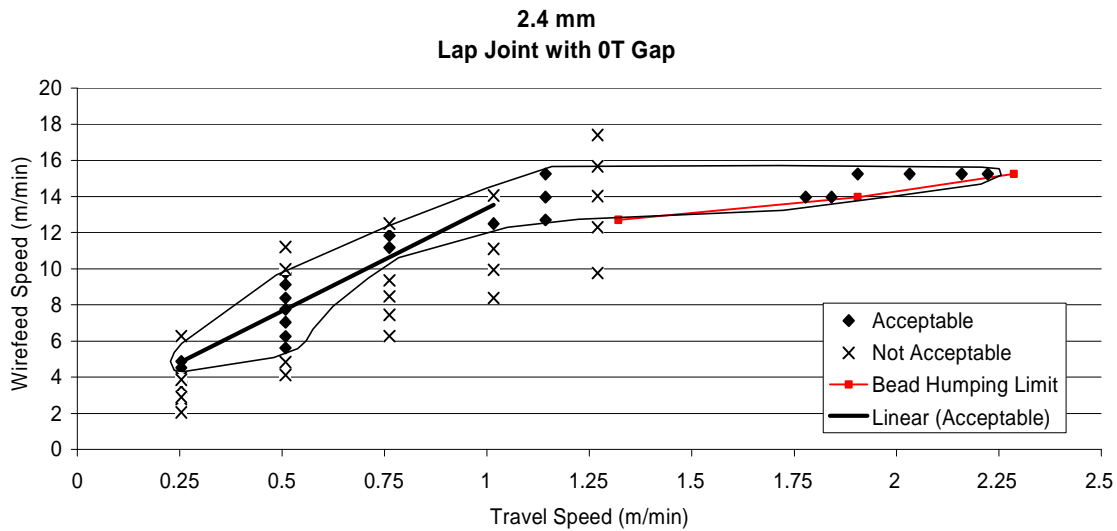


Figure 6.26 Bead Humping Limit and Acceptable Weld Area for High-Speed GMAW-P versus ‘Conventional’ GMAW-P for 2.4-mm Sheet

A weld appearance map showing the appearance of welds made in 2.0-mm sheet is shown in Figure 6.27.




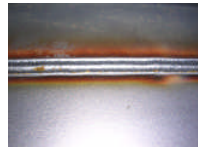
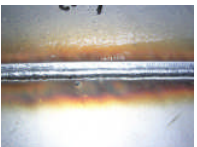
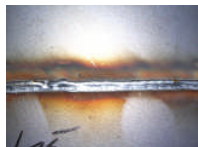

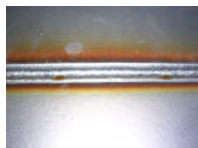
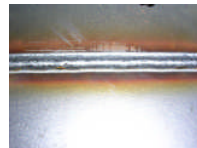




WFS (m/min)	TS (m/min)					
	1.15	1.25	1.35	1.5		
7.6			No Picture			
	1.15	1.5	1.65	1.7		
8.9						
	1.15	1.25	1.5	1.75	2.0	2.2
10.2						

Figure 6.27 Weld Appearance Map for 2.0-mm Sheet Lap-Fillet Joints with 0T Gap and 30-Degree Lead Travel Angle

For the 2.0-mm-thick sheet the area of acceptable welds was increased significantly at the higher TS, as shown in Figure 6.28.

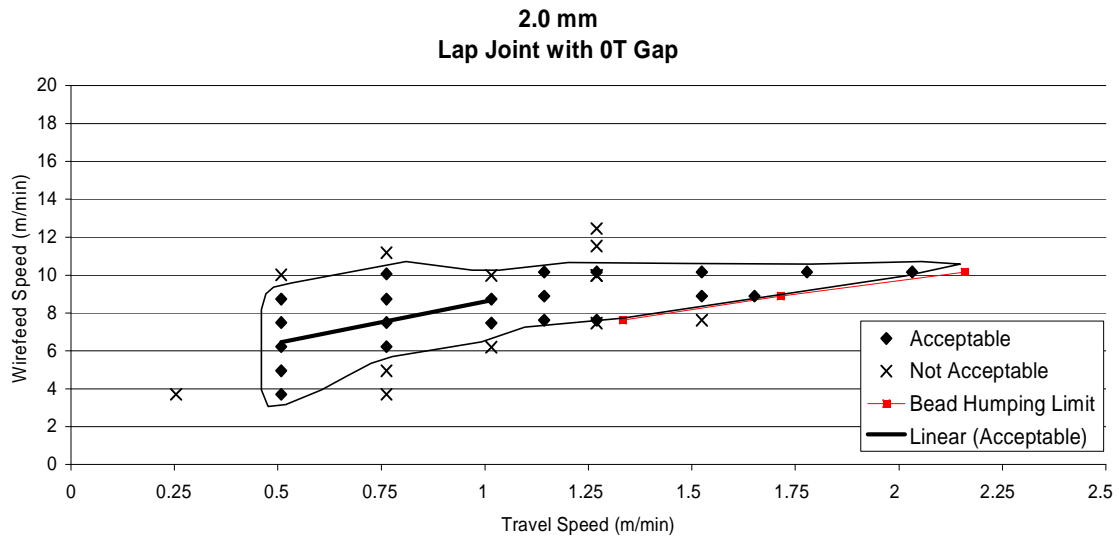


Figure 6.28 Bead Humping Limit and Acceptable Weld Area for High-Speed GMAW-P versus ‘Conventional’ GMAW-P in 2.0-mm Sheet

A weld appearance map showing the appearance of welds made in 1.6-mm sheet is shown in Figure 6.29.

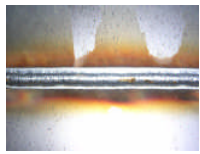


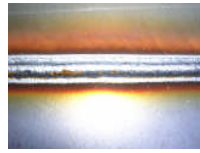
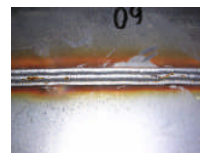

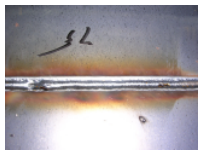


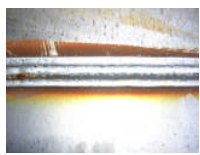

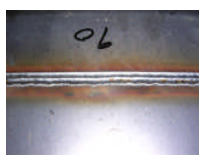


WFS (m/min)	TS (m/min)					
	1.4	1.45	1.5			
7.6						
	1.4	1.5	1.8	1.9	1.95	2.0
8.9						
	1.4	2.0	2.3	2.4	2.45	2.5
10.2					No Picture	

Figure 6.29 Weld Appearance Map for 1.6-mm Sheet Lap-Fillet Joints with 0T Gap and 30-Degree Lead Travel Angle

For the 1.6-mm-thick sheet the area of acceptable welds was increased significantly at the higher TS as shown in Figure 6.30.

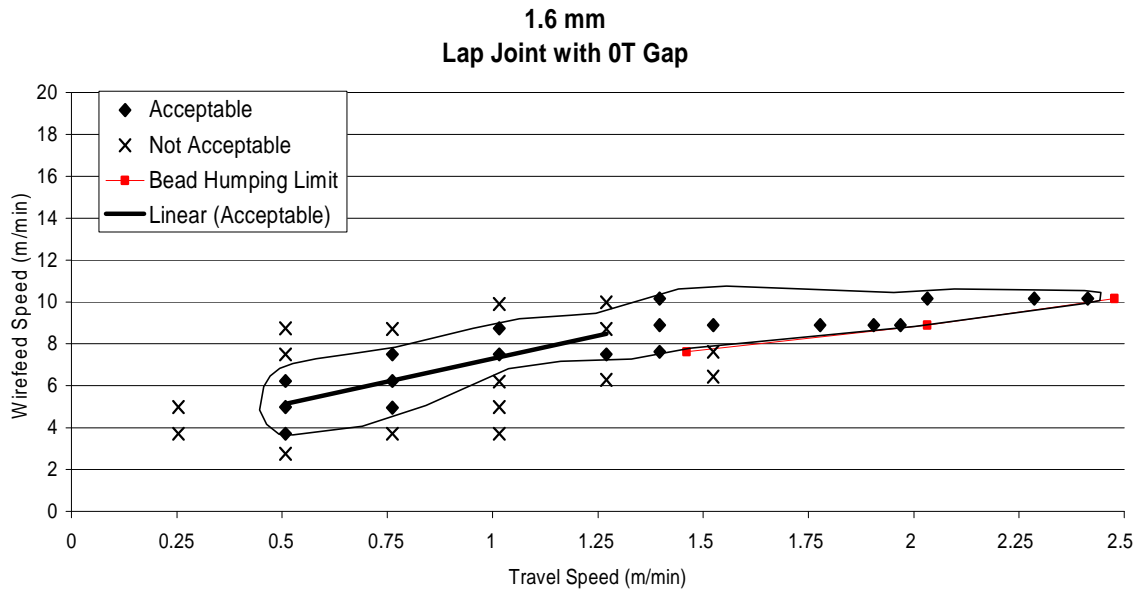


Figure 6.30 Bead Humping Limit and Acceptable Weld Area for High-Speed GMAW-P versus ‘Conventional’ GMAW-P in 1.6-mm Sheet

Bead shapes for the weld beads at the TS limits at which humping was produced are shown in Figure 6.31. The macrosections are taken through the peak of the humped beads in each case to show the typical profile in each case.

There appears to be a minor effect of material thickness on wetting based on the effect of the same heat input on thinner material, allowing a greater effective preheat of the thinner sheet. This is reflected in the higher travel speed achieved for the same welding heat input between 2.0- and 1.6-mm sheet as shown in Figure 6.31.

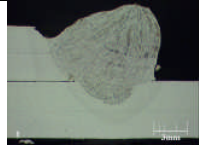


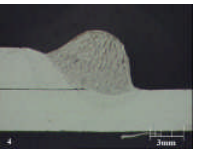
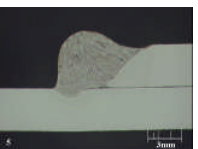
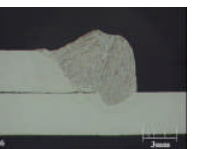
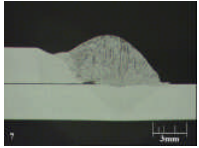

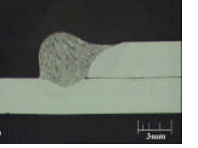
2.4-mm	WFS: 12.7 m/min TS: 1.32 m/min	WFS: 14.0 m/min TS: 1.9 m/min	WFS: 15.2 m/min TS: 2.3 m/min
			
2.0-mm	WFS: 7.6 m/min TS: 1.33 m/min	WFS: 8.9 m/min TS: 1.71 m/min	WFS: 10.2 m/min TS: 2.16 m/min
			
1.6-mm	WFS: 7.6 m/min TS: 1.46 m/min	WFS: 8.9 m/min TS: 2.03 m/min	WFS: 10.2 m/min TS: 2.48 m/min
			

Figure 6.31 Macrosections Through Bead Humps at the Limits of TS for each Material Thickness

In summary, the humping limit was determined for three material thickness combinations of lap joints using a lead travel angle of 30 degrees. This travel angle was shown to substantially increase the maximum travel speed that could be used before humping occurred when compared to similar results achieved using a 90-degree (zero-degree lead) torch travel angle for conventional GMAW-P practice.

6.3 High-Speed GMAW-P T-Joints

The results were produced using the following equipment and set-up conditions:

- CTWD: 19 mm
- Arc length: 3.2 mm
- Torch work angle: 45 degrees
- Torch travel angle: 30 degrees
- Electrode: ER70S-6, 1.2-mm diameter
- Gas: 90/10 Ar/CO₂ mixture
- Power supply: ESAB Digipulse 450i GMAW power supply
- Wire feeder: ESAB Digipulse wire feeder
- Torch: Binzel water-cooled torch

T-butt joints were fillet welded for three material thicknesses (2.4-, 2.0-, and 1.6-mm steel) of carbon steel sheet. The TS limits for acceptable welds were evaluated by successively increasing TS until the bead humping phenomena appeared. Three WFS were chosen for each gauge thickness and the TS was increased until the humping was evident. Macrosections were taken of the weld profile (macro sectioned at hump of beads). The electrode wire was aimed at the root of the joint in each case.

For the welds in 2.4-mm-thick sheet, humping appeared at high WFS, but not before poor wetting conditions were observed. .

- 2.4-mm sheet:
 - 12.7 m/min WFS: Poor wetting at 1.4 m/min, Humping at 1.9 m/min
 - 14.0 m/min WFS: Poor wetting at 1.5 m/min, Humping at 2.03 m/min.
 - 15.2 m/min WFS: Poor wetting at 1.9 m/min, Humping at 2.54 m/min

A weld appearance map is shown in Figure 6.32 illustrating the toe wetting and bead humping conditions. The poor wetting and bead humping conditions were 0.5 m/min apart for welds made with all three WFS. This condition was not observed for welds made using the thinner sheet materials, presumably because of the smaller welds made on the thinner materials so only the bead humping speed is summarized for the thinner materials.

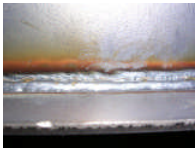





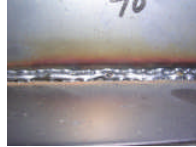

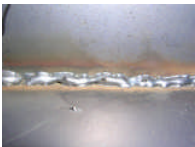
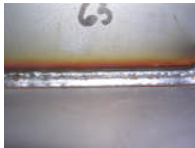





WFS (m/min)	TS (m/min)					
	1.3	1.40	1.5	1.65	1.8	1.95
12.7		No Picture				
	1.5	1.75	1.9	2.0		
14.0						
	1.65	1.9	2.15	2.3	2.4	2.55
15.2						

Figure 6.32 Weld Appearance Map for Fillet Welds on T-Butt Joints Using 2.4-mm Sheet

For the 2.0-mm sheet, bead humping occurred at the following WFS and TS combinations:

- 7.6 m/min WFS: Bead humping at 0.7 m/min
- 8.9 m/min WFS: Bead humping at 0.75 m/min
- 10.2 m/min WFS: Bead humping at 0.95 m/min

This is illustrated in the weld appearance map in Figure 6.33.



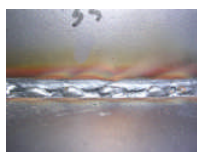



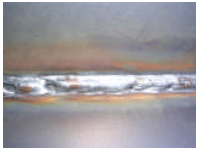
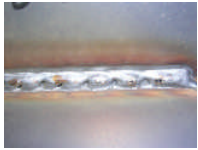
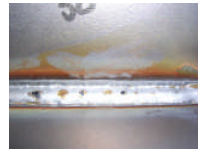
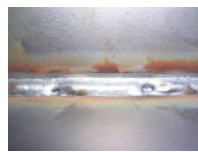

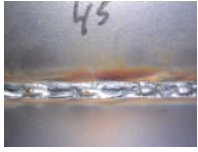
WFS m/min	TS (m/min)					
	0.5	0.75	0.9	1.0	1.15	1.25
7.6						
8.9						
10.2						

Figure 6.33 Weld Appearance Map for Fillet Welds on T-Butt Joints Using 2.0-mm Sheet

For the 1.6-mm sheet, bead humping occurred at the following WFS and TS combinations:

- 7.6 m/min WFS: Bead humping at 0.9 m/min
- 8.9 m/min WFS: Bead humping at 1.1 m/min
- 10.2 m/min WFS: Bead humping at 1.35 m/min

This is illustrated in Figure 6.34.

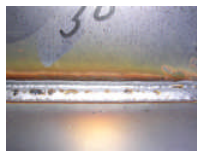
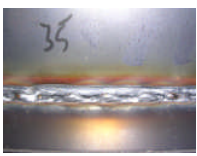
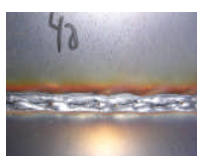


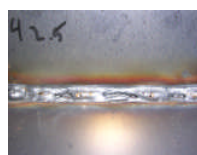
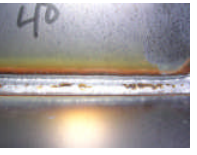
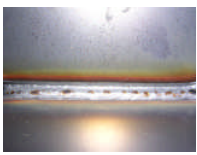
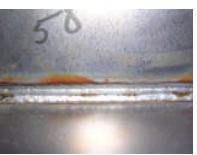
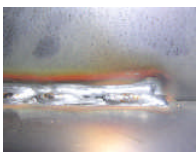
WFS (m/min)	TS (m/min)			
	0.75	0.9	1.0	
7.6				
	0.9	1.0	1.0	
8.9				
	1.0	1.1	1.25	1.35
10.2				

Figure 6.34 Weld Appearance Map for Fillet Welds on T-Butt Joints Using 1.6-mm Sheet

6.4 High-Speed Video (HSV)

The sequence of HSV images (GMAWP186-GMAWP214) in Figure 6.35 shows the predominant direction of weld pool fluid flow at the surface to be rearward. This can be seen from the movement of small silicate slag islands on the weld pool surface in the progression of the images. The sequence of images represents one pulse cycle from the current peak to the next current peak. The small silicate slag islands, that appear in grayish white contrasted by the light grey of the weld pool as a whole, move 0.4 mm from the first image to the next which represents four frames in the HSV at a frame rate

of 250 fps, or 0.1 mm in 0.004 s. The calculated velocity is therefore 25 mm/s or 1.5 m/min.

As the weld pool surface is at an angle of close to 10 degrees relative to the plate surface, this is a close approximation to the surface velocity of the weld pool driven by the convective flow induced by differing thermal gradient and the resulting Marangoni surface tension.

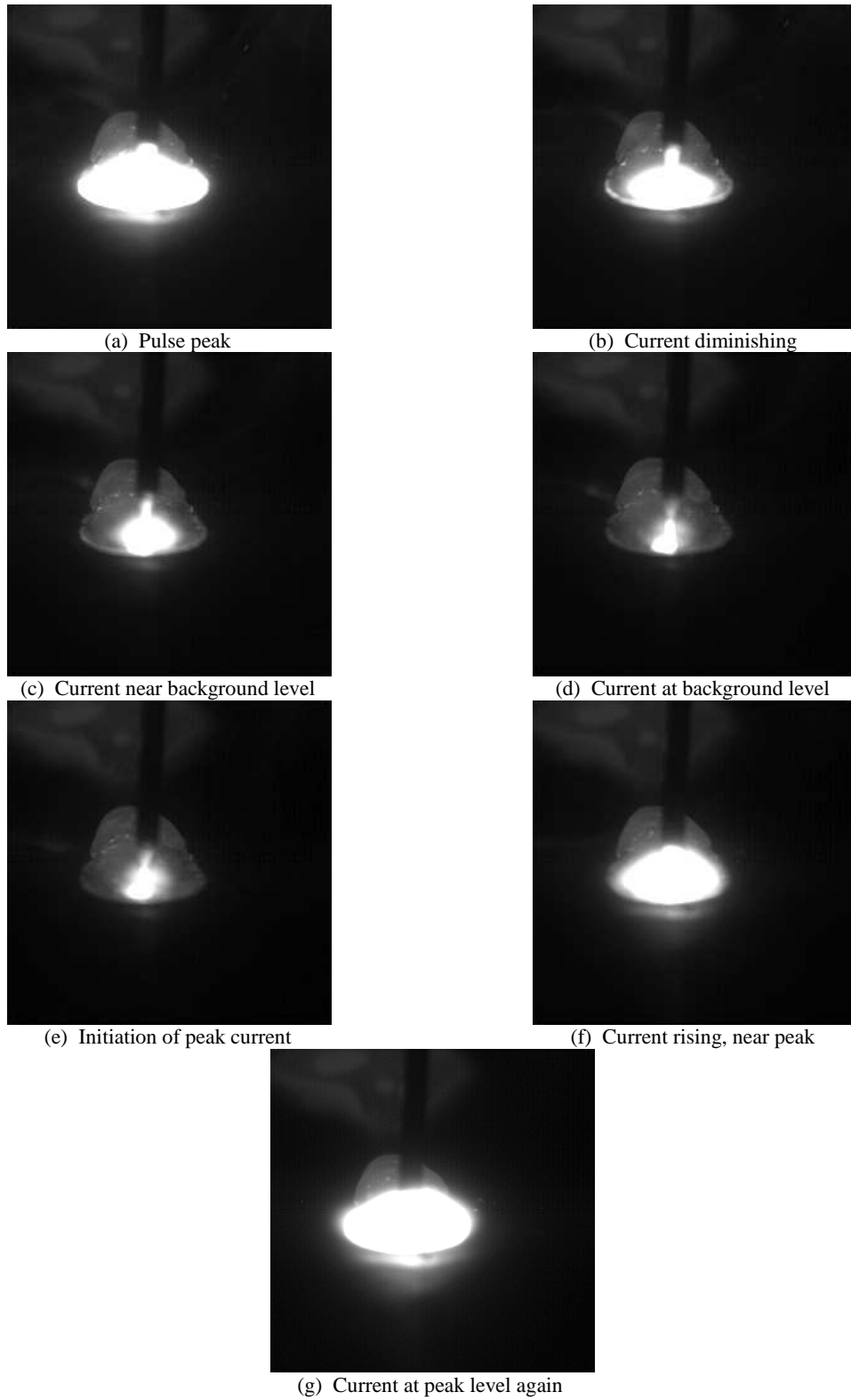


Figure 6.35 Sequence of HSV Images Showing the Predominant Direction of Weld Pool Fluid Flow at the Surface to be Rearward

6.5 Results for Hybrid LBW/GMAW-P

Results and conclusions are presented for the LBW/GMAW-P hybrid welding trials with the PFO (1-kW Nd:YAG laser, 4-kW Nd:YAG laser power, and 5-kW CO₂ laser power).

6.5.1 Welding Trials – GMAW with 1-kW Laser Power and PFO

Trumpf has a PFO scanning head capable of manipulation of 1 kW of laser power. It was designed for making spot welds and short seam welds in a fixed workstation environment. This was integrated into a CNC Nd:YAG/GMAW-P hybrid welding system and trials conducted to evaluate the influence of using the 1-kW laser power to increase heating at the weld toe of the GMAW-P bead, thus increasing weld pool fluidity, wetting and increasing weld toe angles. Heat could be concentrated at the weld toe by a simple linear path offset from the weld centerline, or by increasing the scan width substantially, to 4 mm, to add additional heat to both toe areas simultaneously.

Trials were conducted with a variety of scanning patterns including simple spot and line patterns, Figure 6.36, to achieve conduction mode melting rather than just heating.

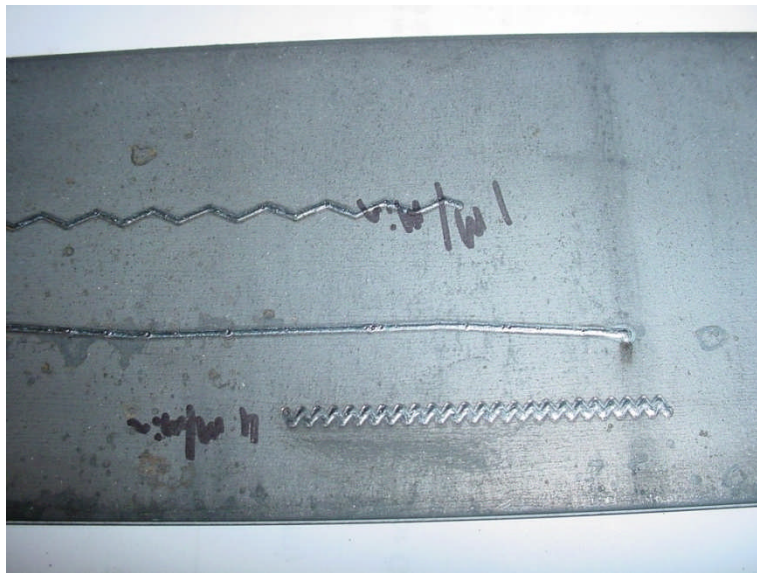


Figure 6.36 Initial PFO Trials with 1-kW Nd:YAG Laser

These trials were used to determine the most effective scanning patterns to achieve improved wetting angles of the GMAW-P weld toes.



Figure 6.37 Spot and Scanned Nd:YAG Laser Profiles in BOP Form

The PFO system was used to produce 2- and 4-mm scan widths and compared to the results achieved with a simple laser spot approach. The resulting bead on plate welds made on steel sheet, Figure 6.37, were correspondingly wider.

The sequence of HSV frames (PFO 4-mm scan width, frames 4065-4185), Figure 6.38 shows operation of the scanning spot manipulated by the PFO using 1-kW Nd:YAG laser power. The sequence shows one complete scan of the laser from right to left and back again. During the scanning sequence the GMAW-P operation undergoes three complete pulse cycles. The laser spot size is 1.2 mm, the same as the wire diameter, and the spot position is just ahead of the leading edge of the weld pool. The programmed scan width was 4 mm, and is verified as such in the sequence of HSV images, 2 mm in each direction from the wire axis.

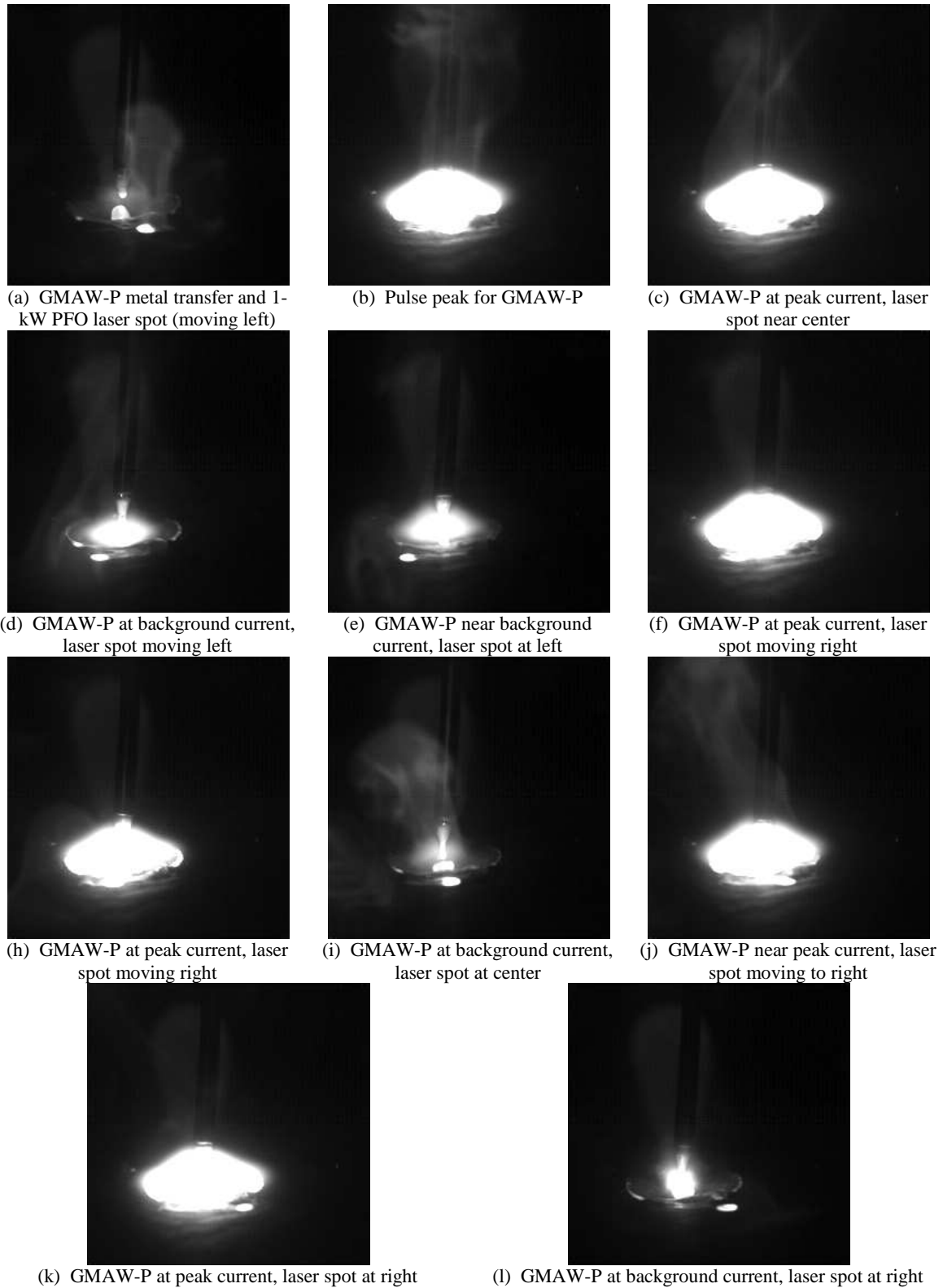


Figure 6.38 Sequence of HSV Frames Shows Operation of the Scanning Spot Manipulated by the PFO using 1-kW Nd:YAG Laser Power

Welds made using the PFO system for spot, and scanned patterns are summarized in Table 6.2. The best results were achieved using the 2-mm scanned width, as illustrated by the macrosections in Figure 6.40.

Table 6.2 1-kW Nd:YAG Trials with PFO

Trial No.	Beam Rasta (mm)	Beam Rasta (Hz)	Beam to Wire Distance (mm)	WFS (m/min)	Arc Volt (V)	CTWD (mm)	TS (m/min)	Torch Travel Angle (degrees)	Torch Work Angle (degrees)	Results/Comments
020204-1	GMAW-P only			15.2	27.8	16	2.05	90	30	Considerable bead humping
020204-2	GMAW-P only			10.2	24.8	16	2.05	90	30	Considerable bead humping
020204-3	Spot	0	1	10.2	24.8	16	2.05	90	30	Improved bead humping
020204-4	Spot	0	1	15.2	27.8	16	2.3	90	30	Considerable bead humping
020304-1a	Spot	0	1	10.2	24.8	16	2.05	90	30	Good
020304-1b	Spot	0	1	10.2	24.8	16	2.3	90	30	Some humping at start
020304-1c	Spot	0	1	10.2	24.8	16	2.55	90	30	Humping for half the weld
020304-2a	2		1	10.2	24.8	16	2.55	90	30	Some humping at bead center
020304-2b	4		1	10.2	24.8	16	2.55	90	30	Humping across whole bead
020304-2c	6		1	10.2	24.8	16	2.55	90	30	Some humping at start
020404-1	Spot		1	10.2	24.8	16	2.05	90	30	
020404-2	GMAW-P only			10.2	24.8	16	2.05	90	30	
020404-3	Spot		2	10.2	24.8	16	2.05	90	30	
020404-4	Spot		2	10.2	24.8	16	2.55	90	30	
020404-5	4		2	10.2	24.8	16	2.55	90	30	
020404-6	4		-2	10.2	24.8	16	2.05	90	30	Trailing LBW - tremendous spatter
020404-7	GMAW-P only			10.2	24.8	16	2.05	90	30	
021704-1	Spot		2	10.2	24.8	16	2.05	90	30	Porosity
021704-2	2		2	10.2	24.8	16	2.05	90	30	Porosity
021704-3	2		2	10.2	24.8	16	2.05	90	30	Realigned air knife
021704-4	Spot		2	10.2	24.8	16	2.55	90	30	Somewhat uneven bead, but OK
021704-5	2		2	10.2	24.8	16	2.55	90	30	Bead looks good
021704-6	4		2	10.2	24.8	16	2.05	90	30	Significant humping
021704-7	6		2	10.2	24.8	16	2.05	90	30	Significant humping

Trial No.	Beam Rasta (mm)	Beam Rasta (Hz)	Beam to Wire Distance (mm)	WFS (m/min)	Arc Volt (V)	CTWD (mm)	TS (m/min)	Torch Travel Angle (degrees)	Torch Work Angle (degrees)	Results/Comments
021804-1	GMAW-P only			15.2	27.8	16	2.05	90	30	Acceptable bead
021804-2	Spot		2	15.2	27.8	16	2.05	90	30	Borderline humping
021804-3	2		2	15.2	27.8	16	2.05	90	30	Acceptable bead
021804-4	Spot		2	15.2	27.8	16	2.3	90	30	Significant humping
021804-5	Spot		2	15.2	27.8	16	2.3	30	30	Significant humping
021804-6	Spot		2	15.2	27.8	16	2.3	30	30	Significant humping

While the scanned laser spot was sufficient to cause surface melting, the scan width available was insufficient to impinge on both GMA weld toes. In addition, the small spot size did not provide a large enough ability to wet the GMA weld toe significantly in the transverse direction relative to the axis of the welding direction. Defocusing the spot size to the 2- to 3-mm-diameter range resulted in insufficient power density to cause surface melting. Providing only enough power density for surface heating did not result in any increase in wetting of the GMAW-P weld toes, and therefore did not result in increased bead width associated with a larger weld toe angle relative to the plate surface. Results for a laser spot, 2- and 4-mm scan widths, are shown in Figures 6.39 through 6.41. These each show a macrosection of the fusion profile running the laser only, and then the resulting hybrid laser/GMAW-P weld macrosection.

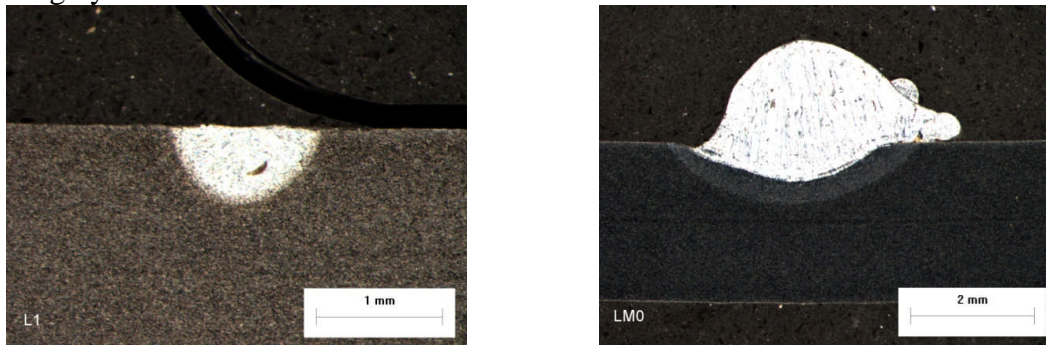


Figure 6.39 Nd:YAG Spot and Corresponding LBW/GMAW-P BOP Weld

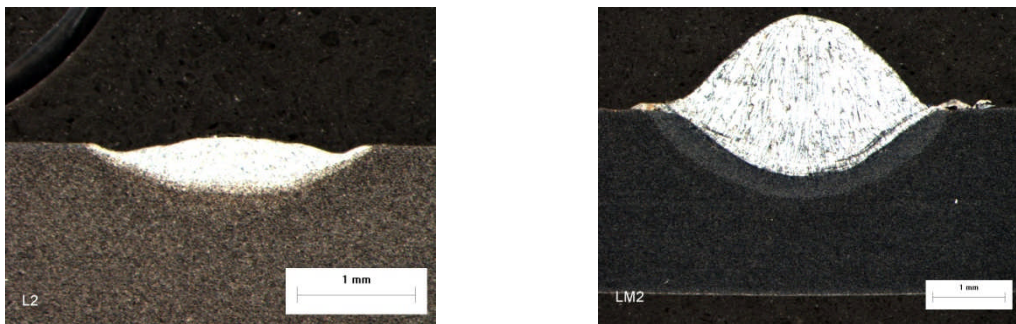


Figure 6.40 2-mm Scanned Nd:YAG and Corresponding LBW/GMAW-P BOP Weld

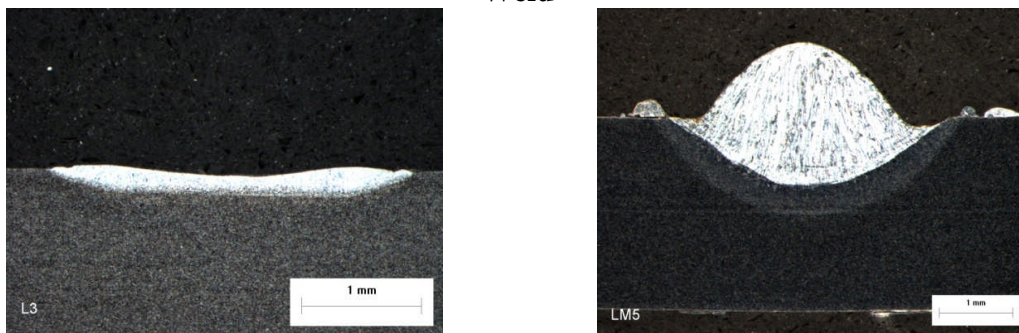


Figure 6.41 4-mm Scanned Nd:YAG and Corresponding LBW/GMAW-P BOP Weld

BOP trials at 2-m/min TS and 10.2-m/min WFS showed classic bead humping, Figure 6.42 (top weld bead), for GMAW-P, but was stabilized using 1-kW Nd:YAG power in a single spot (lower two weld beads, made at the same parameters). Ultimately, it was concluded that insufficient laser power capability, based on the 1 kW capacity of the galvanometer mirrors, would excessively limit the productivity potential, so this technique was eliminated from further study in favor of higher laser power that could achieve similar results at travel speeds in the range of 2-4 m/min.

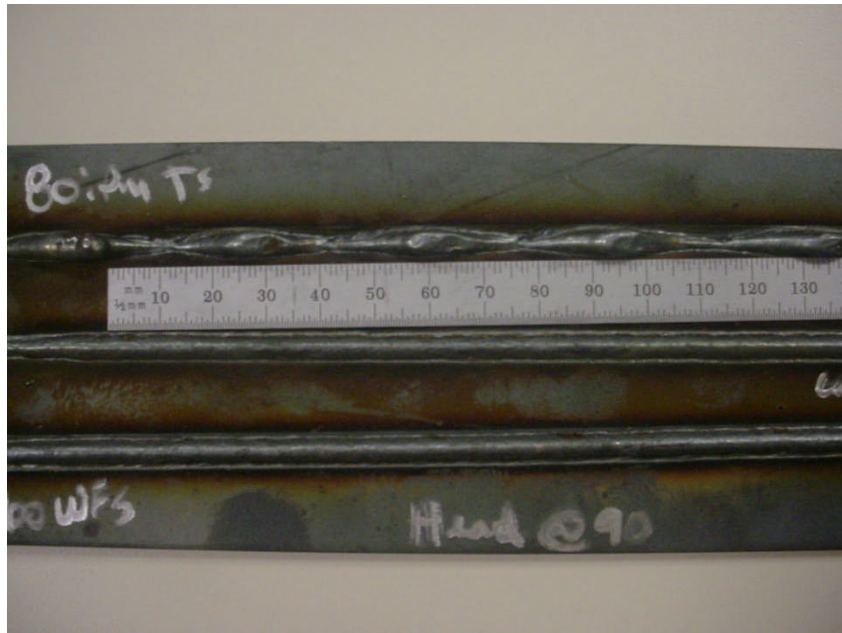


Figure 6.42 Classic Bead Humping (top weld bead) Suppressed with 1-kW Nd:YAG Laser Energy (WFS/TS of 5 - BOP weld) at 2.0-m/min TS

The top weld, Figure 6.42, was made using 2.0 m/min TS, but with GMAW-P only. The bead humping is clearly evident. The bottom two welds were made with 1-kW of Nd:YAG laser power in addition to GMAW-P. All three of the welds were made at 10.2 m/min WFS.

6.5.2 Hybrid GMAW-P/LBW using the Trumpf HAAS 4006 Nd:YAG Laser

Based on the results at 1 kW, the full 4 kW of Nd:YAG laser power was used in the next series of trials to increase the productivity and TS at which humping could be prevented.

The results of measurements of the laser beam profile using the PRIMES device are shown for a single beam, Figure 6.43, and a dual-beam, Figure 6.44, for 4.0-kW laser power. The spot size of the laser at focus was determined in this manner.

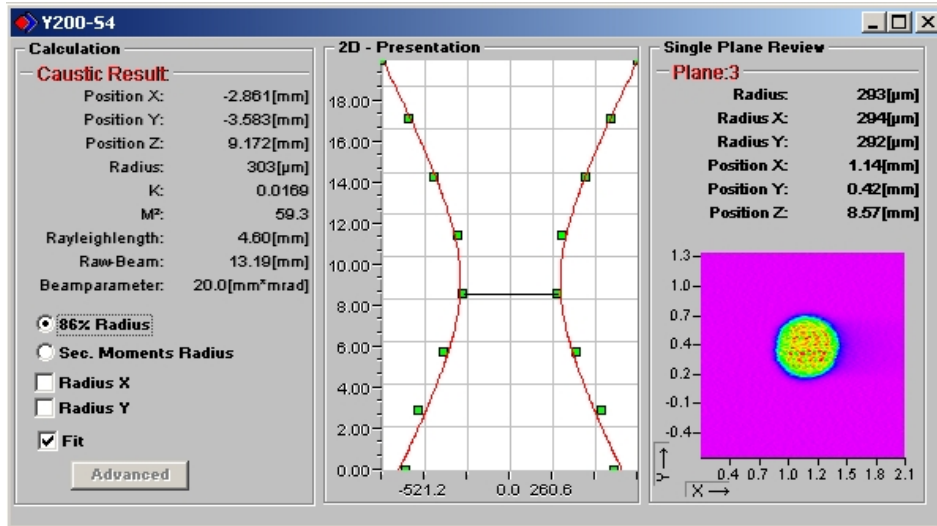


Figure 6.43 Profile for 4-kW Nd:YAG Laser with a Single Beam at Focus with 200-mm Optics

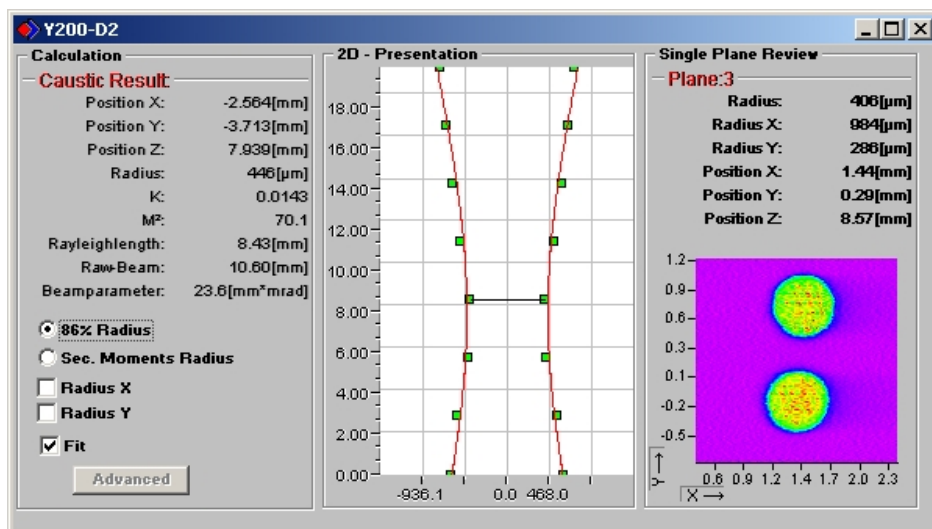


Figure 6.44 Beam Profile for 4-kW Nd:YAG Laser with Dual Beam Using 200-mm Focusing Optics (Profile of One Beam is Shown)

The results show a better depth of focus tolerance for constant beam spot size and power density, Figure 6.44, compared with the single-spot optics.

The dual-spot beam profile at low power was as shown in Figure 6.45. The image shows three separate burn profiles of two spots each. This shows the TEM 01 laser mode clearly along with the consistent shape between the two profiles. The latter illustrates an even power distribution between the two beams.

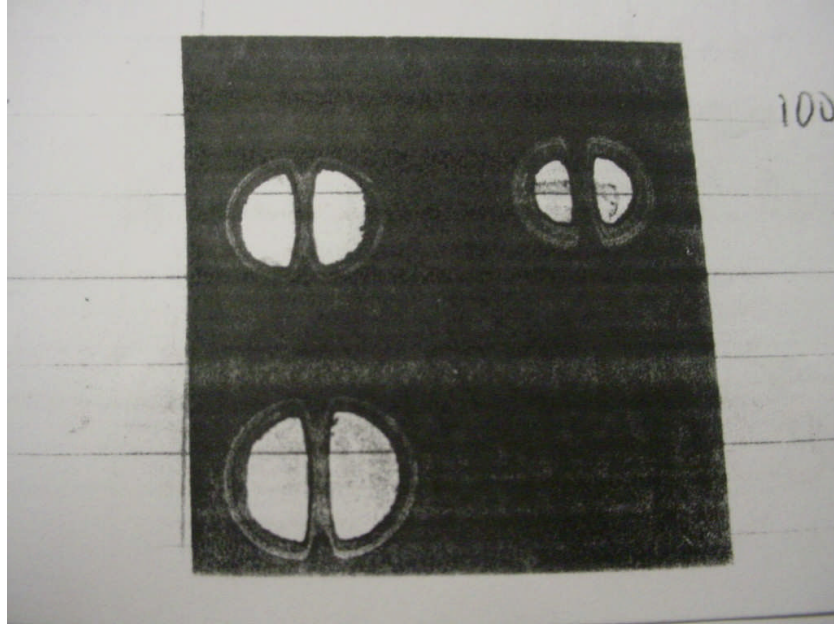


Figure 6.45 100-W Dual-Beam Nd:YAG Laser Burn Pattern on Thermographic Paper to Illustrate TEM 01 Laser Mode

The general approach and results for a single spot are shown in Figure 6.46 with the laser spot offset to coincide with the left-hand weld toe in this case. The laser melt track can be seen at the left hand side of the right hand weld bead in Figure 6.46. The weld on the left is shown for comparison, and made with GMAW-P only. With the added laser energy the heat input is clearly higher in the LBW/GMAW case.



Figure 6.46 Single-Beam Laser Offset to GMAW-P Weld Toe to Increase Toe Wetting Using an Nd:YAG laser at 4 kW

When welding a lap-fillet joint with GMAW-P only, significant weld bead humping occurred, Figure 6.47. Joint gap was set at 0T and the material thickness was 2.4 mm



Figure 6.47 GMAW-P Fillet Weld on a Lap Joint

When adding the laser power to the same joint using the same GMAW-P welding parameters, the weld became much more even and there was no evidence of humping, Figure 6.48. The laser power was 4 kW and the GMAW-P parameters were 15.2 m/min WFS, with a 3.3 m/min TS. Joint gap was 0T and the sheet thickness was 2.4 mm.



Figure 6.48 Hybrid Nd:YAG/GMAW-P Fillet Weld on a Lap Joint

One interesting result was that a very long weld pool could be produced using the hybrid welding configuration with a single laser spot offset to the lower weld toe on the bottom sheet of a lap-fillet joint, Figure 6.49. The beginning and end of the weld pool are marked in blue on the lower sheet in Figure 6.49. This weld, also made on 2.4-mm sheet with 0T gap, had a length to width ratio of 12:1 which exceeded the 10:1 ratio predicted for GMAW by Gratzke (Gratzke, 1992).



Figure 6.49 36-mm-Long Weld Pool with 3-mm Bead Width (12:1) using Single-Spot 4-kW Nd:YAG/GMAW-P Hybrid on a Lap Joint

Table 6.3 1- to 4-kW Nd:YAG/GMAW-P hybrid Trials with Split Optics – Lap Joints

Trial No.	Beam Power (kW)	Spot Size (mm)	Beam to Wire Spacing (mm)	WFS (m/min)	Arc Volt (V)	CTWD (mm)	TS (m/min)	Torch Travel Angle (degrees)	Torch Work Angle (degrees)	Results/Comments
031004-6a	4	3.2	0	15.2	27.8	13	3.3	30	30	
031004-6b	4	3.2	0	15.2	27.8	13	3.3	30	30	
031004-6c	4	3.2	0	15.2	27.8	13	3.3	45	30	
031104-1	4	3.2	0	15.2	27.8	13	3.3	30	30	Wire at top plate
031104-2	4	3.2	0	15.2	27.8	13	3.3	30	30	Wire to joint root - improvement
031104-3	4	3.2	0	15.2	27.8	16	3.3	30	30	Discontinuous humping
031104-4	4	3.2	0	15.2	27.8	9.5	3.3	30	30	Best of present trials, but deep undercut
031104-5	4	3.2	0	17.8	31.1	9.5	3.3	30	30	
031104-6	4	3.2	0	17.8	31.1	13	3.3	30	30	Significant humping
031104-7	4	3.2	0	12.7	24.6	9.5	3.3	30	30	Poor bead profile
031204-1	4	3.2	0	15.2	27.8	9.5	3.3	30	30	Best weld of whole series!
031204-2	4	3.2	-2	15.2	27.8	9.5	3.3	30	30	
031204-3	4	3.2	3.2	15.2	27.8	9.5	3.3	30	30	
031204-4	4	3.2	6.4	15.2	27.8	9.5	3.3	30	30	
031204-5	4	1.6	0	15.2	27.8	9.5	3.3	30	30	
031204-6	4	3.2	1.6	15.2	27.8	9.5	3.3	30	30	
031204-7	4	1.6	0	15.2	27.8	9.5	3.3	30	30	
031204-8	4	1.6	0	15.2	27.8	9.5	3.3	45	30	
031204-9	4	3.2	0	15.2	27.8	9.5	3.3	30	30	
031204-10	4	3.2	0	15.2	27.8	9.5	3.3	30	30	

The parameters used for hybrid Nd:YAG/GMAW-P are summarized in Table 6.3 for the split optics approach. Welds made with a single beam spot used similar set-up conditions and welding parameters for the laser and GMAW-P. This work was able to increase the welding TS to a maximum of 3.5 m/min, but results were not readily reproducible. Maximum consistency was achieved by reducing the TS to 3.3-m/min linear TS on a lap joint in 2.4-mm sheet.

The travel angle and work angles of 30 degrees for the GMAW-P torch were found to be the best to minimize weld toe undercut based on visual weld appearance when using the dual-spot approach, Figure 6.50.



Figure 6.50 Bead Appearance for Dual-Spot Nd:YAG Hybrid Weld made at 3.3 m/min on a Lap-Fillet Joint 2.4-mm Sheet

Macrosections of these welds, Figures 6.51 and 6.52, showed some undercut along the top edge of the top sheet. It should be appreciated that these welds were made as much to determine the TS for the onset of bead humping as anything else. TS in excess of 3.3 m/min did result in humping when welding on the 2.4-mm sheet, as illustrated in Figure 6.52.



Figure 6.51 Macrosection for Dual-Spot Nd:YAG Hybrid Weld Made at 3.3 m/min on 2.4-mm Sheet



Figure 6.52 Macrosection for a Dual-Spot Nd:YAG Hybrid Weld Made at 4.0-m/min on 2.4-mm Sheet

6.5.3 Hybrid GMAW-P/LBW with Rofin Sinar CO₂ Laser, Model RS-850

Lack of availability of the Nd:YAG laser resulted in further study being conducted with a Rofin Sinar CO₂ laser, Model RS-850. A typical beam profile for a CO₂ laser is shown in Figure 6.53. This profile was made on a 6-kW Preco laser as the PRIMES device was not available to measure the 5-kW Rofin laser. However,

similar optics and focal length mean that this beam profile is a close approximation of the one used.

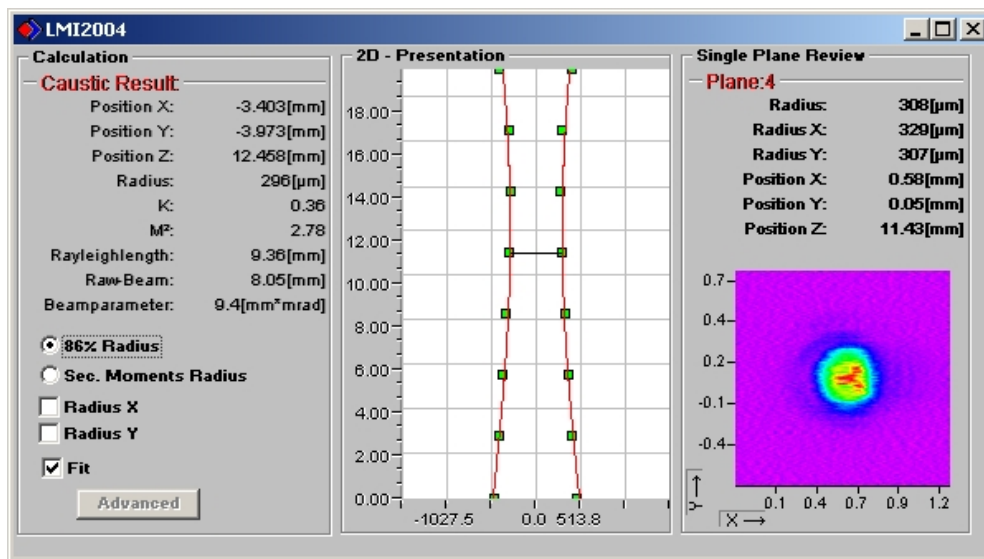


Figure 6.53 Profile of 6-kW CO₂ Laser Beam at Focus with 254-mm Optics

When using dual beams, a burn pattern on blackened Perspex, Figure 6.54, showed the beam pattern which was TEM 01 mode, i.e., bi-modal, with the 'lobes' arranged parallel to the welding direction. The blackening was done to make the burn pattern more visible, not because it was needed for beam absorption.

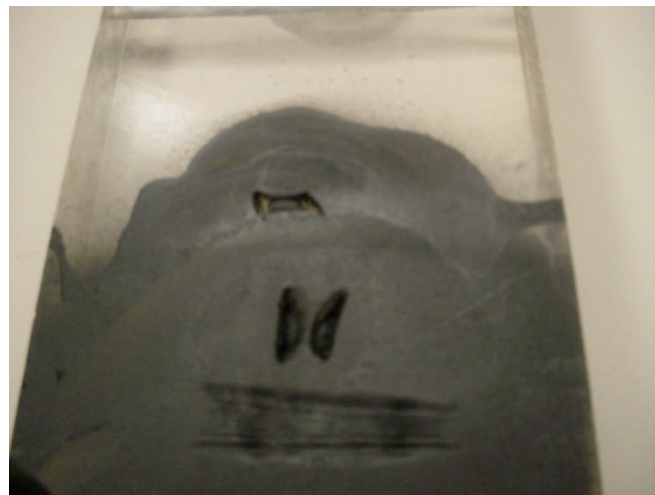


Figure 6.54 CO₂ Laser Burn Pattern on Perspex for Dual Beam in TEM 01 Mode Using 3.2, 6.4 and 9.5-mm Dual Spot Spacing

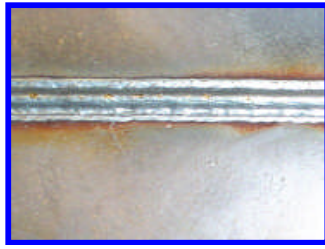
Experiments, including use of HSV showed that use of CO₂ laser power was helpful in reducing weld humping. The offset of the laser beam was critical to the result and laser power was another key parameter. Reduction in bead humping was noted at 1.5 kW but it was not enough to correct existing weld humping. Experiments showed

that the minimum required laser power was 2.7 kW at 0.6 m/min welding speed for dual-spot laser operation. Most results were generated with a single beam with beam power of 3-4 kW as a result, Table 6.4.

BOP welds were used to determine the preferred arrangement of the spot relative to the weld toe and the maximum TS that could be obtained without bead humping occurring.

Table 6.4. Parameters for CO₂ Laser/GMAW-P Hybrid BOP, Lap and T-Butt Joints

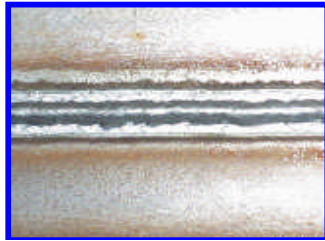
Weld No.	Laser Power (kW)	Travel Speed (m/min)	GMAW-P WFS (m/min)	GMAW-P Arc Voltage (V)	Laser Spot Size and Laser/GMAW-P Spacing (mm)	Comments
3M	3.3	2.5	18.5	28.6	Both 5	BOP hybrid
4M	3.3	3.0	18.5	28.6	Both 5	BOP hybrid
5M	2.5	3.0	N/A	N/A	3	BOP LBW 2 welds
6M	2.5	3.0	N/A	N/A	3	BOP LBW 2 welds
7M	4	3.3	15.2	27.8	Both 3	Lap hybrid
8M	3.7	3.0	15.2	28.2	Both 3	Lap hybrid
9M	3.5	2.8	15.2	28.4	Both 3	Lap hybrid
10M	3.5	2.8	17.8	29	Both 3	Lap hybrid
11M	3.25	4.0	19.7	29	Both 3	Lap hybrid
12M	3.25	4.0	20.3	27.5	Both 3	Lap hybrid
15M	2.5 x 2	1.75	5.0	26	Both 3	T-butt hybrid
16M	2.5	2.0	5.0	26	Both 3	T-butt hybrid
17M	3.5	3.0	11.4	26	Both 3	T-butt hybrid



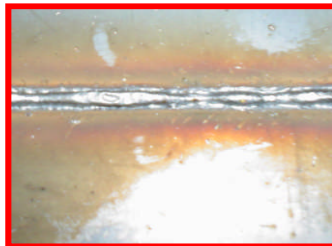
9.5 m/min WFS at 3.0 m/min TS



9.5 m/min WFS at 3.75 m/min TS



18.5 m/min WFS at 3.0 m/min TS



18.5 m/min WFS at 3.75 m/min TS

**Figure 6.55 Weld Appearance for BOP Welds Hybrid CO₂ LBW/GMAW-P
BOP Welds on 2.4-mm Sheet**

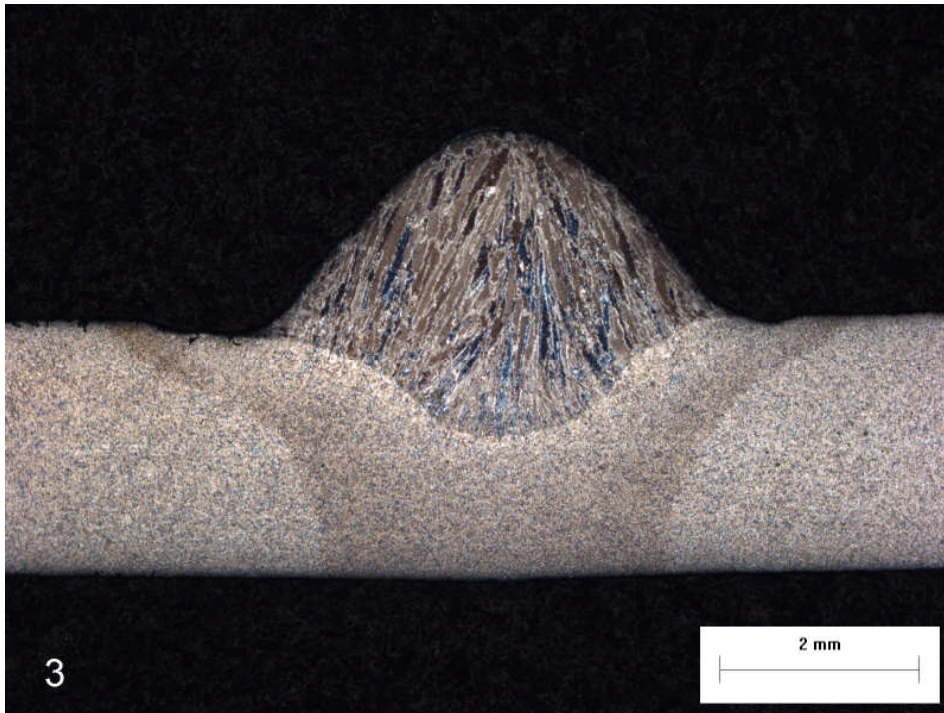


Figure 6.56 BOP Weld Made Using Single-Spot Laser at 3.3-kW and 2.5-m/min TS on 2.4-mm Sheet

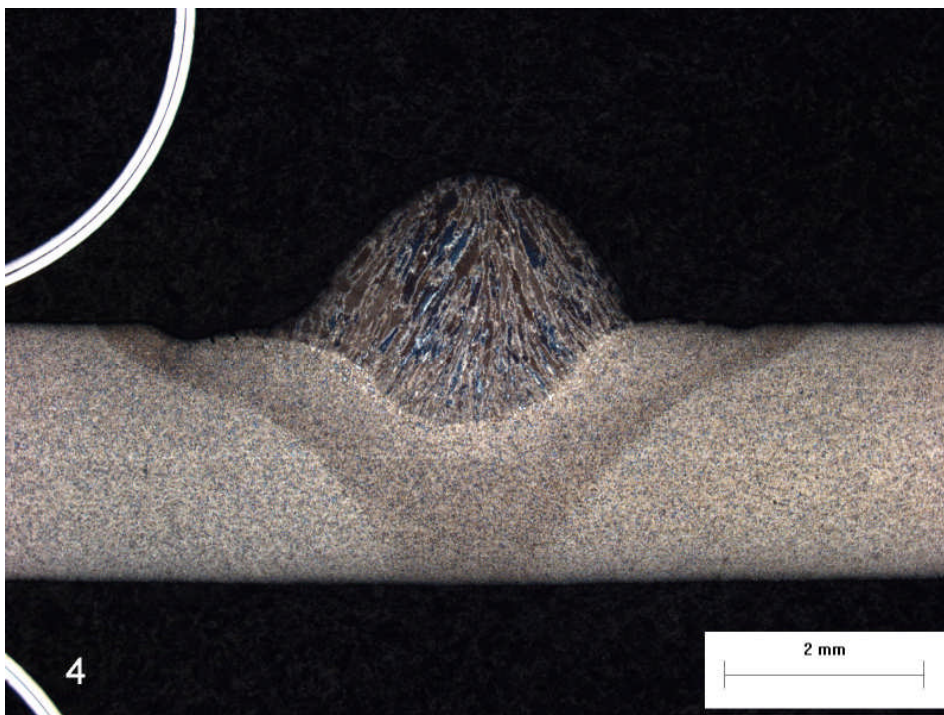


Figure 6.57 BOP Weld Made Using a Single-Spot Laser at 3.3-kW and 3.0-m/min TS on 2.4-mm Sheet

Figures 6.56 and 5.57 show typical results achieved using single laser spots at different TS. The laser impingement was on the left in both cases.

The best results in terms of high productivity and avoidance of bead humping were achieved by using a single laser spot of 3 to 3.5 kW. The beam mode was TEM Mode 00 and was offset onto the lower ligament of the lap fillet joint to increase the wetting of the lower weld toe that is really the limiting factor in making a continuous high-speed fillet weld. Defocusing the laser spot is a balance between sufficient power density and the beam width. The beam width and beam position relative to the lower GMAW-P weld toe is important, since this controls the wetting and ability to widen the weld bead, which itself allows the weld to become wider with a higher wetting angle. If the laser spot is too small, the ability to wet the GMAW-P bead is restricted. At 4-m/min TS, the fastest available with the welding positioner, welds free of humping were achieved for a lap joint in 2-mm sheet, Figure 6.58, increasing the speed by about 100% compared to single-wire GMAW-P, and 25-30% compared to typical twin-wire GMAW. For 2.4-mm sheet, the travel speed at which humping occurred was 3.3 m/min.



15.2 m/min WFS at 3.5 m/min TS on 2.4-mm sheet



15.2 m/min WFS at 3.75 m/min TS on 2.4-mm sheet



17.8 m/min WFS at 4.0 m/min TS on 2.0-mm sheet

Figure 6.58 Weld Appearance for Hybrid CO₂ LBW/GMAW-P Lap-Fillet Welds on 2.4- and 2.0-mm Steel Sheet

For 2.0-mm sheet, the best result in terms of avoiding bead humping was achieved at 4.0 m/min, Figures 6.59 and 6.60. While visually the weld looks good, Figure 6.59, when seen in a macrosection, Figure 6.60, it is evident that there is significant unacceptable undercutting at the upper toe. This can also be attributed to the very

small weld that it is possible to deposit in a continuous manner using these parameters.



Figure 6.59 Bead Appearance for a Lap-Fillet Joint Made Using Single-Spot CO₂ LBW/GMAW-P Hybrid Welding with 3.25-kW Laser Power at 4-m/min TS on 2-mm Sheet



Figure 6.60 Macrosection for a Single-Spot CO₂ LBW/GMAW-P Hybrid Weld Made at 4 m/min on 2-mm Sheet

The same approach was successfully applied to a T-butt weld, Figure 6.61. The offset and defocused CO₂ laser spot was used in GMAW-P/LBW hybrid welding trial sheet metal joints, and speed was 3 m/min for LBW/GMAW-P hybrid welding, Figures 6.62 and 6.63. The maximum TS of 3 m/min was achieved with a single offset laser spot of 3.5 kW. The laser spot size found to be most effective was 2.5-mm diameter, set 3 mm away from the axis of the weld wire.



11.4 m/min WFS at 3 m/min TS



11.4 m/min WFS at 4 m/min TS



14.0 m/min WFS at 4 m/min TS



15.2 m/min WFS at 4 m/min TS

Figure 6.61 Weld Appearance Map for Fillet Welds on T-Butt Joints for 2.4-mm Steel Sheet Using CO₂ LBW/GMAW-P Hybrid Welding

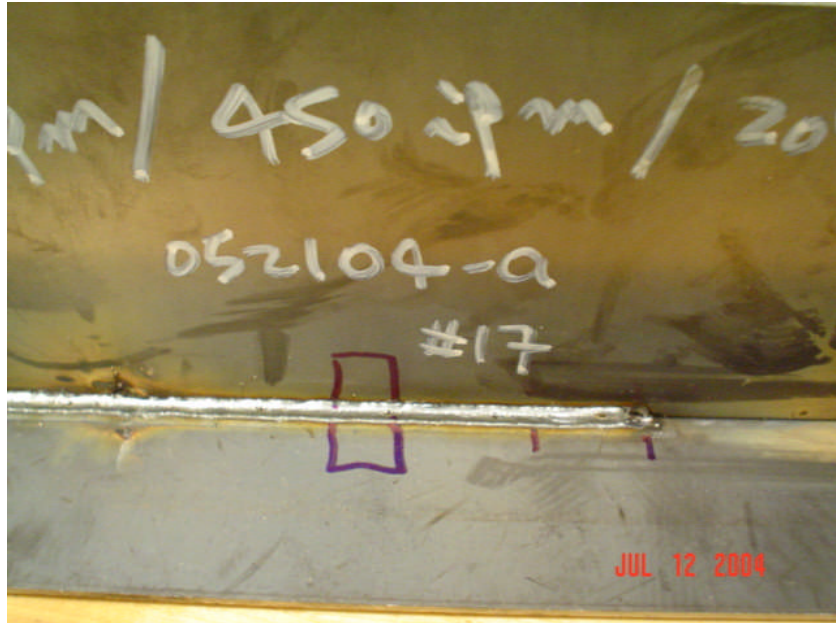


Figure 6.62 Bead Appearance for a T-Butt Joint made using Single-Spot CO₂ LBW/GMAW-P Hybrid Welding at 3 m/min on 2-mm Sheet



Figure 6.63 Macrosection (on left – tack on right) for a Single-Spot CO₂ LBW/GMAW-P Hybrid Weld made with 3.5-kW Laser Power at 3.0 m/min on 2-mm Sheet

Weld leg lengths, weld area, and weld toe angles were measured using ImagePro software for all these hybrid LBW/GMAW-P welds. The results for welds and weld macrosections shown earlier are given in Table 6.5 below.

Table 6.5 Weld Leg Length, Weld Area, and Weld Toe Angles

Weld No.	Length L1 (mm)	Length L2 (mm)	Area (mm ²)	Angle (degrees)	Angle 2 (BOP or T-Butt) (degrees)	Comments
3M	4.7		8.2	128	135	BOP hybrid
4M	4		5.3	164	110	BOP hybrid
5M	1.6/1.8	0.3/0.4	0.3/0.5	N/A		BOP LBW 2 welds
6M	1.7/2.1	0.3/0.4	0.4/0.7	N/A		BOP LBW 2 welds
7M	1.9	4.6	13.4	130		Lap hybrid
8M	2.1	4.8	19.2	108		Lap hybrid
9M	1.8	2.9	9.8	110		Lap hybrid
10M	0.9	3	5.2	152		Lap hybrid
11M	1.1	3.4	7.6	111		Lap hybrid
12M	1.1	3.2	5.8	120		Lap hybrid
15M	2.4	2.1	6.3	115	103	T-butt hybrid
16M	3.4	3.8	10.6	116		T-butt hybrid
17M	2.8	3.4	6.1	180	180	T-butt hybrid

Measurement using ImagePro is illustrated in Figure 6.64, which shows measurement of the two angles, the weld area, and the fillet leg lengths.

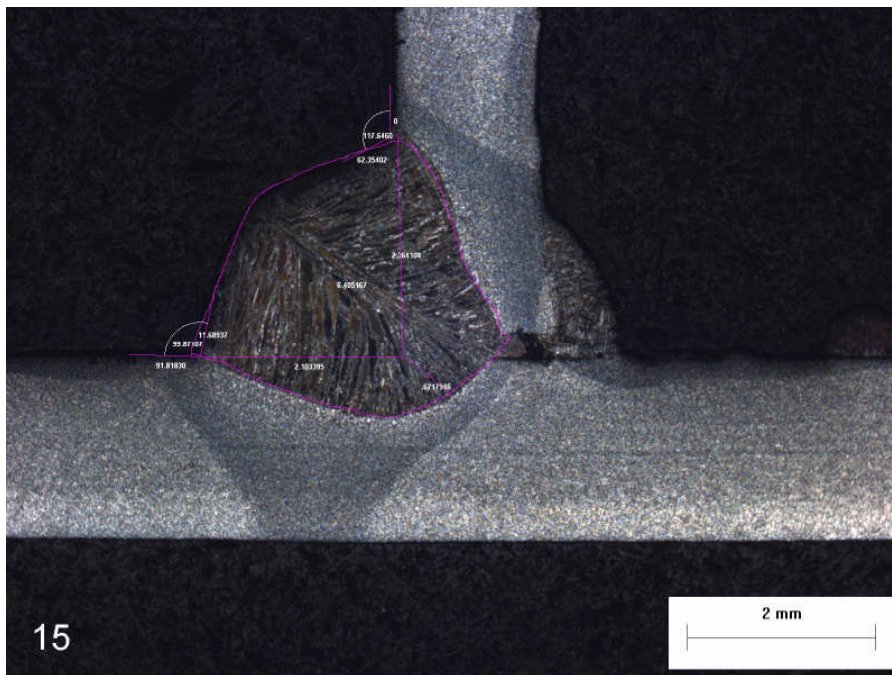


Figure 6.64 Macrosection for a Dual-Spot CO₂ LBW/GMAW-P Hybrid Weld Made at 1.75 m/min on 2-mm Sheet

The toe angles of all these hybrid LBW/GMAW welds were above 90 degrees, meaning that the angle between the face of the sheet and the toe of the weld was in no case reentrant. This was the case whether the weld was BOP, or a fillet welds in either a lap or T-butt joint. When humping takes place the toe angle is usually less than 90 degrees. The weld toe angles were typically in the range of 105-130 degrees,

but in some cases wet very well such that the local angle at the toe was 150 or even 180 degrees.

6.6 Results for Calorimetry

Calorimetry results for GMAW-P showed results ranging from 76 to 83% efficiency for the five measurements made, and averaging 78%, Table 6.6. For hybrid CO₂ LBW/GMAW-P the efficiency ranged from 60 to 63% shown in Tables 6.7, averaging 62% for the four measurements made. Calculations of efficiency were made by comparing known loss of nitrogen weight at room temperature with weight loss based on the known welding heat input. This allows the difference in weight loss to be attributed to the actual heat absorbed by the weld coupon and thus the efficiency to be calculated.

Table 6.6 Results for GMAW-P Calorimetry and Plot of Results

- N loss in raw material: 0.0115 kg
- Weight of raw material: 0.2751 kg
- Heat input: 51,470 J
- Total heat input: 51,470 J

Set	Weld Weight (kg)	N Loss (Heat) (kg)	N Loss (Room) (kg)	Net Heat Loss (J)	Heat Input (J)	Efficiency (%)
1	0.2946	0.3402	0.1248	42,908	51,470	83
2	0.2861	0.3166	0.1212	38,924	51,470	76
3	0.2873	0.3191	0.1217	39,322	51,470	76
4	0.2889	0.3250	0.1224	40,373	51,470	78
5	0.3026	0.3262	0.1282	39,442	51,470	77

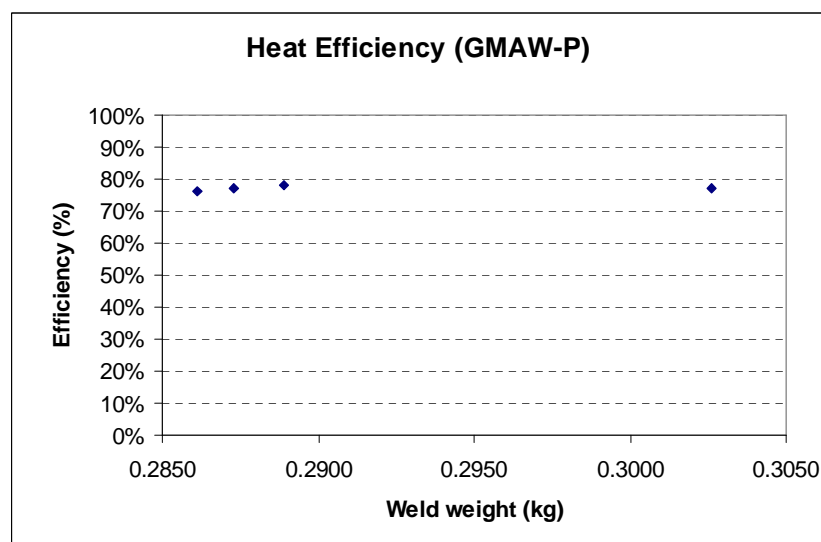
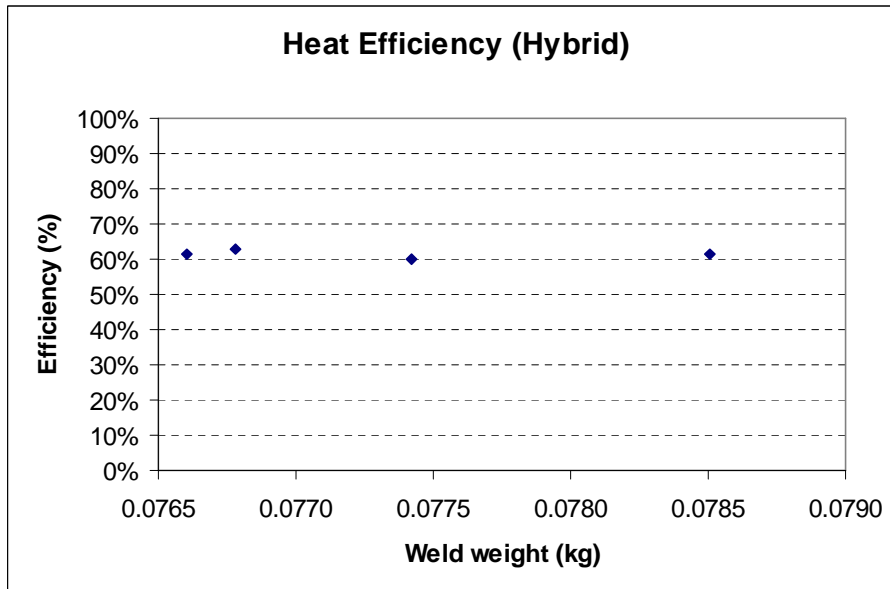


Table 6.7 Results for Hybrid LBW/GMAW-P Calorimetry and Plot of Results

- N loss in raw material: 0.0030 kg
- Weight of raw material: 0.0760 kg

- Heat input: 12,834 J
- Laser input: 5,250 J
- Total heat input: 18,084 J

Set	Weld Weight		N Loss (Heat)		N Loss (Room)		Net Heat Loss (J)	Efficiency (%)
		(kg)		(kg)		(kg)		
1		0.0766		0.0866		0.0307	11,134	62
2		0.0785		0.0874		0.0315	11,148	62
3		0.0774		0.0853		0.0310	10,813	60
5		0.0768		0.0879		0.0308	11,373	63



6.7 Humping Experiments

Experiments were conducted predominantly using GMAW-P BOP welds to examine the formation and morphology of the bead humping defect using HSV recording. This was also conducted to examine the weld pool fluid flow during humping events in lap-fillet welding of sheet steel. The welding parameters used were as listed in Table 6.8. Copies of the individual images and AVI files associated with the specimen numbers were provided on two compact discs along with the thesis.

Table 6.8 Weld Type and Welding Parameters for HSV Trials

Weld ID	Joint	Thickness (mm)	WFS (m/min)	TS (m/min)	Current (A)	Voltage (V)	CTWD (mm)
72805	BOP	2.4	15.2	2.5	225	28	19
72805a	BOP	5	15.2	2.5	225	37	19
72805b	BOP	2.4	15.2	2.5	225	33	19
72805c	BOP	2.4	15.2	2.5	225	31	19
72905a	BOP	5	15.2	2.5	225	33	16
72905-2	BOP	1.6	15.2	2.5	225	35	16
72905-3	BOP	5	15.2	2.5	225	35	16
80205a	BOP	1.6	15.2	2.5	225	34	19
80205b	BOP	1.6	15.2	2.5	225	34	19
80305a	Lap	1.6	15.2	3	225	34	16
80305b	Lap	1.6	15.2	3	225	34	16
82405-4	BOP	1.6	15.2	3	225	31	16
82405-5	BOP	1.6	15.2	3	225	34	16
82405-8	BOP	1.6	15.2	3	225	34	16
83005-1	Lap	1.6	15.2	3	225	34	19
83005-2	Lap	1.6	15.2	3	225	34	31

Figure 6.65 illustrates a typical weld pool cavity melted by GMAW-P using a torch travel angle perpendicular to the workpiece. The resulting weld bead is both undercut along the edges and humped in the middle in the transverse direction. The arc melted cavity at the end of the weld is seen to contain almost no weld metal per-se, Figure 6.65.



**Figure 6.65 Plan View of GMAW-P Weld Pool Cavity for Specimen 72805a
WFS 15.2 m/min, TS 2.5 m/min, 225 A, 37 V, 19-mm CTWD**

Viewed from the side, Figure 6.66, the repeating humping of the weld bead can be clearly seen. The last metal to solidify in each hump is at the top and this can be seen more clearly in the plan view of the same two humps, and is associated with a solidification shrinkage artifact on the top of each hump. In this case the shrinkage feature is on the forefront or leading edge of the peak of the hump.



**Figure 6.66 Side View of GMAW-P BOP Humping for Specimen 72805a
WFS 15.2 m/min, TS 2.5 m/min, 225 A, 37 V, 19-mm CTWD, 5-mm Plate**



**Figure 6.67 Plan View of GMAW-P BOP Humping for Specimen 72805a
WFS 15.2 m/min, TS 2.5 m/min, 225 A, 37 V, 19-mm CTWD, 5-mm Plate**

In Specimen 72805a the shrinkage feature is centered in its position at the peak of the hump, Figure 6.67. The repeating sequence of the humping defect is fairly regular in appearance.

In the following sequence of stills from HSV (072805a GMAW-P HSV humping), Figure 6.68, the hump formed in the GMAW-P BOP weld is seen to solidify at the base and progressively solidify in place. The solidified weld metal can be distinguished from the molten weld pool since it is both a darker shade of grey and movement is inferred by the motion of small silicate slag islands on the surface of the molten weld metal.

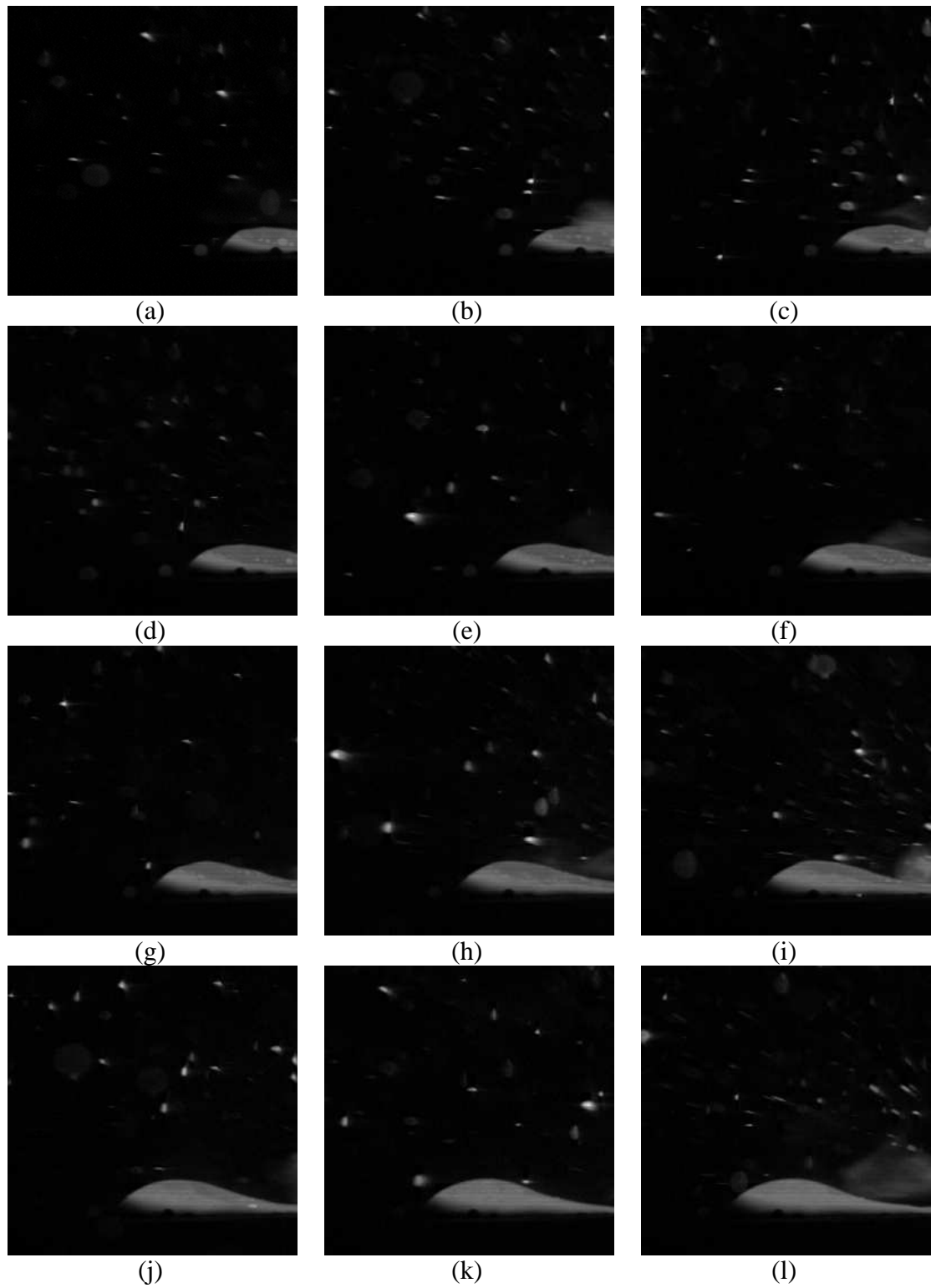


Figure 6.68 HSV Sequence of Bead Humping and Solidification
WFS 15.2 m/min, TS 2.5 m/min, 225 A, 37 V, 19-mm CTWD

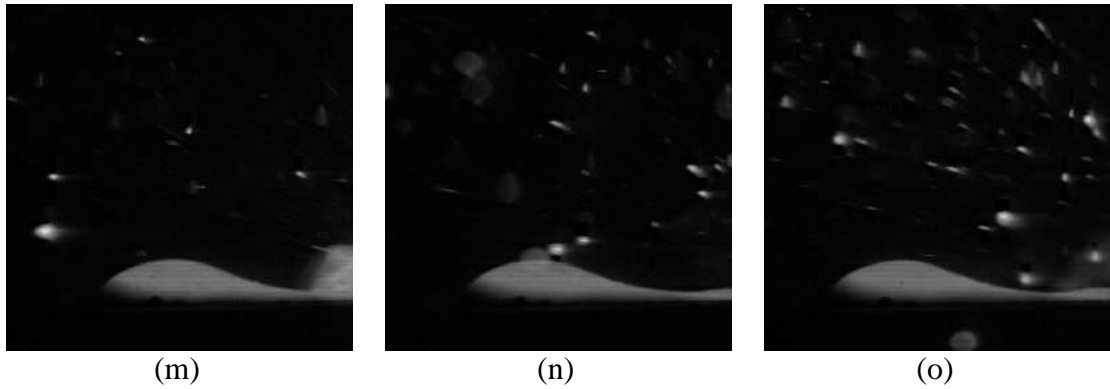


Figure 6.68 (Continued)

The motion of the silicate slag islands on the molten metal surface indicates the direction of the surface motion of the molten metal. These move rearward along the top of the weld bead, and then along the side in a forward motion relative to the welding direction. Once the hump is cut off from the rest of the weld, and another hump is forming, solidification takes place from the base toward the top of the hump as a result of the heat sink below the weld.

There is a noticeable increase in the spatter expulsion in the last frame, albeit that there is spatter being ejected in most of the images. In most of the later video sequences, a pattern in this instability emerges.



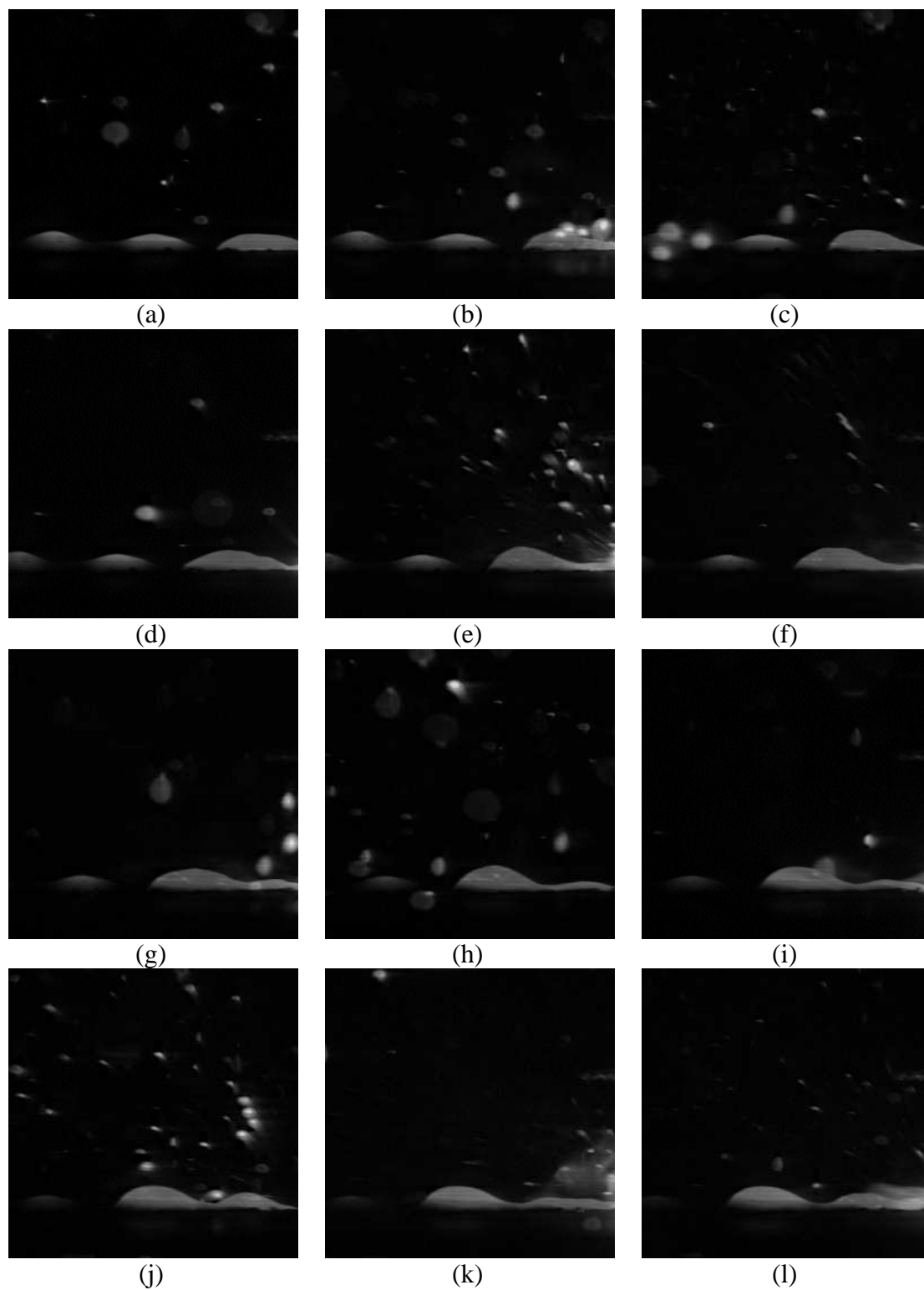
**Figure 6.69 Plan View of GMAW-P BOP Humping for Specimen 72805
WFS 15.2 m/min, TS 2.5 m/min, 225 A, 28 V, 19-mm CTWD, 2.4-mm Plate**

From the plan and side view, Figures 6.69 and 6.70, the ligament of metal connecting one hump to the next can be seen as barely flush with the original surface of the plate. The height of the hump was at least twice that of the material thickness.



Figure 6.70 Side View of GMAW-P BOP Humping for Specimen 72805
WFS 15.2 m/min, TS 2.5 m/min, 225 A, 28 V, 19-mm CTWD, 2.4-mm Sheet

The following series of still images for HSV (072805b GMAW-P Humping), Figure 6.71, of a GMAW-P BOP weld shows a series of small humps that are formed at a closer spacing and with less weld metal in the ligaments connecting the humps compared to 072805a which was made at higher arc voltage on thicker, 4 mm, plate. The apparent higher frequency of humping infers that the smaller ligaments between humps are related to the humping frequency.



**Figure 6.71 HSV Sequence for GMAW-P Bead Humping
WFS 15.2 m/min, TS 2.5 m/min, 225 A, 28 V, 19-mm CTWD**

While the welding is associated with spatter, there are points at which the higher spatter levels appear to be associated with the beginning of another hump. Although not captured in these images directly, later HSV was intended to capture this event by

placing the camera aiming point closer to the rear of the weld pool such that the metal transfer could be observed as well as the humping events.

Figure 6.71 (e) shows another high-level spatter event which is postulated to be associated with the end of one hump and the beginning of another.

In Specimen 72805c the repeating sequence of the humping defect is shorter still, Figures 6.72 and 6.73, and even more irregular in shape. The hump is actually wider than the arc-melted path and the unfilled arc-melted cavity at the end of the weld has a teardrop-shape rather than the elliptical shape of the one in Figure 6.64. This mirrors the change in shape of the molten weld pool at slower TS when humping is not produced.

The side view, Figure 6.73, shows a large loss of weld metal from the cavity produced by the arc melting and also highlights the significant shrinkage evident in all three humps.



Figure 6.72 Plan View of GMAW-P BOP Humping and Weld Pool Cavity for Specimen 72805c WFS 15.2 m/min, TS 2.5 m/min, 225 A, 31 V, 19-mm CTWD, 2.4-mm Sheet



Figure 6.73 Side View of GMAW-P BOP Humping and Weld Pool Cavity for Specimen 72805c WFS 15.2 m/min, TS 2.5 m/min, 225 A, 31 V, 19-mm CTWD, 2.4-mm Sheet

In the following sequence of HSV (072805c GMAW-P Humping), Figure 6.74, the significant level of spatter in the series of images below seems to correlate with the formation of a new hump in the weld metal.

The increased level of spatter in Figures 6.74 (m)-(n) also seems to correlate with the beginning of another hump. It is possible that the loss of this metal from the weld pool in the form of spatter results in the thin ligament of weld metal which appears to solidify first trapping the previous hump and forming the start of the next one.

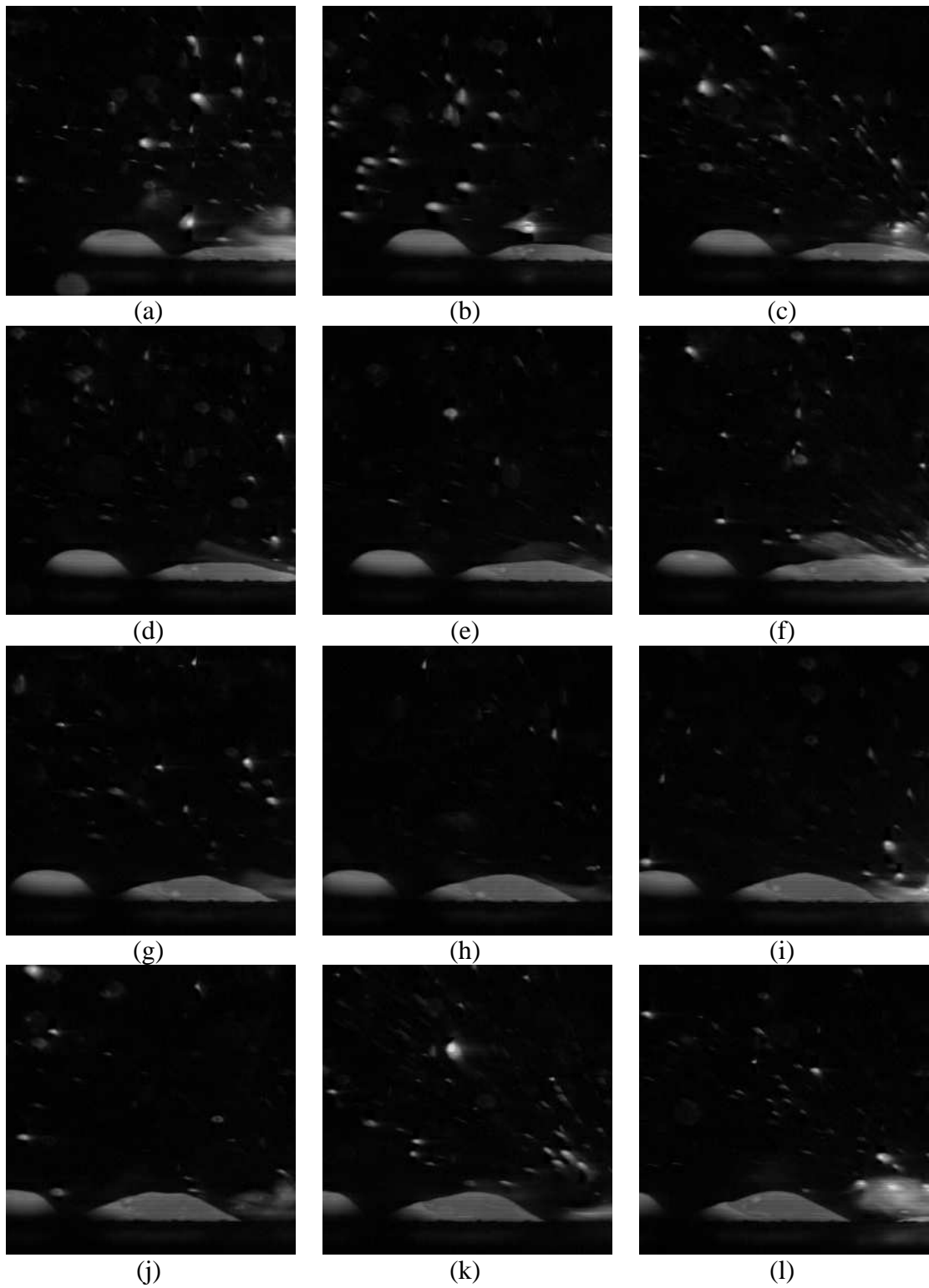


Figure 6.74 HSV Sequence for GMAW-P Weld 72805c WFS 15.2 m/min, TS 2.5 m/min, 225 A, 31 V, 19-mm CTWD

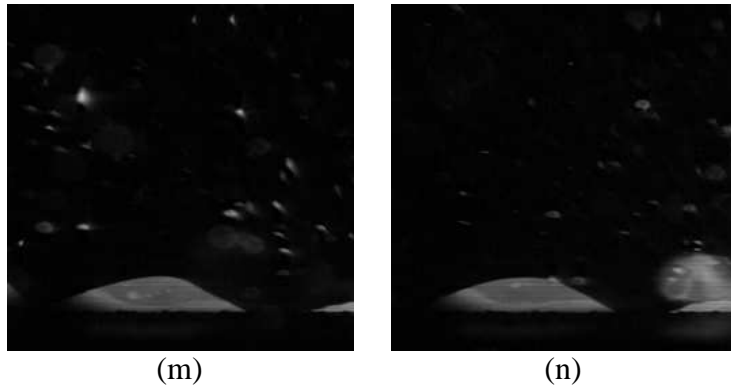


Figure 6.74 (Continued)

In Figures 6.75 and 6.76 the final solidification shrinkage can be seen at the leading edge of the last hump, and the ligament of weld metal between this and the arc-melted cavity at the end of the weld is typical of the longer spacing between bead humps. The ripple profile on the surface of the hump and the length of it as a whole indicate that it likely solidified over a longer period. This can be verified in the sequence of video stills taken from the corresponding HSV.

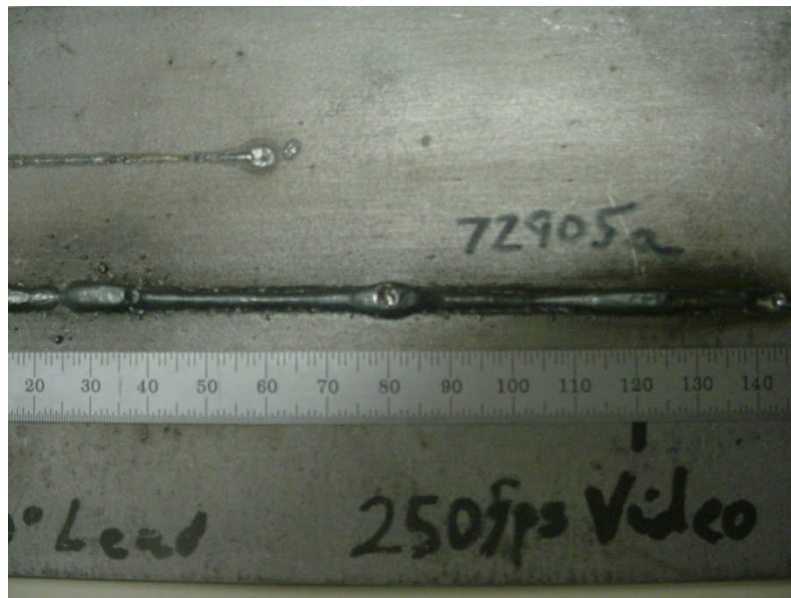


Figure 6.75 Plan View of GMAW-P BOP Humping and Weld Pool Cavity for Specimen 72905a WFS 15.2 m/min, TS 2.5 m/min, 225 A, 33 V, 16-mm CTWD, 5-mm Plate



Figure 6.76 Side View of GMAW-P BOP Humping for Specimen 72905a WFS 15.2 m/min, TS 2.5 m/min, 225 A, 33 V, 16-mm CTWD, 5-mm Plate

The next images, Figures 6.77 and 6.78, clearly show the welding electrode position relative to the weld pool and the cavity between the two created as the molten metal has solidified behind the position of wire entry.



Figure 6.77 Plan View of GMAW-P BOP Humping and Weld Pool Cavity for Specimen 72905-3 WFS 15.2 m/min, TS 2.5 m/min, 225 A, 35 V, 16-mm CTWD, 5-mm Plate



Figure 6.78 Side View of GMAW-P BOP Humping and Weld Pool Cavity for Specimen 72905-3 WFS 15.2 m/min, TS 2.5 m/min, 225 A, 35 V, 16-mm CTWD, 5-mm Plate

The length of the weld pool relative to its width has a ratio measured at 5:1, Figure 6.77. The ability of the welding process to carry a longer weld pool in terms of conductive and convective heat flow appears to have a relationship with the formation of the humps and the frequency of humping as well.

It is noticeable that there is a difference in the formation and shape of the humps relative to the arc-melted gouge profile based on the thickness of the sheet material used. This is illustrated in the next series of images that show different morphologies of humping on thin and thicker plate.

In Figures 6.79 and 6.80, it is noticeable that the humps are more rounded in nature, and tend to be wider than the arc-melted gouge when welding on thicker plate. The transition from one hump to the next can be clearly seen. Once trapped in position by the beginning of a new hump, the prior one solidifies with a resulting solidification shrinkage feature at the top. The beginning of a new hump can be seen to the right in both Figures 6.79 and 6.80 at the end of the weld, as welding progressed from left to right.

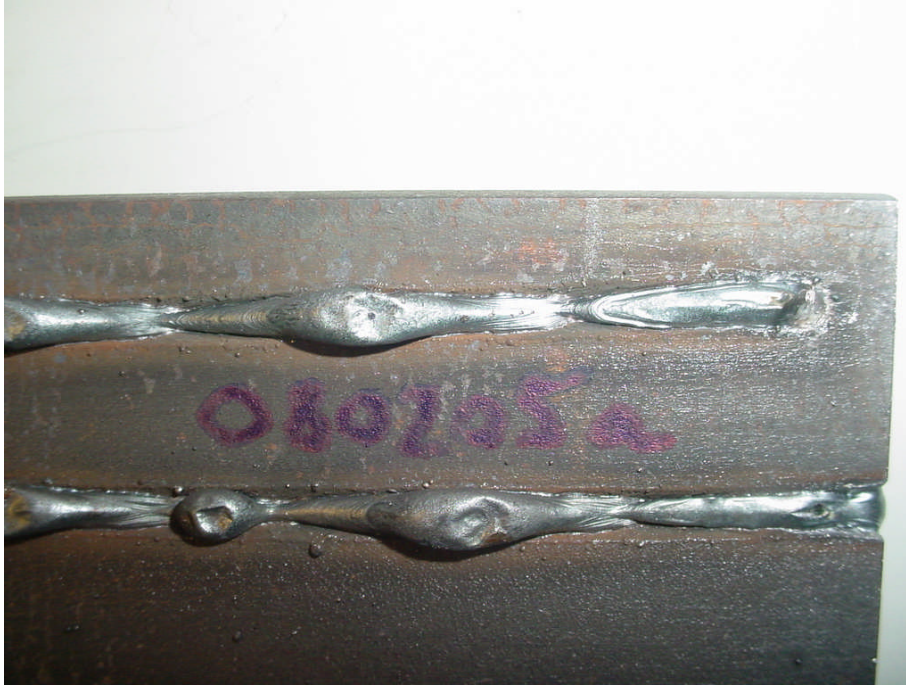


Figure 6.79 Plan View of GMAW-P BOP Humping (Upper Bead) and Weld Pool Cavity for Specimen 80205a WFS 15.2 m/min, TS 2.5 m/min, 225 A, 34 V, 19-mm CTWD, 5-mm Plate



Figure 6.80 Side View GMAW-P BOP Humping and Weld Pool Cavity for Specimen 80205a WFS 15.2 m/min, TS 2.5 m/min, 225 A, 34 V, 19-mm CTWD, 5-mm Plate

When welding on thinner sheet the humping tends to be more elongated and less rounded, and to be only the same width at the arc-melted gouged region, Figures 6.81 and 6.82.



Figure 6.81 Plan View of GMAW-P BOP Humping and Weld Pool Cavity for Specimen 80205b WFS 15.2 m/min, TS 2.5 m/min, 225 A, 34 V, 19-mm CTWD, 1.6-mm Sheet



Figure 6.82 Side View of GMAW-P BOP Humping and Weld Pool Cavity for Specimen 80205b WFS 15.2 m/min, TS 2.5 m/min, 225 A, 34 V, 19-mm CTWD, 1.6-mm Sheet

The noticeably more wavelike humping profile appears typical of the humping morphology seen with BOP welding on thinner sheet, Figure 6.83.



Figure 6.83 Side View of GMAW-P BOP Humping for Specimen 80205b WFS 15.2 m/min, TS 2.5 m/min, 225 A, 34 V, 19-mm CTWD,

For lap joints with fillet welds, Figures 6.84 and 6.85, the high-speed welding combined with a small weld pool results in increased sensitivity to instabilities in arc and metal transfer resulting in the formation of a humping defect.



Figure 6.84 Plan View of GMAW-P Fillet Weld Humping in a LapJoint for Specimen 80305a WFS 15.2 m/min, TS 3.0 m/min, 225 A, 34 V, 16-mm CTWD, 1.6-mm Sheet

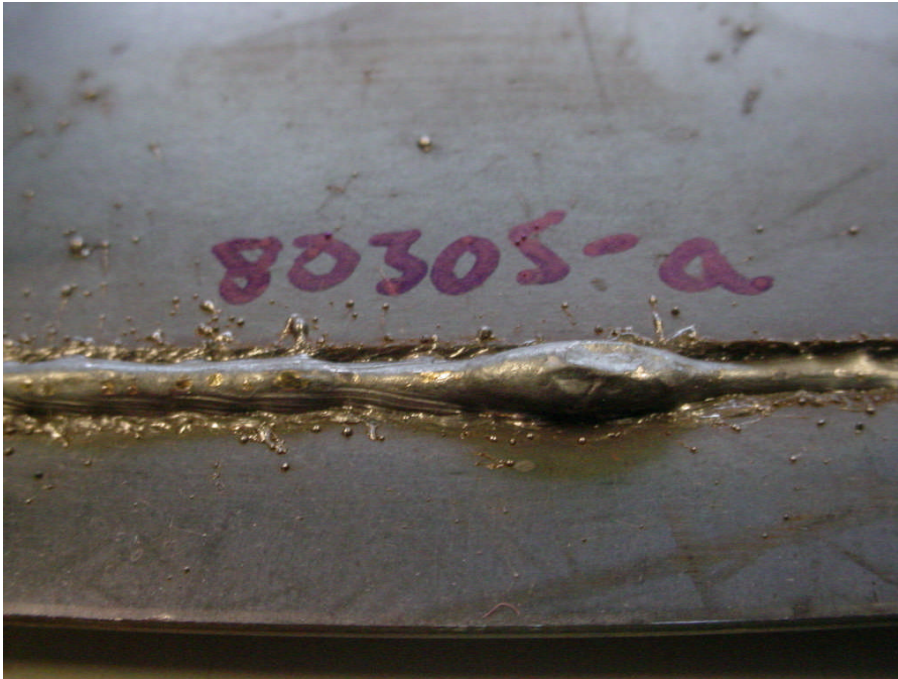


Figure 6.85 Side View of GMAW-P Fillet Weld Humping in a Lap Joint for Specimen 80305a WFS 15.2 m/min, TS 3.0 m/min, 225 A, 34 V, 16-mm CTWD, 1.6-mm Sheet



Figure 6.86 Plan View of LBW/GMAW-P Fillet Weld Humping in a Lap Joint for Specimen 80305b with Wire Offset too Much onto the Top Sheet WFS 15.2 m/min, TS 3.0 m/min, 225 A, 34 V, 16-mm CTWD, 1.6-mm Sheet

Despite the humping resulting from the misalignment of wire and joint, the weld crater can clearly be seen to be filled, Figure 6.87. This is a good indication of the benefit of using the laser to wet the weld toe on the lower side of the joint. The evidence of the laser melting can be seen to the right-hand side of the weld crater on the lower sheet surface. The laser was positioned near the lower weld toe, as for other hybrid welding operations, but the sequencing of the laser and the arc, in terms of the shutdown of each, was not timed to coincide exactly.



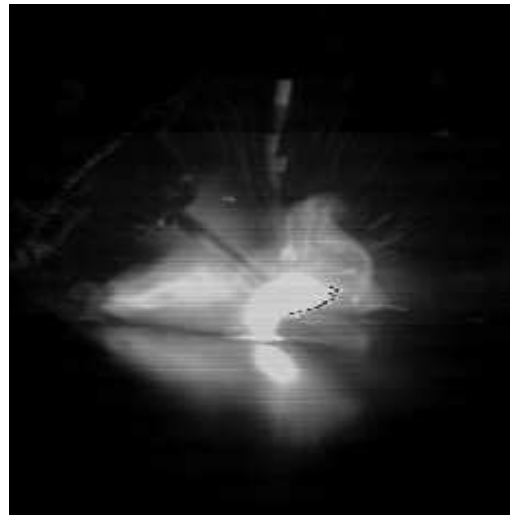
Figure 6.87 Side View of LBW/GMAW-P Fillet Weld Humping in a Lap Joint for Specimen 80305b with Wire Offset too Much onto the Top Sheet WFS 15.2 m/min, TS 3.0 m/min, 225 A, 34 V, 16-mm CTWD, 1.6-mm Sheet

The next HSV stills (80505 HSV) shows a ‘head on’ view of GMAW-P welding of a lap-fillet joint as welding progresses toward the camera, Figure 6.88.

As the images show, the weld pool is largely obscured by the hot welding fume when imaging from in front of the arc. Image 1_808 does show the molten weld pool, but it is obscured by fume in image 1_828. The top sheet edge of the lap-fillet joint can be discerned. The images show the 45-degree torch work angle and the fact that the wire is being aimed at the top edge of the top sheet in the joint, as with all weld trials. The torch travel angle is a 30-degree lead angle.



(a) Image 1_808



(b) Image 1_828

Figure 6.88 HSV Stills of a Lap Fillet Weld Viewed 'Head-On' WFS 15.2 m/min, TS 3.0 m/min, 225 A, 34 V, 16-mm CTWD

An elongated weld hump can be seen in Figures 6.89 and 6.90.



Figure 6.89 Plan View of GMAW-P BOP Humping for Specimen 82405-5 WFS 15.2 m/min, TS 3.0 m/min, 225 A, 34 V, 16-mm CTWD, 1.6-mm Sheet



**Figure 6.90 Plan View of GMAW-P BOP Humping for Specimen 82405-5 WFS
15.2 m/min, TS 3.0 m/min, 225 A, 34 V, 16-mm CTWD, 1.6-mm Sheet (lower
bead)
and for Specimen 82405-4 WFS 15.2 m/min, TS 3.0 m/min, 225 A, 31 V, 16-mm
CTWD, 1.6-mm Sheet (upper bead)**

The upper bead in Figure 6.89 was created by inadvertently selecting a lower arc voltage than intended. This created more frequent short circuits, but had the distinct benefit that it allowed the events to be captured in HSV in a way that showed the wire short circuiting frequently and creating more, shorter humps. Video stills from the HSV are shown in Figure 6.91



(a) Image I- 200



(b) Image I-270



(c) Image I- 346

Figure 6.91 HSV Showing Short Circuiting of the Wire to the Weld Pool in BOP Specimen 082405-4 at the Point when a New Hump is Created

The following sequence of HSV (82405-5), Figure 6.92, shows a side view of the weld pool along with the front of the welding torch, including the contact tip and electrode extension. The welding arc can also be seen in these images. The weld pool can be seen moving forward and then back within two images in the following three images.



(a) Image 1_489



(b) Image 1_490



(c) Image1_491

Figure 6.92 HSV Still Sequence Showing Expulsion and Weld Pool Motion

This sequence repeats every 10 images, as shown in the succeeding two images 10 frames apart from each other and 10 and 20 frames, respectively, from the first such image. It is apparent from the similarity of the images that there is a repeating instability occurring on a regular basis that may correlate with the end of one hump and the formation of another, Figures 6.93 and 6.94.

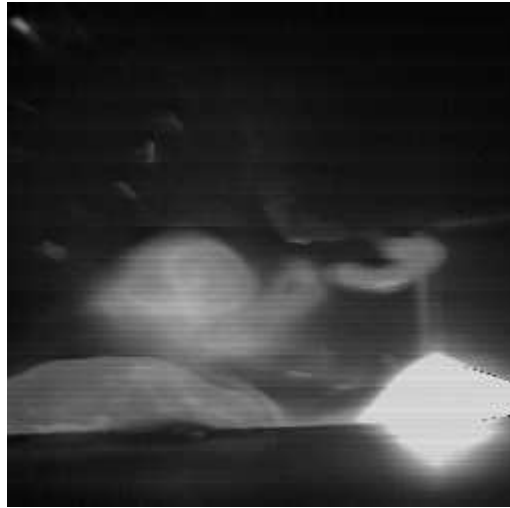


Image 1_500

Figure 6.93 HSV Image Showing Expulsion and Weld Pool Motion



Image 1_510

Figure 6.94 HSV Image Showing Expulsion and Weld Pool Motion

As the welding speed increases the shape of the melted cavity below the arc elongates in a manner very similar to the shape of a weld pool changing from round, to elliptical, to teardrop shaped as the TS is increased. This is illustrated in Figures 6.95 and 6.96 and should be compared with the cavity shape shown in Figure 6.65, page 157.



**Figure 6.95 Plan View of GMAW-P BOP Humping for Specimen 82405-8 WFS
15.2 m/min, TS 3.0 m/min, 225 A, 34 V, 16-mm CTWD, 1.6-mm Sheet**



**Figure 6.96 Side View of GMAW-P BOP Humping for Specimen 82405-8 WFS
15.2 m/min, TS 3.0 m/min, 225 A, 34 V, 16-mm CTWD, 1.6-mm Sheet**

The following HSV still (82405 HSV) images, Figure 6.97, show motion of weld pool surface at the weld toes. The motion is in the direction of welding travel as evidenced by the motion of the 'white' silicate slag islands.

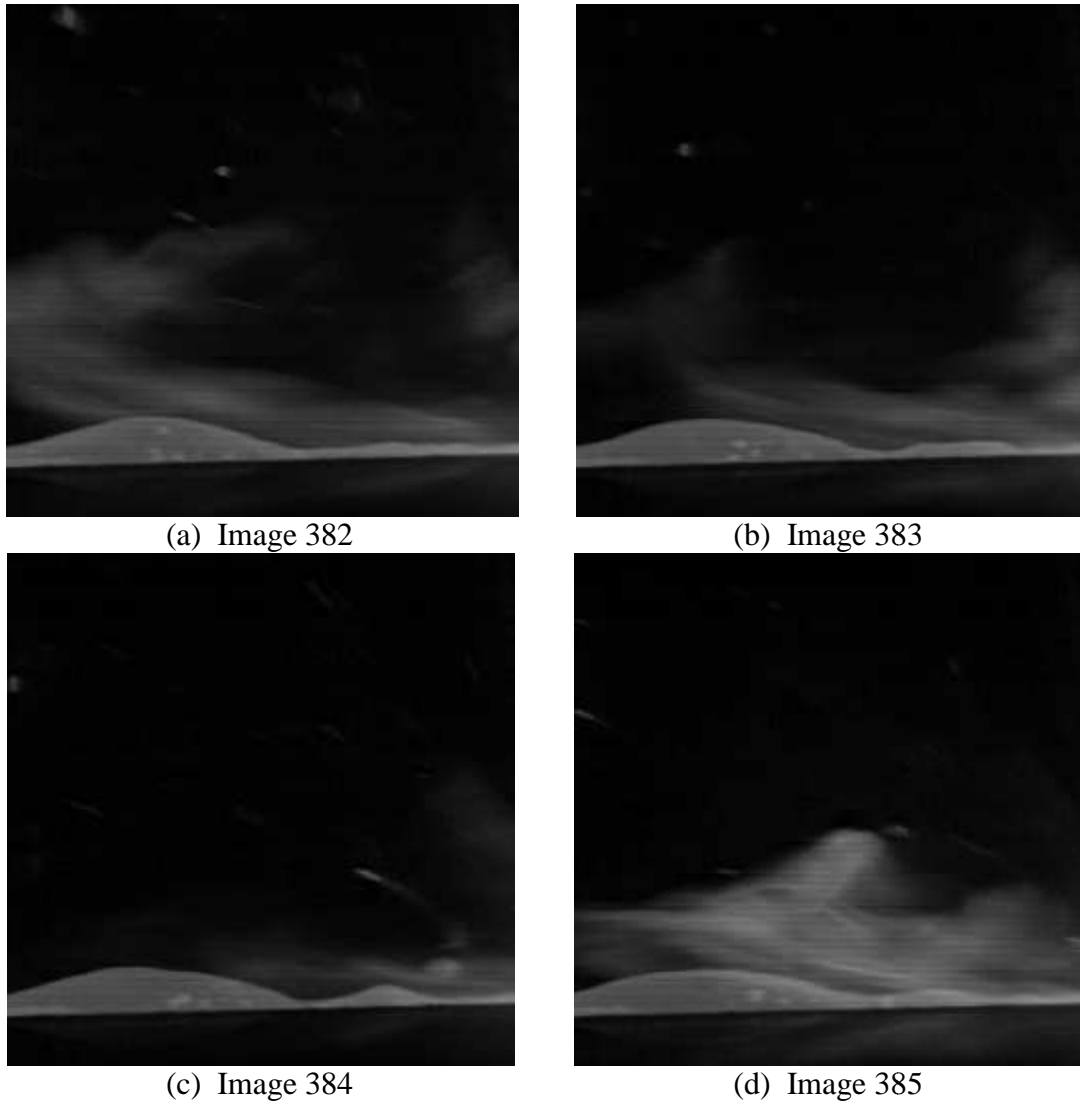
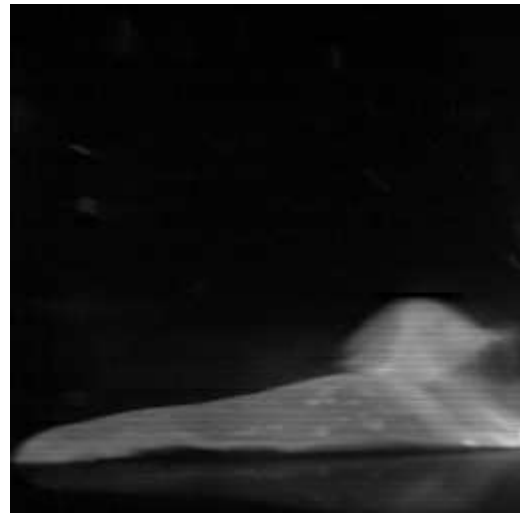


Figure 6.97 HSV Images Showing Weld Pool Motion Through Movement of the ‘White’ Silicate Slag Islands

The weld pool moves forward and then backward again within 2 frames (Images 309, 31, and 310 – the computer saved the three consecutive frames in sequence applying this numbering) at 250 fps, Figure 6.98. The timeframe for this is 0.008 s and cannot be discerned by the human eye. It is considered that this event is associated with the end of one hump and the beginning of the next, with the solidification of the previously molten bridge occurring at this time. As the field of view is 27 mm, this means the weld pool moves forward 15 mm and then back 15 mm in 0.004 s, or at 3.75 m/s.



(a) Image 309



(b) Image 31



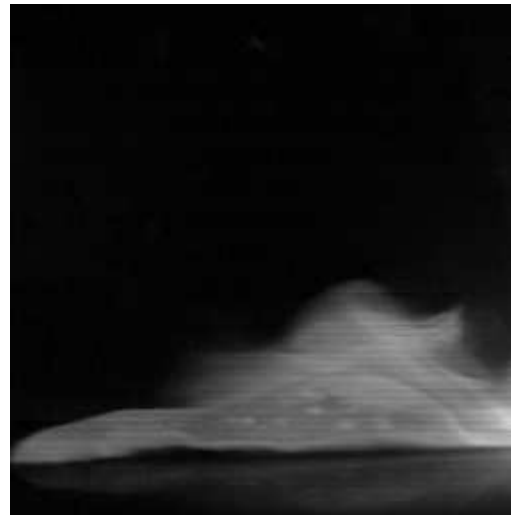
Image #310

Figure 6.98 Three Images in Sequence (082405-8 HSV file) Showing Weld Pool Motion First Forward Then Backward

Within 10 images at 250 fps the cycle repeats whereby the weld pool moves forward again, as shown in the following two HSV images 5 frames apart from each other and 5 and 10 frames, respectively, from Image 310, Figure 6.99. This represents a timeframe of repetition of 0.04 s. This timeframe is very short and this motion could not be detected by the unaided human eye. This is considered to be an important event in understanding the formation and repetitive nature of the humping defect.



(a) Image 315



(b) Image 32

Figure 6.99 Two Images Five Frames Apart (082405-8 HSV file) Showing Repetition of Weld Pool Forward Motion Every 10 Frames

The morphology of discontinuous humping can be seen in Figure 6.100 when welding a lap joint between two sheets of steel. The humping frequency is higher, and the resultant distance between humps is shorter, than in the case of most continuous humping events. The discontinuous nature of the humps has a distinctly different appearance to the continuous type as there is almost no solidified weld metal between each hump. The transition from continuous to discontinuous humping occurred at 3 m/min.

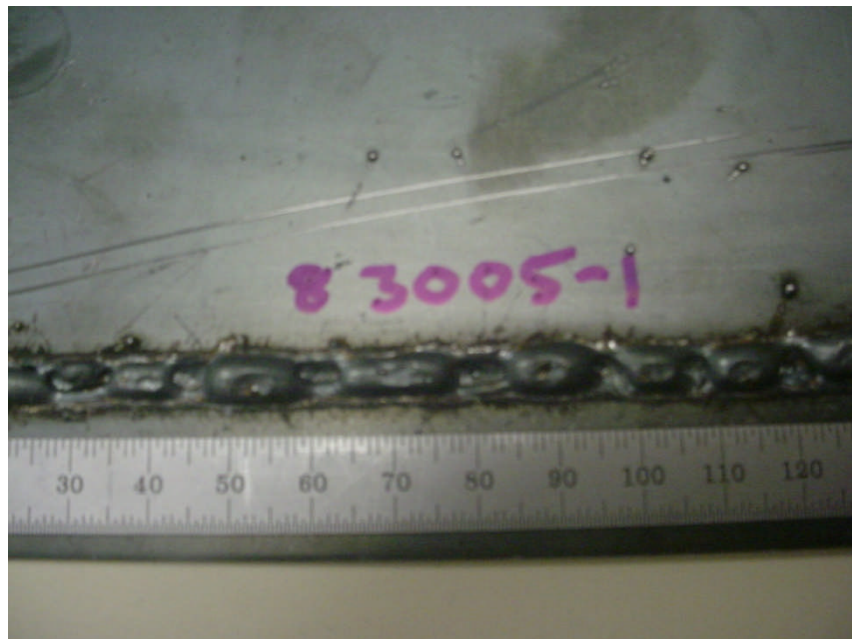


Figure 6.100 Plan View of GMAW-P Fillet Weld Discontinuous Humping in a Lap Joint, Specimen 83005-1 WFS 15.2 m/min, TS 3.0 m/min, 225 A, 34 V, 31-mm CTWD, 1.6-mm Sheet

It appears that the surface tension of the limited amount of weld metal between each hump is such that there is almost complete separation of the individual humps before the weld metal between them solidifies. HSV, Figure 9.101

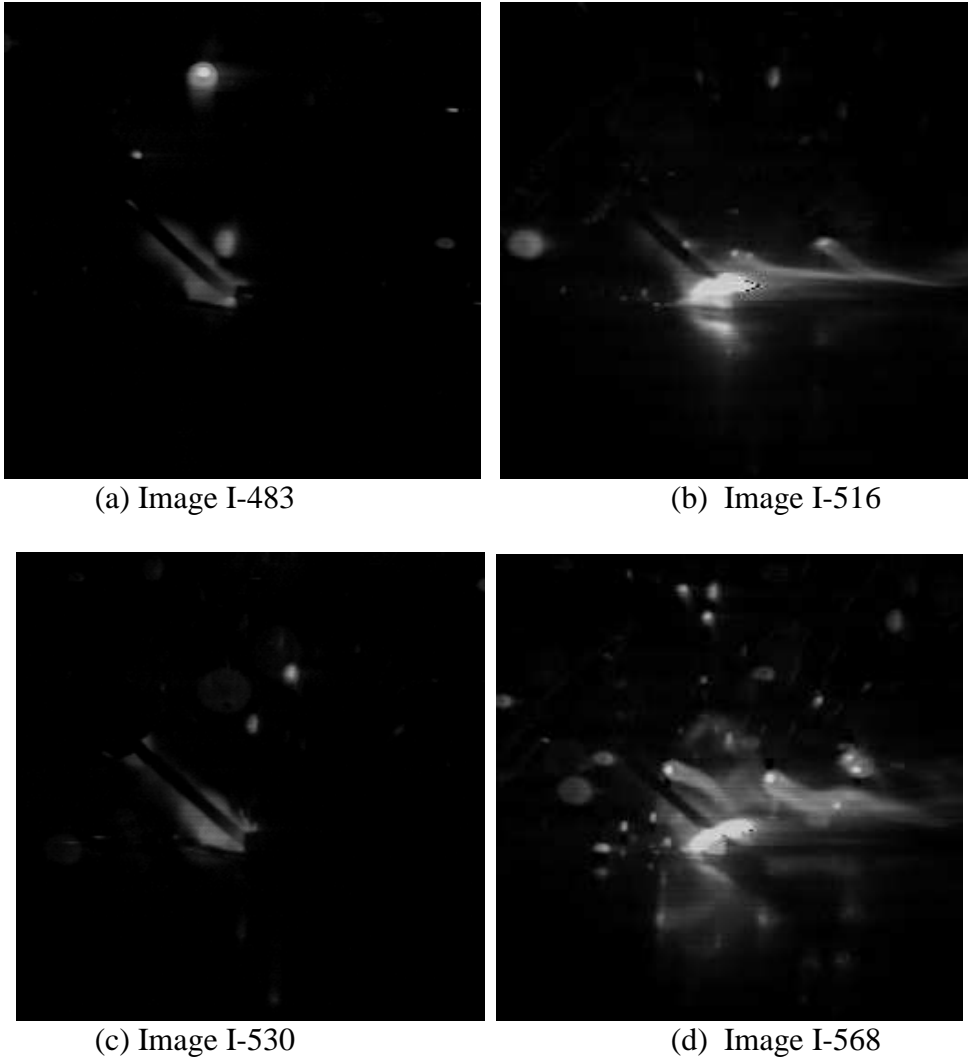


Figure 6.101 HSV Showing Short Circuiting of the Wire to the Weld Pool and Arc Re-Ignition in Lap Fillet Specimen 083005-b



Figure 6.102 Plan View of GMAW-P Fillet Weld Discontinuous Humping in a Lap Joint, Specimen 83005-2 WFS 15.2 m/min, TS 3.0 m/min, 225 A, 34 V, 19-mm CTWD, 1.6-mm Sheet

It appears as if the joint gap between the two sheets contributes to the solidification of the discontinuous hump. This is indicated by the twin ligaments seen between the humps, one on the top sheet and the other on the bottom sheet. Clearly, there is complete melting of the interface as the arc-melted region can be seen at the bottom of the area between each hump.

From these results it is clear that there are a subset of humping morphologies within the general humping defect classification. While the humping defect has been known for years, careful observation of humped welds and associated HSV has provided the basis for determining a fundamental event associated with the humping event. While visual examination of the humped weld bead shows a thin ligament of weld metal between two humps and it has been proposed before that the prior solidification of this ligament separates each hump from the next, the event that precipitates this has not been observed and reported before. HSV images have shown the occurrence of short circuits in the welding process for GMAW-P, which cause the fast movement of the weld pool from the front to rear with respect to the welding direction, Figure 6.98. The event between one hump and the next has also been observed, and is also related to short circuit events in the welding operation. In the latter case, the short occurs at a point when the base of the previous hump has solidified such that a new hump is initiated, Figure 6.91.

7.0 DISCUSSION

Weld bead humping is a major factor limiting the further increase of productivity and TS using single wire GMAW and GMAW-P in current industry application. Often the approach adopted in industry is to simply limit the travel speed of the GMAW and GMAW-P process to 1 m/min maximum because of this and the fact that fit-up is seen as too difficult or too expensive to improve. The lost productivity, over the long term, is considered more expensive than the solution of improving fit-up and increasing travel speed.

The discussion mirrors the general format and presentation order of the results section of the thesis, as follows:

- GMAW-P parameters for welding with 0T and 1T gaps
- High-speed GMAW-P with 0T gap
- Hybrid LBW/GMAW-P using CO₂ and Nd:YAG lasers
- HSV of GMAW-P and bead humping

The majority of arc welds are fillet welds made on T-butt, lap, or edge joints, and most welds are single-pass welds. GMAW-P is the typical tool employed for sheet metal welding, but is limited to 1 m/min in conventional wisdom or 2 m/min depending on power and welding technique. Above these speeds the humping defect is increasingly a problem area when using GMAW-P alone.

The relatively new process combination of hybrid laser and GMAW-P typically uses the laser in the keyhole mode for full penetration, which is not needed in fillet welds, particularly lap joints with fillet welds on sheet metal structures. Thus, the study of, and solutions to, the onset of the humping discontinuity were needed to achieve continuous welds on sheet metal structure at higher travel speed than achieved in current industry practice. The results developed and discussed here provide new data and insight to the issue of generating high-speed welds without the humping defect.

7.1 Weld Sizing

Discussion of fillet weld sizing results, and the effect of various GMAW-P welding parameters, particularly torch travel angle, are discussed in this section. The relevance of the work with 0T and 1T gaps was to illustrate the very important impact on controlling fit-up as far as it influences the weld size and ultimately the TS and productivity that can be achieved with the single torch GMAW-P process.

7.1.1 Deposit Area

To produce a larger deposit area more electrode wire needs to be added to the weld pool per unit distance. Increasing the WFS increases the operating current and the heat input of the process, all other factors remaining equal. Increasing the heat input increases the probability of burnthrough when welding sheet metal.

In all three cases, for the three material thicknesses, the acceptable weld region was shown to be reduced by the introduction of a joint gap. In each scenario the maximum TS was reduced, except the 2.0-mm thickness where the TS remained the

same at 1.0 m/min. In addition, the average width of all three areas was reduced as a joint gap was introduced. This result corroborates the findings by Doherty (Doherty, 1983). The main reason for the reduction in the acceptable weld range is the increased presence of overlap on the bottom toe, against the lower sheet in the lap-fillet weld.

Using the preferred WFS and TS values developed and verified using the data from Figures 6.15, 6.16, 6.17 (on pages 106 and 107) for 0T and 1T gaps for all three material thicknesses, weld areas were calculated using Eq. (7.1). The calculations were performed to help clarify whether the selected welding conditions were appropriate.

$$(7.1)$$

$$WFS \times Aw \times Process\ Efficiency = Deposit\ Area \times Travel\ Speed \quad (7.1)$$

In Eq. (7.1), A_w is the cross sectional area of the wire. The efficiency is the percentage of filler material that is deposited into the weld. It is common for some of the melted filler material to be expelled as spatter or fume during the welding process. The GMAW-P efficiency is approximately 98% (AWS, 1984). The calculated weld areas, from Eq. (7.1), are given in Table 7.1.

Table 7.1 Calculated Weld Deposit Areas for All Three Material Thicknesses Welded Using Preferred WFS and TS

Thickness (mm)	WFS (m/min)	TS (m/min)	Deposit Area (mm²)
2.4	8.4	0.51	17
2.0	7.6	0.76	10
1.6	4.5	0.51	11

This shows the 2.0-mm material having the smallest deposit area. The causes of unacceptable welds were undercut, burnthrough, overlap, and to a lesser extent weld size. Weld areas were accepted for the 1.6-mm material even though the actual size was larger than the weld size for 2.0-mm material. Since the difference in areas was only 1 mm², between the 2.0- and 1.6-mm joints, the welds were not reevaluated.

Image analysis of welds shown in Figures 6.15, 6.16, and 6.17 (on pages 106 and 107) was also performed to compare the actual deposit areas to the calculated deposit areas. The analysis was done by first sectioning both the 0T and 1T gap weld samples and then by taking macrographs. The macrographs were analyzed using ImagePro™ software. The results from the image analysis are given in Table 7.2.

Table 7.2 Weld Deposit Area Measurements Made with ImagePro™ Software of All Three Material Thicknesses Welded Using Preferred WFS and TS

Thickness (mm)	Gap	Deposit Area (mm ²)	Average (mm ²)	Dilution (mm ²)
2.4	0T	27	28	11
2.4	1T	29		
2.0	0T	17	18	8
2.0	1T	18		
1.6	0T	18	19	8
1.6	1T	20		

The difference between the calculated and measured deposit areas is attributed to the dilution from the top plate. The measured weld areas include the top plate dilution because it is not easy to determine how much of the top sheet material was consumed in the weld. The bottom plate dilution was easy to determine, as the amount of material included in the weld is easy to measure. The dilution of the top plate was calculated by subtracting the calculated deposit areas from the measured deposit areas. The measured deposit areas for the 2.0- and 1.6-mm material are nearly the same, with the 1.6-mm material being a little larger.

The thicker 2.4-mm material can support a larger heat input based on its mass compared to the other two sheet thicknesses. The 2.4-mm material may allow for 3-D heat flow, this could allow for the material to cool faster. The increased heat input also accounts for the larger amount of dilution that is present in the deposit area for the 2.4-mm-thick material. The heat is applied mainly to the upper plate, due to the arc location on the top edge of the top sheet. The amount of top plate melting that occurs is directly affected by the amount of heat that is placed into the material. This explains why the amount of average dilution is larger for the 2.4-mm material, and the other two material thicknesses have similar amounts of dilution.

Figure 6.15 (on page 106) shows the macrographs of the welds in the 2.4-mm lap joints, for both the 0T and 1T weld joints. Both macrosections show a high toe angle at the lower toe. The 1T gap section has undercut of the top sheet, but the undercut is less than 20% of the material thickness so it is acceptable. These welds are acceptable as they exhibit full root fusion and no presence of rejectable undercut or overlaps. Figure 6.16 (on page 107) shows welds produced on 2.0-mm material. There is a little underfill on the upper sheet in both welds and a high toe angle at the lower toe. These welds are acceptable for the same reasons as the 2.4-mm material; they exhibit complete root fusion and no rejectable undercut or overlap. Figure 6.17 (on page 107) shows welds produced on 1.6-mm material with a 0T and 1T gap. Both welds have significant penetration as well as no overlap or rejectable undercut, but the welds do appear large relative to the thickness of the material. The 0T gap is on the borderline between acceptable and unacceptable based on excess penetration, but the weld is still characterized as acceptable.

Producing SWAT acceptability windows for a given weld joint and application is a good starting point for weld trials. The result of these trials produces a WFS versus TS relationship that gives a preferred weld area for the given TS.

The nominal basis for weld sizing is usually 0.75 times the material thickness for the leg length for plate thicknesses. However, below 3 mm this becomes somewhat meaningless as the smallest typical leg size for mechanized welding with GMAW is 3 mm. As such, any single-pass weld on material 3 mm or thinner is likely to have a 3-mm leg on the bottom sheet of a lap fillet joint and an upper leg thickness equivalent to the thickness of the upper sheet.

For a horizontal lap fillet weld with a gap

$$A_{HF} = \frac{\pi a(bt)}{4} + G^2 \quad (7.2)$$

where:

- A = weld deposit area
- t = sheet thickness
- a = normal leg, t + G
- G = gap
- b = parallel leg factor.

b is typically 2.0 to 4.0 for conventional GMAW.

With no joint gap this reduces to:

$$A = \frac{[\pi \times a(bt)]}{4} \quad (7.3)$$

Rearranging for b, gives:

$$b = \left[\frac{4A}{(\pi \times a)} \right] t \quad (7.4)$$

Calculations for b, the lower fillet leg length, determined this to be 1.4 for lap-fillet welds of minimum size for all three material thicknesses, when no gap was present. This is considered an important finding in terms of sizing fillet welds on thinner sheet materials. Knowing the value for b, the required weld area can be calculated, and from this the correct combination of WFS and TS can be determined from the WFS/TS ratios determined already from the experimental results.

Weld quality requirements were defined by sheet metal welding standards such as AWS D8.8-97 and D1.3-98 (AWS, 1997 and 1998). Complete root fusion was routinely achieved, as was an acceptable bead profile free from significant inconsistencies. However, freedom from undercut was not achieved at the highest TS approaching 4.0 m/min for hybrid LBW/GMAW. The causes of undercut are well known, Table 7.3.

Table 7.3 Causes and Remedies of Undercut (AWS, 2004)

Possible Causes	Corrective Actions
Travel speed too high	Use slower travel speed.
Welding voltage too high	Reduce the voltage.
Excessive welding current	Reduce wire feed speed.
Insufficient dwell	Increase dwell at edge of weld pool.
Gun angle	Change gun angle so arc force can aid in metal placement.

The welding current and TS need to be maintained at high levels to achieve the desired increase in melting rate and productivity. Edge dwell decreases TS and productivity and consequently is not an option. The arc voltage controls the weld bead width, but at WFS and TS as high as 4.0 m/min, the melted bead width was found to be narrow even at high arc voltages because the arc length became very short. At very high TS underfill of the joint occurred.

Reducing the arc voltage reduces overall power, but does not reduce the melting rate – this is an option that was evaluated, but is limited by arc shorting. When SC occurs, resulting from the arc length being too short, increased arc instability with corresponding poor bead profile occurs.

Changing the work angle was possible – aiming it more at the top sheet – i.e., increasing the work angle as measured from the vertical plane. The work angle was increased from 45 to 55 degrees to use the arc force to direct metal more toward the top sheet while using the laser to wet the lower toe on the lower sheet in the lap-fillet joint.

Increasing the CTWD, resulting in more I^2R heating and reducing the welding current, can be used to increase the melting rate. CTWD was increased from 16-32 mm to alter the amount of resistive heating, Table 6.7 (on page 157). The best results were achieved at a CTWD of 25 mm for hybrid welding.

To increase the toe angle, both laser wetting of the toe and ER70S-6 wire were employed. The results, Table 6.4 (on page 144), showed that a toe angle in the range of 110 to 130 degrees could be maintained using both approaches. This toe angle worked to avoid bead humping in GMAW-P alone, but at significantly lower TS.

7.1.2 Travel Angle

When a lead (push) travel angle is used in GMAW-P the weld pool becomes elongated compared to that produced with a perpendicular (0-degree lead) torch travel angle, all other factors being equal. Elongating the weld pool decreases the power density of the welding arc by distributing the arc energy over a larger weld pool surface area. The decrease in power density reduces the maximum penetration of the weld compared to a weld produced with zero torch travel angle. Reducing the

penetration of the weld is helpful when a high TS is desired. It can become a necessity to avoid excessive penetration and burnthrough when the base material is a sheet product.

The other main result of a lead travel angle is that the weld bead tends to be less convex. This latter result of increasing the travel angle is a key element in mitigating the tendency of a weld bead to have a higher contact angle as the TS is increased. Increasing the lead travel angle is thus a key element of the ability to avoid weld bead humping, particularly for welding with GMAW-P only, .i.e., without a laser, to assist with bead wetting at the GMAW-P weld toes. The results achieved using a 30-degree lead travel angle demonstrated a significant increase in TS achieved before the onset of bead humping, Figures 6.22, 6.23 and 6.24 (on pages 112 and 113). TS of up to 2.4 m/min were achieved using a 30-degree lead travel angle with GMAW-P compared to only 1.0 m/min when using a 0-degree lead travel angle. This represents an increase of 140%.

The location of the arc at the top edge of the top sheet in a lap joint was used to provide additional material from the top sheet to produce a contribution from the base metal to add to that of the added electrode wire.

Standard methods to reduce bead humping are well known and published in the *AWS Welding Handbook*, Table 7.4 (AWS, 2004). Reducing the TS can reduce or eliminate humping, but obviously limits productivity and the objective of this work is to suppress the humping defect to higher TS. Using a push travel angle on the welding torch is understood but often not practiced in industry in the author's experience. Recent research work (Choi, 2006) continues to perpetuate this even for hybrid welding. Choi used a 0-degree travel angle for the GMAW torch in his work. A 30-degree lead travel angle was used in the experiments conducted in the present work since it is the maximum angle that can be used without the torch nozzle interfering with the weld profile, or requiring cutting or otherwise modifying the nozzle to avoid this.

Reducing the arc voltage produces a narrower weld bead and a lower heat input all other things being equal. If the arc voltage is reduced too far, the arc becomes unstable and so this is limited by the practical minimum arc length that can be sustained in a stable transfer mode. In addition, as arc voltage is reduced the weld bead becomes narrower, and ultimately is too convex. This will also lead to increased tendency for humping.

Table 7.4 Methods of Reducing Various Welding Process Defects in GMAW Including the Humping Defect (AWS, 2004)

Possible Causes	Corrective Actions
Humping at high travel speeds	<ul style="list-style-type: none"> • Reduce travel speed • Use push angle • Reduce voltage (arc length)
Poor Wetting	<ul style="list-style-type: none"> • Increase arc voltage • Use high Si wire (steels)
Weld sagging when welding out of position	<ul style="list-style-type: none"> • Weld in flat position, especially when using high currents • Reduce wire feed speed to reduce current and weld pool size • Increase travel speed
Weld bead waviness due to electrode deviation	<ul style="list-style-type: none"> • Reduce contact tip to workpiece distance • Purchase straighter wire or use wire straightener
Magnetic arc blow	<ul style="list-style-type: none"> • Demagnetize tools and fixtures • Move location of workpiece lead connection

7.1.3 Work Angle

The work angle for a typical lap-fillet joint or T-butt joint is 45 degrees, ostensibly bisecting the 90-degree angle between the two sheets when a fillet weld of equal leg length is desired. Positioning the welding torch in a more vertical position does not allow the heat from the welding arc to be equally applied to both joint members. Directing the arc more toward the top sheet, by increasing the work angle relative to the plane perpendicular to the joint, causes more of the top sheet to be exposed to the heat from the arc. This results in a larger amount of melting of the top sheet. Decreasing the work angle, the welding arc is applied more to the bottom sheet, and results in underfill on the top toe of the weld, incomplete fusion defects on the top sheet, or burn-through. Continuous burn-through, analogous to cutting, was produced when a laser was introduced to locally melt the weld toe region on the lower sheet. The results of this work (Figures 6.22, 6.23 and 6.24, on pages 112 and 113) showed that the best results were achieved with a 60-degree work angle (relative to the horizontal plane).

There are practical issues in electrode wire positioning with respect to the joint. There are two types of mislocation: electrode location relative to the joint, Figure 7.1, and differences in CTWD. These are important even at conventional welding speeds in the range of 0.5-1.0 m/min. At higher speeds they become even more important in terms of the stability of metal transfer and the impact, in terms of weld length, that a short interruption in welding torch position can have relative to the joint.

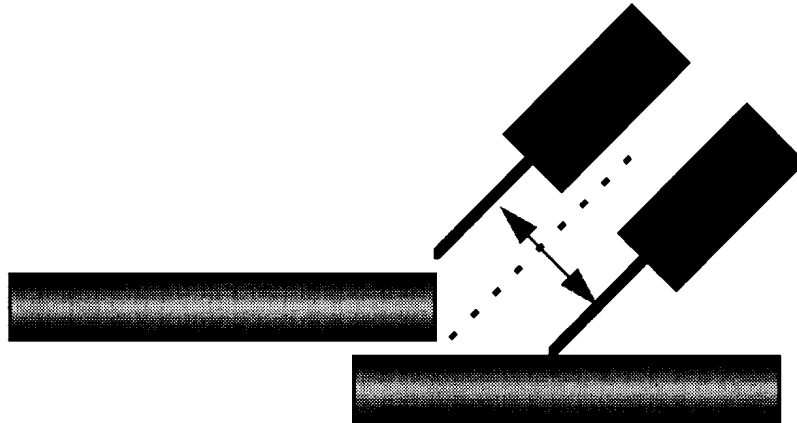


Figure 7.1 Electrode Locating Error

Electrode locating error has the following causes and can have the results listed:

- Cause:
 - Piece-part inconsistencies
 - Improper fixture design
 - Spatter on fixture
 - Cast or helix in electrode
- Result:
 - Incomplete fusion
 - Undersized weld size
 - Undercut
 - Poor weld shape

The critical nature of good fit-up and torch positioning relative to the joint was well illustrated in the hybrid LBW/GMAW-P process when the wire was mislocated onto the top sheet, Figure 7.2. This resulted in discontinuous humping even at 3.0-m/min TS on the fillet weld in the lap joint. The use of the hybrid LBW/GMAW-P process, while it is able to produce a continuous bead at 4.0 m/min when the wire is located at the top edge of the top sheet, cannot tolerate misalignment inboard of this edge at 3.0 m/min.

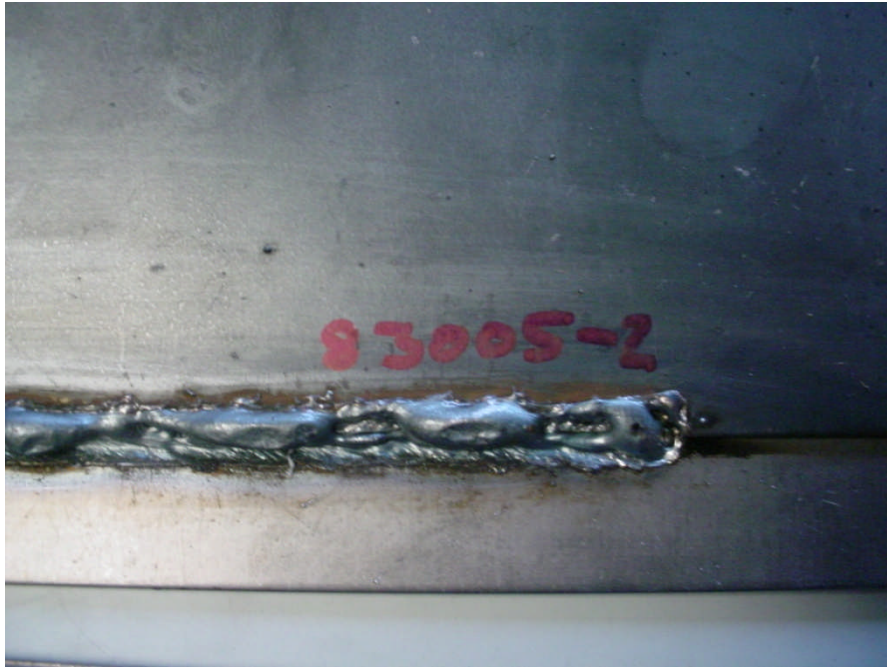


Figure 7.2 Plan View of GMAW Fillet Weld Discontinuous Humping in a Lap Joint, Specimen 83005-1 Resulting from Wire Mislocation onto the Top Sheet

7.1.4 Travel Speed

Significantly higher TS was achieved in GMAW-P using a 30-degree lead travel angle. The results were achieved with 0T gap in each case to demonstrate the improvements that can be achieved when attention is paid to proper joint fit-up and use of the correct travel angles. The results for the 1T gap showed that the travel speed at which an acceptable weld could be produced was considerably slower than when a 0T gap condition was maintained. Combining the 0T gap and lead travel angle resulted in an increase in travel speed before onset of humping by a factor of two compared with that for a 90-degree lead angle and 1T gap.

The heat input of a process is directly related to the welding current and arc voltage, and inversely proportional to the TS. When the TS is increased, the overall heat input to the material is decreased. When the material is thinner, as in the case of the 2.0- and 1.6-mm sheet, the main cause of rejecting the weld was the occurrence of an inconsistency in bead shape resulting in local underfill of the joint. Decreasing the heat input reduces the total amount of liquid metal on the top joint member. The smaller weld pool size appeared to reduce the probability of an underfill condition occurring.

Figures 6.6, 6.10, and 6.14 (on pages 98, 102 and 106, respectively) show the effect of TS and material thickness on the weldability of a 1T gap. Increasing the TS improved the weldability of the two thinner materials but reduces the weldability of the thicker material when a 1T gap was present. This supports the results shown by others (Jelager, 1994) which showed that a slower TS was required for thicker materials to accommodate the same joint gap as a thinner material. Jelager welded T-joints with material thickness combination of 3 mm/3 mm at speeds up to 1.5 m/min. The

materials used in the baseline work performed here with the perpendicular travel angle were 2.4-mm thick or less; the travel angle resulted in lower TS being achieved.

7.1.5 Arc Length

Increasing the arc length increases the arc voltage at a specific current. The increase in voltage increases the heat input of the process because heat input is directly related to voltage. At higher heat inputs, a larger volume of liquid metal is in the weld pool. The larger volume of liquid metal is more likely to produce a ‘skip’ – a region of incomplete joint filling in the weld length as the higher arc voltage produces a wider weld.

Increasing the arc length produces a larger arc impingement area on the base material, which is similar to the case when the travel angle is increased. Increasing the arc impingement area, the heat input per unit area of the process decreases, reducing the penetration into the material. When the torch angle changes the heat input of the process remains the same, but the area over which the heat is applied is increased, thus reducing the power density. When the arc length is increased the heat input of the process increases, but so does the area of arc impingement for a conical arc shape. The arc length was kept intentionally short in the work conducted to achieve better control of the weld pool and to minimize the arc voltage.

Results of HSV show that despite the use of a high arc voltage to minimize arc shorting, this still occurs, Figures 6.91 and 6.101 (on pages 176, and 183-4, respectively). A significant reason is that despite selecting a high arc voltage to maintain spray arc transfer, albeit at the shortest possible arc length, the power source is operating near its available power limit, resulting in a lower delivered arc voltage at high wire feed speed.

7.1.6 Contact Tip to Work Distance

CTWD appears to be a more significant factor in increasing gap weldability for thicker materials, 2.4 and 2.0 mm, and less of a factor for the thinner 1.6-mm steel sheet. Increasing the CTWD resulted in an improvement in gap weldability, and has been shown to be the case by others (Jelager, 1994, and Richardson, 2002).

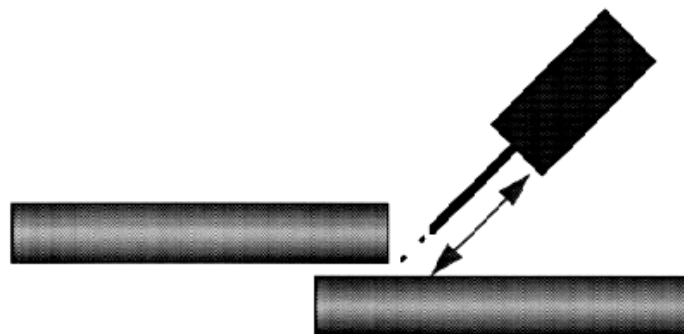


Figure 7.3 CTWD Changes

Changes in CTWD, Figure 7.3, have the following causes and can have the results listed:

- Cause:
 - Piece-part inconsistencies
 - Improper fixture design
 - Spatter on fixture
 - Bent weld guns

- Result:
 - Changes in welding current
 - Reduced or excessive penetration
 - Poor weld shape
 - Excessive spatter
 - Porosity

Increasing the CTWD for a given WFS reduces the resulting heat input. The lower heat inputs were possible due to the increased I^2R resistive heating of the electrode extension, which reduces the current needed to melt the electrode wire for a given WFS and thus maintains the burn-off relationship and stable arc length of GMAW-P. The heat from the welding arc is distributed into the base material, the surrounding environment and the electrode wire. By increasing the electrode extension, the I^2R resistive heating of the longer wire extension increases the initial temperature of the electrode allowing more of the arc heat to melt a larger volume of metal for the same heat input. As this occurs, the current needed to be reduced, for the larger CTWD trials, to produce the same size deposit area as the shorter CTWD trials. By reducing the current for a given WFS, the heat input is decreased. Since it has been shown that the gap weldability decreases with increasing heat input, it follows that increasing the CTWD increases the gap weldability as it lowers the welding current. The evidence for this is that a CTWD of 25 and 32 mm worked best when trying to achieve maximum TS without humping or burnthrough.

7.2 Energy Input and Arc Efficiency

Energy input is the amount of energy applied per unit length of weld and is expressed in joules per millimeter (J/mm). For arc welding this is usually expressed as:

$$H = \frac{VI}{v} \quad (7.5)$$

where:

- H = Energy input, J/mm
- V = Welding arc voltage, volts (V)
- I = Welding arc current, amperes, (A)
- v = Travel velocity of the heat source, mm/s

Arc efficiency is a measure of the net energy input, H_{net} , expressed as:

$$H_{net} = \frac{fVI}{v} \quad (7.6)$$

where:

f = Heat transfer efficiency of the heat source (heat transferred to the workpiece divided by the total heat generated by the heat source)

The heat transfer efficiency is usually referred to as the arc efficiency. With most consumable electrode welding processes the arc efficiency is typically 0.8 to 0.9 (DuPont and Marder, 1985).

The equation for electrode melting rate in GMAW is typically expressed as shown below:

$$MR = aI + bLI^2 \quad (7.7)$$

where

MR = Electrode melting rate, kg/hr
 L = Electrode extension, mm
 I = Welding current, A
 a = Proportionality constant for anode or cathode heating
 b = Proportionality constant for electrical resistance heating including the electrode resistivity, kg/hr \times A² mm

Thus, for hybrid LBW/GMAW-P at high speeds, the use of electrode extensions of 25 to 30 mm and high welding currents were used in this work to maximize the melting rate of the electrode and increase the potential welding speed achievable.

Melting efficiency for 2-D heat flow is a maximum of 0.5. This is effectively reached at 1.78 m/min (30 mm/s) for GMAW-P (DuPont and Marder, 1985). At higher TS used in this work the melting efficiency has been considered to be 0.5 on this basis.

7.3 Calorimetry

Measurement of heat transfer and arc efficiencies requires the use of calorimetry techniques, as was conducted in this work for GMAW-P and LBW/GMAW-P. While the topographical feature of weld bead humping is influenced more by toe wetting than by the thermal efficiency of the process, the anticipated change in efficiency using melt mode laser welding was of interest as it may, if too low, have resulted in a reduced wetting effect compared to that anticipated for a particular nominal power level in kW. The measure of efficiency was also considered when determining the appropriate laser spot size on the workpiece since laser melting, not just heating, was required.

Liquid nitrogen calorimetry was performed for GMAW-P, and CO₂ LBW/GMAW-P. The technique employed was that established at INEL (Kenney et al., 1998) involving recording weight change due to liquid nitrogen boil-off with time. After welding, the part was immediately dropped into an insulated liquid nitrogen container and the

change in weight as liquid nitrogen boiled off was used to calculate the heat content of the part. Equipment calibration was achieved by dropping the same part at room temperature into the liquid nitrogen, enabling adjustment of the results to compensate for the room temperature heat content of the weldment. Analysis of data for GMAW-P showed a process efficiency that averaged 78%. The high efficiency of GMAW-P is attributed largely to the high stability of metal transfer in GMAW-P and the resultant lower level of spatter compared to other transfer modes in GMAW such as GMAW-VP. This compares well with the results obtained by other researchers (Joseph et al., 2003), (Kenney et al., 1998), using liquid nitrogen calorimetry, and those achieved using a Seebeck arc welding calorimeter (DuPont and Marder, 1985).

The efficiency of LBW/GMAW-P was measured at an average of 62%. The lower efficiency of the combined process is attributed to the lower efficiency of conduction mode LBW compared to GMAW-P, which was measured at an average of 78%. The measured efficiency of the combined LBW/GMAW-P process is considered to be the first measured for a high-speed welding operation.

Based on these results, and with the laser operating in the conduction mode rather than the keyhole mode, the anticipated efficiency of the laser process, by simple arithmetic $([78+x]/2 = 62, \text{ where } x = 46)$, would be 46% if each process was operating at the same power level. However, this does not take into account the power difference between the GMAW-P and the laser, which were 12.8 kW and 5.2 kW, respectively. Taking the power ratios into consideration, the effective efficiency of the laser is calculated at 18% $([5.2/12.8] \times 46 = 18)$. As a surface melting effect was intended in the use of the laser, this is a reasonable number for a conduction mode operation.

7.4 Conduction versus Convection

The relative importance of conduction and convection in the overall movement of heat in a weld pool can be assessed from the value of the Peclet number, Pe , given by:

$$Pe = \frac{(u \times p \times L \times c_p)}{k} \quad (7.8)$$

where:

- Pe = Peclet number
- u = Local weld pool velocity, cm/s
- p = Density g/cm^3
- c_p = Specific heat at constant pressure, cal/[g C]
- L = characteristic weld pool length
- k = Thermal conductivity of the melt cal/[cm C s]

For metals with high thermal conductivity, at low speeds, and for small weld pools the value of the Peclet number can be low, i.e., much smaller than 1.

When the Peclet number is much larger than 1.0, heat transport occurs predominantly via convection and heat conduction in the weld pool is of little importance.

For a typical GMAW-P weld in steel:

$$\begin{aligned}u &= 10 \text{ cm/s} \\p &= 7.2 \text{ g/cm}^3 \\c_p &= 0.2 \text{ cal/[g }^\circ\text{C]} \\L &= 1.0 \\k &= 0.1 \text{ cal/[cm }^\circ\text{C s]}\end{aligned}$$

the Peclet number equals 144. This high number confirmed that the heat transport in steel is mostly by convection. This seems reasonable for steel since it does not have high thermal conductivity. The fact that 2-D conductive heat flow predominates in welding sheet steels seems to confirm this. This correlates with the proposition (Mills and Keene, 1990) that weld bead humping is caused by Marangoni convection. However, convection alone does not explain the phenomenon, as also confirmed by others (Gratzke et al., 1992) concerning the breakdown of a liquid cylinder. From the results obtained in the present work, increased wetting resulting from use of a laser, rather than increased arc stability, has been shown to be the predominant mechanism.

The length of the weld pool in LBW/GMAW-P has been shown to be in the range of 20 to 36 mm, so the Peclet number would be considerably higher than in the example calculation shown above. Thus, it is clear that heat transport in LBW/GMAW-P also occurs predominantly via convection, and that the weld pools must impinge to achieve the desired wetting and spreading of the GMAW-P weld pool. It also shows that the predictions of Gratzke based on Rayleigh instability theory of the breakdown of a liquid cylinder are not a complete explanation for bead humping formation as the length to width ratio was 12:1 in the 36-mm-long weld pool noted above and shown in Figure 7.4, rather than the limit of 10:1 proposed by Gratzke for single wire GMAW.



Figure 7.4 36-mm-Long Weld Pool with 3-mm Bead Width (12:1) Using Single-Spot 4-kW Nd:YAG/GMAW-P Hybrid on a Lap Joint

Welding of sheet steel is governed by 2-D heat flow rather than 3-D heat flow. As welding speed increases, so the weld pool becomes more elongated because of the low thermal conductivity of steel and the effect of convective cooling.

The GMAW-P process results in the highest heat and penetration along the bead centerline and the wetting angle is controlled by the overall heat input, particularly the welding current and TS, and Marangoni convection within the weld pool. Surface tension, decreasing with increasing temperature, results in an inward, surface tension-driven fluid flow within the weld pool.

The ability to increase the weld penetration by addition of laser energy is known and used to good effect in welding of plate thicknesses when arranged in axial alignment with the welding arc. However, using the laser energy predominantly to increase the superheat and fluidity of the weld pool by directing it at the weld toes has not previously been investigated. This technique was used in the present work by intentionally directing the laser energy to one, Figure 7.5, or both of the weld toes, thus increasing the superheat and fluidity of the weld pool and thus also increasing the contact angle and wetting between the weld bead and the parent material such that higher welding speeds could be obtained before the onset of weld bead humping.



Figure 7.5 Wetting of the Weld Toe Using a Single Laser Spot (Seen at Left of the Right-Hand Weld Bead)

7.5 Wire Composition and Wetting

Oxygen promotes wetting in GMAW weld beads. Si and Mn are deoxidizers added to solid steel electrodes to remove oxygen and promote higher toughness.

Si promotes wetting also but the ratio of Si and Mn has been shown to have a significant effect on the wetting characteristics (Suzuki and Nakano, 2001). Results with ER70S-3 and ER70S-6 wires show increased wetting for ER70S-6 wires that have about the same amount of Si, but significantly more Mn in the case of ER70S-6. Thus, it appears that the extra Mn in the latter consumable preferentially consumes the

oxygen leaving more of the Si to act as a reducer of surface tension, thus resulting in improved wetting and lower contact angles when using this consumable.

The use of HSV enabled the movement of the slag islands on the liquid weld pool to be viewed. HSV taken from the front of the welding operation, with the weld progressing toward the camera, showed that the direction of weld pool movement was rearward, based on the rearward movement of the 'white' (in the IR image) slag island on the surface of the weld pool. This observation is in agreement with other observers (Nguyen et al., 2005). From HSV taken at 90 degrees to the welding direction, to provide a side view of the weld pool and bead humping, the slag islands were seen to progress forward on the sides of the humps, showing that the weld pool motion was forward in this region of the pool. As the motion of the weld metal is predominantly rearward toward the forming bead hump, it was concluded (Nguyen et al., 2005) that forward movement does not occur. Based on the direct observation of this in the present research, the conclusion of Nguyen is incorrect in this respect.

The extra Mn is added to cater for increased oxygen in the case of welding over rusty steel, or, as in the case examined in this work, welding over hot-rolled steel sheet that has an oxide mill scale. Removing this mill scale should result in better wetting, and could be achieved using grit blasting. However, the coupling of the laser with the steel is improved by an oxide film and thus it was decided to weld the hot-rolled steel in the as-received condition.

As expected, results in the present work showed that better wetting was achieved using ER70S-6 electrode wire than with the ER70S-3 used for the baseline work. The ability of the ER70S-6 wire to produce better wetting characteristics also affects the ability to produce a smaller weld size for a single-pass fillet weld.

The CO₂ LBW/GMAW-P used ER70S-3 initially and then ER70S-6, while all work with hybrid Nd:YAG/GMAW-P used ER70S-6. Better results were achieved with the ER70S-6 electrode wire. The ability to continue to produce welds with 110- to 130-degree toe angles and thus continue to suppress weld bead humping at higher and higher TS is considered to be partially a result of using the wire with higher deoxidants. The Si in the wire is considered to be able to assist with wetting while the less stable Mn oxide is formed, Table 7.5.

Table 7.5 Oxidation Potential of Various Metals and Oxides and their Stability (AWS, 2004)

Oxidation Potential of Metals and Metal Oxides	
Relative Stability*	Relative Reactivity†
1. CaO	1. Aluminum
2. MgO	2. Magnesium
3. Al ₂ O ₃	3. Cobalt and Titanium
4. TiO ₂	4. Tungsten
5. SiO ₂	5. Manganese
6. V ₂ O ₃	6. Vanadium
7. MnO	7. Molybdenum
8. Cr ₂ O ₃	8. Iron
9. WO ₂ and MoO ₂	9. Chromium
10. Fe ₂ O ₃	

* Listed in decreasing order of stability.

† Listed in decreasing order of reactivity.

7.6 Effect of Shielding Gas

Ar-CO₂ shielding gas was used for all the GMAW-P work. A mixture of 90Ar-10CO₂ was employed as this gas promotes high stability GMAW-P metal transfer and minimizes occurrence of arc instabilities. Arc instability at high TS is a major cause of weld bead irregularities and is exacerbated at high TS where the length of time associated with an instability results in a longer length of weld with a resulting irregularity as the welding speed increases.

CO₂ shielding gas promotes a deep bowl-shaped fusion profile which is useful for increasing tolerance to torch misalignment relative to a joint. However, when welding on sheet metal, the deeper profile tends to promote burnthrough. Another significant issue is that CO₂ promotes globular transfer and this mode of metal transfer is characterized by high levels of spatter. In the context of a small fillet weld, spatter loss can represent a significant reduction in the local cross-section of the weld.

Ar-CO₂ mixtures tend to promote streaming spray transfer and increase the stability of axial pulsed spray transfer. The high deposition efficiency of 98-99% typical of spray transfer is important in production of small fillets welds as it minimizes spatter loss and promotes a smooth metal transfer.

While the dissociation energy from ionization of helium provides increased energy in the arc, for sheet metal welding it is considered that the higher arc voltage and broader penetration profile that helium tends to promote are not beneficial to a smaller weld width which is required for welding at high TS. The higher arc voltage promotes a wider weld, albeit that this has a higher weld toe angle with less excess weld metal than an Ar-based gas. Helium gas was, however, used for arc plume suppression in CO₂ LBW.

7.7 Spatter in GMAW

At high welding speeds the volume loss of spatter can cause undercut in a fillet weld by its absence from the solidified weld pool. For spray transfer, with GMAW and GMAW-P, spatter levels are typically no more than 1-2%. For GMAW-SC with CO₂ shielding gas they can be as high as 10%. For a small weld size, spatter losses can become significant in reducing the weld volume. A high arc voltage and high arc length increase weld width which is undesirable for high-speed welding. Process control is best achieved at high speed using a low arc voltage to control the arc length and avoid melting too much weld width in relation to the weld bead size. In this work the wire feed speed and arc voltage were high, but the arc length was low as the power source was being used near its capability limit with an extended CTWD. Arc stability was increased, and the tendency to transition to rotational spray transfer was suppressed, by the stabilizing effect of the laser-stabilized cathode spot on the GMAW-P weld pool.

The welding process melts the material, and the weld pool fluid flow, along with the arc force and spatter condition, determines the degree and distribution of the solidifying weld metal. The arc voltage controls the weld width and the width of the melted area. To fill the area created by the arc melting the weld metal must have sufficient cooling time to wet out and fill this area to avoid undercut. This is why two solutions for undercut are to reduce welding speed and reduce arc voltage. However, the former clearly is not an acceptable solution when one is trying to increase TS and overall productivity.

A high level of spatter is generated in hybrid LBW/GMAW if the laser beam impinges on the weld pool. This is one of the main reasons why the laser aiming point is ahead of the wire aiming point. Despite this, significant spatter was generated at the highest travel speeds, Figure 101,(pages 183-4) as the power source was used near its power limit.

The effect of spatter is also important in controlling welding costs – spatter on fixtures increases the chance of parts mislocating in fixtures leading to increased joint gaps and increased likelihood of burnthrough conditions in sheet products, as well as the need to decrease welding speed to bridge the joint gap.

7.8 GMAW-VP and LBW/GMAW-VP

Higher productivity of GMAW for sheet metal lap-fillet joints is a need that has resulted in the development of advanced power sources. GMAW-VP power sources allow high filler WFS with controlled heat input to the thin substrates, preventing burnthrough defects that had been a limiting factor for deposition rate. At still higher deposition rates with VP power sources, bead humping becomes the limiting factor as these power sources are generally limited to 200 A.

GMAW-VP, by variation of the DCEN and DCEP, arc components is capable of reducing the heat input to a substrate without decreasing the burn off rate, and is cited as having productivity advantages for welding sheet metal compared to GMAW-P (Harwig, 2003). As the heat input to a substrate decreases, the wetting of the molten metal also decreases, so the resulting bead has an undesirable toe angle, with a

narrower width and larger height. Poor wetting and spreading of the weld deposit results in the GMAW-VP process having limited benefits for high-speed welding. Welding speeds of 1.8-2.0 m/min were achieved using CO₂ LBW/GMAW-VP hybrid welding (Choi, 2006). This is high compared to conventional wisdom for GMAW-P, but demonstrated in the current research work to be no better than GMAW-P.

7.9 Hybrid Welding

Use of lasers in conjunction with arc welding was first reported in 1978 (Eboo and Steen) and referred to as arc augmented laser welding. The practical application of this process, now known as laser hybrid welding, has taken almost 20 years. The first commercial exploitation of this process was claimed in Germany in 2002.

Hybrid laser/GTAW and laser/PAW has been developed predominantly by ISF at Aachen University (Dilthey, 2002) and the University of Coventry (Page et al., 2002), and used predominantly for welding of butt joints in automotive tailored blank applications which use laser welding almost exclusively at this time.

Laser/GMAW hybrid welding has been the most widely studied since it offers the most potential for increased productivity and tolerance to fit-up variations typical in most industrial practice. The predominant approach employed to date is to use the laser for penetration and the GMAW wire addition for gap tolerance and joint filling. Much of this work has been directed at the shipbuilding and pipelining markets for welding steel plate and pipe products, respectively, by EWI, Cranfield University, and others. Significant work has also been conducted in laser/GMA brazing of automotive steel sheet (Dilthey, 2000) and on Al sheet products for BIW applications (Graf, 2002). Commercial systems have been developed by companies such as Fronius, Fraunhofer (ISF), Cloos, HighYag, and Daihen.

A review of CO₂ laser/GMAW hybrid welding and BOP trials on steel plate (Downs and Mulligan, 2002) highlighted the benefits of the process for deep penetration and tolerance to joint gap, but did not address the potential process benefits for sheet products. This leaves a gap in the knowledge base that the work conducted and discussed in the current research has addressed.

7.9.1 Comparison of Welding Speed for GMAW-P and LBW/GMAW-P Hybrid

The productivity, in terms of welding speed for a single-pass fillet weld, for various processes has been shown to be as follows:

- Conventional GMAW-P <1.0 m/min
- High-Speed GMAW-P <2.4 m/min
- LBW/GMAW-P hybrid <4 m/min)

Single-wire productivity for a 3-mm fillet weld on a lap-fillet joint is 1 m/min with 25-mm electrode extension and 14-m/min WFS for a 1.0-mm-diameter steel electrode (Fronius, 2005). This result is comparable to the data produced in the current research for GMAW-P. The results achieved in the current research for high-speed GMAW-P show a large increase of 240% compared with the conventional GMAW-P results

TGMAW productivity for a 2-mm fillet weld on a lap-fillet joint is 2-3 m/min with 15-mm electrode extension and WFS of 14 and 12 m/min for a 1.0-mm-diameter steel electrode (Fronius, 2005). This data for TGMAW TS of 2-3 m/min is comparable to the speeds of up to 2.4 m/min achieved for high-speed single torch GMAW-P in the current research. The hybrid LBW/GMAW-P results showed a further increase of up to 4 m/min without humping, and acceptable welds at welding speeds up to 3.3 m/min, Figures 6.58 and 6.61 (on pages 147 and 149, respectively).

7.9.2 GMAW-P and LBW/GMAW-P Bead Humping – Lap Joints

WFS and TS ratios for the onset of bead humping are reported below for GMAW-P and compared to those for the best results achieved with LBW/GMAW-P hybrid welding. Both processes used a 30-degree lead travel angle for the GMAW torch.

- 2.4-mm-thick steel sheet:
 - 12.7-m/min WFS: Bead humping at 1.3 m/min (WFS/TS = 9.6) GMAW-P
 - 14.0-m/min WFS: Bead humping at 1.9 m/min (WFS/TS = 7.3) GMAW-P
 - 15.2-m/min WFS: Bead humping at 2.3 m/min (WFS/TS = 6.7) GMAW-P
 - 15.2-m/min WFS: Bead humping at 3.6 m/min (WFS/TS = 4.3) LBW/GMAW-P.

- 2.0-mm-thick steel sheet:
 - 7.6-m/min WFS: Bead humping at 1.3 m/min (WFS/TS = 5.7) GMAW-P
 - 8.9-m/min WFS: Bead humping at 1.7 m/min (WFS/TS = 5.2) GMAW-P
 - 10.2-m/min WFS: Bead humping at 2.2 m/min (WFS/TS = 4.7) GMAW-P
 - 17.8-m/min WFS: No humping at 4.0 m/min (WFS/TS = 4.4) LBW/GMAW-P.

- 1.6-mm-thick steel sheet:
 - 7.6-m/min WFS: Bead humping at 1.5 m/min (WFS/TS = 5.2) GMAW-P
 - 8.9-m/min WFS: Bead humping at 2.0 m/min (WFS/TS = 4.4) GMAW-P
 - 10.2-m/min WFS: Bead humping at 2.5 m/min (WFS/TS = 4.1) GMAW-P.

The data above, for the onset of weld bead humping, can be summarized for different sheet thicknesses graphically as shown in Figure 7.6. Welds made at TS to the lower right of these lines exhibit humping.

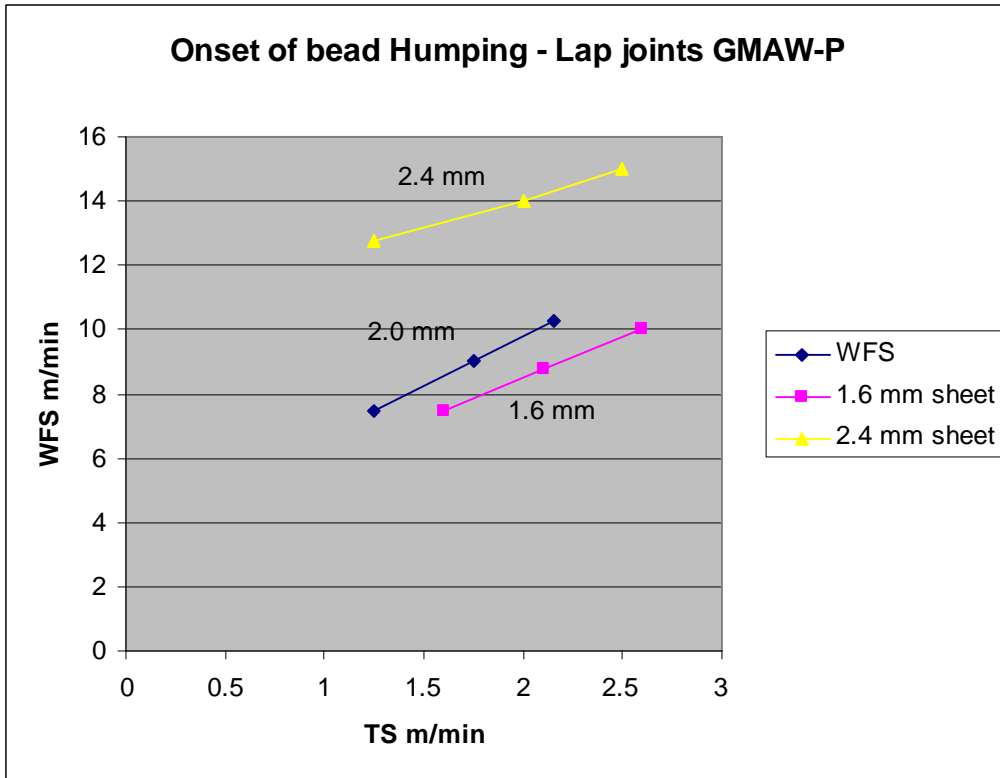


Figure 7.6 Onset of Bead Humping for Lap Joints Made Using High-Speed GMAW-P

When comparing WFS/TS, the results below were developed for robustness to both 0T and 1T gaps when making fillet welds on lap joints with conventional GMAW-P and a 90-degree travel angle:

- 1.6 mm (WFS/TS = 16.5)
- 2.0 mm (WFS/TS = 9.9)
- 2.4 mm (WFS/TS = 8.75).

The larger WFS/TS above is required when a 1T gap must be bridged.

For GMAW-P with a 30-degree lead torch travel angle the comparable results for the highest TS with a 0T gap were as follows:

- 1.6 mm (WFS/TS = 4.1)
- 2.0 mm (WFS/TS = 4.7)
- 2.4 mm (WFS/TS = 6.7).

It is noticeable that the results for high-speed GMAW-P with a closed gap are half to a quarter those for the 1T gap tolerant procedures. Results are compared in Figure 7.6.

For LBW/GMAW-P with a 0T gap the comparable results, Figure 7.7, were as follows:

- 1.6 mm (WFS/TS = 4.3)
- 2.0 mm (WFS/TS = 4.4)
- 2.4 mm (WFS/TS = 4.2).

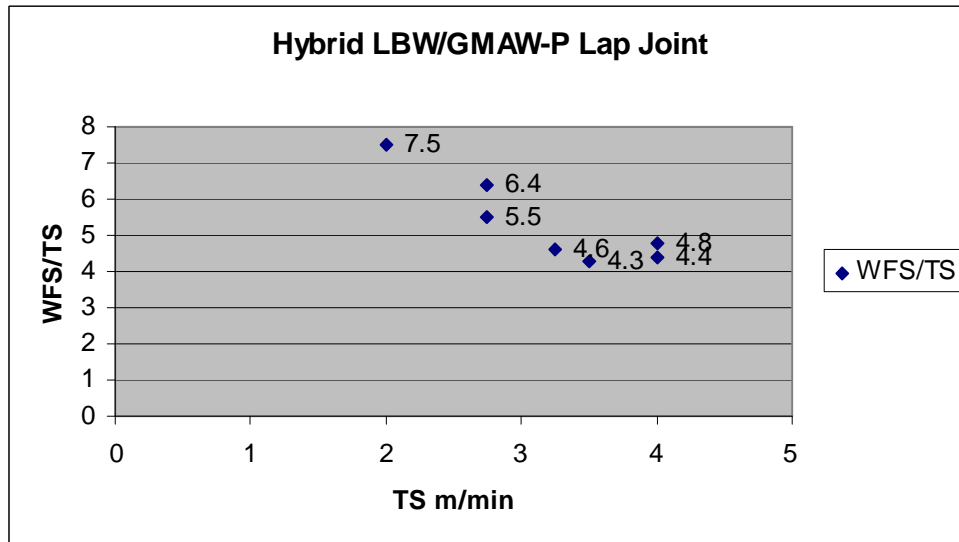


Figure 7.7 WFS/TS Versus TS Showing that Smaller Welds can be Made at Higher TS

It is noticeable that the ratios for GMAW-P and LBW/GMAW-P are essentially the same for 0-gap conditions. This number is the same across both processes and all three material thicknesses. This finding, combined with the calculated factor of 1.4 for the lower leg length (b) of the fillet weld, can therefore be used to size welds for both processes.

Based on the need to cater for avoidance of bead humping and for a 1T joint gap, which includes overwelding for a 0T gap, the weld size, as defined by WFS/TS for conventional GMAW-P is twice that required for the LBW/GMAW-P hybrid welds, Figure 7.8. While this is true this statement has to be modified when excessive undercut is created by use of an excessive arc length or CTWD.

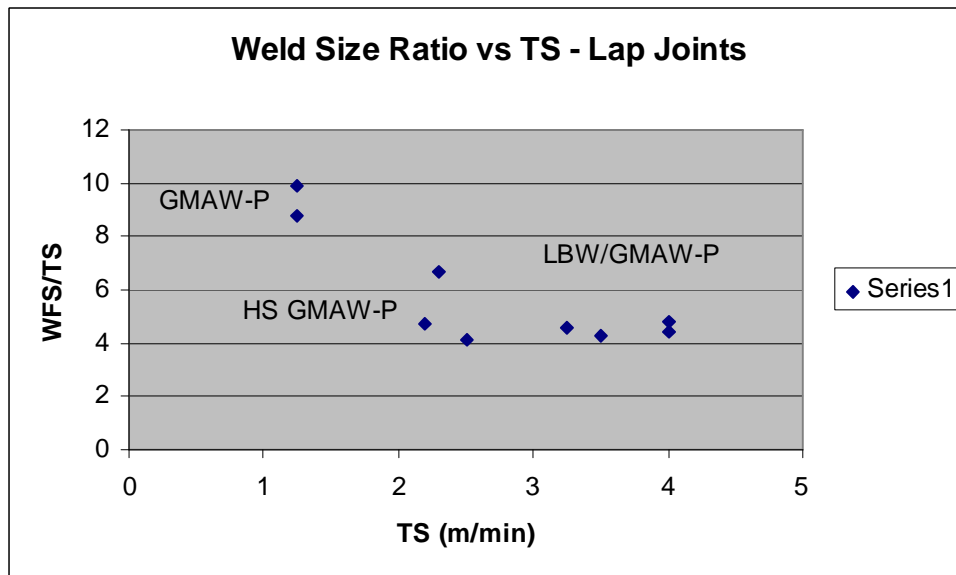


Figure 7.8 Trends for Weld Size Ratio (WFS/TS) versus TS for Lap Joints Made with Conventional GMAW-P, High-Speed GMAW-P, and LBW/GMAW-P

7.9.3 GMAW-P and LBW/GMAW-P Bead Humping – T-Butt Joints

WFS and TS ratios for the onset of bead humping are reported below for high-speed GMAW-P and compared to those for the best results achieved with LBW/GMAW-P hybrid welding. Both processes used a 30-degree lead angle for the GMAW torch.

- 2.4-mm-thick steel sheet:
 - 12.7-m/min WFS: Bead humping at 1.9 m/min (WFS/TS = 6.7) GMAW-P
 - 14.0-m/min WFS: Bead humping at 2.0 m/min (WFS/TS = 6.9) GMAW-P
 - 15.2-m/min WFS: Bead humping at 2.5 m/min (WFS/TS = 6.0) GMAW-P.

For 2.4-mm sheet, the typical WFS/TS was 6-7 for GMAW-P.

- 2.0-mm-thick steel sheet:
 - 7.6-m/min WFS: Bead humping at 0.7 m/min (WFS/TS = 10.7) GMAW-P
 - 8.9-m/min WFS: Bead humping at 0.8 m/min (WFS/TS = 11.7) GMAW-P
 - 10.2-m/min WFS: Bead humping at 1.0 m/min (WFS/TS = 10.5) GMAW-P
 - 14.0-m/min WFS: No bead humping at 4.0 m/min (WFS/TS = 3.4) LBW/GMAW-P.

The comparison of results noted above shows that the TS for onset of humping can be increased by a factor of 3 for 2.0-mm sheet. The typical WFS/TS was 10.5-11.5 for GMAW-P, and 3.5 for LBW/GMAW-P.

- 1.6-mm-thick steel sheet:
 - 7.6-m/min WFS: Bead humping at 0.9 m/min (WFS/TS = 8.6) GMAW-P
 - 8.9-m/min WFS: Bead humping at 1.1 m/min (WFS/TS = 8.2) GMAW-P
 - 10.2-m/min WFS: Bead humping at 1.3 m/min (WFS/TS = 7.6) GMAW-P
 - 12.7-m/min WFS: Bead humping at 3.8 m/min (WFS/TS = 3.3) LBW/GMAW-P.

The comparison of results noted above shows that the TS for onset of humping can be increased by a factor of 3 for 1.6-mm sheet using LBW/GMAW-P compared with GMAW-P alone. For 1.6-mm sheet, the typical WFS/TS was 7.6-8.6 for GMAW-P, and 3.3 for LBW/GMAW-P.

The results show that by using laser melting at the weld toes of the GMAW-P bead, the effective minimum size of a weld bead that can be produced without humping can be reduced by a factor of 3 and a continuous bead can still be produced. The actual TS that can be used based on meeting the required bead size is likely to be less than this to meet welding specification requirements. Results are compared in Figure 7.9. The leftmost three data points are for conventional GMAW-P, the next three for high-speed GMAW-P, and the three to the right are for LBW/GMAW-P.

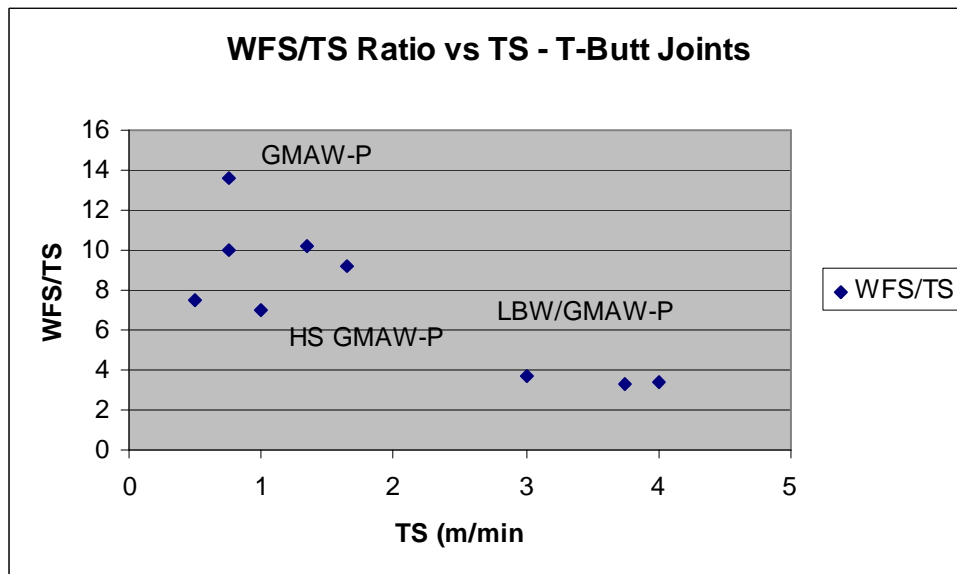


Figure 7.9 Trends for Weld Size Ratio versus TS for Conventional GMAW-P, High-Speed GMAW-P, and LBW/GMAW-P Hybrid Welding in T-Butt Joints

7.9.4 Laser Spot Size, Spacing, and Power Density

To be an effective tool for modifying the GMAW-P weld bead toe angle the laser must have enough power density to melt the base metal and result in wetting of the GMAW-P bead edge.

The required spot size must be relatively large to result in effective wetting and spreading of the GMAW-P weld bead in the transverse direction relative to the welding direction, Figure 7.10. The position of the laser impingement point ahead of the arc impingement point was varied from -2 through 3 mm, and worked best at in the range of 0 to 2 mm ahead of the arc to minimize spatter generation and arc interference. The laser did not stabilize the arc, but rather increased the wetting of the weld pool as described below. As such, a 2-mm spacing is recommended based on the work conducted.

The spot spacing must be such as to impinge or overlap the weld toes of the GMAW-P bead, but only just, so that the inner portion of the laser spot is near the GMAW-P bead toe – this results in the maximum wetting of the GMAW-P bead in the transverse direction, Figure 7.11.

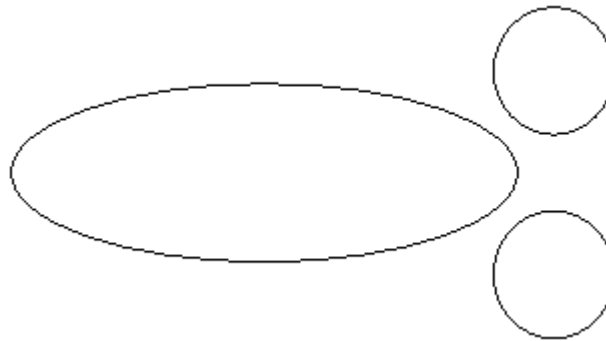


Figure 7.10 Plan View - Arrangement of Laser beam Spots (Round) Relative to the Arc Weld Pool (Ellipse) to Achieve Maximum Weld Toe Wetting and Spreading

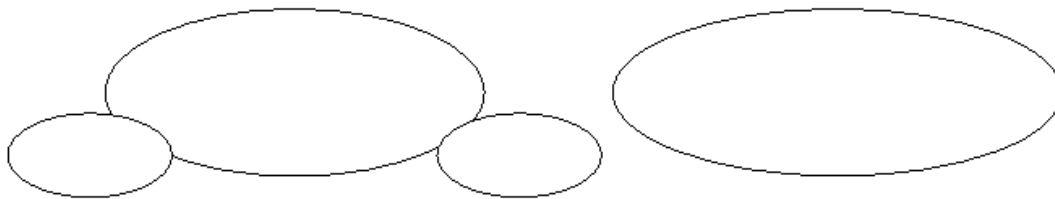


Figure 7.11 Cross-Sectional view - Arrangement of Laser beam Spots (Small Ellipses) Relative to the Arc Weld Pool (Larger Ellipse) at Left, to Achieve Maximum Weld Toe Wetting and Spreading, at Right

If the spot size is too small, Figure 7.12, the degree of wetting is small and the effect on GMAW-P spreading and toe angle is minimal, Figure 7.13.

The requirement to melt the base metal and have an effective spot size to meet the above criteria defines the laser power required for effective wetting and to result in a significant increase in the bead toe angle.

Control of the beam splitting angle is required to achieve the correct spot spacing for transverse separation of the two beam spots such that they impinge on the GMAW-P

bead toes. Without meeting this requirement, the possibility of cold laps and resulting lack of fusion between the GMAW-P weld toe and the melted area of the laser spot can be expected as the weld metal will bridge across the spacing between the two if the spacing is too large. Conversely, if the spacing is too small, then no effective wetting is seen as a result.

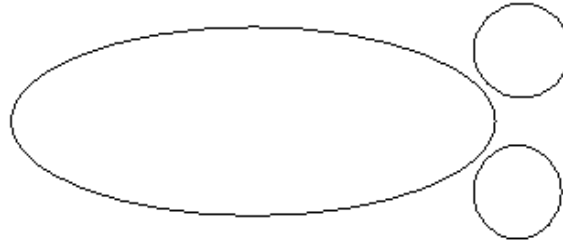


Figure 7.12 Plan View - Size and Arrangement of Laser beam Spots (Round) Relative to the Arc Weld Pool (Ellipse) Resulting in Minimum Weld Toe Wetting and Spreading



Figure 7.13 Cross-Sectional View - Size and Arrangement of Laser beam Spots (Small Elliptical Spot) Relative to the Arc Weld Pool (Ellipse) at Left, Resulting in Minimum Weld Toe Wetting and Spreading at Right

For LBW a typical spot size is 2.0 mm for Nd:YAG and 2.5 mm for CO₂ laser. For wetting in dual-beam LBW/GMAW-P hybrid welding a spot size of 2.5-3.0 mm was found to be effective. This is achieved in practice by setting the laser head out of the true focal plane.

If the laser spot size is too large, Figure 7.14, the power density is too low to generate a conduction weld pool, and thus there is heating rather than melting of the area impinged by the laser spot. This condition does not allow the wetting of the GMAW-P weld pool and thus there is no significant impact on wetting, Figure 7.15, nor consequent increase in the TS before bead humping occurs.

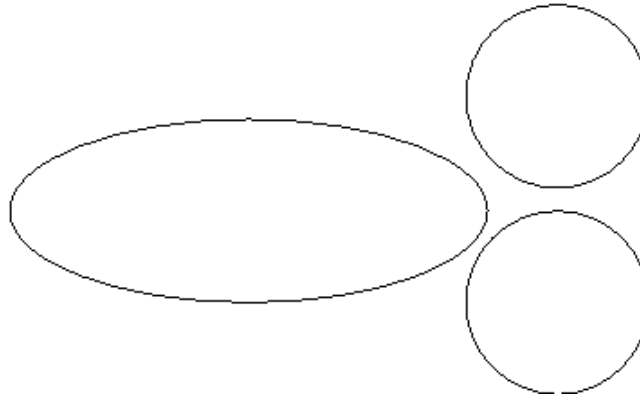


Figure 7.14 Plan View - Arrangement of Laser Beam Spots (Round) Relative to the Arc Weld Pool (Ellipse) Resulting in Insufficient Melting by the Laser and Thus No GMAW-P Toe Wetting and Spreading

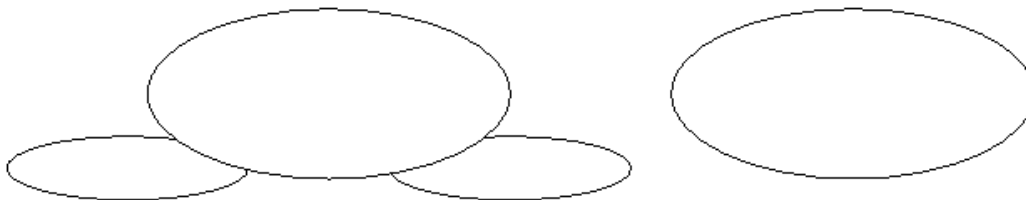


Figure 7.15 Cross-Sectional View - Arrangement of Laser beam Spots (Small Ellipses) Relative to the Arc Weld Pool (Ellipse) at Left, Resulting in Insufficient Melting by the Laser and Thus No GMAW-P Toe Wetting and Spreading, at Right

To achieve the flexibility provided to the CO₂ laser for beam splitting with an adjustable copper mirror, the Nd:YAG laser would require a series of interchangeable fixed optics. The results show that in fact this is not necessary for the best wetting results which are achieved using a single laser spot at the lower weld toe in the fillet weld on a lap-fillet joint. This has the benefit that the laser power, and power density, required to achieve a conduction melt pool can effectively be halved for a single spot operation compared to a dual spot operation mode. Ultimately, this reduction in laser power requirement reduces the cost of the laser needed for the high-speed LBW/GMAW-P operation. This leads to the conclusion that only one LBW spot is necessary, but that this needs to be sufficiently focused to achieve wetting.

There are several statements that can be made based on this research, as follows:

1. The results show that by using laser melting at the weld toes of the GMAW-P bead, the effective minimum size (area) of a weld bead that can be produced without humping can be reduced by a factor of 2 to 3.
2. The results show that by using laser melting at the weld toes of the GMAW-P bead, the effective leg length of a weld bead can be reduced by 35% from 7.5 to 4.8 mm on the lower ligament of the joint, whilst maintaining a typical toe

angle of 110 to 130 degrees compared to 115 to 130 degrees for GMAW-P only. TS was increased from 0.75 m/min with GMAW-P to 4 m/min with hybrid LBW/GMAW-P, an increase of 530%.

3. Maximum speed before the onset of bead humping was increased from 1.15 m/min with ER70S-3 to 2.15 m/min with ER70S-6, to (beyond) 4 m/min with hybrid LBW/GMAW-P, increases of 460 and 185%, respectively, for the hybrid process.
4. The WFS/TS ratios for GMAW-P and LBW/GMAW-P are essentially the same for 0-gap conditions on lap joints. This number is the same across both processes and all three material thicknesses. This finding can therefore be used to size welds for both processes.

7.9.5 Hybrid GMAW-P/LBW with Trumpf HAAS 4006 Nd:YAG Laser

Mechanisms in operation and controlling the tendency or otherwise for bead humping to occur are the arc force, bead size, TS, WFS, laser power, and laser focus spot size, i.e., its power density. HSV has been used to show the interaction of the laser spot and the GMAW weld pool. The laser is set up to lead the weld pool by about 1.5 mm, with a tolerance of ± 0.5 mm. This allows for a stable interaction and focus height between the laser beam and the surface of the steel sheet. It is also routinely observed that if the laser is focused at a point on the GMAW-P weld pool surface that significant spatter is generated resulting in a weld bead size that is too small because of volume loss of weld metal.

Single-spot operation ultimately proved inconsistent. However, a significant result was the achievement of a 14:1 weld length-to-width ratio, Figure 7.16 (beyond the 10:1 maximum ratio predicted for instability by Gratzke et al.), using a 4-kW single-spot Nd:YAG technique. It is considered the extra thermal energy of the laser was sufficient to increase this ratio, delaying the onset of surface tension-driven bead humping.

Using commercially available split optics, operating in the TEM 01 mode, and producing two 0.9-mm-diameter spots at 1.7-mm spacing when at focus, a maximum productivity of 3.3 m/min was reached for a fillet weld on a lap joint between 2.4-mm sheets. The best results were achieved using a 3.2-mm spot spacing. With a 200-mm focal distance, the spot size at the work surface was 1.6 mm.

The power density at the work using two 2-kW beams was:

$$\frac{2000}{(\pi \times r^2)} = 995 \text{ W} / \text{mm}^2 \quad (7.9)$$

for each beam spot.

At 3.3 m/min TS the heat input was 0.3 W/mm²/m, 0.15 W/mm²/m for each beam.

Using a single 3.2-mm-diameter spot with 4 kW of laser power gave a power density of:

$$4000(\pi \times r^2) = 497 \text{ W} / \text{mm}^2 \quad (7.10)$$

This resulted in adequate bead wetting until bead humping was found to occur at 3.3-m/min TS.

At 3.3-m/min TS the heat input was 0.15 W/mm²/m.

Distribution of the energy between each spot was evaluated, and verified using a beam intensity mapping system called PRIMES. Too much power on the lower joint ligament resulted in a tendency for cutting and so a 50:50 power distribution was used.

Nd:YAG laser radiation, with wavelength 1.06 μm, has more energetic photons, and absorption is typically 40% for steel across a wide range of temperature from room temperature up to 2000 K (Steen, 1998). Similar to the case with the CO₂ laser, an arc plasma in contact with the material surface couples the laser beam providing a preferential path for arc rooting of the cathode spot of the welding arc, and higher absorption of the laser energy (Denney, 2004).

The hybrid LBW/GMAW-P results are compared to those achieved with GMAW-P for both lap and T-butt joints in terms of productivity and WFS and TS ratios.

For a 2.5-mm spot size at 3.5-kW laser power, the power density was:

$$\frac{3500}{(\pi \times r^2)} = 713 \text{ W} / \text{mm}^2 \quad (7.11)$$

For a TS of 4 m/min the heat input was 0.18 W/mm²/m.

For a 3.2-mm spot size at 3.5-kW laser power, the power density was:

$$\frac{3500}{(\pi \times r^2)} = 435 \text{ W} / \text{mm}^2 \quad (7.12)$$

For a TS of 4 m/min the heat input was 0.11 W/mm²/m.

Dual-spot laser welding (TEM mode 01), was conducted with laser power of up to 2.5 kW in each spot, but based on the available power, was only able to delay the formation of bead humping to 2.5 m/min for a fillet weld in a lap joint on 2.4-mm sheet.

With a similar 2.5-mm-diameter spot size, the power density was:

$$\frac{3500}{(\pi \times r^2)} = 510 \text{ W / mm}^2 \quad (7.13)$$

For a TS of 2.5 m/min the heat input was 0.20 W/mm²/m.

From these calculations it can be stated that power densities of 435-995 W/mm² were used and that 435 W/mm² was sufficient to achieve melting and hence wetting of the GMAW-P weld toe in the hybrid welding mode.

Similarly, heat input in the range of 0.1 to 0.2 W/mm²/m was sufficient to achieve melting and hence wetting of the GMAW-P weld toe in the hybrid welding mode.

In summary, only one beam spot is required - at the lower weld toe - to result in wetting.

The work angle of the GMAW torch was used to control undercut on the top edge (toe) of the fillet weld in a lap-fillet joint.

There are several statements that can be made based on this research, as follows:

1. Laser power densities of 435-995 W/mm² were used and 435 w/mm² was sufficient to achieve melting and hence wetting of the GMAW-P weld toe in the hybrid welding mode.
2. Laser heat input in the range of 0.1 to 0.2 W/mm²/m was sufficient to achieve melting and hence wetting of the GMAW-P weld toe in the hybrid welding mode.
3. The experiments with the CO₂ laser showed that the best results were achieved using a single-spot LBW/GMAW-P hybrid welding technique and that using 3.5-kW power resulted in suppression of bead humping at 4-m/min TS for lap joints.
4. The maximum TS obtained for robust, repeatable weld quality for Nd:YAG LBW/GMAW-P was 3.3 m/min for a fillet weld on a lap joint using 2.4-mm sheet.

7.9.6 Hybrid CO₂ Laser/GMAW-P Using the Rofin Sinar RS850

CO₂ laser radiation, with wavelength 10.6 μm, is typically absorbed between 10 and 60% dependent of the thickness of the surface oxide, thicker films resulting in higher absorption (Steen, 1998). In the work conducted here the efficiency of the melt mode CO₂ laser was measured at nominally 46%, 18% when taking the 3:1 power ratio of the laser and arc into account, using liquid nitrogen calorimetry. 18% is toward the lower end of this range which is not surprising for a shallow weld pool in the conduction mode. A thicker surface oxide is known to produce better laser energy absorption. This is why welding was conducted with the oxide present on the hot-rolled carbon steel material, and why it was not grit blast prior to welding. An arc plasma in contact with the material surface couples the laser beam providing a

preferential path for arc rooting of the cathode spot of the welding arc, and higher absorption of the laser energy (O'Neill, 1990).

Both the single- and split-beam approaches were intentionally used with the laser somewhat out of focus to increase spot size and allow the melted laser spot to assist in lateral weld bead wetting and spreading to reduce the toe angle and delay bead humping to higher TS. Sufficient power density is required to obtain melting of the base metal by the laser beam. If melting is not achieved, neither is the GMAW-P weld toe wetted and spread laterally by the impingement of the melt zone created by the laser.

7.9.7 Laser Power versus Arc Power

In the work conducted here, laser power, using both Nd:YAG and CO₂ lasers, was typically 3-4 kW, while the power supplied by the GMAW-P system was typically in the range of 10-12 kW. Having a higher arc power is reasonable as most lasers are restricted to 6 kW or less, and the power density of the laser is much higher than that of the welding arc. Ratios of laser power to arc power vary considerably in previous work, depending on material type, joint type, and material thickness. Having similar arc and laser power significantly restricts the maximum productivity obtainable, since it most often results in restricting arc power and deposition rate in GMAW. In most work the laser is in axial alignment with the arc welding system, rather than offset as in the work performed here.

Higher arc power compared to laser power has been reported (Denney et al., 2004) to have a very beneficial effect on arc stability through cathode rooting of the welding arc when conducting Nd:YAG laser/GMAW-P hybrid welding of Ti. In this case the arc power was about 4 kW while the laser power range was 0.2-2 kW. The distinct advantage of a lower laser power is lower capital cost for the laser portion of the welding equipment. More efficient and industrially reliable diode and fibre lasers offer future increases in the overall production reliability of the laser/GMAW-P hybrid welding processes.

7.9.8 Laser Power Distribution

In work involving the wetting of a stationary GMAW weld pool by a laser spot {Cho, 2006}, wetting was found predominantly as a result of a growing GMAW spot size. As the GMAW spot grows the perimeter of the weld impinges on the melted laser spot as it wets in that direction. However, there is not time for this to take place at practical linear welding speeds of interest in the context of high-speed welding. In addition, the wetting in the stationary arc case results in the weld pool wetting in the direction of the laser spot, but this is a case of bridging due to capillary action, and does not result in fusion in terms of the weld cross section or fusion profile between the GMAW spot weld and the laser spot. To achieve fusion in the context of hybrid LBW/GMAW-P, the molten weld pools of the GMAW-P and LBW must impinge on one another, that is to say partially overlap.

The bead wetting action provided by the laser, in the context of a traveling weld pool, is achieved only if the laser melts the base material. Heating alone is insufficient to cause wetting of the GMAW-P bead toe. Melting of the base material alone is

insufficient to cause wetting of the GMAW-P bead if the spacing between the LBW and GMAW-P is more than about 1 mm. The thesis that overlapping the bead toe of the GMAW-P and LBW melted area was proven by experiment. An overlap condition of about 1 mm was shown by experiment to result in bead wetting using a 3 kW laser power and a 3-mm spot size. This also provides sufficient alignment tolerance between a small leg length GMAW-P bead and the melted zone produced by the laser.

If the laser spot is too small, say 1-mm-diameter, alignment becomes more critical, but more importantly, even if alignment is maintained the 1-mm laser spot provides very little opportunity for the GMAW-P bead toe to wet transverse to the welding direction and thus to reduce the weld toe angle, and increase the bead toe wetting angle.

Laser operation was in the conduction mode to produce a relatively large, shallow weld pool. The larger spot size enables the weld toe of the GMAW-P bead to be laterally moved by a larger amount, thus enabling a more significant wetting action to occur. Conduction limiting welding occurs when the power density is insufficient to produce boiling and therefore cannot generate a keyhole at the given TS. The conduction mode LBW weld pool has stirring forces driven by Marangoni forces created by variation in surface tension with respect to temperature, and is thus analogous to an arc weld pool.

As it is a fusion welding process, LBW is subject to similar types of undercut and bead humping in terms of laser power and TS (Albright, 1988). In the work conducted here results were generated using both single laser spot and dual laser spot approaches. The spot size and power density are both important. A larger spot with skin melting is preferred to spread the GMAW-P bead toe and suppress the humping tendency that is increased as the weld toe angle is reduced below 90 degrees.

Keyhole welding would achieve better laser power absorption, but is not practical for sheet metal welds as burnthrough must be avoided, hence, the use of conduction mode welding. For Nd:YAG LBW/GMAW-P a dual spot at focus achieved 3.3-m/min TS with 2- × 2-kW beams while for CO₂ LBW/GMAW-P a single defocused spot achieved 4-m/min TS at 4 kW. The defocused spot approach is favored as it has more tolerance to misalignment between the laser beam and the GMAW-P weld toe as well as achieving a higher TS for the hybrid lap-fillet weld. The laser energy at the GMAW-P weld toe with the 'spreading'/wetting action confirmed the benefits of a single, larger, defocused spot.

7.10 Weld Bead Humping

Gratzke (Gratzke, 1992) indicated instabilities leading to humping at values of 10:1 for the weld length:width ratio. Work here on LBW/GMAW-P hybrid extends this to 12:1, Figure 7.16. This represents a 20% increase in the maximum weld length for LBW/GMAW-P compared to GMAW-P alone. It is likely that the laser imparts increased fluidity/superheat and counteracts the surface tension forces that cause the bead to reduce its wetting angle and result in bead humping. The finding that the laser also stabilizes the repetitive dynamic instability of the GMAW-P metal transfer

at high speed is also considered to be a major factor in the ability to increase the length:width ratio of the weld pool.



Figure 7.16 36-mm-Long Weld Pool with 3-mm Bead Width (12:1) Using Single-Spot 4-kW Nd:YAG/GMAW-P Hybrid on a Lap Joint

The conclusions for prediction of weld pool geometry (Mills et al., 1998) indicated that modeling typically underpredicts the length of the weld pool as conduction models fail to adequately compensate for convective fluid flow in the weld pool. The fact that LBW/GMAW-P can produce a 20% increase in the maximum proposed weld pool length of 10:1 to 12:1 shows that weld pool convection is a significant factor in high-speed welding of sheet material.

7.10.1 Periodicity of Weld Humping in GMAW-P

The frequency or periodicity of bead humping was determined by comparing the humping frequency for a range of WFS/TS ratios.

For T-joints the frequency across a range of WFS/TS averaged 0.6 Hz with a range from 0.45 to 0.78 Hz:

- 0.45 Hz, 14 m/min WFS/ 2.03 m/min TS = 6.9 WFS/TS
- 0.6 Hz, 7.6 m/min WFS / 1.14 m/min TS = 6.7 WFS/TS
- 0.6 Hz, 7.6 m/min WFS / 1.27 m/min TS = 6.0 WFS/TS
- 0.78 Hz, 7.6 m/min WFS / 0.89 m/min TS = 8.6 WFS/TS

For lap-fillet joints the frequency across a range of WFS/TS averaged 0.8 Hz with a range from 0.67 to 1.03 Hz:

- 0.67 Hz, 15.25 m/min WFS / 2.3 m/min TS = 6.7 WFS/TS
- 0.7 Hz, 7.6 m/min WFS / 1.5 m/min TS = 6.0 WFS/TS
- 0.82 Hz, 8.9 m/min WFS / 1.7 m/min TS = 5.2 WFS/TS

- 1.03 Hz, 10.1 m/min WFS/ 2.16 m/min TS = 4.7 WFS/TS

The humping tended to increase in frequency as the WFS/TS ratio increased for fillet welds in T-butt joints. For fillet welds in lap-fillet joints the humping frequency increased as the WFS/TS ratio decreased. The latter result is considered to be the result of more base metal being consumed from the top sheet of the joint. There is not a similar contribution from the base metal in a T-butt joint.

7.10.2 Weld Pool Dynamics and Humping Mechanisms

A significant number of forces are involved in the GMAW-P process, including arc pressure, viscosity and fluid flow, convective heat flow, surface tension, and degree of superheat over the melting temperature. The physical morphology of the weld is additionally affected by welding heat input including welding current, arc voltage, and TS, and their effect on weld pool shape moving from round, to elliptical, to teardrop shaped as welding speed increases. In making practical joints the work angle and travel angle of the welding torch also play a significant role in weld bead shape and the TS at which bead humping occurs.

Work on weld pool dynamics and weld pool fluid flow in the 1980s concentrated mostly on the GTAW process (Kujanpaa, 1983), (Oreper and Szekely, 1984), and (Lin and Eagar, 1985), lower welding currents, and significantly lower TS. Recent work (Mendez and Eager, 2003) dealt with higher current GTAW. However, the GTAW process, without the addition of filler metal, is more amenable to analysis than the considerably more dynamic GMAW process. Theoretical work on GMAW (Ushio and Wu, 1997) and contact tip-to-workpiece effects in GMAW (Kim and Na, 1995) dealt with welding currents up to 250 A. With advances in computational power and weld pool simulation packages such as Flow-3D™ and Fluent™ more recent work (Cao et al., 2004) has dealt with higher welding currents in GMAW that are applicable to the present work and assisted more accurate modeling of the process (Cho, 2007). However, this modeling work has yet to be able to actually predict humping because it is absent the key information determined here, i.e., the event that actually causes the end of one hump and the beginning of the next. This was observed in the current work and is a key piece of information previously lacking in the knowledge base.

The phenomenon of discontinuous bead humping in GMAW was first systematically studied and documented in 1968 (Bradstreet). The literature was reviewed much later (Paskell, 1989), but not much significant work had been done to advance the field. Marangoni convection was proposed as the underlying mechanism (Mills and Keene, 1990) but later work (Gratzke et al., 1992), showed that surface tension and gravity acting in a manner similar to that breaking up a liquid cylinder were important underlying physical mechanisms, and that the length-to-width ratio of the weld pool was more important, the ratio needing to be less than 10:1 for arc welding. This ratio was used in the work reported here by measuring the length-to-width ratio of welds and comparing it to the humping found in practice. In this work it was found that this could be increased 20% to 12:1 using hybrid LBW/GMAW-P.

Results from prior work (Gao and Sonin, 1994) (Schiaffino and Sonin, 1997) showed that the humping instability depends on the conditions at the boundary of the deposit,

i.e., the weld toe region, in the case of a weld bead produced by GMAW. They argued that the driving force involved in bead hump formation is the surface tension of the molten metal surface. As TS is increased, the time required for conduction cooling and solidification of the weld deposit is somewhat decreased, but not in proportion to the TS increase. This leads to a molten weld pool with a relatively large length-to-width ratio, and a fluid geometry that is prone to a dynamic shape instability driven by surface tension. In the case of welding, if the surface tension forces within the weld pool are sufficiently strong, the bead can develop appreciable humps before cooling freezes the deposit geometry.

Based on the HSV results produced in the present work, the humping formation is proposed to result from a momentary, repeated instability in the metal transfer whereby the instability results in metal expulsion. This proposed mechanism is confirmed by examination of still video frames taken at 250 fps. It is proposed that this instability, resulting from an arc short, reduces the arc force momentarily and the weld pool which is being pushed backward by the predominant flow of metal suddenly moves forward and then backward again as the instability ends and the arc force is returned to the former value. This event was seen occurring within two frames of video filmed at 250 fps. This represents a time of $1/125^{\text{th}}$ of a second or 0.008 s. When the welding speed is 4.0 m/min the distance traveled in this time is 0.00053 m, or 0.53 mm. 0.53 mm more typically represents a distance between ripples on the weld bead, but the bead humping events are typically 30-40 mm apart. Thus, while the events captured on HSV did not record the event corresponding to the end of one hump and the beginning of the next in most sequences, the high-speed motion of the weld pool in the fore-aft direction was recorded.

Further examination of two HSV sequences did however show the events between one hump and the next, particularly the sequence for weld 082405-4 for a BOP weld Figure 6.91 (on page 176). In this HSV sequence, the formation of humps was shown to be associated with the repeating arc short circuit event. This was seen in another HSV sequence 083005-1, Figure 6.101 (on page 183-4). for a hybrid LBW/GMAW-P lap fillet weld is thus confirmed as occurring based on the results of experiments conducted. The establishment of this mechanism has not been determined before.

The conclusions of Choi (Choi, 2006) were that capillary instability was not the only factor in weld bead humping, and suggested weld pool fluid flow was also important. The work conducted here has gone beyond these conclusions using HSV to observe weld pool fluid flow and also to determine the mechanism of a repeating arc instability that is associated with the end of one hump and the beginning of the next.

7.11 HSV Images of Bead Humping

HSV of metal transfer and weld pool behaviour has shown weld metal flow patterns and a dynamic instability considered to be associated with the formation of bead humping. In many of the video images the simultaneous view of the weld pool, the bottom of the arc melted groove, and the arc itself is not captured. In video stills and AVI files for video sequences, simultaneous viewing of all three is required to definitively see the event that results in the end of one hump and the beginning of another.

The side view, Figure 7.17, shows a large loss of weld metal from the cavity produced by the arc melting and also highlights the significant solidification shrinkage evident in the humps.



Figure 7.17 Side View of GMAW-P BOP Humping for 2.4-mm Sheet Specimen 72805

Figure 7.17 show the deep gouge resulting from arc melting in plate material. This is characterized by the solidification of the bead humps, and that the valleys between them which are below the surface plane of the plate material. This is characteristic of bead humping in plate material where there is little material between the humps.

The noticeably more wavelike humping profile typical of the humping morphology seen with welding on thinner sheet, is shown in Figure 7.18. In this case the weld metal is constrained in the horizontal axis and humping does not result in weld pool depression below the sheet surface.



Figure 7.18 Side View of GMAW-P BOP Humping in 1.6-mm Sheet Metal for Specimen 80205b

Information and data concerning humping morphology has been gathered used to delay the humping phenomenon in GMAW and largely avoid it in LBW/GMAW, or at least suppress it to TS in the range of 3-4 m/min, the maximum travel speed available being 4 m/min. Weld bead humping develops as the welding speed increases because the pool length becomes excessively long. The weld pool length was found to exceed the 10:1 ratio for GMAW found by Gratzke (Gratzke, 1992), showing that the wetting caused by the use of laser spots near the GMAW-P weld pool can increase wetting further, and thus increase the travel speed at which humping begins.

Metal movement is from under the arc toward the back of the weld pool. HSV of the GMAW-P and 'Dip pulse' GMAW-P transfer modes shows that the weld pool has an oscillation from front to back while it is molten (ESAB ref). Work here has shown a humping periodicity of 0.45 to 1.0 Hz between BOP, fillet welds in lap joints, and fillet welds in T-butt joints.

When the weld metal freezes the last metal to solidify is in the peak of the hump, indicated by a dimpled appearance at the peak of the hump in the as welded condition. The addition of the laser energy at the bead toe changes the temperature in the toe region affecting the surface tension and solidification time at the toe, allowing it to wet out and produce a higher toe angle compared to the case with the GMAW-P bead alone.

A key finding, confirmed in several trials and reported in the results in this thesis, is that a dynamic instability occurs in the metal transfer. The instability generates significant spatter, and the loss of this material from the weld pool precipitates the fore-aft motion of the weld pool. The end of one hump and initiation of a new one

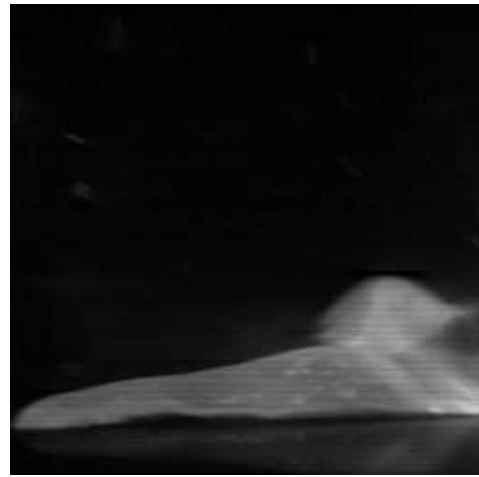
when the liquid bridge between two humps solidifies was not captured directly by HSV. However, this fast motion forward then backward is considered likely to trap the previously deposited metal in the prior hump, and then lead to the formation of another hump.

The weld pool moves forward and then backward again within 2 frames (Images 309, 31, and 310) at 250 fps, Figure 7.19. The timeframe for this is 0.008 seconds and cannot be discerned by the human eye. It is considered that this motion is the cause of the end of one hump and the beginning of the next, with the solidification of the previously molten bridge occurring at this time. As the field of view is 27 mm this means the weld pool moves forward 15 mm and then back 15 mm in 0.008 s, or at a speed of 3.75 m/s.

Within 10 images at 250 fps the cycle repeats whereby the weld pool moves forward again, as shown in the following three HSV images. This represents a timeframe of repetition of 0.004 s. This timeframe is very short and this motion could not be detected by the unaided human eye. Neither was this detected in the LaserStrobe work conducted by Nguyen (Nguyen et al., 2005). This motion is considered to be an important event associated with understanding of the formation and repetitive nature of the humping defect.



(a) Image 309 in 082405-8 HSV file



(b) Image 31 in 082405-8 HSV file



(c) Image 310 in 082405-8 HSV file



(d) Image 315 in 082405-8 HSV file



(e) Image 32 in 082405-8 HSV file

Figure 7.19 Repetitive Forward and Backward Motion of the GMAW-P Weld Pool Within 2 frames (Images 309, 31, and 310) at 250 fps

The rapid motion of the weld pool forward, when the instability occurs, and then backward as the dynamic equilibrium is met again, is the result of the cycle of events occurring at high speed in the weld pool. The images above show this event to occur very rapidly, and when weld metal is lost from the weld pool as a consequence of the dynamic instability where spatter is ejected from the weld pool along with a short section of weld wire.

The following sequence of HSV (82405-5), Figure 7.20, shows a side view of the weld pool along with the front of the welding torch, including the contact tip and electrode extension. The welding arc can also be seen in these images. The weld pool can be seen moving forward and then back within two images in the following three images.



(a) Image 1_489



(b) Image 1_490



Image1_491

Figure 7.20 HSV Still Sequence Showing Weld Wire Expulsion and Weld Pool Motion

This sequence repeats every 10 images, as shown in the succeeding two images 10 frames apart from each other and 10 and 20 frames, respectively, from the first such image, Figures 7.21 and 7.22. It is apparent from the similarity of the images that

there is a repeating instability occurring on a regular basis that also seems to correlate with the ripples formed on the surface of each hump, and the formation of another, Figures 6.75 (page 164).

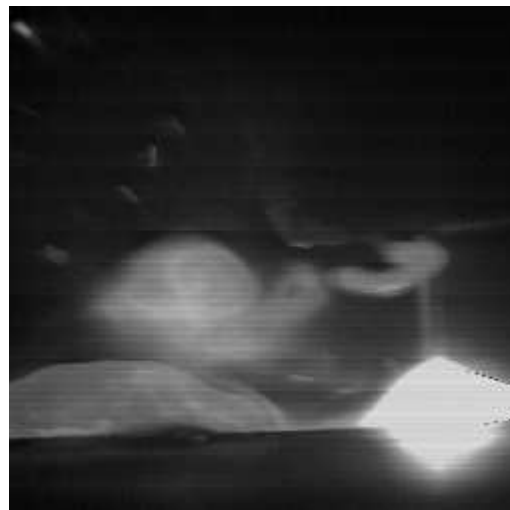


Image 1_500

Figure 7.21 HSV Still Showing Weld Wire Expulsion and Weld Pool Motion



Image 1_510

Figure 7.22 HSV Still Showing Weld Wire Expulsion and Weld Pool Motion

The loss of this volume of metal, clearly shown in Figures 7.20, 7.21, and 7.22, results in the rearward force applied to the molten weld pool being temporarily reduced, allowing the weld pool to move forward. When the arc recovers from the momentary instability the arc force is again applied to the molten weld metal and pushes the weld metal rearward again, Figures 7.19 (a) through (e).

The majority of HSV images captured the weld pool motion in a repeating forward and rearward motion, but have been shown as associated with a repetition frequency associated with weld ripple profile at a spacing of about 0.5 mm. They did not

capture the events at the end of one hump and the beginning of next, based on the weld wire often not being in the field of view, and/or the arc gouge groove depth relative to the camera viewing angle. The following images for a BOP weld, Figure 7.23, and a lap weld, Figure 7.24, show the weld wire in the field of view and the bottom of the arc gouge is sufficiently aligned with the HSV camera since the weld pool is shallow. These images (backed up by jpg and avi files supplied on CD with the written document) show the moment of arc short circuit in each case. At 70 frames in 250 fps, and with a TS of 3 m/min (50 mm/sec), the distance travelled in $(70/250 = 0.28)$ 0.28 s, is 14 mm. This corresponds closely to the repeat sequence of humps in Figure 6.90, on page 164, for weld 082405-4.



(a) Image I- 200



(b) Image I- 270

Figure 7.23 HSV Showing Short Circuiting of the Wire to the Weld Pool in BOP Specimen 082405-4



(c) Image I-346

Figure 7.23 (cont.) HSV Showing Short Circuiting of the Wire to the Weld Pool in BOP Specimen 082405-4

These images (backed up by jpg and avi files supplied on CD with the written document) show the moment of arc short circuit in each case. At about 50 frames in 250 fps, and with a TS of 3 m/min (50 mm/s), the distance travelled in $(50/250 = 0.20)$ 0.20 s, is 10 mm. This corresponds closely to the repeat sequence of humps in Figure 6.100 (on page 180), for weld 083005-1.



(a) Image I-483



(b) Image I-516

Figure 7.24 HSV Showing Short Circuiting of the Wire to the Weld Pool and Arc Re-Ignition in Lap Fillet Specimen 083005-1

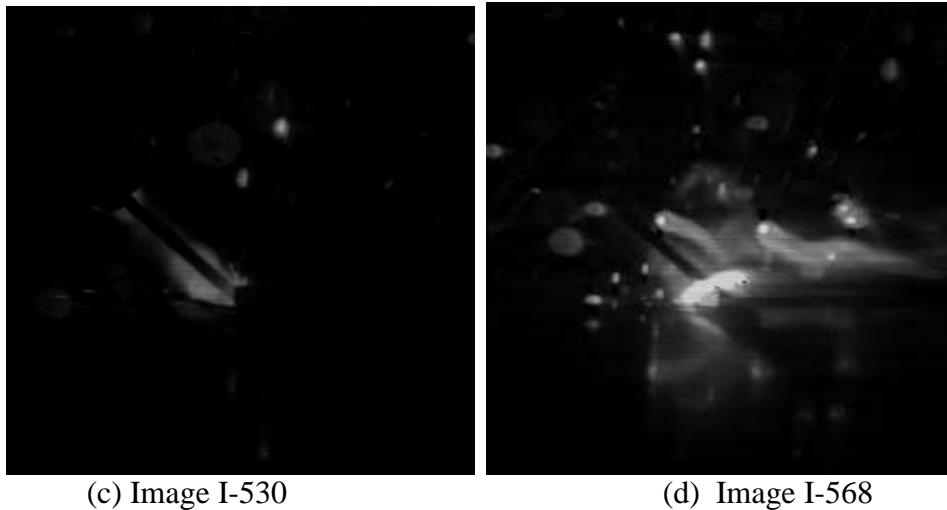


Figure 7.24 (cont.) HSV Showing Short Circuiting of the Wire to the Weld Pool and Arc Re-Ignition in Lap Fillet Specimen 083005-1

From these results it is clear that there are a subset of humping morphologies within the general humping defect classification. While the humping defect has been known for years, this work is considered to have found a fundamental event that occurs that can be considered as associated with the formation of the humping defect. While visual examination of the humped weld bead shows a thin ligament of weld metal between two humps and it has been proposed before (Nguyen et al., 2005) that the prior solidification of this ligament separates each hump from the next, the event that precipitates this has not been previously observed and reported.

When adding a small amount of laser energy to a GMA weld pool it has been shown (Shinn et al., 2004) that the laser spot on the weld pool surface stabilizes the arc cathode spot for low-power arcs at low TS. The work reported here shows that this does not occur for high power arcs at high travel speed. However, reduction or suppression of the humping event can be achieved at high travel speeds, up to 4 m/min for small fillet welds in steel sheet metal by increasing the wetting at the weld toes, particularly using lasers. This has been shown whether using 1 kW at 2 m/min, Figure 7.25, or higher laser energy in one or two spots. The best results were achieved using a single laser spot.



Figure 7.25 Classic Bead Humping (Top Bead) for GMAW-P Suppressed with 1-kW Nd:YAG Laser Energy (Middle and Bottom) (WFS/TS of 5 - BOP Weld) at 2.0-m/min TS

Thus, it appears that the addition of laser energy and the increased wetting of the toe of the GMAW-P weld bead is the main reason why the humping defect is suppressed with the right combination of welding parameters. Continuous weld beads were produced with only 1 kW of laser power when the welding speed was only 2.0 m/min. Higher laser power is required at higher TS since the heat input and power density to maintain a conduction melt pool needs to be maintained for suppression of humping to continue at TS up to 3.3 for 2.4-mm sheet, or even 4.0-m/min for 2-mm sheet.

In terms of the new information generated in this work it has been set against the context of conventional industrial practice with GMAW using an ER70S-3 electrode and accounting for commonly encountered gap ranges from 0T to 1T.

Using a 0T gap approach, a leading torch angle and an ER70S-6 wire represents the state of the art within the bounds of a high-speed single-torch GMAW-P approach. Against this are set hybrid LBW/GMAW-P trials which represent new knowledge when comparing single and dual-beam laser spots for weld toe wetting and bead humping suppression at high welding speeds in the range of 2-4 m/min.

7.12 Impact of Results and Process Economics

General industry is ostensibly light manufacturing. Combining automotive, automotive suppliers, and general industry accounts for a total of 60% of consumable usage, Figure 7.23. Thus, the impact of increasing TS and productivity for GMAW would affect at least half of the applications where solid-wire GMAW is used throughout the world.

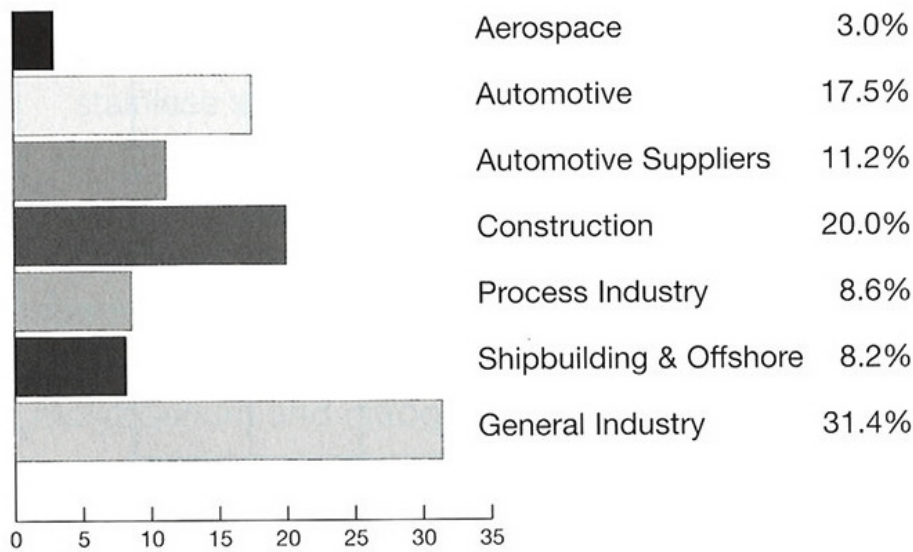


Figure 7.26 Distribution of Welding Consumable Use by Industry (Pekkari, 2004)

All processes should be considered, especially single- and multiple-torch GMAW (tandem) versus laser and laser/GMAW hybrid. For single-pass welding – welding productivity, i.e., TS is key to production rate. As such, the results developed in this thesis research can have a significant impact in the understanding of high-speed welding both for GMAW and hybrid LBW/GMAW.

The baseline is 0.76 m/min for GMAW in terms of productivity and cost. The work conducted in this thesis research has shown that this can be increased to 2.0 m/min for single-torch GMAW-P as long as appropriate attention is paid to part accuracy in first operations and proper fit-up for welding. High-speed welding of thinner materials will have a very significant cost impact, if implemented. Costs for hard automation or for a 6-axis robotic cell should be considered, rather than the cost of GMAW-P equipment versus that for lasers.

TGMAW, with systems available from Fronius, Cloos, and Lincoln Electric has significant cost advantage compared to laser systems when considering system cost versus TS capability. The lower thickness limit suggested by Fronius is 1.6 mm. As strength to weight issues continue to drive materials type and thickness selection to higher strength and lighter weight, the use of hybrid welding systems will become increasingly attractive for materials thinner than 2.0 mm.

Considering the case for a 3-kW CO₂ laser versus a 3-kW fiber laser, the lower running cost, compact laser and much reduced cooling requirements for the fibre laser are very attractive. Robotic versus hard automation – flexible manufacturing cells – Nd:YAG is easily deliverable over long distance to flexible robotic or other automation cells, as are fibre lasers, while the CO₂ laser is much less flexible based on its mirror and waveguide beam delivery limitations.

The smaller footprint of the laser and chiller, and the portability for pipeline root welding, or other field applications along with high reliability and the same fiber delivery (based on 1.06- or 1.07- μm wavelength), generate similar results for a fibre laser compared to a Nd:YAG for the same kilowatt laser. The advantage of the fibre laser is that it is already available in 10-kW units, while the Nd:YAG laser is limited to 4 kW in most cases.

When considering the benefits of hybrid LBW/GMAW-P compared to those of GMAW-P, commercial heads are available from Fronius, HighYag and Cloos for hybrid welding.

A cost justification has been made and applications developed in Germany at Meyer Werft and VAG (Graf and Staufer, 2002). Potential for automotive and light manufacturing, i.e., frame rails for trucks made with C-channels rather than hydroforming are anticipated in the future. In shipbuilding, thinner higher strength steels are being used for welding stiffeners to panels, making fillet welds with better toe angles, and better fatigue performance can be developed. With sufficient access, hybrid laser welding can make full-penetration T-butt welds in a single pass compared to two-sided fillet welds used in present construction practice.

The case for Hybrid has not yet been made in the U.S. with shorter ROI requirements than in Europe. Volkswagen has invested in over 300 robotic LBW/GMAW-P systems for fabricating Al sheet products for vehicles. In Europe ROI is often premised on a one year timeframe, while in the U.S. this is more often only 6 months.

Combining CO₂ lasers and diode-pumped Nd:YAG lasers with GMAW-P in hybrid LBW/GMAW-P can clearly be seen as an energy efficient method of welding for manufacturing in the future, Figure 7.27.

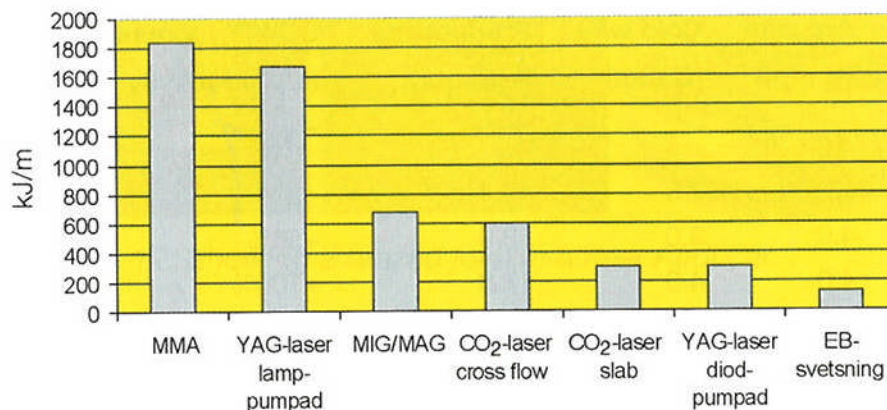


Figure 7.27 Energy Usage and Efficiency for an Array of Commonly Used Welding Processes (Pekkari, 2004)

In terms of flexibility for automation, comparing Nd:YAG and CO₂, the Nd:YAG is clearly more flexible as it can be delivered by fiber-optic to the robotic welding system. The CO₂ system requires a cumbersome mirror beam guide. Application possibilities exist with CO₂ lasers for fixed automation and/or straight seams versus

complex parts. Use of coordinated motion positioners to manipulate parts or assemblies rather than laser manipulation is also possible.

An even better case can be made for fibre lasers in the future, including operating cost, Figure 7.28. They are 25% electrically efficient compared to only 3% for Nd:YAG lasers, Only 10% of floor space cost compared to comparable power for Nd:YAG: next 'wave of the future' They are also deliverable by fibre-optic as with Nd:YAG, so offer retrofitting possibilities. High-power fiber lasers have only been available for about 6 years in the commercial marketplace. They have high initial capital cost, are highly expandable (additional diode banks), and 'low' running cost based on diode life.

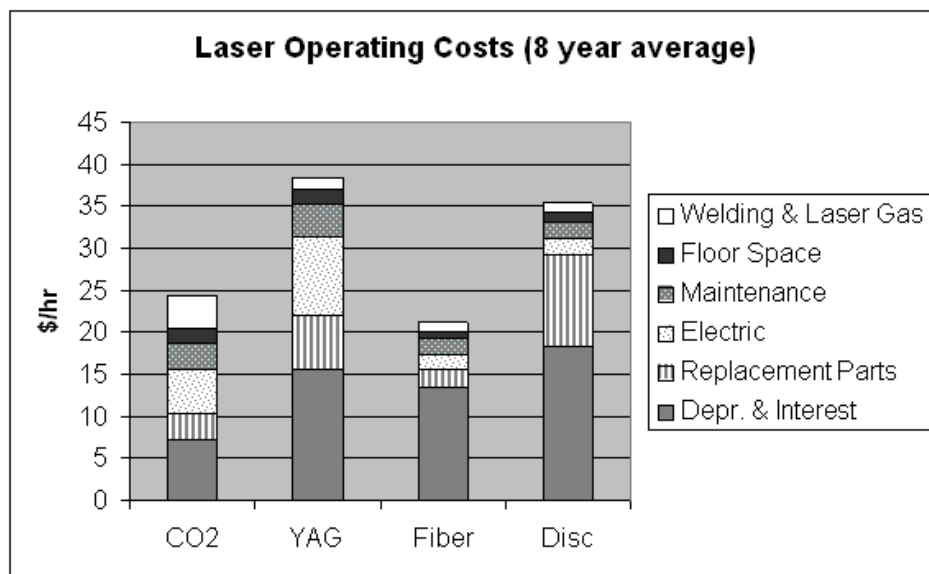


Figure 7.28 Laser Operating Cost Summary (Ream, 2004)

The data developed here can provide a foundation for future studies that evaluate different joint designs, materials, and processes. The results derived provide data for accurate benchmarking and robustness assessment. The deployment of this technology should enable the optimization of weld size and minimize production costs of sheet metal structures, including automotive truck frames, and similar products.

8.0 CONCLUSIONS

The initial hypothesis was that the humping defect can be suppressed and continuous beads deposited at much higher speeds by applying a laser beam in the conduction mode at the weld toes to improve bead wetting thus minimizing bead convexity which, at toe angles below 90 degrees tends to promote the formation of the humping defect. This was investigated by a research program intended to develop an understanding of the cause of the humping defect, including HSV to determine the root cause, from which the mechanisms were determined.

The hypothesis that weld pool humping can be suppressed to TS well beyond that achievable with either GMAW or LBW alone by directing the laser at the weld toes was demonstrated in the results achieved and their comparison to data generated for single wire GMAW-P. For the three main types of welding technique investigated, the following maximum TS can be stated:

1. Conventional GMAW-P – typical maximum TS of 1 m/min
2. High-speed GMAW-P – typical maximum TS of 2 m/min
3. Hybrid conduction mode laser with GMAW-P – typical maximum TS of 3.3 m/min

As 60% of industrial use of consumables is in industries using sheet metals predominantly, and as 80% of these are single pass fillet welds, the results achieved here have the possibility of very wide ranging application.

The main conclusions are as follows:

1. Laser assisted GMAW-P allows increases in TS before humping. The hypothesis that weld bead humping can be suppressed by using laser melting at the GMAW-P weld toes was shown by experiment to be valid.
2. HSV of GMAW-P showed a repetitive arc instability that caused the weld pool to move first forward and then backward at the moment of the instability. It also showed arc shorting leading to the end of one hump and the beginning of the next.
3. A 30-degree lead travel angle for the GMAW welding torch achieved a maximum welding speed in GMAW-P and LBW/GMAW-P welding and was beneficial in suppressing humping.
4. A work angle of 60 degrees, wire on the top edge of the top sheet, and aiming the laser at the bottom toe of the GMAW-P weld is the best configuration.
5. Aiming the wire at the top edge of the top sheet delayed the onset of bead humping to higher TS than aiming at the root.
6. Long weld pools (12:1) and no humping were achieved with a single 4 kW laser spot. Only one beam spot is required – aimed at the lower weld toe - to result in wetting.

7. The value of the overwelding 'b' factor was determined to be 1.4. This is a constant value for lap-fillet welds in sheet thicknesses – and applies for sheet from 1.6- to 2.4-mm thicknesses. Knowing the value for b, the required weld area can be calculated, and from this the correct combination of WFS and TS can be determined for GMAW-P.

9.0 FUTURE WORK

Three areas are noted below for future work based on the results and conclusions of the present work. It is recommended that fibre lasers are used for this work.

9.1 High-Speed Single-Pass Hybrid Welding

Larger diameter wires will be required for achieving the required weld sizes at TS of 4 m/min and greater. Future work is needed to evaluate 1.4- and 1.6-mm-diameter ER70S-6 wires for fibre laser/GMAW-P. Based on results achieved for 2 and 4 m/min TS, the following extrapolation of TS and WFS (based on 1.2-mm diameter wire) are made, for higher productivity, Figure 9.1. Use of 10 kW Fibre lasers and TGMAW is anticipated.

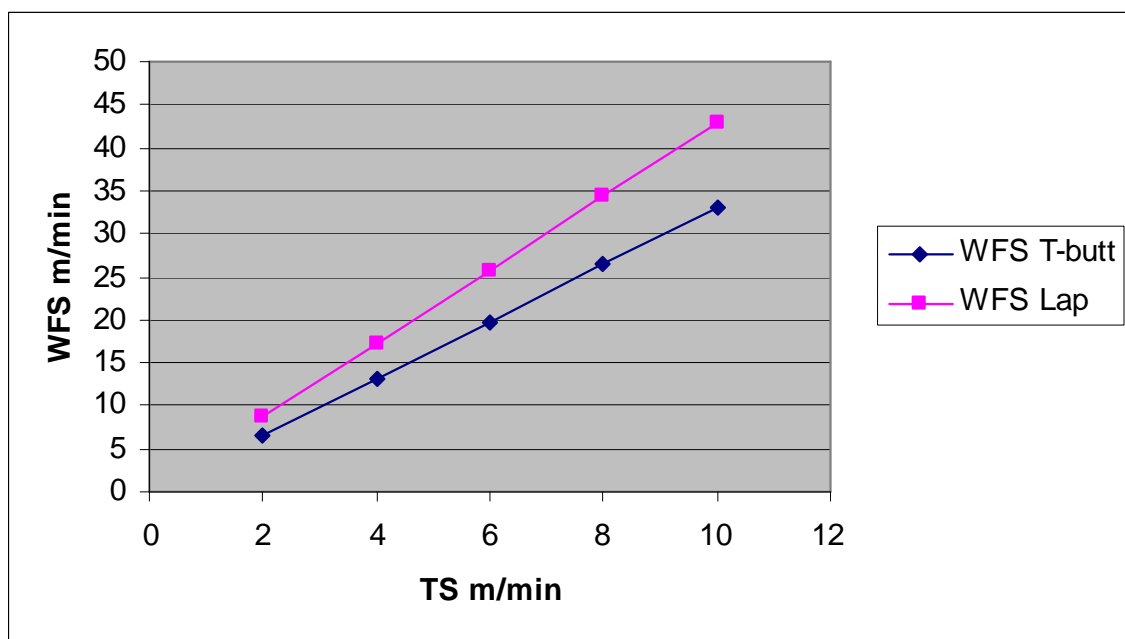


Figure 9.1 Extrapolation of TS and WFS for Higher Productivity Using Hybrid LBW/TGMAW-P

9.2 Multi-Pass Hybrid Welding

The use of split-beam laser hybrid GMAW-P for multi-pass welds in narrow-gap (NG) joints was demonstrated and improved weld toe wetting, improving bead tie-in at sidewalls. Further investigation of this technique is recommended for future work.

9.3 Modeling

More work should be conducted to incorporate the repeating arc instability that causes the humping in GMAW into the models developed using Fluent™, Flow-3D™, and Truchas (Nat Lab) software packages.

10.0 REFERENCES

- Abe, N., Kunugita, Y., Hayashi, M., Tsuchitani, Y., Mihara, T., and Miyake, S. 1998. Combination mechanism of high speed leading path laser-arc combination welding. *Trans. JWRI*, Vol. 27, No.2, pp. 7-11.
- Abe, N., Kunugita, Y., Hayashi, M., Tsuchitani, Y. 1998. Welding mechanism of laser-arc combination high speed welding. *Trans. JWRI*, Vol. 27, No.1, pp. 109-110.
- Abe, N., Higashino, R., Nakagawa, N., Tsukamoto, M., Noguchi, S, and Miyake, S. 2000. High speed welding of thin steel plates with high power and high power density diode laser system. *Trans. JWRI*, Vol. 29, No. 1.
- Abe, N., Higashino, R., Tsukamoto, M., Noguchi, S, and Miyake, S. 1999. Materials processing characteristics of a 2 kW class high power density direct diode laser system. *Trans. JWRI*, Vol. 28, No. 2.
- Aden, M. Kreutz, E.W., and Hausen, O. 1998. Influence of the laser radiation on the plasma dynamics during arc-laser welding. *Proc. 17th Intl. Congress on Applications of Lasers and Electro-Optics (ICALEO)*, pp. 139-148.
- Albright, C.E. and Chiang, S. High speed laser welding discontinuities. *Proc. 7th Int. Conf. on Applications of Lasers and Electro Optics*, ICALEO 88, pp 207-213, Oct./Nov. 1988.
- Anon. TRUCHAS Physics and Algorithms. Los Alamos National Lab, Telluride Project, Oct. 2004.
- AWS Welding Handbook*, Eighth Edition, Vol. 2, Welding Processes, American Welding Society, Miami, FL, 955 pp, 1991.
- AWS Welding Handbook*, Ninth Edition, Vol. 1, Welding Science and Technology, American Welding Society, Miami, FL, 918 pp, 2001.
- AWS/SAE Joint Committee on Automotive Welding. Specification for automotive and light truck components weld quality – arc welding. AWS/ANSI D8.8-97. American Welding Society, Miami, FL, 1997.
- AWS Sheet metal welding code. ANSI/AWS D9.1:2000. American Welding Society, Miami, FL, 2000.
- AWS Structural Welding Committee. Structural welding code – sheet steel. ANSI/AWS D1.3-98. American Welding Society, Miami, FL, 1998.
- Bagger, C. and Olsen, F.O. Review of laser hybrid welding. *Journal of Laser Applications*, Vol. 17, No. 1, pp. 2-14, Feb. 2005.
- Biffin, J. Plasma augmented lasers shine ahead in auto body application. *Welding and Metal Fabrication*, pp. 19-21, Apr. 1997.

- Blundell, N., Biffin, J., Johnson, T., and Page, C. High speed augmented laser welding of thin sheet metals.
- Bonss, S., Seifert, M., Barthel, K., Brenner, B., and Beyer, E. New developments in high power diode laser welding.
- Boring, M.A., and Harris, I.D. Weld sizing and gap weldability for arc welding production robustness in sheet metal. EWI Members Report MR015X, Dec. 2004.
- Bradstreet, B.J. Effect of surface tension and metal flow on weld bead formation. *AWS Welding Journal*, pp. 314s-322s, July 1968.
- Bratt, C. and Noel, J. 2004. Laser hybrid welding of advanced high strength steels for potential automotive applications. *Proc. 23rd Int. Congress on Applications of Lasers and Electro-Optics (ICALEO)*.
- Cao, Z., Yang, Z., and Chen, X.L. Three-dimensional simulation of transient GMA weld pool with free surface. *AWS Welding Journal*, pp. 169s-176s, June 2004
- Cho, Y. and Na, S-J. 2003. Temperature measurement of laser arc hybrid welding plasma. *Proc. 22nd Int. Congress on Applications of Lasers and Electro-Optics (ICALEO)*.
- Cho, M.H., Lim, Y.C., and Farson, D.F. Simulation of weld pool dynamics in the stationary pulsed gas metal arc welding process and final weld shape. *AWS Welding Journal*, pp. 271-s to 283-s, Dec. 2006.
- Cho, M.H. and Farson, D.F. Simulation study of a hybrid process for the prevention of weld bead hump formation. *Welding Journal*, Vol. 86, No. 9.. pp. 253s-262s. Sept. 2007.
- Choi, H.W., Farson, D.F., and Cho, M.H. Using a hybrid laser plus GMAW [MIG/MAG welding] process for controlling the bead humping defect. *Welding Journal*, Vol. 85, No. 8.. pp. 174s-179s, Aug. 2006.
- Choo, R.T.C., Szekely, J., and Westhoff, R.C. Modeling of high-current arcs with emphasis on free surface phenomena in the weld pool. *AWS Welding Journal*, pp. 346s-361s, Sept. 1990.
- Denney, P.E., Shinn, B.W., and Fallara, P.M., 2004. Stabilization of pulsed GMAW in titanium welds with low power lasers. *Proc. 23rd Int. Congress on Applications of Lasers and Electro-Optics (ICALEO)*.
- Dilthey, U. Increased productivity by GMA tandem welding and brazing and by laser GMA hybrid welding. *Proc. Conf. Gas Metal arc Welding for the 21st Century*, Orlando, FL, pp. 133-143, Dec. 6-8, 2000.
- Dilthey, U., Leuder, F., and Wieschemann, A. 1998. Technical and economic advantages by synergies in laser hybrid welding. *Welding in the World*, pp. 141-152.

- Dilthey, U. and Wieschemann, A. 2002. Perspectives offered by combining a laser beam with arc welding procedures. *Welding International*, Vol. 16, No. 9, pp. 711-719.
- Doherty, J. and Holder, S.J. Adaptive control of MIG welding of thin sheet steel. *Developments and Innovations for Improved Welding Production, 1st International Conference*. Paper 45. Birmingham, U.K., pp. 45.1-45.14, Sept. 13-15, 1983: .
- Downs, D. and Mulligan, S. Hybrid CO₂ laser MAG welding of carbon steel – a literature review and initial study. TWI Members Report 739/2002, TWI, U.K., Mar. 2002.
- Dupont, J.N. and Marder, A.R. Thermal efficiency of arc welding processes. *AWS Welding Journal*, pp. 406s-416s, Dec. 1985.
- Eboo, M., Steen, W.M., and Clarke, J. 1978. Arc augmented laser welding. *4th Int. Conf. On Advances in Welding Processes*, Harrogate, U.K., Paper 17, pp. 257-265.
- El Rayes, M., Walz, C., and Sepold, G. The influence of various hybrid welding parameters on bead geometry. *AWS Welding Journal*, pp. 147s-153-s, May 2004.
- Fabbro, R., Coste, F., Goebels, D., and Kielwasser, M. 2004. *Study of Nd:YAG laser welding of Zn-coated steel thin sheets. Proc. 23rd Int. Congress on Applications of Lasers and Electro-Optics (ICALEO)*.
- Farson, D.F. Hybrid laser GMAW process for fatigue-resistant welding. EWI Members Report MR015X, June 2004.
- Fellman, A., Salminen, A., and Kujanpaa, V. 2004. The comparison of the effects of welding parameters on weld quality and hardness of t-butt joints welded with CO₂ laser, ND:YAG laser and CO₂ laser-GMA hybrid welding. *Proc. 23rd Int. Congress on Applications of Lasers and Electro-Optics (ICALEO)*.
- Fronius data tables of recommended parameters including travel speed for single torch GMAW, tandem GMAW and LBW/GMAW for steel lap-fillet welding. Received as a result of private discussions, 2005.
- Gao, F., and Sonin, A.A. Precise deposition on molten microdroplets; the physics of digital microfabrication. *Proc. Mathematical and Physical Sciences*, Vol. 444, No. 1922, pp. 533-554, Mar. 1994.
- Goebels, D., Kielwasser, M., and Fabbro, R. 2003. Improvement of laser welding of Zn-coated steel and aluminum alloy thin sheets using shaped laser intensity distribution. *Proc. 22nd Int. Congress on Applications of Lasers and Electro-Optics (ICALEO)*.
- Graf, T. and Staufer, H. 2002. Laser hybrid welding at Volkswagen. IIW Doc. XI-1730-02.

- Gratzke, U., Kapadia, P.D., and Dowden, J. 1991. Heat conduction in high-speed laser welding. *Journal. of Inst. of Physics*, pp. 2125-2134.
- Gratzke, U., Kapadia, P.D., Dowden, J., Kroos, J., and Simon, G. 1992. Theoretical approach to the humping phenomenon in welding processes. *J. Phys. D: Appl. Phys.*, Vol. 25, pp. 1640-1647.
- Green, B. I. et al. 2001. A systematic method for sheet metal parameter development using sloping weld area testing. EWI Report No. 42634. EWI, Columbus, OH.
- Hackl, H. 1998. MIG-brazing of galvanized thin sheets. *Schweissen und Schneiden*, Vol. 50, No. 6, pp. E102-104.
- Harris, I.D. Evaluation of STT for nickel alloys in FGD scrubbers. EWI Report 42168CSP for The Lincoln Electric Company, Oct. 1998.
- Harris, I.D. Application of synergic MIG/GMA welding – phase IV – power source characteristics. TWI GSP Report, Apr. 1987. (Out of embargo).
- Harris, I.D., Denney, P., Farson, D., Cho, M.H., Choi, H.W., and Yong, C.L. Scanning hybrid laser-GMAW welding for sheet metal and fill passes on plate. EWI Members Report MR0151, July 2005.
- Harris, I.D. Welding procedure development for a stainless steel gas tank welding. EWI Report 45010CSP for Pilot Industries, July 2002.
- Harris, I.D., and Norfolk, M. I., Development of Hybrid Laser arc Welding for Pipeline Construction, Proceedings of the 7th international Pipeline Conference, IPC 2008, Paper IPC2008-64129.
- Harwig, D. D., A wise method for assessing arc welding performance and quality *Welding Journal*, Vol. 79, No. 12, pp. 35-39, 2000.
- Harwig, D. D. Arc behaviour and metal transfer in the VP-GMAW process. Ph.D. Dissertation, Cranfield University, SIMS, Cranfield, U.K., 2003
- Harwig, D. D. et al. Characteristics of variable polarity (AC) GMAW power supplies. ICAWT 2000, Orlando, FL, Dec. 6-8, 2000.
- Hedegard, J., Andersson, J., Tolf, E., Weman, K., and Lundin, M., 2004. Enhanced prospects for tandem-MIG/MAG Welding. IIW Doc. XI-1808-04.
- Heiple C.R. and Roper, J.R. Mechanism for minor element effect on GTA fusion zone geometry. *AWS Welding Journal*, pp. 97-2 to 102-s, Apr. 1982.
- Herbert, S. Laser-hybrid welding of ships. *AWS Welding Journal*, pp. 39-43, June 2004.
- Howse, D.S. MAG weld procedure development for galvaneal coated high strength steel sheet. TWI Members Report 697/2000, Mar. 2000.

- Hu, B., and den Ouden, G. 2003. Welding efficiency of laser-assisted arc welding. IIW Doc. 212-1036-03.
- Hu, B. and Richardson, I.M. 2003. Absorption of laser energy by a welding arc. *Proc. 22nd Int. Congress on Applications of Lasers and Electro-Optics (ICALEO)*.
- Ishide, T., Tsubota, S. Watanabe, M., and Ueshiro, K. 2003. Development of TIG-YAG and MIG-YAG hybrid welding. *Welding International*, Vol. 17, No. 10, pp. 175-780.
- Jelager, T. et al. Determination of welding parameters for filling of gaps in fillet welds. *International Journal of Joining Materials*, Vol. 6, No. 1, pp. 34-38, Mar. 1994.
- Johnson, T.A., Biffin, J., and Bacon, M.C. Laser/plasma technique welds sheet metal. *Industrial Laser Review*, pp. 21-24, Nov.1995.
- .Joseph, A. Harwig, D.D., Dierkscheide, J., and Richardson, R. Capability of variable polarity GMAW for automotive applications. *AWS Sheet Metal Welding Conference X*, Sterling Heights, MI, May 15-17, 2002.
- Joseph, A. Harwig, D., Farson, D.F., and Richardson, R. 2003. Measurement and calculation of arc power and heat transfer efficiency in pulsed gas metal arc welding. *Science and Technology of Welding and Joining*, Vol. 8, No. 6, pp. 400-406.
- Joseph, A., Webb, C., Haramia, M., and Yapp, D. Variable polarity improves weld brazing of galvanized sheet. *AWS Welding Journal*, pp. 36-40, Oct. 2001.
- Kenney, K.L., Miller, K.S., and Smartt, H.B. Heat transfer in pulsed gas metal arc welding. *Proc. 5th Int. Conf 'Trends in Welding Research*, Pine Mountain, GA, pp. 357-361, June 1-5, 1998.
- Ketron, D.L. Assessment and development of twin wire GMAW. *EWI CRP Progress Report PR0006*, May 2000.
- Kim, J.W. and Na, S-J. 1995. A study on the effect of contact tube to workpiece distance on weld pool shape in gas metal arc welding. *AWS Welding Journal*, pp. 141s-151s.
- Kim, T. and Suga, Y. 2001. Application of hybrid welding combined TIG arc and YAG laser to thin steel plate welding. *Proc. 7th Int. Symp. JWS*, Kobe, Japan, pp. 409-414.
- Klimpel, A. and Wolnik, A. 2002. High-power diode-laser welding of butt joints in high-strength steel plates. *Welding International*, Vol. 16, No. 7, pp. 522-529.
- Kristensen, T. and Olsen, F. Improving laser welding using self-fixturing weld parts. *Second European Conference on Joining Technology, Eurojoin 2*. Florence, Italy, :pp. 305-314, May 16-18, 1994.

- Kristensen, J.K. and Weldding, J. Laser based welding of structural steels – recent trends and properties of hybrid YAG-laser/MAG welds. *Proc. Intl. Conf. on Joining of Materials*, JOM-11, Helsingor, Denmark, pp. 1-13, May 25-28, 2003.
- Kodama, M., Kawano, T., and Iwabuchi, H. 1997. Development of high speed horizontal fillet welding process in GMAW process. IIW Doc. XII-1489-97.
- Kujanpaa, V.P. Weld defects in austenitic stainless steel sheets – effect of welding parameters. *AWS Welding Journal*, pp. 45s-52s, Feb. 1983.
- Kumar, A. and Debroy, T. Toward a unified model to prevent humping defects in gas tungsten arc welding. *AWS Welding Journal*, pp.292-s to 304-s, Dec. 2006.
- Lin, M.L. and Eagar, T.W. Influence of arc pressure on weld pool geometry. *AWS Welding Journal*, pp. 163s-169s, June 1985.
- Maddox, S.J., Tips on Fatigue Design of Weldments, Proceedings of International Conference on Fatigue, Toronto, Canada, pp. 19-27, May 9-10, 1994.
- Makhnenko, V.I. et al. 1997. Calculating the kinetics of changes of the gap in laser butt welding panels. *The Paton Welding Journal*, pp. 419-424. Vol. 9, No. 8.
- Malin, V., Sciammarella, F.M. 2004. Calorimetric system for measurement of net power in laser and arc welding and cladding. *Proc. 23rd Int. Congress on Applications of Lasers and Electro-Optics (ICALEO)*.
- Mendez, P.F. and Eagar, T.W. Penetration and defect formation in high-current arc welding. *AWS Welding Journal*, pp. 296s-306s, Oct. 2003.
- Michie, K., Blackman, S., and Ogunbiyi, T.E.B. Twin-wire GMAW: process characteristics and applications. *AWS Welding Journal*, pp. 31-33, May 1999.
- Mills, K.C. and Keene, B.J. 1990. Factors affecting variable weld penetration. *Int. Mater. Review*, Vol. 35, pp. 185-216.
- Mills, K.C., Keene, B.J., Brooks, R.F., and Shirali, A. 1998. Marangoni effects in welding. *Phil. Trans. Royal Society*, London, Vol. 356, pp. 911-925.
- Mischler, H.W. 1986. Gas metal arc welding at high travel speeds. *CMF Focus*, Vol. 2, No. 1.
- Moorehead, T. Automatic multiwire GMAW multiplies productivity. *AWS Welding Journal*, pp. 40-43, June 2003.
- Moran, S.P. and Kotnik, J.F. Twin wire GMA welding 409 stainless steel. *Proc. Conf. Gas Metal arc Welding for the 21st Century*, Orlando, FL, pp. 113-119, Dec. 6-8, 2000.
- Morgan, S.A. and Williams, S.W. 2005. Hybrid laser conduction welding. IIW Doc

- Nakata, K., Tanaka, M., Takao, S., Ueyama, T., Yazawa, I., Nakano, T., Koshiishi, F., and Chen, L. 2004. Hybrid laser-MAG welding of galvanized steel sheets. IIW Doc. XII-1820-04.
- Ng, E. and Watson, I.A. Characterization of CO₂ and diode laser welding of high carbon steels. *Journal of Laser Applications*, Vol. 11, No. 6, pp. 273-278, Dec. 1999.
- Nguyen, T.C., Weckman, D.C., Johnson, D.A., and Kerr, H.W. 2005. The humping phenomenon during high speed gas metal arc welding. *Science and Technology of Welding and Joining*, Vol. 10, No. 4, pp. 447-459.
- Nilsson, K., Heimbs, S., Engstrom, H., and Kaplan, A. 2003. Parameter influence in CO₂ laser/MIG hybrid welding. IIW Doc. IV-843-03.
- Oreper, G.M. and Szekely, J. 1984. Heat and fluid-flow phenomena in weld pools. *J. Fluid Mech.*, Vol. 147, pp. 53-79.
- Page, C.J., Devermann, T., Biffin, J., and Blundell, N. 2002. Plasma augmented laser welding and its applications. *Science and Technology of Welding and Joining*, Vol. 7, No. 1, pp. 1-10.
- Paskell, T.D. Defect formation and control during high-speed gas metal arc welding. EWI Research Brief, Jan. 1989.
- Pekkari, B. 2004. The future of welding and joining. *Svetsaren*, No. 1.
- Rippl, P. 1998. Improved performance in MIG/MAG welding due to the twin-wire technique. IIW Doc. XI-1528-98.
- Petring, D. Hybrid laser welding. *Industrial Laser Solutions*, pp. 12-15, Dec. 2001.
- Petring, D., Benter, C., and Poprawe, R. Fundamentals and applications of diode laser welding.
- Petring, D., Fuhrmann, C., Wolf, N., and Poprawe, R. 2003. Investigations and applications of laser-arc hybrid welding from thin sheets up to heavy section components. *Proc. 22nd Int. Congress on Applications of Lasers and Electro-Optics (ICALEO)*.
- Ream, S. 2004. Laser welding efficiency and cost: CO₂, YAG, fiber, and disc. *Proc. 23rd Int. Congress on Applications of Lasers and Electro-Optics (ICALEO)*.
- Richardson, R. W. et al. Statistical process design for robotic GMA welding of sheet metal. *Welding Journal*, pp. 69-s-77-s, May 2002:.
- Rodwell, M. Surface tension effects in welding. *TWI Research Bulletin*, pp. 194-200, June 1985.

- Rossi, B. Fibre lasers target manufacturing. *Industrial Laser Solutions*, pp. 17, 20, 22, Apr. 2000.
- Salminen, A., Siltanen, J., Jansson, A., and Kujanpaa, V. 2003. Effect of joint configuration on high power diode laser welding of steel. *Proc. 22nd Int. Congress on Applications of Lasers and Electro-Optics (ICALEO)*.
- Sanchez-Castillo, A. and Garcia-Lara, H. 2003. Welding of AISI 1045 steel plates by high power diode laser. *Proc. 22nd Int. Congress on Applications of Lasers and Electro-Optics (ICALEO)*.
- Savage, W.F., Nippes, E.F., and Agusa, K. Effect of arc force on defect formation in GTA welding. *AWS Welding Journal*, pp 212-s-224-s, July 1979.
- Schiaffino, S. and Sonin, A.A. 1997. Formation and stability of liquid and molten beads on a solid surface. *J. Fluid Mech.*, Vol. 343, pp. 95-110.
- Schiaffino, S. and Sonin, A.A. Motion and arrest of a molten contact line on a cold surface; an experimental study. *Phys. Fluids*, Vol. 9, No. 8, pp. 2217-2226, Aug. 1997.
- Sekimoto, K., Oguma, R., and Kawasaki, K. 1987. Morphological stability analysis of partial wetting. *Annals of Physics*, Vol. 176, pp. 359-392.
- Schnitzler, C., Giesekus, J., Leers, M., Meyer, R., Hoffmann, D., and Poprawe, R. 2003. A compact fibre coupled high brightness diode end pumped slab laser with kW output power. *Proc. 22nd Int. Congress on Applications of Lasers and Electro-Optics (ICALEO)*.
- Shinn, B.W., Farson, D.F., and Denney, P.E. 2005. Control of weld bead shape with the hybrid welding process. *IIW Doc. IV-879-05*, pp. 1-10, IIW.
- Stauffer, H. Laser hybrid welding in the automotive industry. *AWS Welding Journal*, Vol. 86, No. 10, pp. 36-40, Oct. 2007.
- Steen, W.M. and Eboo, M. Arc augmented laser welding. *Metal Construction*, pp. 332-335, July 1979.
- Steen, W.M. Arc augmented laser processing of materials. *J. Appl. Phys.*, Vol. 51, No. 11, pp. 5636-5641, Nov. 1980.
- Swift-Hook, D. T. and Gick, A.E.F. Penetration welding with lasers. *AWS Welding Journal*, Vol. 52, No. 11, pp. 492s-499s, Nov. 1973.
- Suzuki, R. and Nakano, T. 2001. Development of MAG welding wires for thin steel sheets in automotive industry. *IIW Doc. XII-1679-01*.
- Tanimoto, J. et al. Development of the AC pulsed MAG welding process. *IIW Asian Pacific Regional Welding Congress, 36th Annual A.W.I. Conference*, Milson's Point, Australia, pp. 678-696, Nov. 14-18, 1988.

- Thomy, C., Seefeld, T., and Vollertsen, F. Industrial potential for high power fibre laser welding. *The Industrial Laser User*, Issue 42, pp. 22-25, Mar. 2006.
- Tomita, N., Ueyama, T., Hasegawa, S., Yasufuku, T., and Ueda, Y. 2004. Development of laser-arc hybrid welding robot system. IIW Doc. XII-1791-2004.
- Tusek, J. and Suban, M. 1999. Hybrid welding with arc and laser beam. *Science and Technology of Welding and Joining*, Vol. 4, No. 5, pp. 308- 311.
- Ueyama, T., Tong, H., Harada, S., Passmore, R., and Ushio, M. AC pulsed GMAW improves sheet metal joining. *Welding Journal*, pp. 40-46, Feb. 2005.
- Ushio, M. and Wu, C.S. 1997. Mathematical modeling of three-dimensional heat and fluid flow in a moving gas metal arc weld pool. *Metall. Mater. Trans. B*, Vol. 28, pp. 509-516.
- Wahab, M.A. and Painter, M.J. 1997. Numerical models of gas metal arc welds using experimentally determined weld pool shapes as the representation of the welding heat source. *Int. J. Pressure Vessels & Piping*, Vol. 73, pp.153-159.
- Wahab, M.A., Painter, M.J., and Davies, M.H. 1998. The prediction of the temperature distribution and weld pool geometry in the gas metal arc welding process. *Journal of Materials Processing Technology*, Vol. 77, pp. 233-239.
- Walduck, R.P. and Biffin, J. Plasma augmented laser welding. *Welding and Metal Fabrication*, pp. 172-176, Apr. 1994.
- Yapp, D. Recent Developments in Hybrid Laser Arc Welding, Comm. XII, Intermediate Meeting, Denmark, IIW Doc., April, 2008.
- Zhou, J., Tsai, H.L., Wang, P.C., Menassa, R.J., and Marin, S.P. 2003. Modeling of hybrid laser MIG keyhole welding process. Proc. 22nd Int. Congress on Applications of Lasers and Electro-Optics (ICALEO).